

SYNTHESIS OF NOVEL SURFACTANTS FROM
BIOMASS DERIVABLE STARTING MATERIALS AND
ANALYSIS OF THEIR PROPERTIES

Rebecca Donovan

PhD

University of York

Chemistry

January 2023

ABSTRACT

This thesis explores the synthesis and properties of novel bioderivable surfactants, focusing on the hydrophobic components, in an attempt to find replacements for perfluorinated surfactants. Perfluorinated surfactants have excellent thermal and chemical stability, excellent surface tension reduction and extreme hydrophobicity and oleophobicity. However, perfluorinated surfactants are also toxic and persistent in the environment. Globally, the production and use of perfluorinated surfactants is being phased out due to regulatory pressures from Europe and the US. Therefore, sustainable replacements for their varied applications which do not pose a threat to the environment are needed.

Lignocellulosic biomass, specifically from waste biomass so as not to compete with food production, is an ideal renewable feedstock for sustainable surfactant production. High density alkanes produced in biofuel research were selected as platforms for the synthesis of novel surfactants to increase hydrophobicity in comparison to typical linear chain surfactants.

Novel surfactant hydrophobes were synthesised primarily through aldol condensations to give branched ketones followed by hydrogenation to produce fatty alcohols. Several methodologies were attempted to attach a variety of head groups to the hydrophobic structures to produce a range of surfactants. These include sulfonation of the α,β -unsaturated ketones, amination of the α,β -unsaturated ketones and etherification of alcohols to produce a poly (ethylene glycol) head group, all of which were unsuccessful. This led to the use of an ester link between the head and tail groups which also promotes biodegradability of the surfactant. Esterification was successfully achieved using an acyl chloride as an intermediate producing 9 novel compounds with potential to behave as surfactants.

Standard industry techniques confirmed that all 9 compounds exhibited surfactant properties and were benchmarked against industrially produced surfactant blends. Analysis methods included Wilhelmy plate static surface tension method, dynamic surface tension measurements and dynamic light scattering measurements. From these analysis techniques the size of the micelles formed was discussed, as well as the speeds at which each surfactant migrated to a newly formed surface and the critical micelle concentrations (CMC) of each compound were determined.

This thesis is dedicated to Nathan Mansell. A true and wonderful friend whose absence is felt keenly.

LIST OF CONTENTS

Synthesis of novel surfactants from biomass derivable starting materials and analysis of their properties.....	1
Abstract.....	2
List of Tables	7
List of Figures	9
List of Schemes.....	14
Acknowledgments.....	17
Declaration.....	18
1 Introduction	19
1.1 Green and sustainable chemistry.....	21
1.1.1 Principles and metrics	21
1.1.2 The circular economy.....	26
1.1.3 Platform molecules	27
1.2 Surfactants and sustainability	28
1.2.1 Definition and applications	28
1.2.2 PFA's and their properties.....	33
1.2.3 Effects on people and the environment	39
1.2.4 Regulations.....	44
1.2.5 Current alternatives to perfluorinated surfactants.....	46
1.3 Project outline	52
1.3.1 HSPiP	52
1.3.2 The route to hydrophobes from fuel precursors and the role of the hydrodeoxygenation stage	57
1.3.3 The scope of possible starting materials for innovative hydrophobes from biomass.....	68
1.4 Conclusion	72
2 Synthetic routes to novel hydrophobic surfactants.....	75
2.1 Introduction to synthetic goals	76
2.2 Lignocellulose as a feedstock	76
2.3 Justification for target compound 56 and access from lignocellulosic biomass ..	78
2.4 Preparation of compound 56 and 56a.....	83
2.5 Structural identification of compound 56	94
2.5.1 Infrared spectroscopy	95
2.5.2 Gas chromatography and mass spectrometry	98
2.5.3 NMR spectroscopy	100

2.6	Cyclisation of 2-nonanone (90) and 2-dodecanone (93).....	102
2.7	Addition of head groups.....	105
2.8	Amination.....	105
2.9	Sulfonation.....	109
2.9.1	HSPiP's predictive role in alternative solvents for compound 56 dissolution 112	
2.10	Addition of tetraethylene oxide (115).....	115
2.11	Esterification.....	119
2.12	Aldol condensations and the hydrogenation and reduction of aldol condensates 122	
2.13	Deprotection.....	126
2.14	Conclusion.....	128
2.15	Experimental.....	129
2.15.1	General Experimental.....	129
2.16	Reaction procedures and experimental.....	129
2.16.1	Preparation of ether, carboxylic acid and intermediates.....	129
2.16.2	Aldol Condensations.....	132
2.16.3	Hydrogenation of aldol condensates.....	133
2.16.4	Sodium borohydride reduction of ketones.....	135
2.16.5	Preparation of esters from acyl chloride.....	137
2.16.6	General procedure for the aldol condensation of 2-hexanone using Q-tube apparatus 147	
2.16.7	Preparation of Mg-Al-O.....	148
3.1	Introduction and aims.....	150
3.2	Measuring hydrophobicity and creating a surfactant monolayer on a solid substrate.....	159
3.2.1	The Sessile drop technique.....	159
3.2.2	The Retraction Method.....	161
3.2.3	Loading hydrophobic liquids onto silica.....	167
3.2.4	Airbrushing.....	171
3.2.5	Depositing compounds onto silver.....	172
3.2.6	Contact angles of Crodamol AB solutions on glass.....	179
3.2.7	Surface tension.....	183
3.2.8	CMC definition.....	184
3.2.9	Wilhelmy plate static surface tension method.....	185
3.2.10	Dynamic light scattering.....	196
3.2.11	Maximum bubble tensiometry.....	204

3.2.12	The Hydrophobic-lypophobic balance (HLB) scale	211
3.2.13	The Hydrophobic-lypophobic difference equation.....	212
3.2.14	Key parameters for surfactant behaviour and performance determined from combinations of analysis.....	213
3.2.15	Preliminary bench test for an indication of emulsion type	214
3.3	Conclusion	216
3.4	Overall conclusion	217
4	References	219
4.1	Appendix.....	228

LIST OF TABLES

Table 1 Examples of surfactants classified according to head group type with example structures.	31
Table 2: Catalyst screening for the condensation of 2-hexanone (1). Reagents and conditions: 2-hexanone (1, 2 mmol), toluene (3 mL), 200 mg of catalyst, 150 °C, 3 hours. Work carried out by Sacia et al. * calcined hydrotalcite.	85
Table 3: Reaction conditions for the aldol condensation and cyclisation of 2-hexanone (54). Dean-Stark set up. * conversion by mass.	86
Table 4: Reaction conditions for the condensation of 2-hexanone (54). Conversion of 54 determined by GC-FID. MgAlO is hydrotalcite calcined at 700 °C for 2 h with an oven ramp rate of 2 °C prior to use. ** percentage conversion to total products calculated by mass without further analysis after removing remaining 54 through rotary evaporation until no further loss of mass.....	87
Table 5: Catalyst treatment after calcination at 700 °C for 2 h with an oven ramp rate of 2 °C. Reagents and condition: 2-hexanone (compound 54, 2 mmol), toluene (3 mL) and 200 mg of catalyst reacted under pressure at 170 °C.	89
Table 6: Infrared spectral data and assignments for 2-hexanone (54) and compound 56/56a.....	97
Table 7: Reaction details of nonanone (90) and dodecanone (93) aldol condensations. * Calcined at 450 °C for 2 hours prior to reaction.	103
Table 8: Reaction conditions and yields for the reaction between the benzyl protected acyl chloride of poly (ethylene glycol) and fatty alcohols.....	121
Table 9: Final compounds and the bioderivable alcohols used to produce hydrophobes.	152
Table 10: Industrial products and information on manufacture and structure for the industrial produced used for comparison with compounds 145-153.	153
Table 11: Contact angle and water droplet volume results obtained via the retraction method of sample preparation.....	164
Table 12: Contact angle measurements of the silver coated glass slides after treatment with PFOA and octanoic acid solutions of different concentrations.	173
Table 13: Contact angles of Crodamol AB with 0.5% additives on glass slides.	180
Table 14: Results table for the surface tension vs surfactant concentration analysis of compound 149.	189
Table 15: CMC values for final compounds determined through surface tension measurements using the Kruss K100 vs surfactant concentration. *compound 147 is insoluble in DI water and was dissolved in 5% IPA in DI water prior to CMC analysis.	194
Table 16: Dynamic light scattering data for samples at 0.1% surfactant concentration in ultrapure water measured at 25 °C.	198
Table 17: Dynamic light scattering data for surfactants at 0.1% solution in 5% IPA in DI water at 25 °C. * Bank is 5% IPA in Di water and has a derived count rate of 606 kcps. ...	202
Table 18: Concentration and derived count rate for CMC determination of compound 149.	203
Table 19: CMC values determined by DLS (see appendix for data tables, plots, line equations and intercept co-ordinates for each compound).....	204
Table 20: Masses used and results table for the emulsion type bench test.	215
Table 21: Concentration and derived count rate for CMC determination of compound 149.	228

Table 22: Results table for the surface tension vs surfactant concentration analysis of compound 149	230
Table 23: Surface lifetime (SL) / s and surface tension (ST) / mN/m for compound 149 ...	231
Table 24: Concentration and derived count rate for CMC determination of compound 148	232
Table 25: Results table for the surface tension vs surfactant concentration analysis of compound 148	233
Table 26: Surface lifetime (SL) / s and surface tension (ST) / mN/m for compound 148 ...	235
Table 27: Concentration and derived count rate for CMC determination of compound 150	236
Table 28: Results table for the surface tension vs surfactant concentration analysis of compound 150	238
Table 29: Surface lifetime (SL) / s and surface tension (ST) / mN/m for compound 150 ...	239
Table 30: Concentration and derived count rate for CMC determination of compound 153	240
Table 31: Results table for the surface tension vs surfactant concentration analysis of compound 153	241
Table 32: Surface lifetime (SL) / s and surface tension (ST) / mN/m for compound 153 ...	242
Table 33: Concentration and derived count rate for CMC determination of compound 146	244
Table 34: Results table for the surface tension vs surfactant concentration analysis of compound 146	245
Table 35: Surface lifetime (SL) / s and surface tension (ST) / mN/m for compound 146 ...	246
Table 36: Concentration and derived count rate for CMC determination of compound 145	247
Table 37: Results table for the surface tension vs surfactant concentration analysis of compound 145	248
Table 38: Surface lifetime (SL) / s and surface tension (ST) / mN/m for compound 145 in deionised water with 5% IPA	250
Table 39: Concentration and derived count rate for CMC determination of compound 151	251
Table 40: Results table for the surface tension vs surfactant concentration analysis of compound 151	252
Table 41: Surface lifetime (SL) / s and surface tension (ST) / mN/m for compound 151 ...	254
Table 42: Concentration and derived count rate for CMC determination of compound 152	255
Table 43: Results table for the surface tension vs surfactant concentration analysis of compound 152	256
Table 44: Surface lifetime (SL) / s and surface tension (ST) / mN/m for compound 152 in deionised water with 5% IPA	258
Table 45: Concentration and derived count rate for CMC determination of compound 147	259
Table 46: Results table for the surface tension vs surfactant concentration analysis of compound 147	260
Table 47: Surface lifetime (SL) / s and surface tension (ST) / mN/m for compound 147 in deionised water with 5% IPA	261

LIST OF FIGURES

Figure 1: The 12 Principles of Green Chemistry.....	21
Figure 2: Schematic for comparison of the traditional linear economy and the circular economy.	26
Figure 3: Examples of petrochemically derived base chemicals used by the chemical industry.	27
Figure 4: Examples of platform molecules that can be obtained from biomass at scale.....	27
Figure 5: Schematic of the typical structure of a surfactant and the head group categories.	28
Figure 6: Self-assembly of surfactants around an oil droplet in a micelle (left), at the air/water interface of a foam (centre) and at the air/water interface of a solution (right). 29	
Figure 7: The four sub-categories of surfactants according to charge on the head group. .	29
Figure 8: Structures of fluorinated polymer PTFE and perfluorinated surfactants PFOA and PFOS.	33
Figure 9: Logarithmic hexadecane/air partition coefficients vs molar volume for a range of 684 organic compounds. ²⁷	34
Figure 10: Saturated liquid vapour pressures at 25 °C of 200 organic compounds and 6 perfluorinated alkanes vs molar volume. ²⁷	35
Figure 11: Advertisements for Gore-Tex (top left), Scotchguard (bottom left) and Teflon (side right) products. <i>Image credits: "MirroTeflon037-1968-CompAds" (right) from DukeUnivLibraries is licensed under CC BY-NC-SA 2.0. "GORE-TEX® Experience Tour: Design sketch of Marco Vanella" (top left) by GORE-TEX brand is licensed under CC BY-NC-ND 2.0. "3M Scotchguard" (bottom left) by is licensed under CC BY-NC-ND 2.0.</i>	37
Figure 12: Bar chart demonstrating increasing attention paid to PFAS in the scientific community since 1998. Number of publications v year of publication sourced from the Web of Science database. Search terms used: PFAS and perfluoro* or PFOS or PFOA.	38
Figure 13: Health effects identified by the C8 health project as having probable links to PFAS.	40
Figure 14: Examples of ways in which PFAS may enter the environment.	41
Figure 15: Structures of prevalent PFAS used as replacements for PFOA, PFOS and other restricted PFAS.	47
Figure 16: Compounds used for the chemisorbed monolayer films formed from the deposition of normal alkanethiols, CF ₃ -terminated alkanethiols, and methyl-terminated partially fluorinated thiols. ¹¹⁸	48
Figure 17: The Chemical structure of highly branched fluorinated thiol (BRFT) and of linear 1H,1H,2H,2H perfluorodecanethiol (PFDT).	49
Figure 18: Polymer chain with M3T side chain. ¹²²	50
Figure 19: HSPiP plot of perfluorocarbons and hydrocarbons. Hydrogen bonding contribution on the X-axis, molecular permanent dipole on the y-axis and dispersion forces (Van der Waals forces) on the Z-axis.	54
Figure 20: HSP plot for molecules found within the range of HSP values observed for perfluorinated structures.....	55
Figure 21: HSP plot containing hydrocarbons, perfluorinated molecules and molecules occupying a similar HSP space to perfluorinated molecules.	56
Figure 22: The structure of lignocellulosic biomass.....	77

Figure 23: Diagram of Q-tube for small scale reactions (left) and Dean-Stark apparatus set-up for scale-up (right).	84
Figure 24: Calibration curve for starting material (hexanone) and internal standard (dodecane).	88
Figure 25: Schematic representation of crystal structure of Mg-Al-O after rehydration via liquid phase (top) and gas phase (bottom). ¹⁹⁷	92
Figure 26: Effect of water addition to catalyst. % conversion = conversion of 2-hexanone. % A = major cyclic isomer. % B minor cyclic isomer, %C minor cyclic isomer.	93
Figure 27: Investigating a greener solvent replacement for toluene. % conversion = conversion of 2-hexanone (54). % A = major cyclic isomer. % B minor cyclic isomer, %C minor cyclic isomer.	94
Figure 28: Infrared spectra of 2-hexanone (54).	96
Figure 29: Infrared spectra of a mixture of compounds 56 , 56a and 57	96
Figure 30: GC-FID chromatogram for reaction mixture, Table 5, Entry 4, in acetone.	98
Figure 31: GC-MS Chromatogram for RD130 crude reaction mixture.	98
Figure 32: Mass spectra for the peak of dimer from the GC-MS chromatogram.	99
Figure 33: Mass spectra for the peak of trimer from the GCMS chromatogram.	99
Figure 34: ¹ H NMR of product compounds 56 , 56a (400 MHz, Chloroform-d) δ 5.68 (s, 0.15H), 2.28-1.79 (m, 7H), 1.49-0.96 (m, 13H), 0.96-0.58 (m, 12H).	100
Figure 35: The structure of compound 56 and 56a with ¹ H NMR assignments. * represents the chiral centre.	101
Figure 36: Key reaction products of 2-hexanone (54), 2-nonanone (90) and 2-dodecanone (93).	102
Figure 37: ¹ H NMR snapshot comparing the alkene region of cyclohexenone (a), the sulfonation product of cyclohexenone (b), isophorone (c) and isophorone's sulfonation product (c).	110
Figure 38: Graphical representation of different solvents in Hansen space. Compound 56 at the centre of the mesh sphere. Solvents within the sphere are most likely to dissolve the target molecule. Toluene and water ratios (90:1, 70:30, 50:50) calculated from predictions.	113
Figure 39: Reagents used by Fini et al for sulfonation that produced low yields after 4 days at 22 °C.	114
Figure 40: Structure of compound 133	122
Figure 41: Structure of compound 136	125
Figure 42: Final synthetic compounds with surfactant potential	127
Figure 43: Final compounds 145-153 synthesised in this study and subjected to analysis for identification and comparison of surfactant properties.	150
Figure 44: Representative structures for the Industrially produced surfactant samples (purify unknown but likely to be a distribution of fatty chain lengths from natural oils and variation of ethoxylate chain length) alongside the structures of compounds 145-148	154
Figure 45: Fatty Acid Methyl Ester Carbon Chain length distribution in Palm Oil and Coconut Oil.	155
Figure 46: Contact angle of an ultrapure water droplet on a solid surface.	157
Figure 47: Schematic of the measurement of contact angle of water droplet on solid substrate.	159
Figure 48: Surface descriptions based on the degree of wetting of that surface with a droplet of water using the sessile drop technique.	160
Figure 49: Schematic of the retraction method ²³⁷	161

Figure 50: A comparison of perfluorooctanocic acid (25 , PFOA) and octanoic acid (160).	162
Figure 51: Schematic of water droplet on top of fluorosurfactant monolayer exhibiting superhydrophobic contact angle.	163
Figure 52: Bar chart for a visual representation of the contact angles described in Table 11. Error bars are based on one standard deviation.	164
Figure 53: Photograph of back-lit sample slide prepared via the retraction method.	166
Figure 54: Schematic of drying and crystallisation process during the drying time of the retraction method.	166
Figure 55: Schematic of the expected effect on contact angle with a de-ionised water droplet of coating silica in octanol.	168
Figure 56: Silica samples treated with octane (top), octanol (middle) and octanoic acid (bottom) at 20%, 40%, 60%, 80% and 100% w/w with respect to silica from left to right.	169
Figure 57: Schematic of the wetting mechanism of coated silica on a glass slide.	170
Figure 58: Microscope image of silica treated with octanoic acid spread across adhesive tape.	171
Figure 59: Photographs of the slide preparation process using Tollen's reagent to produce a silver coated slide (left) and the silver coated slide raised up on the side of a petri dish ready for the solution of the component of interest to be pipetted over (right).	173
Figure 60: Scatter plot of contact angles produced by octanoic acid on a silver surface described in Table 12.	175
Figure 61: Superhydrophobic surface with droplets of water showing large contact angle.	176
Figure 62: Photograph of the hydrophobic effects of octanoic acid at 10 mM.	176
Figure 63: Schematic of plasma jet treatment of a polymer sheet.	178
Figure 64: Schematic of the expected effect of adding hydrophobic surfactants to Crodamol AB.	181
Figure 65: Bar chart showing how the average contact angle of Crodamol AB changed when additives were added at 0.5% wt/wt.	182
Figure 66: Photograph showing the effect of additives to Crodamol AB on contact angles on a glass surface.	182
Figure 67: Surface tension diagram.	184
Figure 68: Schematic of the distinct changes in physical properties of a surfactant before and after the critical micelle concentration.	185
Figure 69: Schematic diagram of Wilhelmy plate static surface tension method.	187
Figure 70: Photograph of the Kruss K100 with automated dilution.	188
Figure 71: Surface tension vs concentration of compound 149 in deionised water.	189
Figure 72: Comparison of surfactant concentration vs surface tension relationships for the final compounds * compound was insoluble in DI water and was dissolved in 5% isopropanol in water.	191
Figure 73: Structures of final compounds 149 , 153 and 150 .	192
Figure 74: Chemical structures of compounds 149 , 145 and 148 .	193
Figure 75: Structures of compounds 153 and 150 .	193
Figure 76: Critical micelle concentration vs number of carbons in the tail group.	195
Figure 77: Structures of compounds 153 , 150 and 149 .	195
Figure 78: Chemical structures of the compounds from Table 16.	197
Figure 79: Chemical structures of the compounds 145-153 .	201
Figure 80: Derived count rate vs concentration of compound 149 .	203
Figure 81: Radius size of gas bubble eluting from a capillary tube.	205

Figure 82: Schematic representing the change of gas pressure over time as a bubble elutes from a capillary tube.....	206
Figure 83: Surface tension vs surface lifetime data collected from the maximum bubble pressure method. Surfactant concentration was 0.1% wt/wt in 5% IPA in deionised water.	208
Figure 84: Surface tension vs surface lifetime data collected from the maximum bubble pressure method. Surfactant concentration was 0.1% wt/wt in deionised water.....	209
Figure 85: Structures of compounds 146 and 148	210
Figure 86: Structures of compounds 153 and 150	211
Figure 87: Schematic diagram of the emulsion type bench test.	214
Figure 88: The structure of compound 149	228
Figure 89: Derived count rate (kcps) vs Surfactant concentration (% wt/wt) for compound 149	229
Figure 90: Surface tension vs Concentration of compound 149 in deionised water.....	229
Figure 91: Surface tension vs surface lifetime for compound 149	230
Figure 92: The structure of compound 148	231
Figure 93: Derived count rate (kcps) vs Surfactant concentration (% wt/wt) for compound 148	232
Figure 94: Surface tension vs concentration of compound 148 in deionised water.....	233
Figure 95: Surface tension vs surface lifetime for compound 148	234
Figure 96: The structure of compound 150	236
Figure 97: Derived count rate (kcps) vs Surfactant concentration (% wt/wt) for compound 150	237
Figure 98: Surface tension vs Concentration of compound 150 in deionised water.....	237
Figure 99: Surface tension vs surface lifetime for compound 150	238
Figure 100: The structure of compound 153	239
Figure 101: Derived count rate (kcps) vs Surfactant concentration (% wt/wt) for compound 153	240
Figure 102: Surface tension vs Concentration of compound 153 in deionised water.....	241
Figure 103: Surface tension vs surface lifetime for compound 153	242
Figure 104: The structure of compound 146	243
Figure 105: Derived count rate (kcps) vs Surfactant concentration (% wt/wt) for compound 146	243
Figure 106: Surface tension vs Concentration of compound 146 in deionised water.....	244
Figure 107: Surface tension vs surface age for compound 146 at 0.1% wt/wt concentration	245
Figure 108: The structure of compound 145	246
Figure 109: Derived count rate (kcps) vs Surfactant concentration (% wt/wt) for compound 145	247
Figure 110: Surface tension vs Concentration of compound 145 in deionised water.....	248
Figure 111: Surface tension vs surface age for compound 145 at 0.1% concentration in deionised water with 5% IPA	249
Figure 112: The structure of compound 151	250
Figure 113: Derived count rate (kcps) vs Surfactant concentration (% wt/wt) for compound 151	251
Figure 114: Surface tension vs Concentration of compound 151 in deionised water.....	252
Figure 115: Surface tension vs surface age for compound 151 at 0.1% concentration in deionised water with 5% IPA	253

Figure 116: The structure of compound 152	254
Figure 117: Derived count rate (kcps) vs Surfactant concentration (% wt/wt) for compound 152	255
Figure 118: Surface tension vs Concentration of compound 152 in deionised water	256
Figure 119: Surface tension vs surface age for compound 152 at 0.1% concentration in deionised water with 5% IPA	257
Figure 120: The structure of compound 147	259
Figure 121: Derived count rate (kcps) vs Surfactant concentration (% wt/wt) for compound 147	259
Figure 122: Surface tension vs Concentration of compound 147 in deionised water	260
Figure 123: Surface tension vs surface age for compound 147 at 0.1% concentration in deionised water with 5% IPA	261

LIST OF SCHEMES

Scheme 1: Aldol condensation scheme and mechanism between furfural and acetone. ...	60
Scheme 2: Cross aldol condensation between furfural (1) and the product of the aldol condensation of furfural and acetone (3).....	61
Scheme 3: Furfural and cyclopentanone aldol condensation products using a deep eutectic solvent to yield C10 and C15 fuel precursors.	62
Scheme 4: Synthetic route to decalin from the hemicellulose/cellulose derived platform molecule furfural.	63
Scheme 5: Mechanism for the reductive rearrangement of furfural to cyclopentanone	63
Scheme 6: Mechanism for the self-aldol of cyclopentanone	63
Scheme 7: Preparation of bicyclopentane and tricyclopentane from cyclopentanol.	64
Scheme 8: Conversion of 2,5-hexanedione to polycyclic alkanes via one-pot process over dual catalyst bed.	64
Scheme 9: Self and cross aldol condensation products (55 , 56 , 57 , 58) of 2-hexanone (54)	65
Scheme 10: Diels-Alder products of cyclopentadiene, dicyclopentadiene and 2-MF.	66
Scheme 11: Mannich-Diels-Alder route to C10 spiroalkane precursor to high density fuel.	67
Scheme 12: The Mannich-Diels-Alder addition of biomass derived hydroxycyclopentenone and cyclopentadiene (59)	67
Scheme 13: Chemical structure of γ -decalactone (76).	68
Scheme 14: A collection of structures from the literature review.	69
Scheme 15: 2-hexanone (54) condensation and cyclisation reaction. Reaction conditions taken from Sacia et al: 2-hexanone (54 , 2 mmol), toluene (3 mL), 200 mg catalyst. *Mg-Al-O = calcined hydrotalcite	69
Scheme 16: Possible reaction routes to surfactants from compound 56 , synthesized through the aldol condensation of 54	71
Scheme 17: Major product of 2-hexanone (54) sequential self-aldol condensation with conditions specified by Sacia et al. ¹⁷⁰	78
Scheme 18: Potential synthetic structures to novel surfactants from 2-hexanone (54).	79
Scheme 19: Synthetic route from fructose to 2-hexanone (54) via platform molecule 5-HMF (16).	79
Scheme 20: Mechanism for the dehydration of fructose catalysed by HCl in a deep eutectic solvent system. ¹⁸⁵	80
Scheme 21: Mechanism for the hydrogenolysis of HMF (16) to 2,5-DMF (87). Reaction conditions: perovskite-supported Ni catalyst, 6 h, 230 °C, 5 MPa H ₂	81
Scheme 22: Mechanism for the ring opening hydrogenation of 2,5-DMF (87) to 2-hexanone using Pd/C (5% wt) at 120 °C, 4.1 Bar H ₂	82
Scheme 23: Mechanism of 2-hexanone (54) self-aldol condensation, addition and cyclisation. MgAlO* hydrotalcite calcined at 200 °C for 2 hours.	83
Scheme 27: Synthetic routes to surfactants from compound 56	102
Scheme 28: Aldol condensation of 2-nonanone and 2-dodecanone (90 , 93)	104
Scheme 29: Amination of cyclohexenone (3 mmol) (96) with excess diethyl amine (82 , 24 mmol). Solvent free reaction with stirring. Yields determined by GC-FID analysis of reaction mixtures *100% conversion of cyclohexenone with 0% selectivity to the desired product.	106

Scheme 30: Amination of isophorone (2.4 mmol) (98) with excess diethyl amine (82 , 19 mmol). Solvent free reaction with stirring. Yields determined by GC-FID analysis of reaction mixtures.	106
Scheme 31: Amination of compound 56 (1.5 mmol) with excess diethyl amine (82 , 12 mmol). Solvent free reaction with stirring, Yields determined by GC-FID analysis of reaction mixtures.	106
Scheme 32: Amination of cyclohexenone (3 mmol) (96) and excess butyl amine (24 mmol)(101). Solvent free reaction with stirring. Yields determined by GC-FID analysis of reaction mixtures.	107
Scheme 33: Amination of isophorone (2.4 mmol) (98) and excess butyl amine (19 mmol)(101). Solvent free reaction with stirring. Yields determined by GC-FID analysis of reaction mixtures. **96.1% conversion of starting material with 33% selectivity to the desired product **100% conversion of starting material with 31% selectivity to the desired product.....	107
Scheme 34: Amination of 1 (1.5 mmol) (56) and excess butyl amine (15 mmol)(101). Solvent free reaction with stirring. Yields determined by GC-FID analysis of reaction mixtures.	108
Scheme 35: Sulfonation of 56 (4 mmol) with sodium metabisulfite (4 mmol) in aqueous solution (10 mL deionised water) with stirring. Solvent removed by rotary evaporation before analysis by FT-IR and ¹ H NMR.	109
Scheme 36: Sulfonation of cyclohexenone (96) (3 mmol) with sodium metabisulfite (3 mmol) in aqueous solution (2.5 mL deionised water) with stirring. Solvent removed by rotary evaporation before analysis by FT-IR and ¹ H NMR.	109
Scheme 37: Sulfonation of isophorone (98) (2 mmol) with sodium metabisulfite (2 mmol) in aqueous solution (2.5 mL) deionised water with stirring. Solvent removed by rotary evaporation before analysis by FT-IR and ¹ H NMR. Conditions: a) H ₂ O, room temperature, 30 minutes with ultrasonic probe (RD187-A) b) H ₂ O, 50 °C, 30 minutes with ultrasonic probe (RD187-B) c) H ₂ O, room temperature, 12 days (RD190-A)	109
Scheme 38: Sulfonation of isophorone (5) with sodium bisulfite with stirring. Solvent removed by rotary evaporation before analysis by FT-IR and ¹ H NMR. a) 4 (2.8 mmol) and sodium bisulfite (8.5 mmol) in deionised water (20 mL) b) 4 (2.8 mmol), sodium bisulfite (8.5 mmol) and acetic acid (0.5 mL) in deionised water (20 mL) c) isophorone (3 mmol) and sodium bisulfite (6 mmol) in deionised water (10 mL) and isopropanol (10 mL). Conditions: a) H ₂ O, room temperature, 12 days (RD190-B) b) H ₂ O, acetic acid, room temperature, 12 days (RD190-C) c) Isopropanol, H ₂ O, 50 °C, 65 hours (RD192)	111
Scheme 39: Sulfonation of 1 (3.3 mmol) with sodium bisulfite (6.6 mmol) in specified solvents with stirring. Yields determined through ¹ H NMR and FT-IR after removal of solvent via rotary evaporation. Conditions: a) H ₂ O, isopropanol, 50 °C, 24 hours b) H ₂ O, isopropanol, 65 °C, 3 days c) H ₂ O, isopropanol, reflux, 24 hours d) H ₂ O, cyrene, reflux, 4 days e) H ₂ O, toluene, reflux, 4 days.....	112
Scheme 40: Showing the hydrogenation of levoglucosenone (LGO) to form Cyrene and hydration of Cyrene to the geminal diol.....	113
Scheme 41: Two equilibrium present in bisulfite solution.	114
Scheme 42: Route to bioethylene oxide from bioethanol through ethylene.....	115
Scheme 43: Synthetic route to tetraethylene glycol monobenzyl ether (75%) from tetraethylene glycol (1 mol), benzyl chloride (0.1 mol) and sodium hydroxide (0.12 mol) heated to 100 °C for 24 hours.....	116
Scheme 44: Synthesis of compound 119	116

Scheme 45: Unsuccessful etherification of compound 119 and 2-dodecanol	117
Scheme 46: Appel reaction to produce alkyl bromide from compound 117	117
Scheme 47: Unsuccessful etherification of compound 121	117
Scheme 48: Finkelstein reaction with TBAI for the etherification of compound 121	118
Scheme 49: Synthesis of alkyl iodide 122	118
Scheme 50: Proposed etherification of compound 122 and 2-dodecanol (124).....	118
Scheme 51: Addition of carboxylic acid to compound 117 using bromoacetic acid	119
Scheme 52: T3P mediated esterification attempt	119
Scheme 53: Steglich esterification attempt using compound 126 and 2-dodecanol	120
Scheme 54: Using oxalyl chloride to produce an acyl chloride for esterification with fatty alcohols	120
Scheme 55: Esterification with fatty alcohol via acyl chloride formation	120
Scheme 56: Esterification mechanism via acyl chloride	122
Scheme 57: Aldol condensation of furfural (36) and cyclopentanone (40).....	123
Scheme 58: Cross aldol condensation mechanism of furfural (36) and cyclopentanone (40)	123
Scheme 59: Hydrogenation of aldol condensate product 39	124
Scheme 60: Sodium borohydride reduction of compound 140	124
Scheme 61: Proposed mechanism for the aldol condensation of compound 54	124
Scheme 62: Aldol condensation of 2-nonanone (90)	125
Scheme 63: Hydrogenation over Pd/C and reduction with sodium borohydride of 2- nonanone double aldol condensate.	125
Scheme 65: Deprotection of head group to yield final compounds with surfactant potential	126
Scheme 66: Acid and base catalysed mechanisms for the addition of poly(ethylene oxide) head groups.	156
Scheme 67: Mechanism of the reaction between dextrose and Tollen's reagent.	172

ACKNOWLEDGMENTS

Firstly, I'd like to thank my supervisors for giving me this opportunity to develop my knowledge, my skills and myself. To Tom, Will and Rob, you have been incredibly welcoming, supportive and understanding as supervisors and you have been both influential and inspiring as chemists. I'd also like to thank all of the support staff that have facilitated me and provided essential support and guidance including Richard, Suranjana, Hannah, Scott, Helen, Phil, Katy and Rachel from the grad office. From my industrial sponsor Croda, James Humphreys has provided stimulating insights and invaluable professional opinions.

Lastly, I'd like to thank my family and friends. The road never did run smooth but the unwavering support from my family and friends gave me strength when I had none. To my parents, Sandra and Stephen, my Auntie and Uncle, Susan and Ian, my sister Louise and the best of friends, Hannah and Roxana, you shared the load, you uplifted and sustained me and deserve more thanks than I can give.

DECLARATION

I declare that this thesis is a presentation of original work and I am the sole author. This work has not previously been presented for an award at this, or any other, University. All sources are acknowledged as References.

Chapter 1

1 INTRODUCTION

1.1 GREEN AND SUSTAINABLE CHEMISTRY

1.1.1 Principles and metrics

Green Chemistry can be summarised as an approach to chemistry that brings the consideration of environmental impacts to the forefront when designing chemical processes. The seminal work of Anastas and Warner in 1998 lays out the 12 principles of green chemistry.¹ Their work described how to go about reducing waste (especially harmful waste), reducing energy expenditure and avoiding producing environmentally damaging products in the first place. Through the application of the 12 principles of green chemistry, a systematic, definable and somewhat measurable approach can be used to move towards achieving the overall goal of green chemistry; to allow progress whilst protecting the environment.¹⁻³ The 12 principles of green chemistry, shown in Figure 1, are central to this study and have been considered where appropriate throughout.⁴

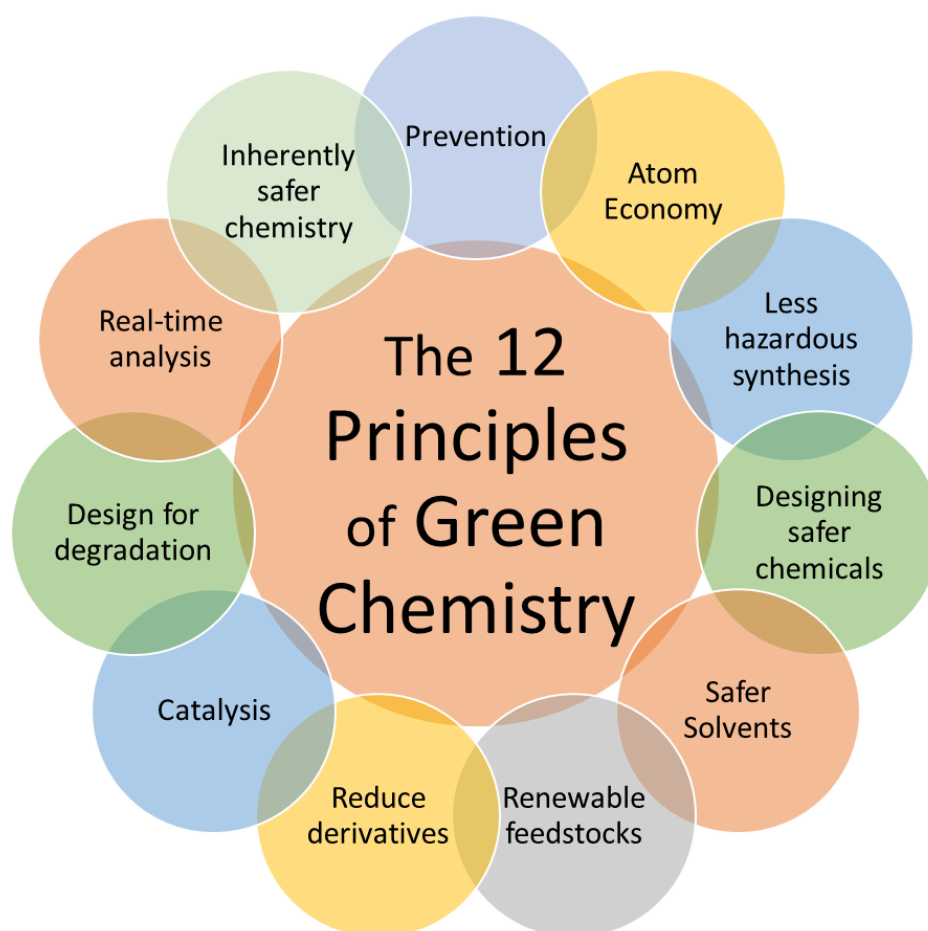


Figure 1: The 12 Principles of Green Chemistry.

The 12 principles of green chemistry:¹

1. Prevention

The prevention principle aims to reduce the waste produced through chemical reactions and processes because it is better to prevent the production of waste than it is to dispose of the waste or treat it. This is the first principle of green chemistry and some aspect of this goal runs through all 12 principles.

2. Atom Economy

Atom economy is a green chemistry metric which quantifies the percentage of atoms from the reactants that are utilised in the desired product, and therefore how much is wasted. Addition reactions for example would have a high atom economy because all atoms of the reactants are present in the desired product. The atom economy principle is rooted in the aim to apply a green chemistry metric while designing processes to maximise the efficiency of reactions therefore reducing waste production.

3. Less Hazardous Chemical Synthesis

This principle aims to reduce the usage of hazardous materials in synthesis. If a reaction uses or produces hazardous materials, either as starting materials, products or by-products, alternative routes should be considered against the 12 principles. The safety of the workforce carrying out the reaction in the first instance is of paramount concern as well as the safety of the general public if accidentally exposed to hazardous waste. This principle also incorporates the prevention principle, as it is better to avoid creating hazardous waste than to clean it up or treat it.

4. Designing safer chemicals

The design of safer chemicals aims to reduce hazards created through use and disposal of hazardous chemicals by not producing them in the first place. Consideration should be made of the probable toxicity and environmental damage a product has the potential to cause throughout its life cycle. This principle is one of the more challenging aspects of green chemistry because trends in toxicity and biodegradability are not yet well understood. Furthermore, in the interest of progress, newly designed chemicals should not only be safer but also maintain or improve the efficacy and functionality of its predecessor.

5. Safer solvents and auxiliaries

Solvents are often the reaction component that causes the greatest concern for safety due to volatility, flammability and toxicity. Solvents are also often heated, distilled, filtered and cooled in various energy and resource heavy processes to finally be removed from the final products (where low levels can cause toxicity problems in products) and either recycled or more often incinerated. This principle aims to reduce the use of solvents ideally with solventless reactions. This immediately greatly reduces the hazards and production of waste in most cases. It would however be unrealistic and chemically unsound to assume that solvents do not play a vital role in the chemistry and therefore solventless reactions are not always possible.

Solvents often play a crucial role in removing the heat of reaction, providing safety from runaway reactions and unwanted side products. To combat this the engineering process at the industrial scale of solventless reactions may require more efficient monitoring and cooling systems and would therefore lend themselves to flow chemistry. The design of safer solvents is critical to reduce hazards where a solventless reaction is not possible. Often solvents are a necessity for example when issues with safety, viscosity and selectivity through solvent effects arise however the choice of solvent should be carefully considered, using safer solvents where possible.

6. Design for energy efficiency

This principle is concerned with minimising the energy required to complete a chemical process. Ambient temperatures and pressures are preferred as they greatly reduce the consumption of energy. Reactions and processes should be carefully considered where conditions are concerned. For example, a small reduction in yield may be agreeable when a large amount of energy (and therefore money) can be conserved. Principle 6 is particularly topical through the current demands on energy providers and the costs associated.

7. Renewable feedstocks

Where possible feedstocks should not be derived from depletable resources but instead from renewable resources. The advancement of this principle has created a vast research area surrounding the circular economy and the production of fuels and chemicals from biomass using biorefineries.

8. Reduce derivatives

Reactions and processes that involve the protection and deprotection of functional groups during reaction sequences should be redesigned where possible to avoid these steps as they often increase energy consumption and waste production. Enzymes are particularly useful to achieve this goal as their high specificity reduces the need for protecting groups and the production of by-products is also reduced.⁵

9. Catalysis

Catalysis is preferable to stoichiometric reagents because the amount of waste produced is reduced and the catalyst can usually be recycled many times over.⁶

10. Design for degradation

When designing target molecules for synthesis consideration should be given to the environmental impact of the products. Any compounds known to be persistent in the environment should not be made and much caution used when designing similar compounds. Products should be designed in a way that allows for breakdown in the environment when released because it is unreasonable to assume no accidental releases will occur or that a disposal problem will not be created in the future. This principle is closely related to principle 4, designing safer chemicals, as chemicals which are persistent in the environment have been known to bioaccumulate through food webs and effect the human and animal populations.⁷

11. Real time analysis

The use of real time analysis or in-process monitoring enables adjustments to be made during the course of the reaction leading to better and more consistent outcomes. The production of waste is also minimised. For example, a batch of product has been made and does not pass quality control and is now not fixable once out of the reactor but may have been fixable with real time alterations. Furthermore, real time monitoring can improve safety through the feedback of vital information such as temperature and pressure which could provide early warning of hazards, such as runaway reactions.

12. Inherently safer chemistry for accident prevention

This principle combines principles 3,4 and 5 but focusses specifically on accident prevention. All 12 principles work on the basis that prevention is better than a cure and in this instance the elimination of potential hazards is always much more effective in

term of safety than additional monitoring or personal protection equipment for the workforce.

Over time metrics such as atom economy and the principles of green chemistry have helped quantify positive changes to chemical processes and the impact their products have. However, these principles have limitations such for example no consideration of carbon emissions or the purpose and use of a product. Life cycle assessments (LCAs) can be used to consider the wider use and impact of products beyond their manufacture. LCAs take into account the environmental impact of a product from cradle to grave. The manufacture, emissions during manufacture and use, recyclability, polluting power during use and waste produced at the end of life are all considered in LCAs. LCAs are difficult to accurately calculate because they typically encompass a great many factors and therefore can have a considerable margin for error. However, they represent a more rounded and considered approach to the assessment of a product, allowing comparison between products when questions beyond manufacture and processing are raised. Furthermore, the wider assessment of the environmental impacts of a product provided by LCAs can be combined with life cycle sustainability assessments and life cycle costing assessments to provide a holistic overview of the product. The increasing complexity of these calculations combined with non-standardised techniques for calculation leaves much room for error however is a significant step towards a holistic understanding of a product's impact on the world.

1.1.2 The circular economy

The circular economy is an idealised model of production and consumption. The circular economy takes the traditional linear production and consumption model which can be described as ‘take, make, use, pollute’ and transforms it into a circular economy which extends the life of products and transform them into new products leading to drastic reduction in the production of waste (see Figure 2 for a visual representation).

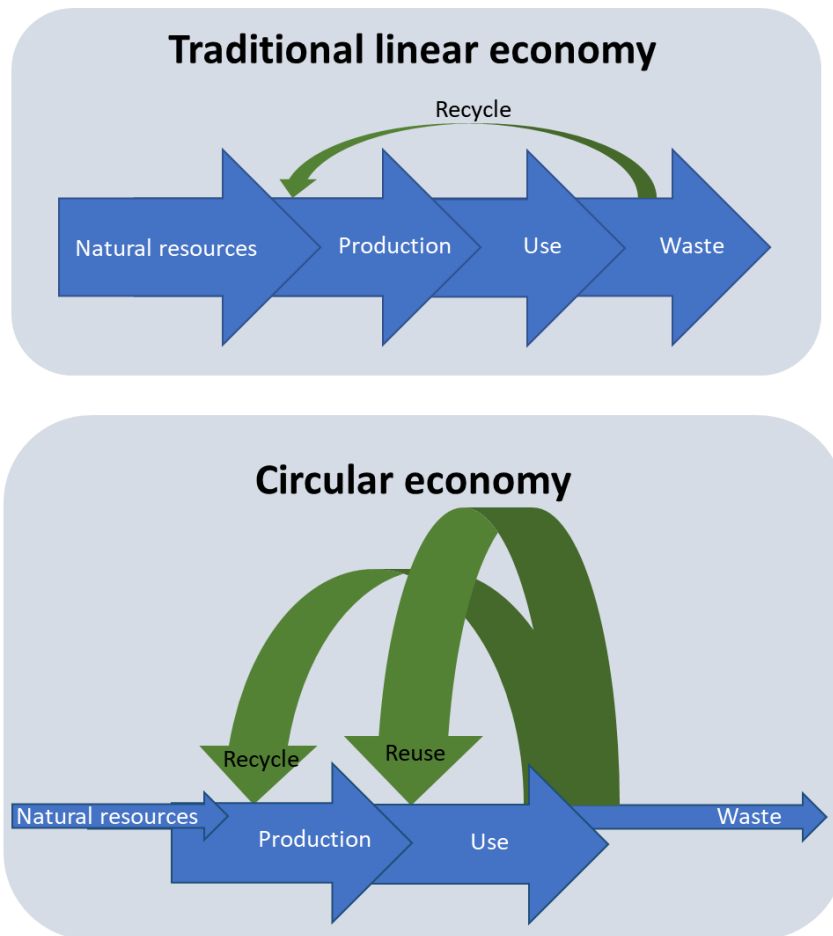


Figure 2: Schematic for comparison of the traditional linear economy and the circular economy.

As seen in the diagram of the circular economy in Figure 2, the amount of natural resources used can be reduced by designing products that have longer lifetimes, can be reused, can be remanufactured after the initial use period and can be recycled at the end of life. Reusing and recycling in this way also effectively reduces the waste produced as the majority of the waste is inserted back into the economy as a feedstock for new products.⁸⁻¹¹

1.1.3 Platform molecules

Platform molecules are green chemistry's answer to the base chemicals we traditionally use to synthesise the vast array of compounds produced in the chemical industry. The traditional base chemicals, examples (compounds **1-6**) of which are shown in Figure 3, are derived from non-renewable petrochemicals. The chemical industry therefore has an unsustainably heavy reliance on fossil fuels.¹²

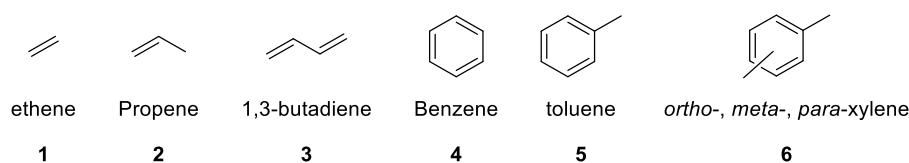


Figure 3: Examples of petrochemically derived base chemicals used by the chemical industry.

From a sustainability viewpoint, renewable feedstocks would be preferable to petrochemically derived. Biomass is an ideal candidate as a renewable feedstock as it is replenished globally in a matter of years rather than millennia and is available cheaply and in abundance as a waste product from industries such as the paper industry, forestry, farming. Food production is also a rich source of biomass which can be ethically sourced when using unavoidable food waste such as fruit peels, spent cooking oils and used tea leaves amongst other things.

Biomass can be converted into renewable base chemicals, referred to as platform molecules, within biorefineries. Biorefineries however are in their infancy compared to the well-established crude oil and natural gas base chemical supply lines.

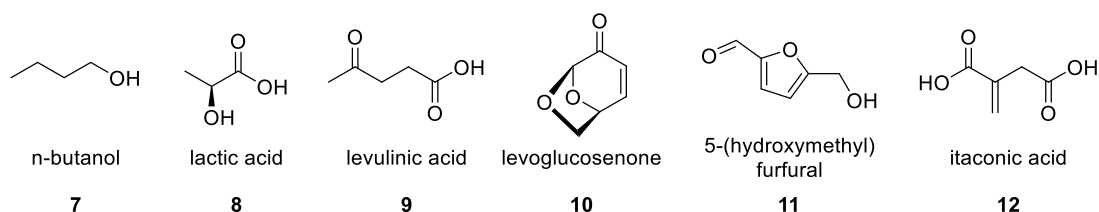


Figure 4: Examples of platform molecules that can be obtained from biomass at scale

Figure 4 shows some examples of established platform molecules such as levoglucosenone (**10**) and 5-(hydroxymethyl) furfural (**11**).

1.2 SURFACTANTS AND SUSTAINABILITY

1.2.1 Definition and applications

‘Surfactant’ is a term used to describe amphiphilic molecules and is derived from the longer term ‘surface active agent’.¹³ Molecules in this class have a lipophobic portion which dissolves well in aqueous solution and a lipophilic portion which dissolves well in organic solvents and oils. As a result, surfactants self-assemble at interfaces such as the interface between oil and water, oil and air or water and air. Figure 5 shows a common representation of a surfactant, the lipophobic or hydrophilic group is referred to as a head group and the lipophilic or hydrophobic portion is referred to as the tail group.¹⁴

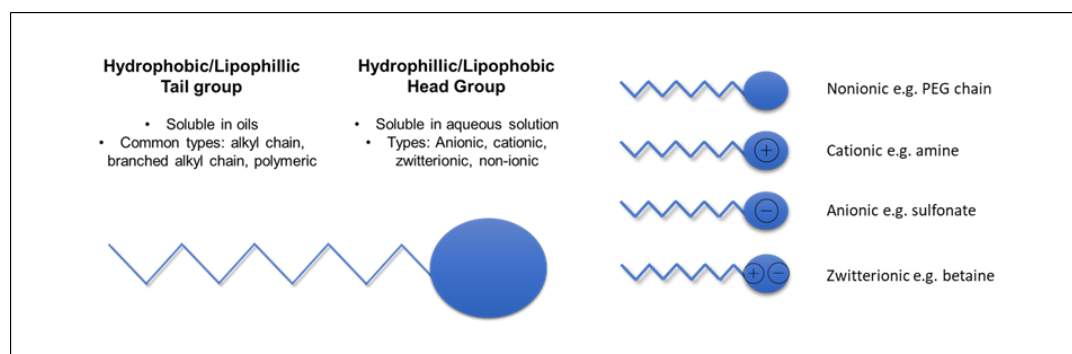


Figure 5: Schematic of the typical structure of a surfactant and the head group categories.

The presence of surfactants at surfaces and interfaces lowers surface tension. To describe surface tension, consider a beaker of liquid. The cohesive forces in the bulk of a liquid are more favourable than the cohesive forces between the liquid and the air above it. As a result of this the surface of the liquid occupies the minimum amount of space, to favour the interactions in the bulk rather than with the gas molecules above the surface. The minimisation of the occupied space creates tension at the surface to different degrees, similar to a taut sheet.

The amphiphilic nature of surfactants which allows them to lower surface tension also gives them the ability to self-assemble into higher order structures such as micelles (Figure 6). The

various ways in which the surfactants self-assemble gives rise to a large variety of effects such as foam stabilisation, detergency and friction reduction among many others.¹⁵

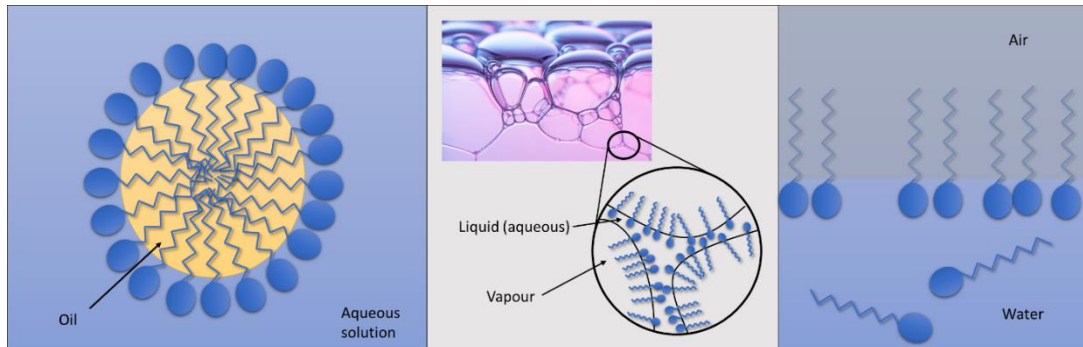


Figure 6: Self-assembly of surfactants around an oil droplet in a micelle (left), at the air/water interface of a foam (centre) and at the air/water interface of a solution (right).

There are a broad range of head groups divided into four categories: anionic, cationic, nonionic and amphoteric. The overall charge of the head group denotes the classification, see Figure 7:

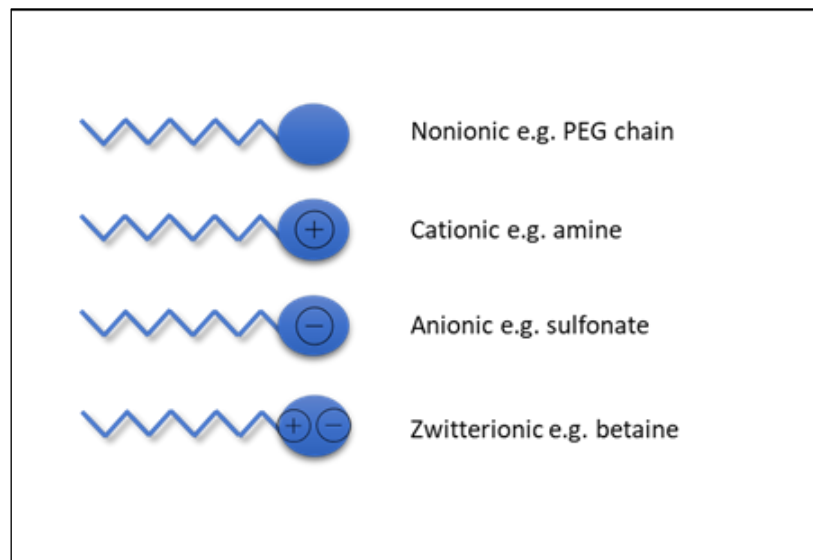


Figure 7: The four sub-categories of surfactants according to charge on the head group.

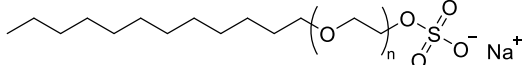
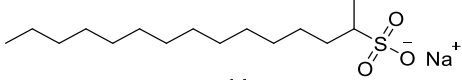
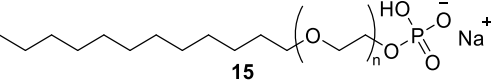
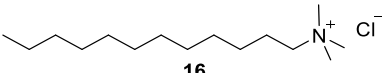
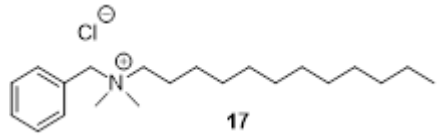
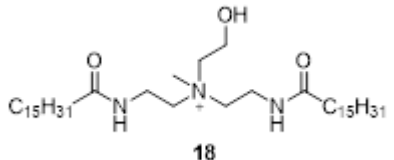
Nonionic surfactants have no overall charge associated with the head group, cationic have a positive charge and anionic have a negative charge. Finally, amphoteric surfactants have both positive and negative charge, which is balanced at the isoelectric point and therefore

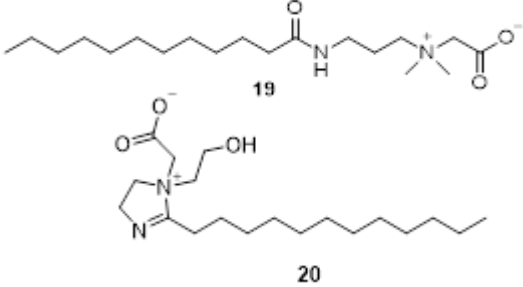
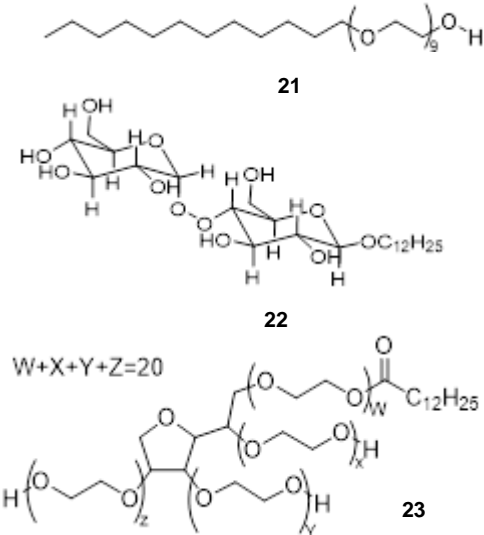
are able to act as a cationic or anionic surfactant dependent on pH. Amphoteric surfactants are often referred to interchangeably as zwitterionic surfactants due to ability of the surfactant to form a zwitterion, a molecule with positive and negative charges but a net charge of zero, at the isoelectric point. Well known examples of each category are shown in Table 1.

A large proportion of all surfactants produced are ionic surfactants.^{16, 17} Ionic surfactants tend to have good foaming capability and are effective for removing particulate soil from natural fabrics however are sensitive to salt content and hard water. Consequently, they require detergent builders to complex with the magnesium and calcium in hard water to remain effective in detergent formulations. The positive charge on cationic surfactant head groups makes them good for applications in which a coating is formed such as fabric softeners and hair conditioners because most of these types of surfaces are slightly negatively charged. Amphoterics tend to have low irritability and good stability against pH ranges, electrolytes and hard water and are compatible with anionic and cationic surfactants. Nonionics are generally low foaming and effective for removing oily stains from synthetic fabrics. Usually they are less irritant to the skin, not effected by salt and hard water and are compatible with cationic and anionic surfactants.^{14, 18} A classification of surfactants can be seen in Table 1.

As can be observed in Table 1, while head groups differ greatly in structure, size, functional group and charge, surfactant tail groups typically consist of an alkyl chain. The variation in tail groups comes from levels of unsaturation, chain length and branching with some surfactants having more than one tail group. The alkyl chain is often either synthetic or derived from natural oils such as coconut oil, palm oil and tannins from sheep's wool. Purification of such oils to separate the mixture of chain lengths is costly and unnecessary in many cases as a mixture of chain lengths often enhances performance over a wider range of applications. However some more specialised, higher value surfactants have narrower chain length ranges. More specialised surfactant tail groups include polymeric chains, fluorocarbon chains and siloxane chains.

Table 1 Examples of surfactants classified according to head group type with example structures.

Classification	Example Structure
<p>Anionic:</p> <ul style="list-style-type: none"> • Good at lifting particulate soil • High foaming • Sensitive to water hardness • Incompatible with cationics 	<p>Ether sulfates <i>i.e.</i>, Sodium laureth ether sulfate (SLES)  13</p> <p>Alkane sulfonates <i>i.e.</i>, Sodium 2-hexadecanesulfonate  14</p> <p>Phosphate esters <i>i.e.</i>, Sodium dodecyltetraethoxy phosphate  15</p>
<p>Cationic:</p> <ul style="list-style-type: none"> • Absorb rapidly to textiles • Less effective in cleaning applications • Often used in fabric softeners • Incompatible with anionics 	<p>Alkyl quat ammonium salts <i>i.e.</i>, <i>N</i>-hexadecyltrimethylammonium chloride  16</p> <p>Benzylalkyldimethylammonium salts <i>i.e.</i>, Benzyl-dodecyldimethylammonium chloride  17</p> <p>Amidoamine quaternary ammonium salts <i>i.e.</i>, Methyl-<i>bis</i>(hexadecylamidoethyl)-2-hydroxyethyl ammonium chloride  18</p>

Classification	Example Structure	
<p>Amphoteric (zwitterionic):</p> <ul style="list-style-type: none"> Function similarly to cationic and anionic surfactants dependent on pH 	<p>Betaines and amido betines <i>i.e.</i>, Cocoamidopropyl betaine</p> <p>Amphoacetates <i>i.e.</i>, Sodium lauroamphoacetate</p>	 <p>19</p> <p>20</p>
<p>Nonionic:</p> <ul style="list-style-type: none"> Good emulsifiers Tolerant to water hardness and a range of pHs Compatible with anionic and cationic surfactants Often low foaming Generally less irritant than anionics 	<p>Ethoxylated alcohols <i>i.e.</i>, Dodecanol 9-mole ethoxylate</p> <p>Alkyl polyglucosides <i>i.e.</i>, Lauryl diglucoside</p> <p>Ethoxylated sorbitan esters <i>i.e.</i>, Polysorbate 20</p>	 <p>21</p> <p>22</p> <p>23</p> <p>$W+X+Y+Z=20$</p>

1.2.2 PFA's and their properties

The development of a group of specialized surfactants called per- and polyfluorinated surfactants (PFAS) began in 1938 when Roy Plunkitt made the accidental discovery of polytetrafluoroethylene (PTFE) while experimenting with new ideas for coolants. He found that a gas cylinder he had left overnight retained its initial mass however no longer emitted gas flow when opened. The gas had polymerized overnight and produced a white waxy solid which was highly resistant to temperature change and exposure to corrosives and was insoluble in aqueous and organic solvents.¹⁹ Throughout the 1940s companies DuPont and 3M began to experiment with other perfluorinated compounds and make use of their unusual properties in a range of applications.

Polyfluorinated substances are organic compounds of which two or more hydrogens on the carbon backbone have been substituted for fluorine. Perfluorinated are those with a carbon backbone which has had all hydrogens replaced by fluorine. The example structures illustrated in Figure 8 are the perfluorinated polymer PTFE and the two most abundantly manufactured perfluorinated surfactants, perfluorooctanoic acid (PFOA) and perfluorooctane sulfonate (PFOS).²⁰

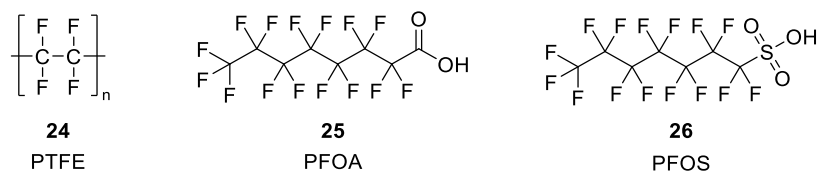


Figure 8: Structures of fluorinated polymer PTFE and perfluorinated surfactants PFOA and PFOS.

Perfluorinated compounds were found to be more hydrophobic than their hydrocarbon counterparts as well as oleophobic and thermally stable.²¹ The replacement of carbon-hydrogen bonds for carbon-fluorine bonds reduces conformational freedom and dramatically reduces the effects of Van der Waals forces in perfluorinated species and the enhanced stability of the C-F bond in comparison the C-H bond aids with thermal stability.²² These properties give rise to more stable surfactants with anti-fouling abilities that have a greater tension reduction at lower concentration than previously used.

Organic molecules containing a high level of fluorination differ greatly in their behaviour at surfaces and in bulk solution compared to most other organic species. Replacing all hydrogen with fluorine on a carbon backbone reduces conformational freedom. The covalent radii of hydrogen and fluorine are 0.31 Å and 0.57 Å respectively and the volume of space CH₂ groups occupy is 27 Å³ compared to CF₃ which occupies 38 Å³. This reduction in conformational freedom and free space for rotation results in a more rigid backbone with a tendency towards a more helical structure than their hydrocarbon counterpart.^{23, 24}

Highly electronegative fluorine, 3.98 on the Puling scale,²⁴⁻²⁶ holds its electron cloud closely and therefore has low polarizability and induced dipole-dipole interactions are greatly reduced. The lack of Van der Waals forces (specifically Debye and London forces) between perfluorinated chains renders perfluorocarbons oleophobic and hydrophobic. Gross et al investigated the effect of perfluorination on intermolecular interactions in comparison with typical organic compounds.²⁷ Figures 9 and 10 compare fluorocarbons with numerous classes of organic compounds and highlight the effect that a high level of fluorination has on intermolecular interactions.

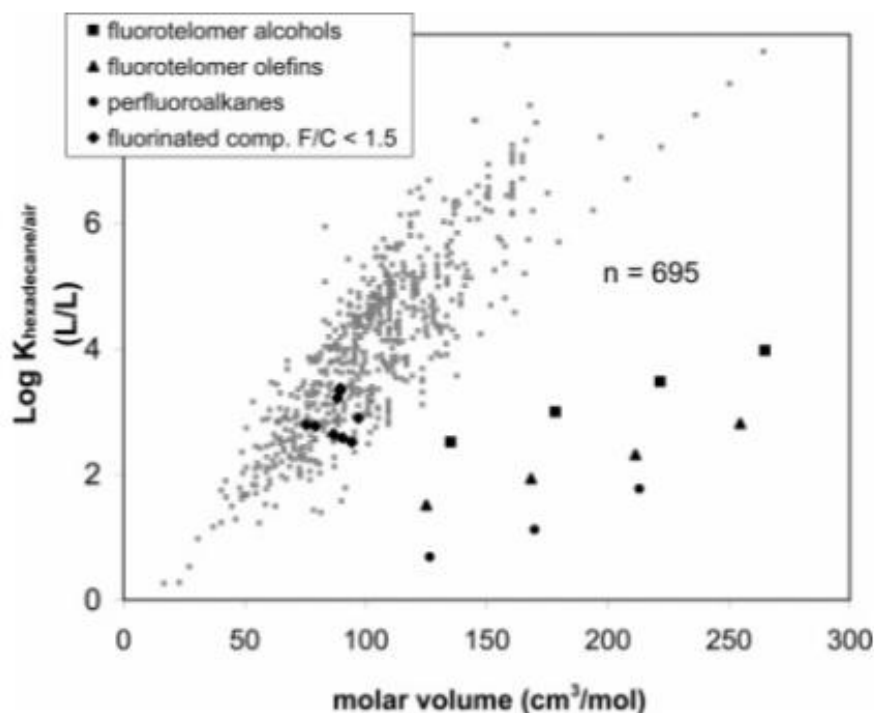


Figure 9: Logarithmic hexadecane/air partition coefficients vs molar volume for a range of 684 organic compounds.²⁷

Figure 9 shows that fluorinated compounds with a fluorine/carbon ratio >1.5 lie far outside the window for which 684 organic chemicals of varying compositions lie with respect to the relationship between the hexadecane/air partition coefficient and molar volume. The partition coefficient is reliant on a two-stage mechanism. Stage 1 involves the opening of a cavity in the bulk solution capable of accepting the volume of the solute molecule and is therefore related to the molar volume. Stage 2 involves the interactions between the bulk and solute molecule being more favourable compared to that at the surface with air, where interactions are scarce. Since the bulk is hexadecane, these interactions are Van der Waals interactions. This graph therefore shows the lack of Van der Waals interactions that highly fluorinated compounds experience explaining their preference to the liquid-gas surface where there are fewer interactions.

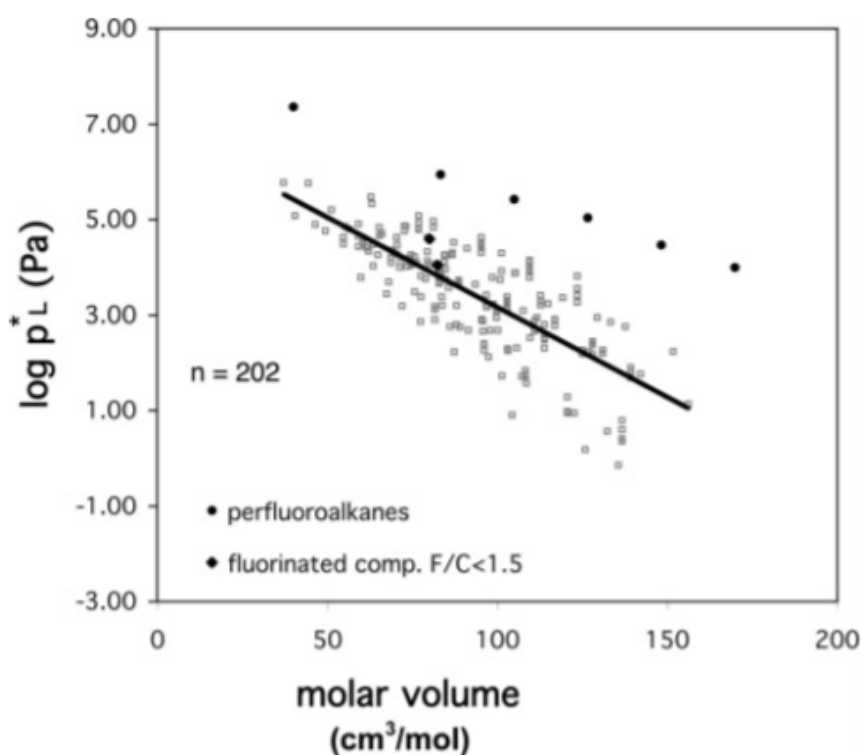


Figure 10: Saturated liquid vapour pressures at 25 °C of 200 organic compounds and 6 perfluorinated alkanes vs molar volume.²⁷

Figure 10 similarly demonstrates the lack of Van der Waals interactions as it shows the significantly higher saturated liquid vapor pressure of highly fluorinated alkanes compared to other classes of organic compound. This highlights the greater affinity of highly fluorinated alkanes to dissociate from their bulk solutions compared to other organics. This

is shown in Figure 9 and 10 due to absence of Van der Waals interactions within their bulk phases.

The absence of carbon-hydrogen bonds has the effect of greatly reducing induced dipole-dipole interactions compared to that in hydrocarbon chains. The carbon-hydrogen bonds have been replaced with carbon-fluorine bonds in which the fluorine holds its electron density very closely and thus induced dipole-dipole interactions are greatly reduced. The loss of hydrogen bonding ability and polarisation provides unique characteristics to perfluorinated surfactants in that they have a strong affinity to align at the liquid vapor surface, have low boiling points and are oleophobic and superhydrophobic.²⁶ Perfluorinated surfactants form micelles at much lower concentrations than their hydrocarbon analogues due in part to a reduced solubility in water. This is demonstrated by the comparative CMC values for perfluoro and hydrocarbon surfactants which are around 2 orders of magnitude lower.²³

Furthermore, this superhydrophobicity and oleophobicity is enhanced by the rod-like packing of perfluorinated chains. Perfluorinated surfactants exhibit this rod-like packing because of the lack of polarizability of the carbon-fluorine bond and the space taken up by the fluorine reducing the conformational freedom of the carbon chain. This rod-like shape allows for close alignment of neighbouring molecules at the liquid-air surface and contributes to the hydrophobicity and oleophobicity as the close packing makes penetration of molecules in contact with the surface less likely.

They have been developed and used with preference over hydrocarbon-based surfactants where extreme surface tension reduction is needed as perfluorinated surfactants are far superior. Perfluorinated surfactants exhibit very low surface tension in aqueous solution, even in small concentrations.²⁸

The extreme surface tension reduction emanates from the lack of Van der Waals interactions for perfluorinated chains. Perfluorinated surfactants also have increased thermal stability due to the strength of the carbon fluorine bond, commonly known as the strongest bond in organic chemistry as fluorine has the strongest single bond to carbon.^{21,}
²⁹ The strength of C-F compared to the C-C and C-H bonds makes highly fluorinated surfactants highly chemically and thermally stable and therefore useful for applications in extreme conditions, for example Teflon coatings on cookware, industrial pipelines for reactive and corrosive chemicals, wire insulation or in the aerospace industry to produce carbon fibre composites and fiberglass composites.³⁰

Fluorinated surfactants are one of the main components of firefighting foams due to their very low surface tension in water and high thermal and chemical resistance.²⁸

Fluorine has low polarizability; hence the Van der Waals interactions between fluorinated chains are weak, leading to low cohesive energy of fluorocarbons, high vapour pressure, high compressibility, high gas solubility, low surface tension and a high surface activity in aqueous solutions and low critical micelle concentration (CMC).^{21, 29, 31}. Fluorocarbon chain is highly hydrophobic and exhibits an unique property being hydro- and oleophobic, meaning they are surface active in both aqueous, and hydrocarbon solutions and have been used in pharma and medical areas^{32, 33}. The ability of the compounds to repel both oil and water was ideal for cookware, outdoor clothing, and stain resistant textiles such as Teflon pans, Scotchgard spray and Gore-tex jackets which were released onto the market sold worldwide. These products were effective and incredibly popular, and production escalated quickly (Figure 11):

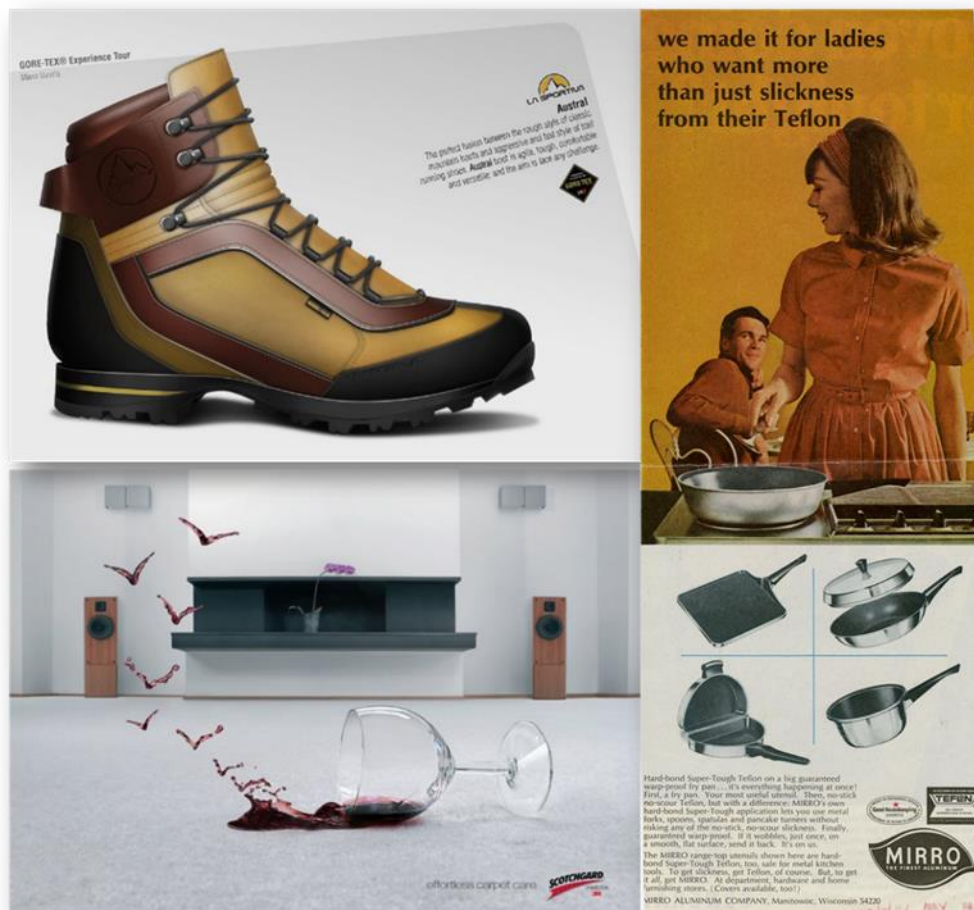


Figure 11: Advertisements for Gore-Tex (top left), Scotchgard (bottom left) and Teflon (side right) products. Image credits: "MirroTeflon037-1968-CompAds" (right) from DukeUnivLibraries is licensed under CC BY-NC-SA 2.0. "GORE-TEX® Experience Tour: Design sketch of

Marco Vanella" (top left) by GORE-TEX brand is licensed under CC BY-NC-ND 2.0. "3M Scotchguard" (bottom left) by is licensed under CC BY-NC-ND 2.0.

Further applications were explored to exploit the unique properties of PFAS. Despite high costs of manufacture, the unique characteristics of PFAS at low concentrations lead to their proliferation into over 200 use categories.^{21, 34} Alongside well known examples such as textile impregnation, anti-stick cookware, anti-fog food packaging and firefighting foams we now see PFAs used for watch making and in tennis rackets, guitar strings, sealants, printer ink, photographic films, pharmaceuticals, cosmetics and insecticides.^{21, 34-36} Through their use, a variety of PFAS have entered people's homes around the globe through the clothes they wear, furniture they sit on and the food they eat. From their conception up till the 1990's little was known outside of industrial expertise about PFAS and their effects on people and the environment and therefore there was no monitoring or regulation of PFAS despite their presence in an ever-increasing line of products. Figure 12, a bar chart showing the number of publications per year discussing PFAS, serves as an indication of the lack of exploration and knowledge in the literature pre-2000 and the escalation to over 1000 papers published in 2021. Much of this interest can be attributed to human health concerns brought into the fold by a farmer who sued a PFAS manufacturer.

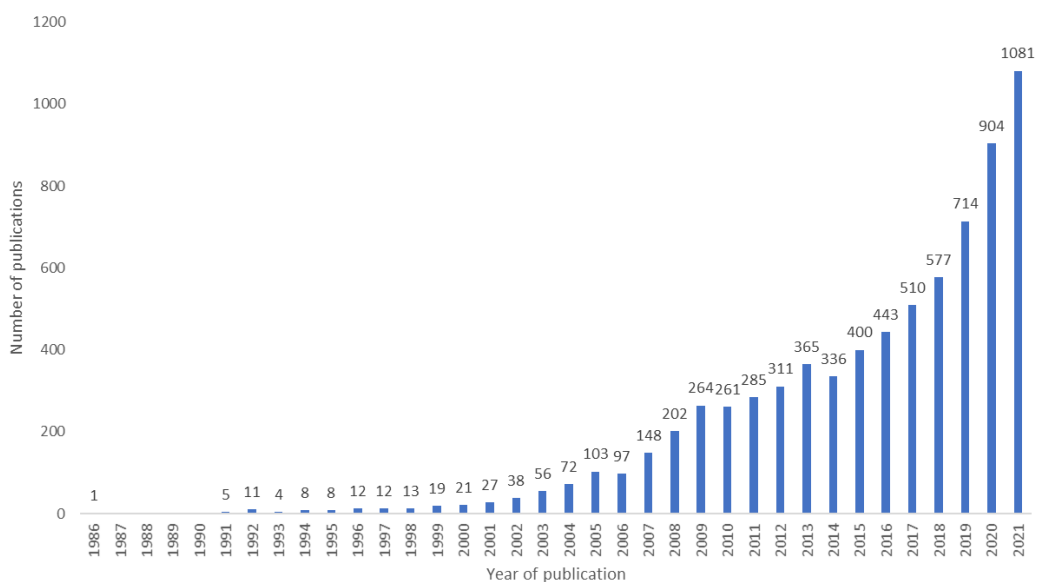


Figure 12: Bar chart demonstrating increasing attention paid to PFAS in the scientific community since 1998. Number of publications v year of publication sourced from the Web of Science database. Search terms used: PFAS and perfluoro* or PFOS or PFOA.

1.2.3 Effects on people and the environment

In 1999 Robert Bilott filed a federal suit against Dupont on behalf of Wilbur Tennant, the owner of a farm adjacent to a site which Dupont had purchased for non-hazardous landfill waste from the nearby Washington works plant in Parkersburg. In the years following the opening of the landfill site the animals of Mr. Tennant farm began dying prematurely and exhibiting unusual ailments such as blackened teeth and vomiting blood. Upon the crude autopsy performed by Mr. Tennant himself the cattle appeared to have swollen and discoloured organs such as gallbladders. A report was later released by Dupont used in their defense which denied culpability and blamed Tennant's poor animal husbandry. Mr. Tennant insisted that the large number of cattle deaths was due to ground water and runoff from the Dupont landfill site which contaminated the water source for the cattle.

This case triggered Robert Bilott to file a class action lawsuit against DuPont. Approved in 2005, the class action lawsuit resulted in a settlement agreement which included the creation of a science panel consisting of three epidemiologists tasked with identifying any probable links between PFOA (known as C8 within the Dupont company) and human disease. As part of the agreement Dupont paid 70 million US dollars to fund a community study of the residents of Parkersburg entitled the C8 health project which collected blood samples from approximately 69,000 people and became one of the largest known epidemiological studies of the time. The science panel concluded that there were probable links between PFOA and pregnancy-induced hypertension, testicular cancer, kidney cancer, thyroid disease and ulcerative colitis.³⁷⁻⁴¹ The National Health and Nutrition Examination Survey (NHANES) examined blood samples from the US population in 1999 and found PFAS in 98% of samples.^{42, 43} It is known that mothers transfer PFAS to their offspring during pregnancy and through breast feeding and that high dosage of PFOA and PFOS had reproductive effects on rats such as reduced birth weight, neonatal death, and reduced postnatal growth.⁴⁴⁻⁴⁶

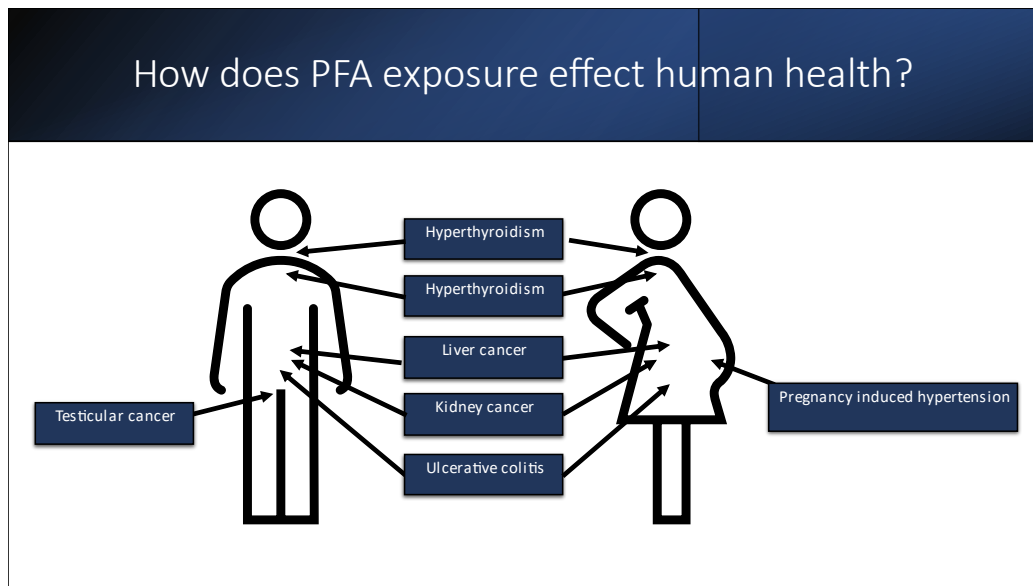


Figure 13: Health effects identified by the C8 health project as having probable links to PFAS.

The plant workers and resident of Parkersburg who were exposed to higher levels of PFAS than the general population through inappropriate handling of manufacturing waste into waterways were entitled to sue Dupont through individual personal injury claims headed initially by Robert Bilott. After several lawsuits were won by Robert Bilott for individual residents Dupont agreed to settle the remaining cases, of which there were more than 3,500. Including the lawsuits brought after those already mentioned Dupont has paid damages to residents over personal injury claims relating to expose to PFOA in drinking water exceeding the amount of 753 million US dollars and additionally settled for 4 billion US dollars over liabilities with respect to PFAS.

The class action lawsuit and subsequent personal claim lawsuits filed against DuPont over their handling of PFAS, their responsibility to their staff and local residents with respect to their health and their responsibilities with respect to the environment brought the media's attention to the health risks of PFAS. The public health risks posed by PFAS and the need for regulation has become topical in recent times and has been covered by news articles from publications such as National Geographic and The Guardian, documentaries such as 'Poisoning America: The Devil we know' which aired on the BBC, a segment on the popular American TV show 'The Daily Show' and the 2019 feature film Dark Waters starring Mark Ruffalo.^{47-52,53-56} PFAS have been dubbed 'forever chemicals' in many of these articles over fears associated with the stability and persistence in the environment.

The aforementioned characteristics of perfluorinated surfactants made them a popular choice in many applications and formulations where extreme surface tension reduction, anti-fouling properties or thermal stability were advantageous. As previously mentioned the use of PFAS grew from the popularity of well-known products such as Gore-tex® waterproof jackets, Teflon® pans and Scotchguard® stain resistant textile treatments into over 200 use categories, examples of which can be found in Figure 14.^{22, 34} PFAS have entered the environment well before appropriate and cost effective methods of detection and removal have been established.

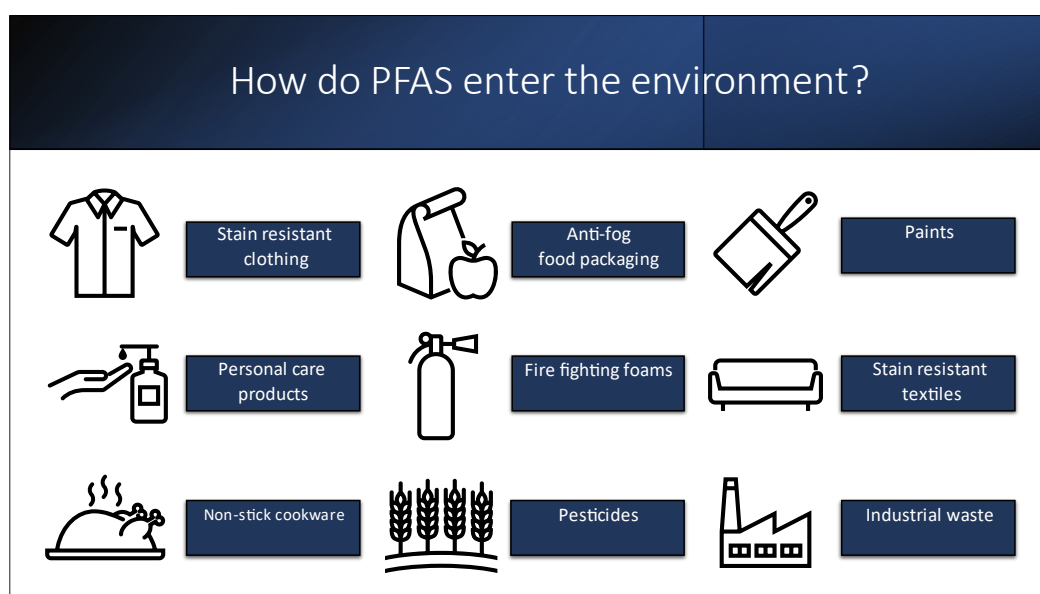


Figure 14: Examples of ways in which PFAS may enter the environment.

The resulting popularity has had a large environmental impact. Their stability and high thermal tolerance make degradation in the environment extremely slow which is of particular concern as many applications result in release directly into the environment for example with the use of fire-fighting foams. As a result, they are of considerable concern with regards to bioaccumulation and biomagnification through food webs.^{57,58,59} PFAs can be detected globally in water supplies, marine mammals, fish and amphibians.^{59,60} PFA's are known to have an affinity for binding to proteins and it was found that the binding constants and bioconcentration factors in fish were dependent on chain length.⁶¹ Perfluorooctanoic acid (PFOA) is the most widely used and the worst offender with regards to pollution, accounting for >35% of perfluoroalkyl (PFA) concentration found in urban water environments.⁶²

A recalcitrant substance is a substance which decomposes extremely slowly or resists decomposition. Even if the world's population complied uncompromisingly with a complete ban of the production of PFAS and stopped wearing them and cooking with them their recalcitrance leaves them strewn throughout the environment, detectably interwoven in global water systems, ground water and soils. The known mobility informs us that the presence of PFAS in the food supply and bloodstreams of the human and animal population of the planet cannot be reversed and will remain for several decades to come.

The high stability of the fluorinated molecules makes them non-biodegradable. To extract the fluorinated surfactants from water, techniques such as the use of membranes, activated carbon, polymers for precipitating surfactants (*i.e.*, cationic polymers to precipitate anionic surfactants), ion exchange or electrochemical decomposition have been used.^{28, 35, 63, 64} Fluorinated surfactants bind to activated carbon irreversibly and an economically feasible regeneration is not possible.⁶⁵ Electrochemical decomposition into hydrogen fluoride (HF) under electrochemical oxidation was possible without organic waste and exhibited a longer service life and lower operating costs than activated carbon or resins.⁶⁴ The same study showed that ion exchange treatment using a resin was seven times more efficient than activated carbon, but less efficient than electrochemical oxidation in removing fluorinated compounds from wastewater. However, when coupling electrochemical decomposition with activated carbon polishing the operating costs were reduced and the capacity of the carbon bed increased tenfold.⁶⁴

Firefighting foams are generally used by airports, oil refineries and motor fuel storage, fire training facilities and military bases. Any fire related incidents can result in the discharge of large amounts of foams containing PFAs directly into the environment. A significant environmental disaster was registered in Sandoz, Switzerland in 1986. The Sandoz disaster started when 1350 tonnes of highly toxic chemicals suddenly went up in flames at one of the company's warehouses. More than 20 tonnes of extinguishing foam containing PFAs were spilled and had a disastrous impact on Rhine's ecology. The river turned red and killed an entire eel population and caused drinking water problems in the Netherlands. It took years for this situation to be recovered.⁶⁶

Another environmental disaster was registered in France, in 1988, when an explosion and a fire erupted on a chemical plant, which had a poorly maintained safety management system. The release of 630 m³ of toxic effluents into the Brenne and Loire rivers led to temporary shut-down of businesses and water shortages in the area for days. Cyanide-

containing products killed aquatic life in 23 km of the Brenne and 5 km of the Cisse.⁶⁷ Human casualties were reported during the accident and in the aftermath: one person from the plant was hospitalised and unable to work for 6 months, 2 firemen and 15 members of the rescue team were intoxicated during the intervention. These environmental catastrophes became known internationally and led countries to tighten the risk management of companies by national and international regulations.

The manufacture of PFAs has been underway for more than seven decades; however, only recently has their toxicity come under scrutiny by the public eye, earning the name 'forever chemicals'. The C-F bond is the strongest bond known to nature and it can take up to 1000 years for some PFAs to degrade, under typical soil conditions, based on modelling degradation tests.^{68, 69} The degradation of PFAs depends in part on the location they are deposited in and their ability to travel. Regardless of the degradation pathway of PFAs, the risk of forming more PFAS by incomplete destruction needs to be carefully evaluated. It is generally very difficult to predict the end-of-life products because most of the PFAs products have confidential chemistry, synthesis pathway, by-products types or applications.⁷⁰

Against the bad reputation of 'forever chemicals', recent literature proved that 'nothing lasts forever'.⁷¹ Recently, it was found that there are bacteria that can catalyse defluorination of PFAS and PFOA.^{72, 73} Up to 60% of PFOA and PFOS were reduced during 100-day microbial incubations with the release of fluorine anion and molecules shortening from perfluorooctanoate to perfluoroheptanoate and then to perfluorohexanoate and so on.⁷² Although this is excellent news in terms of ridding the environment of ever increasing amounts of PFAs, more efficient enzymes would be needed for a realistic timelines of defluorination of perfluorinated surfactants to justify manufacturing them. The biodegradation of fluorinated compounds also presents some other disadvantages: it can take weeks to months and the range of chemicals degraded is limited and different levels of defluorination are achieved depending on their length.^{74,73, 75, 76} The plant uptake and accumulation of PFAs shows that short chain PFAs bioaccumulate in leaves and long chain PFAs bioaccumulate in roots. They degrade into more stable polyfluoroalkyl phosphates (PFAAs) in the environment and biota, while the biodegradability depends on their non-fluorinated functionality.⁷⁷

Many efforts have been made by today's environmental scientists to understand the behavior of perfluorinated compounds working with global regulatory agencies to tackle

the toxicity of the 'forever chemicals'.⁷⁰ They enter into the environment at every stage of their life cycle: from starting material to end product usage then into the recycling waste where they can leak from landfill.^{78, 79, 80} Once they have entered the environment, PFASs easily migrate to terrestrial and aquatic systems. They have been detected everywhere you could think to look; in the air, the human body (including breastmilk), the bodies of animals and birds, soil and plants and the water system (rain, tap water, rivers and oceans).^{78, 79, 81-}
⁹⁰ The uptake of PFAs into plants transfers and bioaccumulates in the humans and animals that consume them. Hence, dietary intake has been considered the main route of non-occupational humans' exposure to PFAs. PFAs have been identified in vegetables and other agricultural crops, drinking water and fish.⁹¹⁻⁹⁴ Humans are exposed to PFAs from plants, fish and meat eaten, air breathed and water drunk.⁹⁵

PFAS such as PFOS and PFOA were found in 99% of American's bodies.⁴² Since the groundbreaking NHANES study published this finding, the same has been recorded the world over.⁹⁶ Once they enter the human body, they accumulate and lead to cancer, liver and thyroid diseases, hormone disruption and birth defects..⁹⁷⁻¹⁰⁰ Even if most of these substances are restricted, these issues are likely to persist in our lives because techniques to remove PFAs from the human body are not well known or understood and removal from the environment is costly and still poses many difficulties and unanswered questions.

1.2.4 Regulations

The human health effects associated with the global contamination of water supplies and concerns over effects on wildlife and the environment through bioaccumulation resulted in heavy regulation and restriction now coming into place globally, limiting their release into the environment and encouraging the use of alternatives in an attempt to phase them out completely. International collaboration was achieved against the issue through the Stockholm Convention on Persistent organic pollutants. In the US the environmental protection agency (EPA) monitors and regulates production of certain PFAS and in Europe the European Unions' Registration, Evaluation, Authorisation and Restriction of Chemicals (REACH) regulations have also targeted certain PFAS which must be phased out of production. Simultaneously companies Dupont and 3M voluntarily phased out production in the early 2000's.¹⁰¹

The Stockholm Convention on Persistent Organic Pollutants (POPs) is a global treaty which aims to protect human health from the effects of POPs which become globally distributed and can lead to serious health effects such as birth defects and cancers. The treaty, which has 152 signatories and was adopted in 2001 came into force in 2004 and requires its parties to take steps towards reducing and eliminating the production of the POPs it identifies. No perfluorinated compounds were originally identified however since then in 2009 PFOS, PFOA and closely related substances were added to the list of POPs to be reduced and eliminated.¹⁰²

In Europe, PFAS are regulated by the European Union. PFOS, PFOA and the ammonium salt of PFOA (APFO), C11–C14 PFAS and others are included in the Candidate List of Substances of Very High Concern for Authorisation under the European Chemicals Regulation, REACH, article 57.¹⁰³

In the US, amendments have been made to current legislation to include perfluorochemicals, for example the Toxic Substances Control Act (TSCA) and the Safe Drinking Water Act. TSCA is a United States law passed in 1976 by 94th United States Congress and administrated by the United States Environmental Protection Agency (EPA).¹⁰⁴

The drinking water industry proposed that the EPA should use its' authority under the TSCA to prevent perfluorochemicals (PFOA and PFOAS specifically) entering drinking water sources. There are no federal drinking water standards however the EPA insist on removing permissions to use perfluorochemicals for non-stick coatings and stain-resistant treatments. The TSCA imposes restrictions on the manufacture and use of PFAs and fluorinated polyolefins to prevent them from impacting on human health and the environment. In March 2022, the EPA sent an open letter to manufacturers, processors, users, distributors, and waste disposal organisations about the potential for PFAs to form and migrate from fluorinated high-density polyethylene (HDPE) plastics.¹⁰⁵

In 2006, the EPA proposed that big companies such as DuPont, BASF, Solvay, Daikin, Arkema, Asahi, Clariant and 3D/Dyneon reduce the emissions of PFOA or its precursors by 95%. The PFOA Stewardship Program was successful and realised its goal by 2010. Also, the complete elimination of these chemicals from products was proposed by 2015 and all companies met this deadline.¹⁰⁵ Moreover, in 2021 Maine became the first U.S. state to ban PFOS, PFOA and PFAs in all products by 2030, unless 'currently unavoidable'.¹⁰⁶

The Madrid statement is an articulation of the scientific consensus surrounding the negative global impacts specifically caused by the use of perfluorinated surfactants which was released in 2015 and was signed by 206 authors and professionals.¹⁰⁷ These concerns voiced by the scientific community come a decade after the initial voluntary phase out of production of PFOA by Dupont and 3M, the legal battles which sparked public awareness and global regulation, regulation in the US and regulation in Europe through REACH. The release of this document highlights the work still needed to be done to eradicate the production of PFAS and find appropriate alternatives.

1.2.5 Current alternatives to perfluorinated surfactants

The key to successfully phasing out all production of PFAS is to find suitable or superior alternatives rendering them unnecessary or inferior. Many alternatives to currently restricted or banned PFAS are already on the market. Initially, as regulations such as the European REACH regulations focused on perfluorinated chains of above 7 carbons research was conducted using shorter chain lengths, reducing the level of fluorination or a combination of both to achieve similar performance. A review from 2007 on the bioaccumulation of PFAs concluded that it is directly related to chain length and that in short chains ($C < 7$) bioaccumulation was several orders of magnitude lower and are therefore not classed as bioaccumulative with regards to widespread regulatory criteria.⁵⁷ Several alternatives to PFOA and PFOS were developed under trade names such as GenX, ADONA and F-53B. The structures of the main components of these short chain alternatives are shown in Figure 15. Hexafluoropropylene oxide dimer acid (HFPO-DA) commonly known by its trade name, GenX, was developed as a PFOA alternative. The key differences between PFOA and GenX are the reduction in chain length from 8 to 6 carbons, which changes the classification from long chain to short chain PFAS and the addition of the ether group, a group intended to be more susceptible to degradation in the environment.

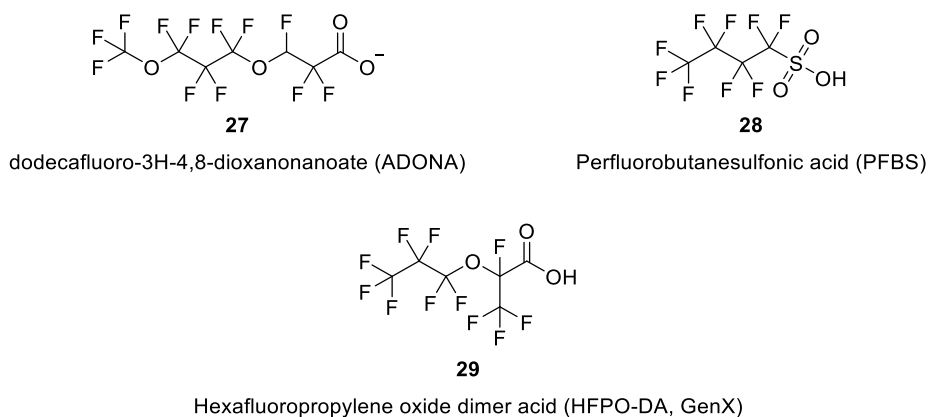


Figure 15: Structures of prevalent PFAS used as replacements for PFOA, PFOS and other restricted PFAS.

Short chain alternatives are known to be persistent and have been found in bottle and tap water in various locations across the globe, suggesting high mobility via waterways.^{96,84} A recent review on the current literature on short chain (C = 2–7) PFAS found that although short chain PFAS have been found in various places including deep polar seas we do not have a complete image of their environmental fate as most previous studies focussed on the longer chain PFAS as they are more common and have established methods of detection.¹⁰⁸ Although a larger more widespread data set on short chain perfluorinated compounds is needed it is known that these short non-biodegradable surfactants such as perfluorobutanesulfonic acid and perfluoro-2-propoxypropanoic acid (GenX) (Figure 15) build up and have been detected in British rivers.^{109,7}

An industrial shift to the use of short chain PFAS will likely not be beneficial in reducing persistent organic pollutants and in fact may result in a need for further restrictive legislation in the future. Those who have concerns over the final degradation products among the heavily increasing demand for short chain PFAS have criticised the view that short chain PFAS are less harmful to people and the environment as short sighted or a mere side-stepping of restriction criteria.^{110,111,112,103,82.} Such were the concerns of Brendel et al who laid out a desired strategy for REACH regulation.¹⁰³

The use of these currently used short chain replacements is likely to be short-lived. In the US, the EPA have already begun issuing improvements to national drinking water standards and revising wastewaters standards for manufacturers in March 2021 and announced in December 2021 that drinking water utilities are to collect data on 29 perfluorinated compounds including short chain PFAS such as HFPO-DA and PFBS with the intention of using this data for further regulation.¹¹³⁻¹¹⁵ The EPA have also published a roadmap to

addressing PFAS contamination and their commitments through 2021 to 2024 which includes attention to short chain perfluorinated surfactants such as GenX.¹¹⁶ In Europe, those compounds relating to GenX (HFPO-DA and its salts and acyl halides) have now been added to the European substances of very high concern list.¹¹⁷

There have also been studies on significantly less fluorinated compounds as replacement for long chain PFAS for example hydrocarbon backbones with perfluorinated end caps or branching. An investigation into the effect of capping a hydrocarbon based surfactant with a CF₃ found that surprisingly the CF₃ capped chains were more wettable to polar liquids than their hydrocarbon counterparts.¹¹⁸ It was theorised that this was due to the proximity of the HC-FC bonds creating a dipole at the surface. Capping the end of partially fluorinated thiols, shown in Figure 16, with a methyl group reduced the hydrophobicity to below that of both the perfluorinated or hydrocarbon analogues.

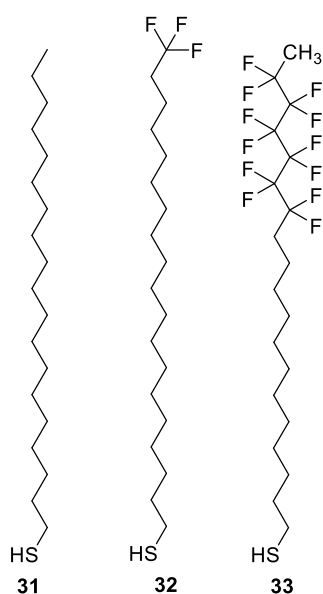


Figure 16: Compounds used for the chemisorbed monolayer films formed from the deposition of normal alkanethiols, CF₃-terminated alkanethiols, and methyl-terminated partially fluorinated thiols.¹¹⁸

Another paper recommended highly branched fluorinated thiols (Figure 17, compounds **33** and **34**) as a replacement for long chain perfluorinated surfactants.¹¹⁹

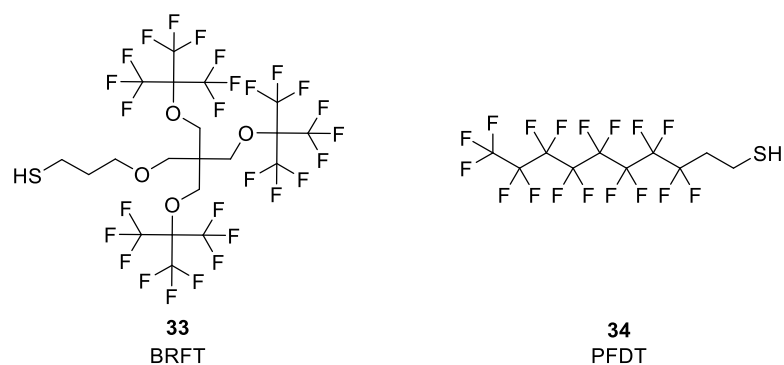


Figure 17: The Chemical structure of highly branched fluorinated thiol (BRFT) and of linear 1H,1H,2H,2H perfluorodecanethiol (PFDT).

The ether bonds in the core of compound **33** are intended to increase biodegradability however questions are raised as to the bioaccumulation of the resulting molecules which may potentially be ultra-short chain forms of the current perfluorinated pollutants. In other papers perfluorinated surfactants have been synthesised with ‘weak points’ similar to the ether bond to enhance biodegradation of the molecule however the degradation products raise the same concerns over environmental persistence and at this point their degradation data remains unpublished.¹²⁰

An additional issue with these lines of alternatives is that the performance of perfluorinated surfactants is greatly dependent on the chain length.¹²¹ Decreasing chain length is known to reduce hydrophobicity and repellence of perfluorinated surfactants. The proposed replacements are less effective shorter chain perfluorinated surfactants which will also persist in the environment and therefore bear no advantage other than avoidance of restrictions.

Moving away from perfluorination completely, a series of novel polymers with highly branched siloxane units (Figure 18, compound **35**) providing an oleophobic and hydrophobic layer close to that of fluorinated chains were reported by Lei *et al*¹²² in 2017 as a possible PFAS replacement. To achieve the anti-stain properties with an 80,000 g mol⁻¹ molecular weight copolymer a 20% wt/wt concentration was needed to achieve good anti-stain performance and with a 9000 g mol⁻¹ molecular weight polymer the copolymer required was 50% wt. With increasing M₃T the surface tension of the polymer decreased to its minimum at 13 mN mol⁻¹ achieved with a 72% molar ratio of M₃T. Although a more efficient co-polymer which required less loading would be desirable the resulting surface tension is similar to that of fluoropolymers.

An investigation is needed into the migrating ability of the monomer for use as a polymer additive could open a pathway to reducing the loading, and as a result the expense, of the polymer. Also, more needs to be established about the biodegradability of the M₃T polymer in order to establish this route as a viable replacement for long chain PFAS.

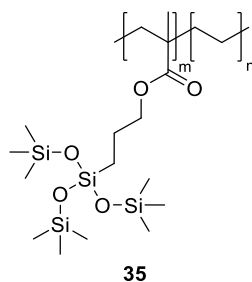


Figure 18: Polymer chain with M3T side chain.¹²²

Arguably the application of PFAs in the most urgent need for abolishment is in fire-fighting foams.¹²³ Access to firefighting foams is essential to safety and during use they are released directly into the environment.^{52, 123} Thankfully there are already replacements available for PFAS in firefighting foams in the form of zwitterionic betaines, alkyl glucose amides and organosilicones among others.¹²⁴⁻¹²⁶ Firefighting foams originally incorporated PFAS because they can provide the very low surface tension in aqueous solution enabling a positive spreading coefficient of aqueous solution over solvents. This traps the solvent vapors which feed the fire and the fire is extinguished. They are also useful for this application because they are thermally stable at high temperatures.²⁸ Fluoride containing firefighting foams are resistant to destabilization from oil droplets and therefore generally superior to fluorine-free formulations, however studies show that with alterations to the foam expansion ratio the performance of the fluorine free formulations are comparable.^{125,}

127

In the biomedical imaging, drug delivery and coatings research areas much work has been done to find replacements for PFAs. Shorter chain PFAs and fluorotelomers have been trialed in these industries, however it has often been found that they do not perform as well as long chain PFAS and are also likely to be legislated against in the near future. Some natural amphiphilic compounds from microorganisms such as bacteria, yeasts, and fungi have also been trialed as PFAs replacements.¹²⁸⁻¹³⁰ They showed low toxicity and good biodegradability. The most widely studied would be the phospholipids (*i.e.*, egg yolk

phospholipids). Several natural proteins are currently used as foaming agents and surfactants in food processing, cosmetics, medical and pharmaceutical applications. Lipid-based colloidal bubbles ('microbubbles') are used for detection and treatment of cardiovascular diseases. However, they generally do not reseal after rupture, but their stability is improved by adding DNA or a protein.¹³¹ Perfluorocarbon-based artificial oxygen carriers ('blood substitutes' or 'white blood') must be not toxic. Perfluorinated organic compounds are not soluble in water and their intravascular carryover requires their emulsification by using a thin surfactant layer. The natural surfactants used for this purpose are egg yolk phospholipids (e.g. Oxycyte[®], Oxyfluor[®] and Oxygent[®]) and poloxamers.²⁹

In conclusion, the unique properties of perfluorinated surfactants makes it unlikely that a similar class of compounds could be made with similar properties without incurring similar issues surrounding bioaccumulation and their diversified uses means that much work is needed to find alternatives. It seems to be apparent that the individual needs for each application be carefully considered while choosing replacements as a blanket set of replacement compounds is unlikely. Some application specific current alternatives on the market are satisfactory however some are problematic and cast doubt upon future viability due to concerns over the biodegradability and health effects of the replacement. Side-stepping legislation in this way is neither good for public health nor for long term business gains. Although some acceptable substitutions have been found there remains a large market for appropriate or superior replacements for perfluorinated surfactants in their diverse portfolio of applications.

1.3 PROJECT OUTLINE

The aims of this project are to design and synthesise alternatives to persistent, bioaccumulative and toxic long chain perfluorinated surfactants. An ideal candidate to replace long chain PFAS would take into account the degradation products and therefore would avoid the integration of CF₃ and CF₂ groups which have the potential to form short or ultra-short chain PFAS as previously discussed. Other groups such as silicates which may pose undesirable health risks or be persistent in the environment but the analysis of which are outside of the scope of this work are also eliminated from consideration.

From a green chemistry perspective making use of the circular economy and developing alternatives to PFAS from biomass waste is ideal and can be achieved through the use of platform molecules. To identify synthetic targets which could potentially share similar properties to long chain PFAS a computational tool, HSPiP, was used to analyse the contributions to their intermolecular forces. Using this tool, it is possible to compare the contributions to intermolecular forces of PFAS with other compounds and therefore identify potential synthetic targets.

1.3.1 HSPiP

The Hansen solubility parameter in practice (HSPiP) software is based on Hansen solubility parameters which were first outlined by Charles M. Hansen in 1967 and allow the prediction of solubility based on Equation 1, which takes into account dispersion forces (δ_d), molecular permanent dipole interactions (δ_p) and hydrogen bonding (δ_h).¹³²

$$\delta^2 = \delta_d^2 + \delta_p^2 + \delta_h^2$$

Eq. 1

HSPiP assigns a molecule co-ordinates within 3 dimensional 'Hansen space' based on the the molecule's presumed ability to hydrogen bond, have dipole interactions and experience Van der Waals and dispersion forces. The co-ordinates allow comparison with other molecules and using the 'like dissolves like' theory can give a good estimate of how likely it is for a solute to dissolve in a solvent. This software has been widely used for the screening

of solvents and the estimation of interactions and incompatibilities between materials in areas such as printing applications, solubility, surfactants, polymers, nanocoatings, rheology and many more.¹³³⁻¹³⁵ This software has also been used as a tool to choose appropriate green solvent alternatives.

When plotted in 3-dimensional space the HSPiP software uses the Hansen Solubility Parameters to give a visual representation of how similar intermolecular interactions of different species are, which can be further defined through the use of vectors.

There is a limitation in the application of Hansen Solubility Parameters in this case as the amphiphilic nature of surfactants means they have two zones with distinctly different solubilities. The HSPiP coordinates are calculated by taking an average over the whole molecule, therefore the interactions are going to cancel out, or partially cancel out, the two distinct parts of the surfactant and not give an accurate picture of the solubility of the head or the tail group. Therefore, in this instance the tail groups have been isolated for the calculation of the co-ordinates, to provide a more accurate view of the Hansen space PFAS lie in.

The Hansen solubility sphere method was used to measure the HSPs of antifoaming agents and a foam-forming surfactant based on HSP theory and the defoaming effect.¹³⁶ The Hansen Solubility Parameters (HSP) was also used to predict surfactants adsorption on a solid surface in inkjet printing processes.¹³⁷ The quality of inkjet printing depends on the wettability characteristics of the printhead and the surface tension of the ink. Hence, surfactants are added to the ink solutions to reduce the surface tension and improve the spreading of the ink droplet.

This computational tool can be used to assess potential surfactants and attempt to move towards the Hansen space occupied by perfluorinated surfactants shown in Figure 19.

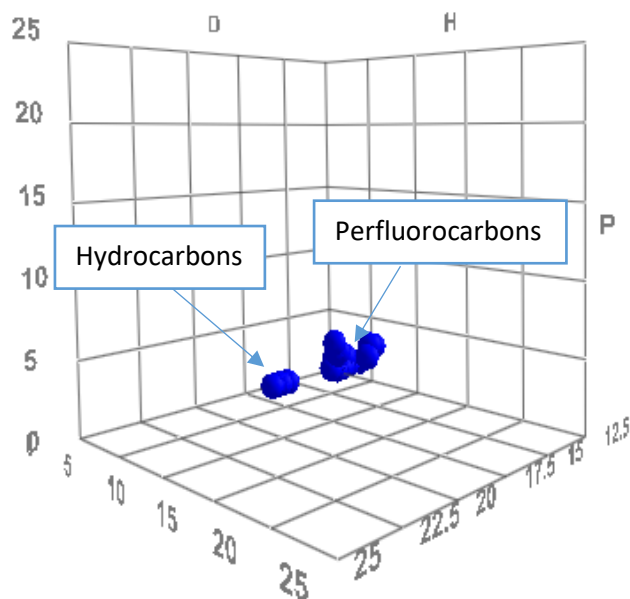


Figure 19: HSPiP plot of perfluorocarbons and hydrocarbons. Hydrogen bonding contribution on the X-axis, molecular permanent dipole on the y-axis and dispersion forces (Van der Waals forces) on the Z-axis.

As expected, the hydrocarbons occupy a space away from the perfluorocarbons due to Van der Waals or dispersion forces. For simplicity the hydrophobic tail section of the perfluorinated and hydrocarbon surfactants in Figure 19 have been plotted in isolation. This removes the influence of the head group on the polarity of the molecule, especially on those of smaller molecular volume. For fair comparison either a common head group must be shared or all of the tail groups must be plotted in isolation. The HSP distance, described using a vector, between perfluorooctanoic acid and octanoic acid is 5.43. These structures differ only by exchange of fluorine for hydrogen on the carbon backbone.

A database of 10,000 organic molecules provided by HSPiP was searched in order to investigate molecules that may have occupy similar Hansen space and have similar molecular interactions to perfluorocarbons. The HSP value range for the perfluorinated molecules available in the database was entered into the search engine to locate molecules within the same HSP space.

The search resulted in a list of short chained hydrocarbons ($C < 6$), highly branched short chain hydrocarbons, siloxanes, silanes and some chlorine and bromine containing highly fluorinated small organic structures for example 1-bromoperfluoroheptane. The space

occupied by these structures is shown in Figure 20, all with very low polarity, hydrogen bonding and dispersion (Van der Waals) forces.

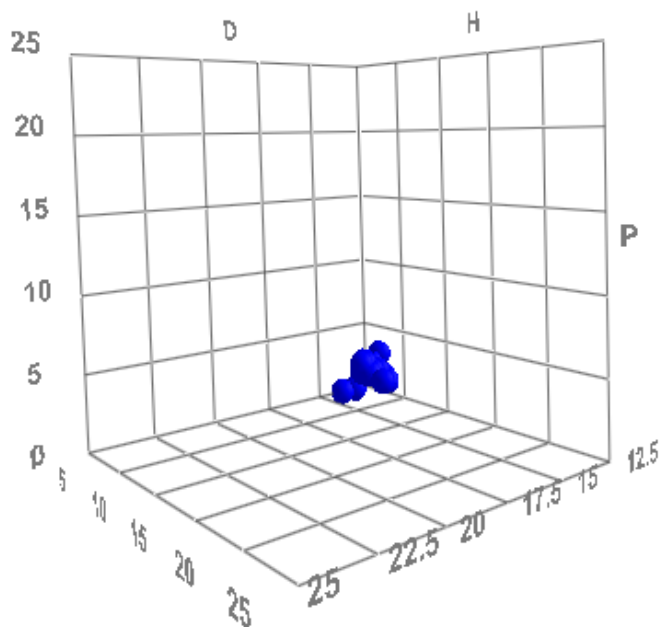


Figure 20: HSP plot for molecules found within the range of HSP values observed for perfluorinated structures.

Figure 20 contains hydrocarbons of increasing chain length alongside all molecules present in Figure 19 which occupied the desirable HSP space enabling high hydrophobicity and in the case of perfluorinated chemicals, oleophobicity. The chain length necessary for adequate surfactancy is at least 6 carbons, those hydrocarbons above 6 carbons can clearly be seen apart from this group. As chain length increases and the effect of dispersion forces increases, the hydrocarbons move away from the space along the dispersion (D) axis.

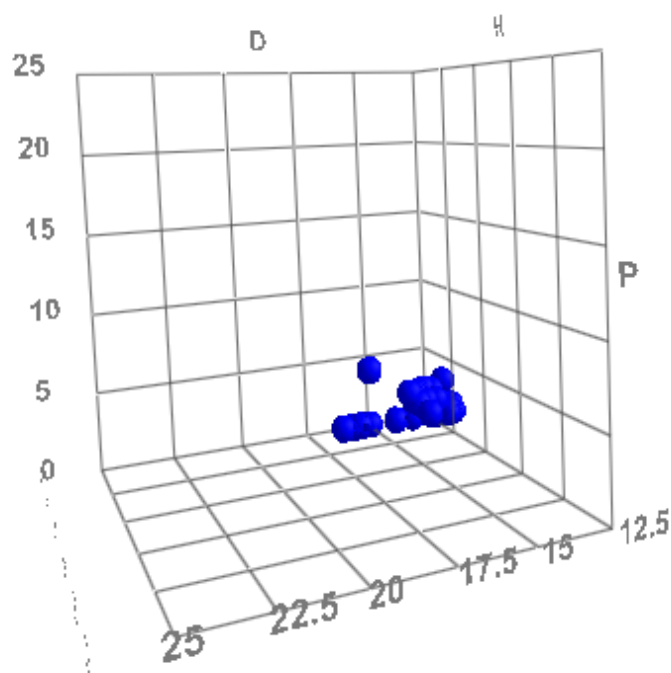


Figure 21: HSP plot containing hydrocarbons, perfluorinated molecules and molecules occupying a similar HSP space to perfluorinated molecules.

Clearly longer chains will be necessary however it may be possible to achieve the same HSP distance from water as perfluorinated molecules. This would forego oleophobicity of course. Another option would be to assess the use of highly branched tail groups, however packing at a surface greatly contributes to the efficiency of a surfactant especially when used for repellency and branching may counteract that. Additionally, highly branched materials are often found to be non-biodegradable.^{119, 138} Some of the siloxanes and silanes found in the search are currently being legislated against by REACH and therefore have been removed from consideration as target molecules as they may have poor bio-degradability.

Currently most tail groups are alkyl chains derived from triglycerides such as those in coconut and palm oil. An argument can be made against the use of extracts and in favour of using waste through the food vs fuel argument.

1.3.2 The route to hydrophobes from fuel precursors and the role of the hydrodeoxygenation stage

The movement within the chemical industry to produce chemicals from renewable resources has produced a vast amount of research in recent years¹³⁹⁻¹⁴⁴. Most notably within the energy, biofuel and aviation fuel industries^{140, 145-148}. The U.S. department of energy aims to have biomass feedstocks responsible for the energy supply of 5% of the country, 20% of the transportation fuels and 25% of chemicals by 2030. The aviation fuel industry is under constant pressure to reduce carbon emissions as they are a major contributor and are therefore vital to the global efforts to reduce emissions. To achieve this goal biomass has been identified as the most abundant renewable resource and therefore of great importance. For ethical reasons, to avoid conflict with the food production industry, waste biomass is most suitable for use as a feedstock. However, complications arise during processing due to the immense variations in biomass feedstock and therefore its chemical composition.

Many industries already use biomass resources in the form of extracts such as oils, dyes, tannins, terpenes and triglycerides. A variety of personal care products, including hand soaps, deodorants, body lotions, skin moisturizers, shaving creams, perfumes, lipsticks, and shampoos have been manufactured from biological sources. Animal fats, vegetable oil, plant fragrances, and other botanical ingredients are widely used to produce these biocosmetics.¹⁴⁹

Although some compounds can be extracted at high quantity and are already industrially established, these industries can also come into direct competition with the food chain in some instances, such as the use of coconut and palm oil in the production of surfactants. This ethical confliction combined with the abundance of waste biomass available globally as a raw material may shift the focus of these industries onto chemical alternatives derivable from platform molecules as opposed to extracts. This becomes increasingly likely as the body of research forming around platform molecules increases. This work intends to use the research into renewable fuels as a springboard for the production of longer chain hydrophobic molecules for other uses, such as synthesis of surfactants.

1.3.2.1 Lignocellulosic biomass as a feedstock

The most abundant component of all biomass regardless of origin is lignocellulose, itself composed of three distinct components; cellulose, hemicellulose and lignin. Cellulose and hemicellulose account for ~70% wt/wt of lignocellulosic biomass and it is from these that the US department of energy identified top value-added chemicals from biomass in a report from 2004 which aimed to unite and focus research efforts. The majority of those identified are classed as platform molecules, a group of base chemicals that the industry can produce in one step and at scale from biomass and use as raw materials for the production of other chemicals.¹⁵⁰

1.3.2.2 Transport fuels industry

The aviation industry accounts for a very large proportion of carbon emissions has become a heavily funded avenue of current biomass research. This industry will also be a driver for the production of biomass derived platform molecules because of the large quantities required year on year which are only increasing in demand. A key synthetic step between platform molecules and fuels is the elongation of the C₅ and C₆ carbon chains derived from the cellulose, hemicellulose and lignin biopolymer units. Integration of fuel and value-added chemicals into the biorefinery concept are key to making biorefineries economical.

For this reason, this study investigates some current opportunities for functionalization of these elongated compounds synthesized as precursors to aviation fuels to produce other functional compounds. The hydrophobic nature of aviation fuels lends itself well to functionalization of precursors to surfactants, bioplastics, lubricants, pesticides and adhesives amongst others.

There are already established routes to aviation fuels from oil, syngas, alcohols and sugars. Of these routes from oils and syngas (oils-to-jet and syngas-to-jet) are commercialized and have approval from ASTM method D7566 to blend with aviation fuel^{147, 151}. Others, such as sugars to aviation fuels are not yet commercialized and remain an area of intense research.

While the synthesis of aviation fuels is a definite area of interest the synthesis of branched hydrocarbons for use as renewable gasoline is also of great interest as the main components of aviation fuels are linear alkanes. Given that branched and linear alkanes are

prominent in current renewable gasoline research, there has been an extensive review of current methods elsewhere¹⁴⁷ and therefore that shall not be discussed here however we endeavour to shed light onto opportunities to further functionalize molecules before the final deoxygenation and reduction stages which commonly eliminate interesting and useful functional groups.

1.3.2.3 Missed opportunities

Many studies have been undertaken into the most logical routes to the many complex chemicals that must eventually be produced from biomass should the circular economy be properly employed and the world were to move away from using fossilized carbon and onto using 'new carbon' for all of its power, fuel and chemical needs. One such study developed a tool named the Biologic Tool¹⁵². This tool enables direct comparison of the atom economies of reaction pathways and allows a visual representation of the 'sanity' of the reaction pathway. This tool allows us to choose the best synthetic starting point in the view of atom economy, an important green chemistry metric.

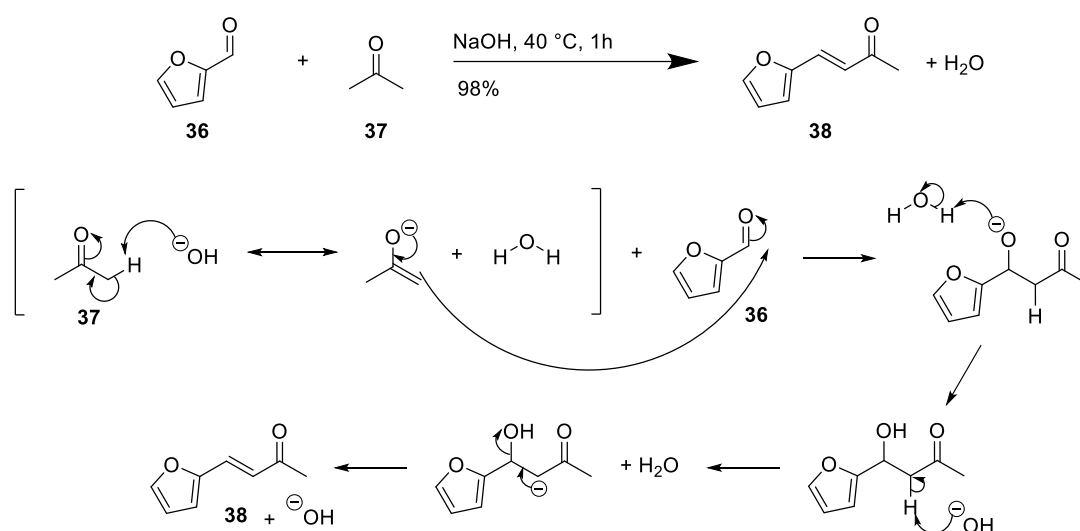
Commonly lignocellulosic biomass is treated in acidic media in order to convert it to platform molecules such as furfural and methyl ketones. To increase the chain lengths in order to produce efficient and high value fuels the platform molecules commonly undergo C-C coupling reactions such as aldol condensation¹⁵³, Michael additions, Diels-Alder additions¹⁵⁴, Guerbet reaction¹⁵⁵, Robinson annulations¹⁵⁶ and oligomerizations¹⁵⁷. Aldol condensations usually utilize basic catalysts and the incompatibility of these catalysts with the up-stream acidic catalysts increases processing costs.

1.3.2.4 Aldol condensations

Utilization of aldol condensations became popular as a method of elongating the short C₅ and C₆ units derived from cellulose and hemicellulose for fuel production after the pioneering work of Huber¹⁵⁸, Dumesic¹⁵⁹ and Corma¹⁶⁰ who studied the chemistry of producing liquid alkanes from biomass derived oxygenated hydrocarbons and the chemical engineering challenges associated with it. Aldol condensations have good atom economies and there are a range of well-established enolisable molecules derivable from biomass such

as furfural, cyclopentanone, methyl isobutyl ketone and 2-hexanone. In particular, furfural has had a lot of attention as a platform molecule for fuel production due to its established large-scale production. The C₈-C₂₃ oxygenates produced and isolated prior to the HDO step retain heteroatoms, ketones and unsaturation.

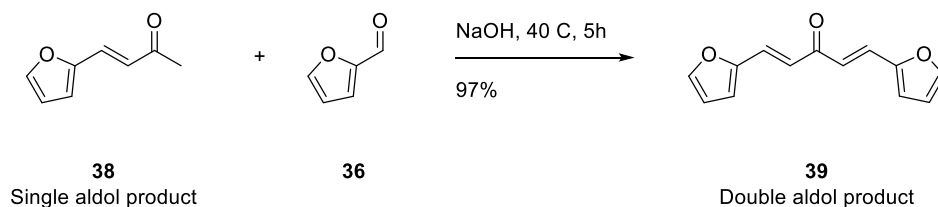
Aldol condensations are commonly base catalysed, often with recyclable solid catalysts and have good atom economies, in-line with the principles of green chemistry. The aldol condensation of furfural and acetone has been studied under numerous basic catalysts including piperazine, aminopropyl triethoxysilane and triazabicyclodecene (TBD) of which TBD gave good yields with 100% conversion of furfural and 100% selectivity to the single aldol product in one hour under mild conditions.¹⁶¹ Scheme 1 shows a potential mechanistic route to the acetone-furfural aldol condensate under basic conditions. The synthesis of the double aldol product has also been investigated using a porous organic framework enhanced with SO₃ as a catalyst, deviating from commonly used basic catalysts, however the conversion of furfural was low (25%) and the selectivity to the double aldol product (35%) also poor¹⁶².



Scheme 1: Aldol condensation scheme and mechanism between furfural and acetone.

A far superior yield of the double aldol product (Scheme 2) of 97% was achieved over 5 hours under very mild conditions (40 °C) using a homogeneous catalyst, sodium hydroxide, which was found to have good recyclability after filtration and was used 5 times without appreciable reduction in yield¹⁶³. The same study applied a further three steps, selective

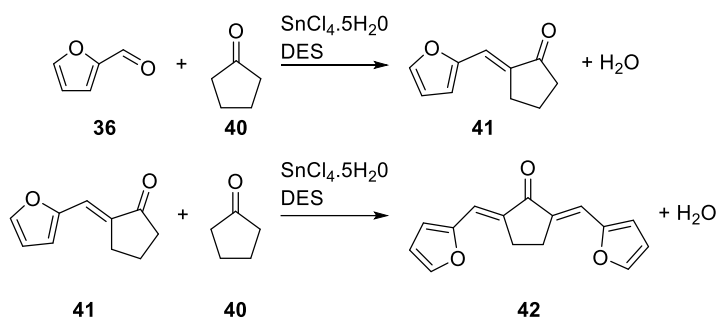
hydrogenation, further aldol condensation and hydrodeoxygenation, to obtain a C₂₃ alkane suitable for use as a high-quality lubricant. Under optimal conditions an 83.8% yield was obtained for the C₂₃ aldol adduct under mild conditions. The resulting oxygenate retains conjugation over 12 carbons, two furanic branches and a ketone group.



Scheme 2: Cross aldol condensation between furfural (**1**) and the product of the aldol condensation of furfural and acetone (**3**).

An investigation focusing on replacing NaOH with solid base catalysts due to the technical and environmental advantages of heterogeneous catalysts used the aldol condensation of furfural and cyclopentanone as an example. It was found that when comparing KF/Al₂O₃, CaO, MgO and hydrotalcite derivatives that KF/Al₂O₃ was the optimal catalyst and produced a 95% yield faster under milder conditions (2h, 333 K) than seen before ¹⁶⁴. Ethanol was used as a solvent and thus more waste is produced than the solvent free methods and an additional separation step is required however the low cost and availability of biomass derived ethanol and improved efficiency of reaction reducing the energy demand partially mitigates this.

An elegant solution put forward by Liu *et al* uses a deep eutectic solvent which can be used to convert biomass to furfural at low temperatures and after addition of cyclopentanone catalyse the aldol condensation producing C₁₀ and C₁₅ fuel precursors ¹⁶⁵. The optimal conditions identified produced a 92% combined yield (C₁₀ and C₁₅) at 100 °C for 120 minutes. The improved efficiency in making a 'one-pot' process from raw biomass to a fuel precursor opens up synthetic opportunities for these compounds once isolated through the ketone and furan functionality for hydrophobic compounds.



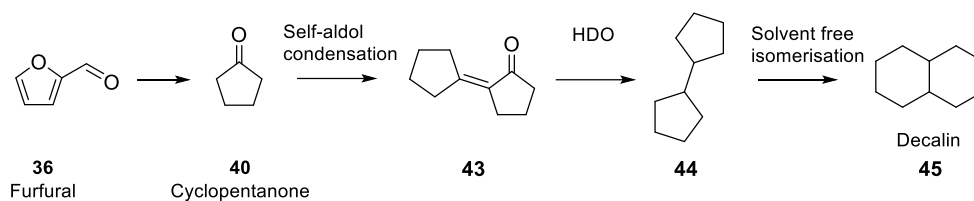
Scheme 3: Furfural and cyclopentanone aldol condensation products using a deep eutectic solvent to yield C10 and C15 fuel precursors.

Solvent free conditions over a solid catalyst have been studied by Wang *et al*¹⁶⁶. Lower yields were recorded at 24% and 37% for the C10 and C15 furfural and cyclopentanone aldol products respectively and the reaction times longer. The optimal conditions were 60 °C for 6 hours at 0.4 g of catalyst (Nafion) per 60 mmol cyclopentanone. The water produced from the aldol condensation may have promoted hydrolysis and polymerisation of furfural forming humins which blocked the catalyst pores and stopped the reaction coming to completion. If the end goal was in fact these fuel precursors these mild solvent free conditions are more favorable in terms of safety and waste production however further study into reducing the humin yield and therefore in theory increasing the product yield would be necessary.

Recent further work by Wang *et al* studied a recyclable dual catalysis system incorporating simultaneous hydrogenation to the aldol condensation of cyclopentanone and furfural over Pd/C and CaO. A carbon yield of >98% was achieved for the partially hydrogenated dual aldol condensate in solvent free conditions with 4 MPa H₂ at 423 K after 10 hours. The HDO step to convert the oxygenate to fuel (86.1% carbon yield) produced a fuel with density of 0.82 g mL⁻¹ and a low freezing point (241.7 K)¹⁶⁷. This work intends to intercept and isolate compounds such as the double aldol condensate from Scheme 3 and use them as a hydrophobic tail group for surfactant synthesis instead of following with a HDO step to create a fuel.

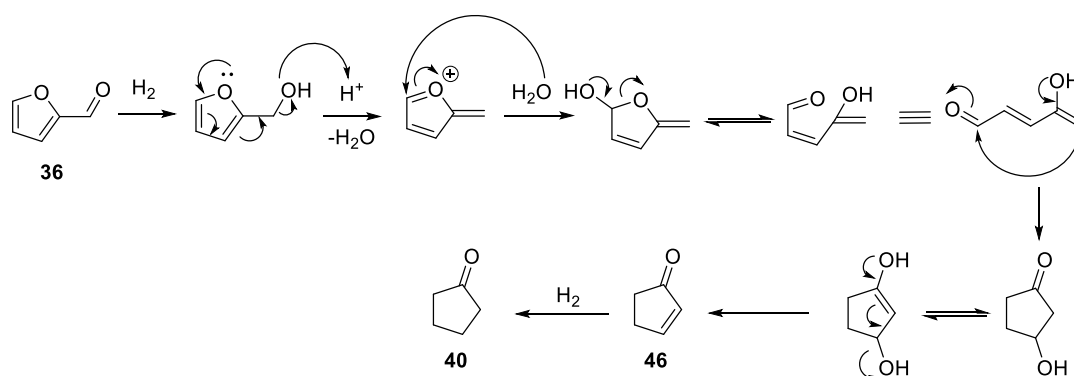
Decalin, another common fuel compound, is traditionally synthesized through the hydrogenation of naphthalene derived from fossil fuels. Decalin is used as a high-performance jet fuel and as an additive to lower grade jet fuels due to the high thermal stability and low freezing point. As a bioderived drop-in replacement decalin can be derived

from furfural via cyclopentanone followed by self-aldol condensation, HDO and isomerization (Scheme 4)¹⁶⁸.



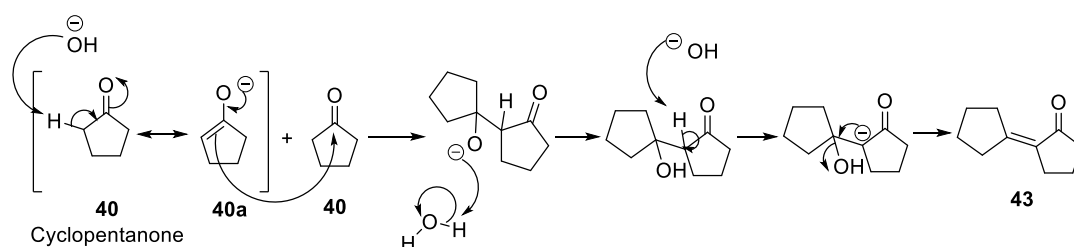
Scheme 4: Synthetic route to decalin from the hemicellulose/cellulose derived platform molecule furfural.

A plausible mechanism for the reductive rearrangement of furfural to cyclopentanone is shown in Scheme 5:



Scheme 5: Mechanism for the reductive rearrangement of furfural to cyclopentanone

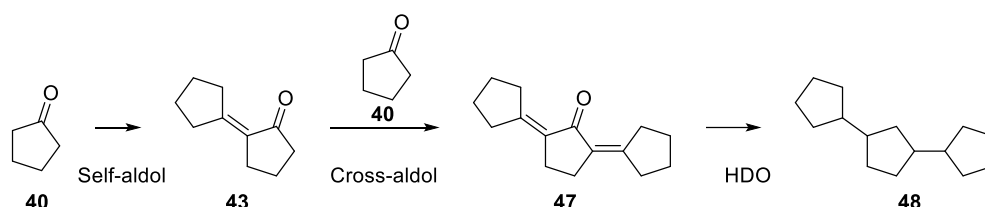
The self-aldol condensation (68.5% carbon yield, Scheme 6) produces an exploitable α,β -unsaturated ketone with the potential for further condensation to a higher carbon number which is lost in the subsequent HDO reaction.



Scheme 6: Mechanism for the self-aldol of cyclopentanone

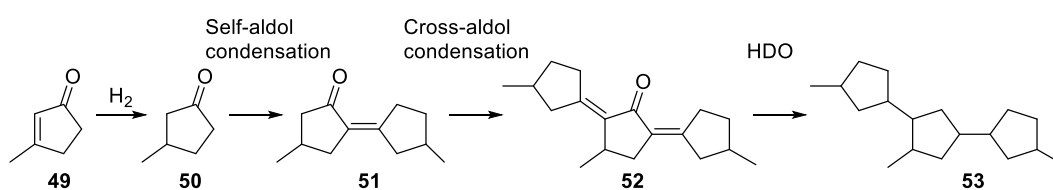
Cyclopentanone can be synthesized on a large scale from the selective hydrogenation of furfural and was used by Sheng *et al* to produce bi(cyclopentane) and tri(cyclopentane) at

95.6% combined yield for use as high density aviation fuels (Scheme 7).¹⁵⁵ Cyclopentanone undergoes self and cross aldol condensation and yields C10 and C15 ketones. Co-catalysts magnesium-aluminium hydrotalcite (MgAl-HT) and Raney Ni were the most successful and also catalysed the hydrogenation of the ketones to C10 and C15 alcohols to produce a total yield of 96.7% yield of C10 and C15 oxygenates. Hydrodeoxygenation of the oxygenates produces alkanes suitable for use as jet fuels.



Scheme 7: Preparation of bicyclopentane and tricyclopentane from cyclopentanone.

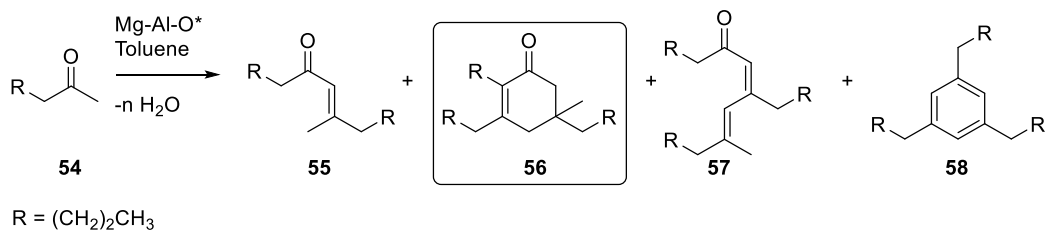
A process has recently been established and reported by Lui *et al* which enables the conversion of cellulose derived 2,5-hexanedione (separation yield of 71.4%) (platform molecule) to a mixture of C12 and C18 polycycloalkanes through addition of hydrogen over a catalyst bed in a one-pot process with a carbon yield of 74.6%. Usually, this process is carried out in a series of steps, first an intramolecular aldol condensation to methylcyclopentenone then a hydrogenation followed by the C-C coupling reactions (self-aldol and cross aldol) and finally hydrodeoxygenation (HDO) as shown in Scheme 8.



Scheme 8: Conversion of 2,5-hexanedione to polycyclic alkanes via one-pot process over dual catalyst bed.

The HDO reaction removes functionalities required for C-C couplings and therefore finding a one pot solution has been elusive however through use of a unique dual catalyst bed Lui *et al* have combined the two processes to increase efficiency and save energy.¹⁶⁹ This results in a mixture of C10 and C15 products prior to the HDO step. The products (**51**, **52**) are of

potential interest as surfactant hydrophobes with suitable functionality available for the addition of a head group through the ketone.

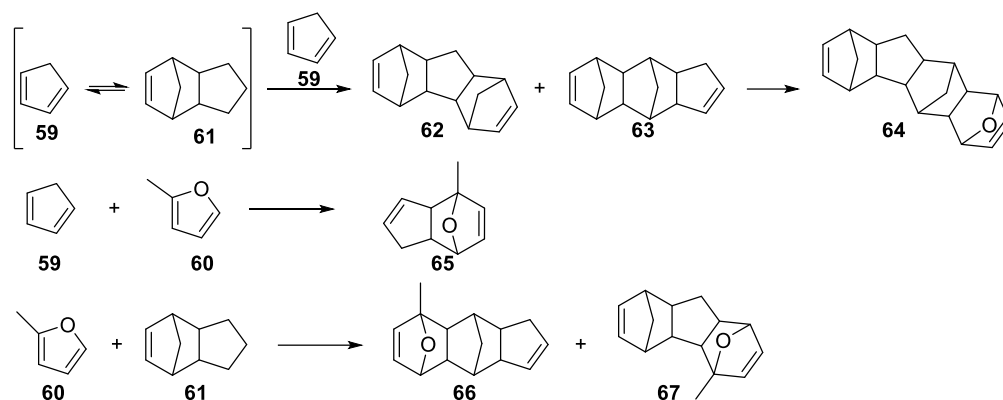


Scheme 9: Self and cross aldol condensation products (**55**, **56**, **57**, **58**) of 2-hexanone (**54**)

Sacia *et al* produced a mixture of highly branched C12-C18 addition products (Scheme 9) from 2-hexanone (**54**) in toluene over Mg-Al-O, a catalyst produced by calcination of hydrotalcite at 700 °C for 2h with an oven ramp rate of 2 °C per minute.¹⁷⁰ The products (**55**, **56**, **57**, **58**) were then hydrodeoxygenated by Sacia *et al* to produce high density fuels. The highly branched cyclic, **56**, is a structure of interest in this study as the branching may increase hydrophobicity and is oriented in a more fixed manner by the ring. The α,β -unsaturated ketone of **56** could act as a Michael acceptor for the addition of a head group to form a surfactant with a highly branched novel hydrophobe.

1.3.2.5 Diels-Alder reaction

Fused ring systems with high densities for advanced jet fuels can be derived from the Diels-Alder reaction of biomass derivable 2-methylfuran (2-MF, **60**) and dicyclopentadiene (DCPD, **61**) at 150 °C over a zeolite catalyst^{171,172}. The Diels-Alder yields a range of fused ring systems (**62-67**, Scheme 10).

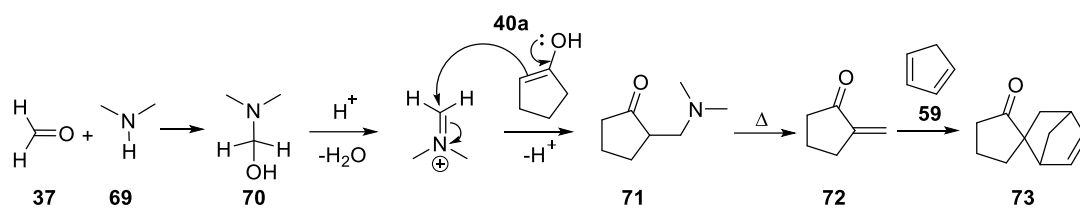


Scheme 10: Diels-Alder products of cyclopentadiene, dicyclopentadiene and 2-MF.

Compounds **64**, **65**, **66** and **67** preserve heteroatoms derived from 2-MF, **60**. The ether could be targeted to add a surfactant head group. The authors concluded that this mixture of compounds had superior characteristics than widely used jet-fuel JP10.¹⁷¹

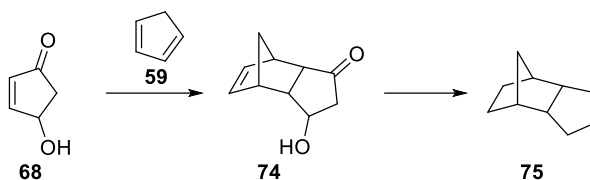
The route to cyclopentadiene involves the rearrangement of furfuryl alcohol followed by hydrogenation and dehydration. The self-Diels-Alder of cyclopentadiene produces a bicyclic system (**61**, Scheme 10) with 95.5% yields, the product of which can be hydrogenated and sold as an alternative to bio-derived JP-10, a high-quality, high-density jet fuel.

Scheme 11 shows the route to a spirocycloalkane (**73**) through the Mannich-Diels-Alder reaction of biomass derivable starting materials: formaldehyde (**37**), cyclopentanone (**40**) and cyclopentadiene (**59**).¹⁷³ The reaction, carried out by Pan and coworkers, used a recyclable zeolite catalyst with an Si/Al molar ratio of 130 over which the product, **73**, was afforded at 80.9% yield.¹⁷³ Pan and coworkers found that **73** had a higher density and volumetric neat heat of combustion than JP-10, a well-known and popular jet fuel.



Scheme 11: Mannich-Diels-Alder route to C10 spiroalkane precursor to high density fuel.

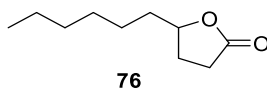
Scheme 12 shows how JP-10 can be derived from biomass via the Mannich-Diels-Alder of hydroxycyclopentenone (**68**) and cyclopentadiene (**59**) followed by a hydrodeoxygenation step to yield bioderived JP-10, compound **75**. Compound **74**, prior to the HDO step retains a hydroxyl and ketone group which is ideal for addition of a surfactant head group.



Scheme 12: The Mannich-Diels-Alder addition of biomass derived hydroxycyclopentenone and cyclopentadiene (**59**)

1.3.2.6 Hydrodeoxygenation

One-pot HDO of biomass is currently a hot topic of research intended to reduce costs and energy consumption when converting biomass to fuels. Furfurylidenelevulinic acid can be derived from furfural and levulinic acid which are both widely produced from lignocellulosic biomass¹⁷⁴. Using furfurylidenelevulinic acid as a starting material, such a one-pot synthesis is reported by Li *et al* in with a 93.16% yield of nonane and decane achieved at 170 °C for 4 hours under 3 MPa of H₂.¹⁷⁴ Their process was developed around using a Pd/C catalyst combined with phosphotungstic acid (HPW). However, after just 30 minutes the overall yield is 60% and the reaction mixture consists of approximately 20% γ -decalactone (**76**) and 30% decanoic acid. These molecules can be further functionalized individually or as a mixture, for use as surfactants and other products which may be of higher value than nonane and decane¹⁷⁴. This would also save energy by reducing the heating time.



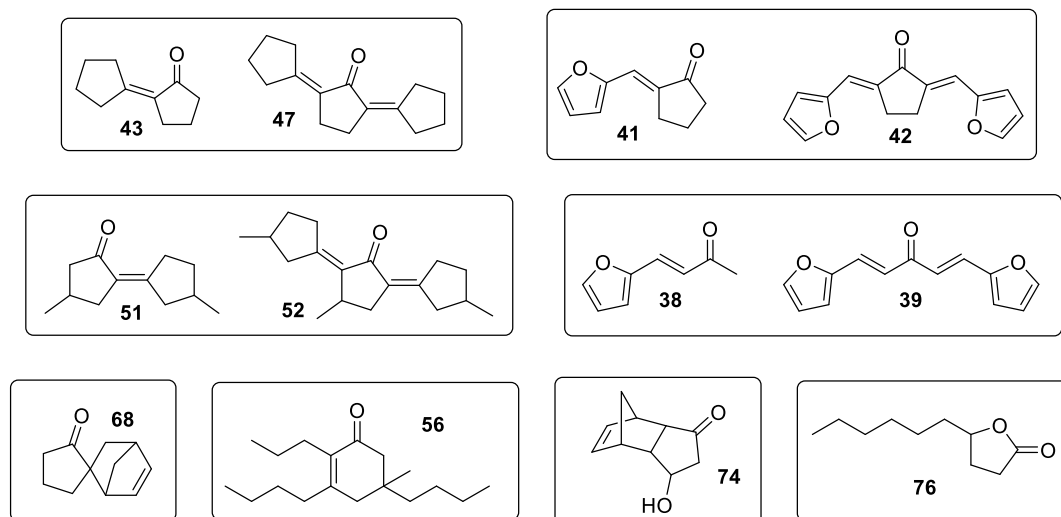
Scheme 13: Chemical structure of γ -decalactone (**76**).

1.3.3 The scope of possible starting materials for innovative hydrophobes from biomass

Perfluorinated surfactants have had widespread application due to their chemical and thermal stability, high surface activity at low concentration, and both hydrophobic and lipophobic character. However, their high stability resulted in them being labelled as PBTs (persistent, bioaccumulative and toxic).²⁰ Due to their easily migration and persistence in the environment, these man-made perfluorinated surfactants have shown toxicity to humans and animals and were found in blood and tissues. Driven by the increasing need for fluorinated products in everyday life and their long-term toxicity to humans and environment, the interest of scientists in replacing these compounds with safer alternatives has increased over the years.^{107, 128, 175}

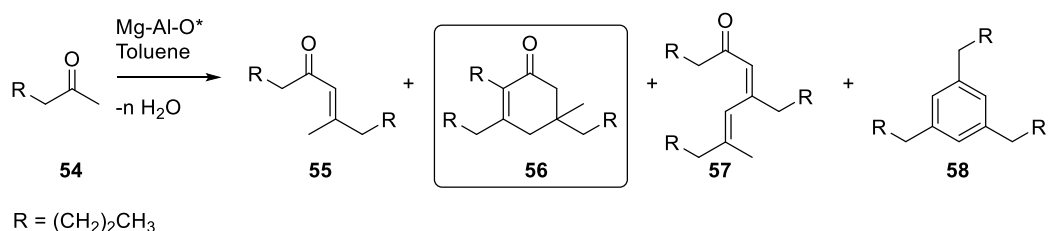
Several structures taken from biofuel research have been proposed as potential synthetic starting points to synthesise novel bioderived surfactants with the aim or replacing

perfluorinated surfactants for water repellent applications. The structures chosen, shown in Scheme 14, are structures intended to undergo hydrodeoxygenation to produce dense alkanes for use as jet fuels. Compound **56**, of Scheme 14, a structure synthesised by Sacia *et al*¹⁷⁰ (Scheme. 15) intended as an aviation fuel derived from biomass was chosen as the initial synthetic starting point.



Scheme 14: A collection of structures from the literature review.

This structure was investigated by Sacia and coworkers with reduction down to a gasoline-like hydrocarbon structure as the eventual goal. However, this misses the opportunity to make use of the diverse chemical functionality, particularly the potential to add hydrophilic units *via* either the ketone or the Michael accepting centre. Based on prior expertise and interest in the group regarding Michael accepting compounds we targeted this cyclic branched compound derivable from sequential aldol condensations of fatty ketones.



Scheme 15: 2-hexanone (**54**) condensation and cyclisation reaction. Reaction conditions taken from Sacia *et al*: 2-hexanone (**54**, 2 mmol), toluene (3 mL), 200 mg catalyst. *Mg-Al-O = calcined hydrotalcite

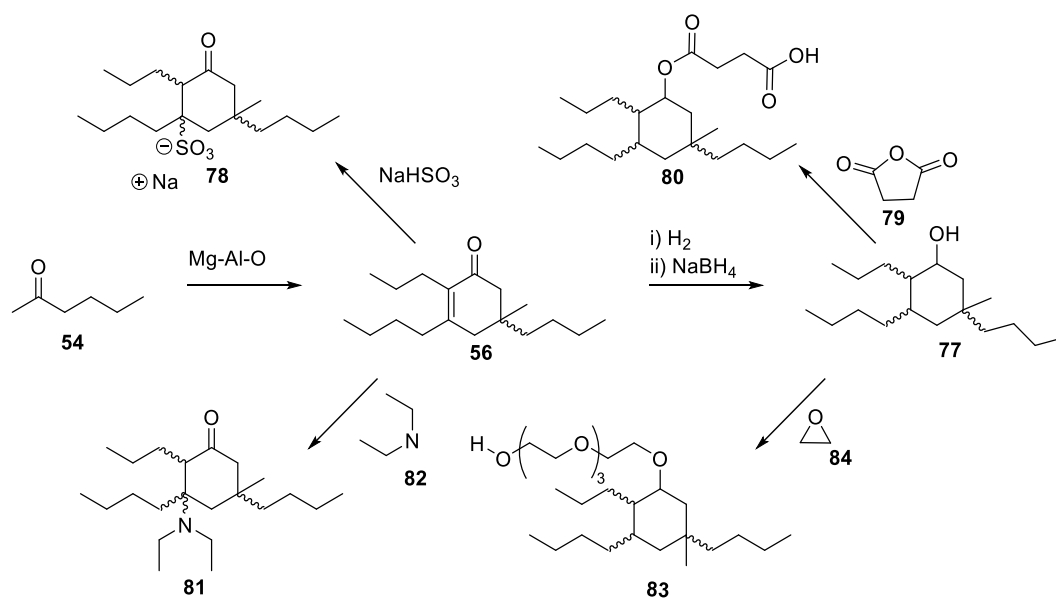
The additional hydrocarbon chains in **56** of Scheme 14, compared to that in a conventional linear tail group, are intended to improve hydrophobicity.¹⁷⁶ This structure also introduces the concept of using a ring to increase hydrophobicity whilst using space to keep the structure away from the Hansen space of conventional hydrocarbon chains.

The starting material, 2-hexanone (**54**), can be derived from biomass, as can other ketones capable of undergoing the same reaction to produce the highly branched cyclic α , β -unsaturated ketone. 2-Hexanone is accessed from biomass by dehydration of glucose, forming the platform molecule 5-(hydroxymethyl) furfural (HMF) followed by hydrodeoxygenation in high yield to 2,5-dimethylfuran (2,5-DMF, **87**). From 2,5-DMF (**87**), ring opening hydrogenolysis yields **54** with 98% selectivity. Additionally, longer chain methyl ketones are accessible via the Dakin-West reaction of enolisable carboxylic acids (such as fatty acids) with acetic anhydride in the presence of base.¹⁷⁷

The cyclic condensation products from **54**, compounds **55–58** of Scheme 15, show promise as highly hydrophobic molecules and have a α , β -unsaturated ketone sites available as points to functionalise for the creation of a head group. The structure, a highly branched cyclic with head group connectivity direct to the ring, would produce a novel surfactant should the resulting compound exhibit surfactancy once a head group is added.

The structures of the expected products from the condensation and cyclisation **54** are shown in Scheme 15. Compound **54** undergoes an aldol condensation forming four diastereoisomers, which then form cyclic trimers, through either Michael addition or 1,2 addition (dependant on stereochemistry) and subsequent cyclisation to produce **56**.

Scheme 16 shows some potential routes to surfactants from compound **56**. A range of head groups could be added using the α - β unsaturated ketone as a Michael acceptor.



Scheme 16: Possible reaction routes to surfactants from compound **56**, synthesized through the aldol condensation of **54**.

The review of biofuel research and computational predictions in HSPiP has led us to a range of potential structures which may have a stronger hydrophobic effect than conventional linear chains. Based on prior expertise and interest in the group regarding Michael accepting compounds we targeted a family of cyclic branched compounds derivable from sequential aldol condensations of fatty ketone.

1.4 CONCLUSION

PFA's make unique and powerful surfactants which are unlikely to be matched in performance by biodegradable surfactants. This is because perfluorination leads to several desirable traits for a surfactant, namely excellent thermal and chemical stability and excellent surface tension reduction. These desirable characteristics however, go hand in hand with the toxicity and persistent nature of perfluorinated surfactants. Therefore the aims of this work are adjusted to synthesising alternatives to PFAs while accepting that performance is unlikely to be matched or improved. A more realistic aim therefore is to improve on the performance of traditional linear alkane surfactants while maintaining biodegradability and applying green chemistry principles.

The principles of green chemistry run through the core of this project to design safer alternatives to perfluorinated surfactants. PFA's are toxic, persistent and bioaccumulative and are a real threat to public health. Designing safer alternatives leans into several green chemistry principles such as prevention, less hazardous chemical synthesis, designing safer chemicals, design for degradation and inherently safer chemistry for accident prevention. The design process considers the toxicity and persistent nature of perfluorinated surfactants and endeavours to avoid their manufacture through provision of alternatives. The synthesis design at the outset is inherently less hazardous as fewer hazardous materials are used and produced.

Principle 7, concerning renewable feedstocks is also incorporated. The choice of feedstock is lignocellulosic biomass which is both abundant and renewable and therefore all starting materials for final products are derivable from biomass. Choosing lignocellulosic biomass as a feedstock has several advantages. It is sustainable and renewable and promotes the circular economy model as it can be sourced as waste materials from other industries, such as forestry. Lignocellulosic biomass is also abundant and therefore cheap as it is also a waste material. Choosing to use a waste feedstock to synthesise speciality chemicals such as surfactants would also increase value significantly and strengthen the economic viability of the biorefineries which currently produce platform molecules.

Biofuel research typically takes platform molecules and utilises their functional groups (which traditional base chemicals lack) to perform C-C coupling reactions to produce longer chains before a final hydrodeoxygenation step to remove any unsaturation and any oxygen containing functional groups to create a fuel. This work intends to take the products from

the C-C coupling step before removing the functional groups such as alcohols and ketones to use them as the hydrophobic portion of surfactant molecules. Several potential synthetic starting points have been suggested from structures taken from biofuel research.

Chapter 2

2 SYNTHETIC ROUTES TO NOVEL HYDROPHOBIC SURFACTANTS

2.1 INTRODUCTION TO SYNTHETIC GOALS

The aim of this work is to synthesise novel biobased surfactants which are able to fill a gap in the market created by the heavy regulation of toxic and environmentally persistent fluorinated surfactants. The unique characteristics of fluorinated surfactants include resistance to stains through creation of hydrophobic and oleophobic surfaces and resistance to thermal and chemical decomposition.¹⁷⁸ There are many uses of fluorinated surfactants which utilise these unique characteristics which now require replacements. This study does not aim to replicate all of these characteristics. Designing another thermally and chemically recalcitrant structure as a replacement would likely produce another environmentally persistent compound. This work also aims to elevate the revenues available from biorefineries, enhancing their validity whilst reducing waste. Given the nature of the starting materials available to biorefineries (lignocellulosic biomass), achieving the combined oleophobicity and hydrophobicity is an impractical and unrealistic goal. Therefore, the aim of this work is to produce a novel highly hydrophobic surfactant with an environmentally considered design.

Biobased fuel production is a research area of high priority as many countries aim to reduce their dependence on petrochemicals. Several studies with this goal produced highly branched potentially highly hydrophobic structures with the intention to serve as biobased aviation fuels. The needs of this research area align with that of this work and therefore have been used as a springboard for the synthesis of novel biobased highly hydrophobic surfactants.

2.2 LIGNOCELLULOSE AS A FEEDSTOCK

Lignocellulosic biomass is a highly abundant renewable resource through waste streams such as unavoidable food waste and forestry waste making this feedstock economically viable. Utilizing our lignocellulosic waste streams has the potential to replace the traditional building block chemicals sourced from crude oil with platform molecules which have a greater range of structures and functionality.¹⁷⁹

The primary components of lignocellulosic biomass are the three biopolymers: cellulose, hemicellulose and lignin which form the basis of the plant cell wall (Figure 22):

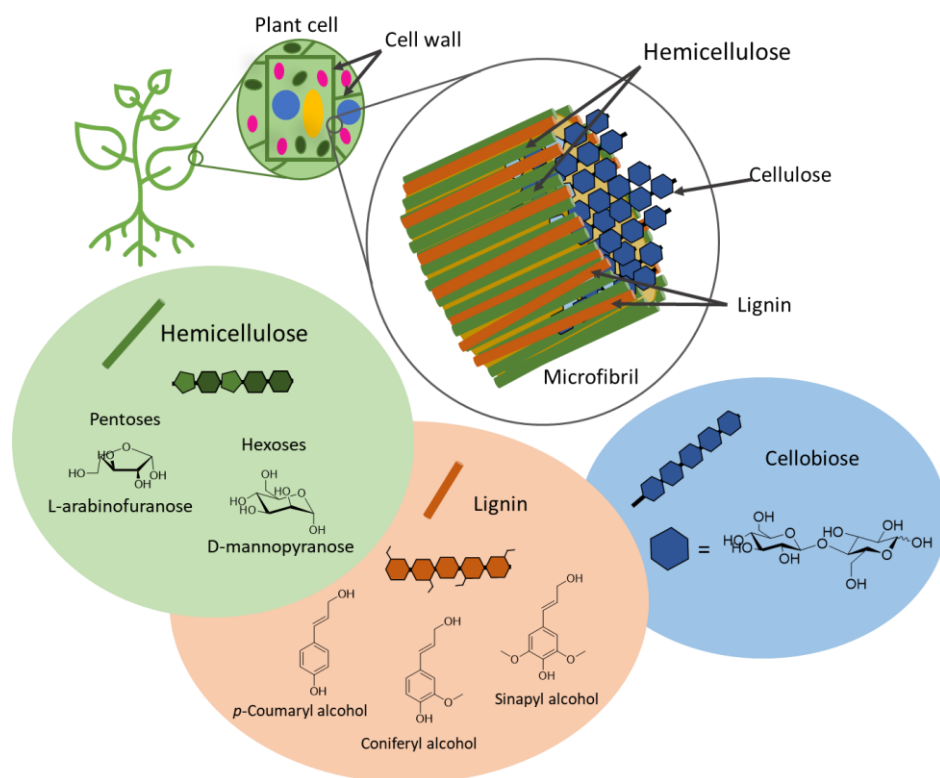


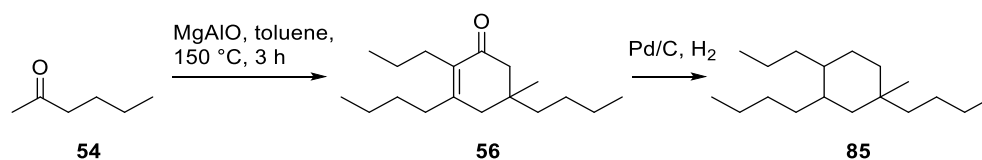
Figure 22: The structure of lignocellulosic biomass.

Monomeric units can be obtained from these biopolymers to synthesise platform molecules. The complex structure of lignocellulosic biomass contributes to its recalcitrance to enzymatic degradation. Hemicellulose and lignin provide structural strength and form a strongly bonded matrix, covalently and through hydrogen bonding, which envelops the cellulose. To efficiently utilise the hexoses (cellulose, hemicellulose), pentoses (hemicellulose) and phenolics (lignin) within the biopolymers a pre-treatment process is considered essential to improve the yields of the individual monomeric units of the components, such as sugars.¹⁸⁰

Because of the variation in feedstock for lignocellulosic biomass there are a variety of pre-treatment methods which can be used alone or in combination with others. The pre-treatment processes can be categorised into four methods: 1) physical, such as milling or microwave pre-treatments, 2) chemical, such as acid or alkaline pre-treatments, 3) physiochemical, such as steam or ammonia fibre explosion and 4) biological such as through use of enzymes.^{179, 180}

2.3 JUSTIFICATION FOR TARGET COMPOUND 56 AND ACCESS FROM LIGNOCELLULOSIC BIOMASS

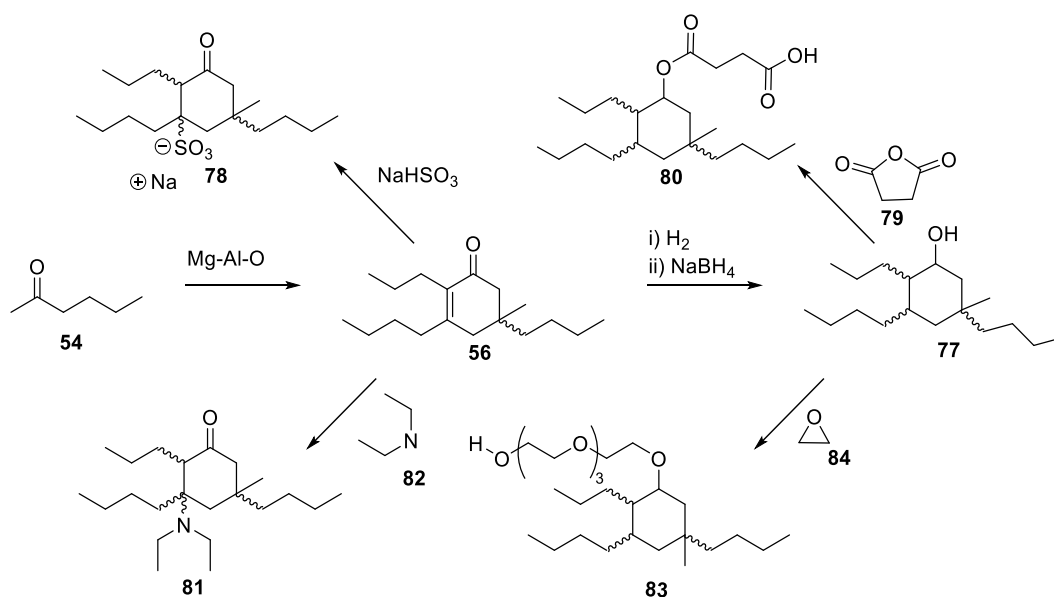
A structure synthesised by Sacia *et al.*¹⁷⁰ (compound **56**, Scheme 17) intended as an aviation fuel derived from biomass was chosen as one potential synthetic starting point. This structure was investigated by Sacia *et al.* with reduction down to a gasoline-like hydrocarbon structure (compound **85**, Scheme 17) as the eventual goal. However, this overlooks the opportunity to make use of the diverse chemical functionality, particularly the potential to add hydrophilic units via either the ketone or the Michael acceptor. Based on prior expertise and interest in the group regarding Michael accepting compounds we targeted this cyclic branched compound derivable from sequential aldol condensations of fatty ketones similar to ketone **54**.¹⁸¹⁻¹⁸⁴



Scheme 17: Major product of 2-hexanone (**54**) sequential self-aldol condensation with conditions specified by Sacia *et al.*¹⁷⁰

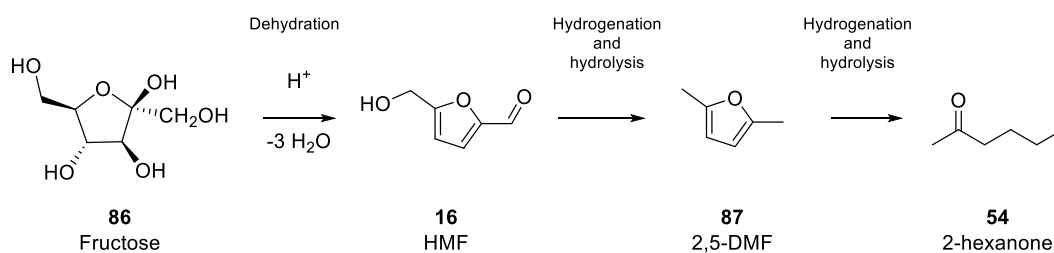
The additional hydrocarbon chains in compound **56** of Scheme 17, compared to the conventional linear tail groups commonly found in surfactants such as SLES, are intended to improve hydrophobicity.¹⁷⁶ This structure also introduces the concept of using a ring to increase hydrophobicity by moving away from the Hansen space of conventional hydrocarbon chains whilst using the relatively fixed and predictable conformation of the ring structures to orient the hydrocarbon chains. One of the cyclic condensation products of compound **54**, compound **56** of Scheme 17, shows promise as a highly hydrophobic molecule and has an α,β -unsaturated ketone site as a potential point to functionalise for the creation of a head group.

The addition of a headgroup utilising the α,β -unsaturated ketone would result in a structure that is highly branched and cyclic with head group connectivity direct to the ring. Once a head group is added the synthesis should yield a novel compound which exhibits surfactant properties. Suggested examples of such structures (**78**, **80**, **81**, **83**), which could potentially behave as surfactants, are shown below in Scheme 18.



Scheme 18: Potential synthetic structures to novel surfactants from 2-hexanone (**54**)

The starting material, 2-hexanone (**54**) can be derived from lignocellulosic biomass, as can other methyl ketones such as 2-butanone, 2-pentanone and 2-heptanone which are all capable of undergoing the same reaction to produce the highly branched cyclic α,β -unsaturated ketones (Scheme 19):

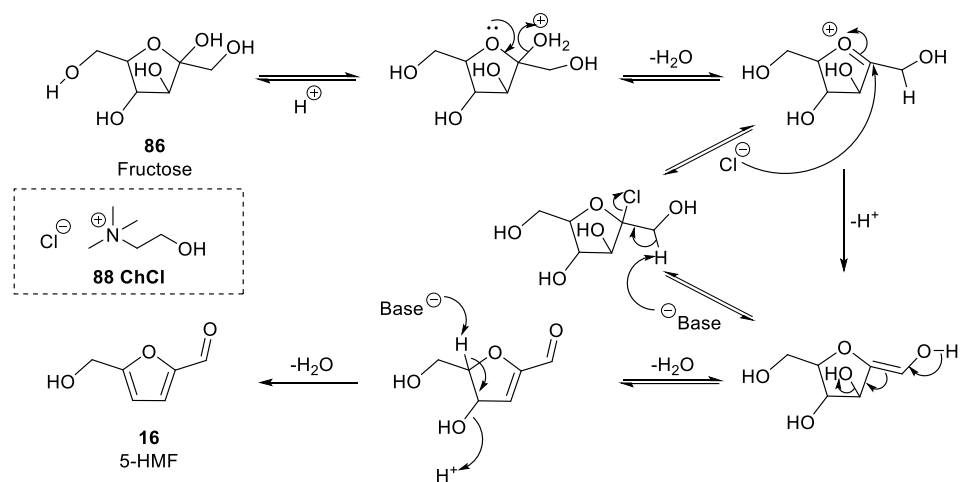


Scheme 19: Synthetic route from fructose to 2-hexanone (**54**) via platform molecule 5-HMF (**16**).

As seen in Scheme 20, 2-hexanone (**54**) is accessed from biomass through isomerisation of glucose to fructose (**86**), dehydration of fructose forming the platform molecule 5-(hydroxymethyl)furfural (5-HMF, **16**). This then followed by hydrogenation and hydrolysis in high yield to 2,5-dimethylfuran (2,5-DMF, **87**). Hydrogenation and hydrolysis of 2,5-DMF (**87**) yields 2-hexanone (**54**) with 98% selectivity. Additionally, longer chain methyl ketones

can be derived via the Dakin-West reaction of enolisable carboxylic acids (such as fatty acids) with acetic anhydride in the presence of base.¹⁷⁷

The initial step towards deriving 2-hexanone from biomass is pre-treatment of lignocellulose, which was discussed earlier in the chapter. Pre-treatment methods typically produce sugars such as glucose and fructose and some platform molecules such as 5-hydroxymethylfurfural (5-HMF, **16**). A mechanistic route to 5-HMF (**16**) from fructose (which can be derived either from pre-treatment yields or from isomerisation of glucose) is shown in Scheme 20:



Scheme 20: Mechanism for the dehydration of fructose catalysed by HCl in a deep eutectic solvent system.¹⁸⁵

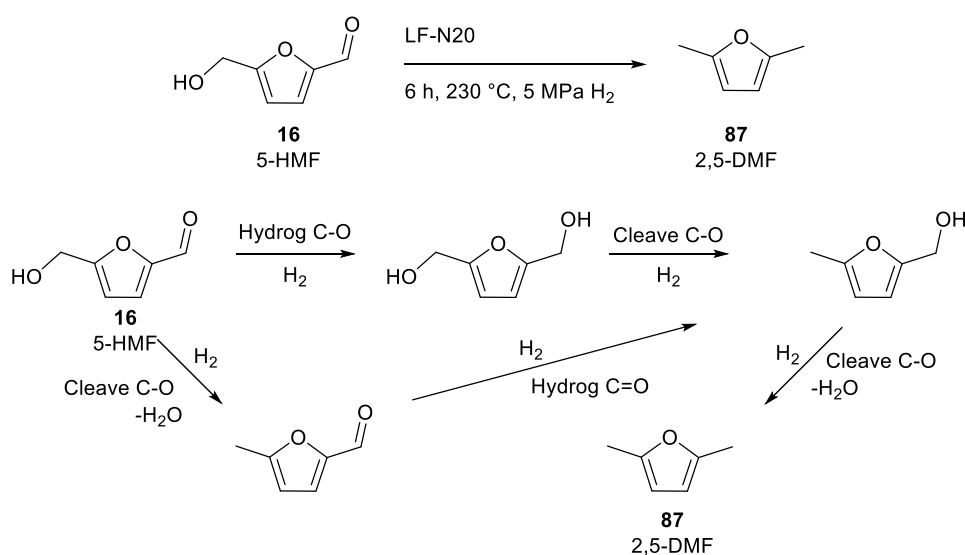
This high yielding reaction (90.3%) is a HCl catalysed, 4-hour reaction at 100 °C making use of fructose (**86**) and choline chloride (ChCl, **8**) as a deep eutectic solvent (DES) pairing. Deep eutectic solvents (DESs) are binary mixtures of Lewis/Bronsted acid and bases which form a eutectic mixture which has a lower melting point than either pure compounds due to hydrogen bonding between the two.¹⁸⁶

DESs provide excellent solvation over a wider range of temperatures which is beneficial and aids with the recalcitrance of lignocellulosic biomass. As a result, research is currently ongoing in using deep eutectic solvents in pre-treatments for lignocellulosic biomass.¹⁸⁷ DESs are becoming more frequently used in green chemistry applications because solvents such as ChCl (a common solvent used in DES mixtures) are cheap, have low volatility, are non-toxic and biodegradable. In this instance the reactant, fructose, also acts as a deep

eutectic solvent which interacts through hydrogen bonding with choline chloride (Scheme 21).¹⁸⁸

Hydrogenolysis produces 2,5-DMF (**87**) from 5-HMF (**16**). As a biomass derived fuel, 2,5-DMF (**87**) has advantages when compared to bio-ethanol and bio-butanol, such as lower water solubility and higher research octane number.¹⁸⁹ Dumesic and coworkers published a reaction pathway for the hydrogenolysis of 2,5-DMF (**87**) from fructose (**86**) with a 76–79% yield, using a Cu/Ru/C catalyst in 2007.¹⁹⁰ Since then much research has been undertaken into efficient catalysis, the work initially focussing on precious metals with some papers seeking non-precious metal based catalysts for industrial applications such as copper and nickel.¹⁹¹

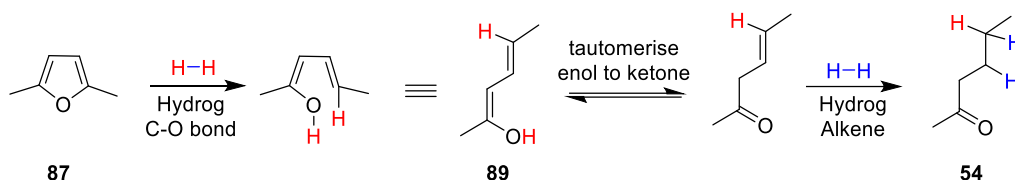
A perovskite-supported Ni catalyst (LF-N20) was reported to achieve a 98.3% yield for the hydrogenolysis of 5-HMF (**16**) to 2,5-DMF (**87**) under optimised conditions (6 hours at 230 °C, 5 MPa H₂). The group reported that the heterogeneous catalyst retained good activity through 5 cycles and gave an insight to the mechanism (Scheme 21):



Scheme 21: Mechanism for the hydrogenolysis of HMF (**16**) to 2,5-DMF (**87**). Reaction conditions: perovskite-supported Ni catalyst, 6 h, 230 °C, 5 MPa H₂.

The final step in the synthetic route from lignocellulosic biomass to 2-hexanone (**54**) is the ring opening hydrogenation of 2,5-DMF (**87**) to 2-hexanone (**54**). Work carried out by Louie *et al* demonstrates that the ring opening hydrogenation of 2,5-DMF (**87**) can be carried out in a single step and optimised to produce 2-hexanone (**54**) at 92% yield (Scheme 22).¹⁹² The

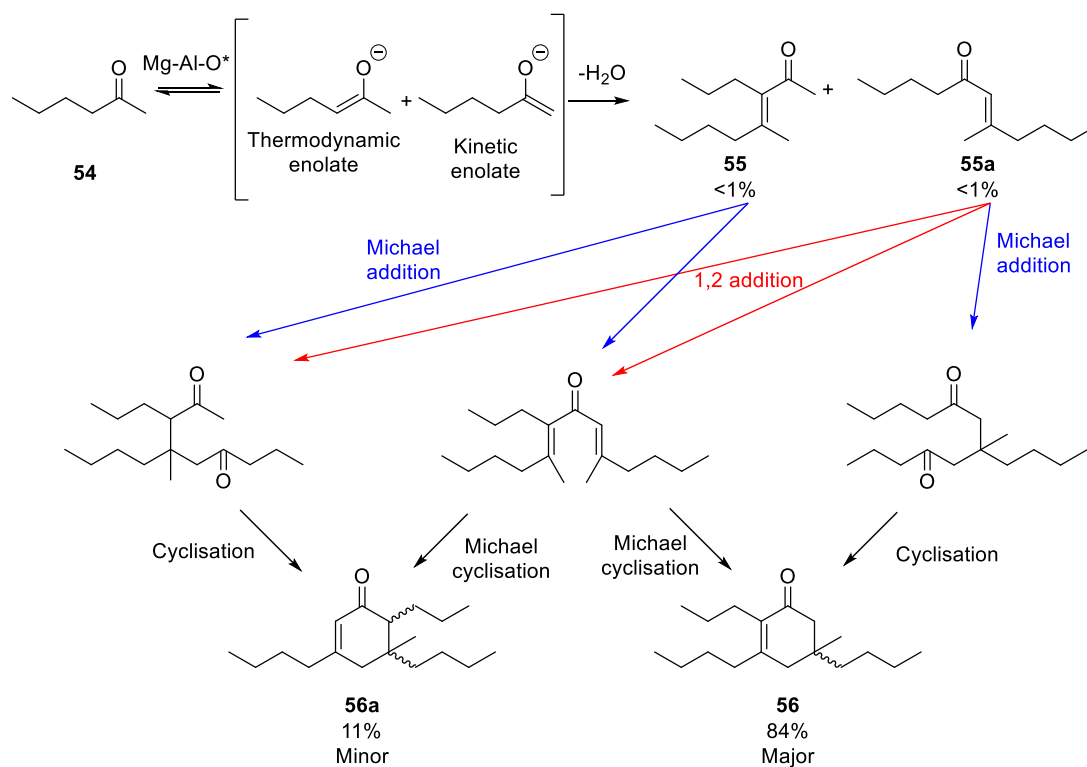
reaction was carried out in nonanone at 120 °C and 4.1 bar hydrogen with 5% Pt/C catalyst at 0.2 mol%. The mechanism, shown in Scheme 22, involves ring opening 2,5-DMF (**87**) through hydrogenation of the C-O bond followed by tautomerisation of the enol to form the ketone and further hydrogenation of the alkene to form 2-hexanone (**54**):



Scheme 22: Mechanism for the ring opening hydrogenation of 2,5-DMF (**87**) to 2-hexanone using Pd/C (5% wt) at 120 °C, 4.1 Bar H₂.

Side products include the fully hydrogenated furan, 2,5-dimethyltetrahydrofuran, and 2-hexanol which is formed when the enol alkene is hydrogenated followed by the second alkene. The group found that the ring opening of 2,5-DMF (**87**) was much faster than the ring opening of the saturated 2,5-dimethyltetrahydrofuran (2,5-DMTHF) and therefore deduced that the process shown in Scheme 23 represents a plausible route to 2-hexanone (**54**) from 2,5-DMF (**87**) under these conditions.¹⁹²

Compound **56** can then be accessed through reaction of **54** over MgAlO in toluene at 150 °C. The structures of the expected products from the sequential self-aldol condensation and cyclisation of 2-hexanone (**54**) are shown in Scheme 23. First, compound **54** is expected to undergo aldol condensation, forming two structural isomers, compounds **55** and **55a** (Scheme 23). Compounds **55** and **55a** then form cyclic trimers, **56** and **56a**, through either Michael addition or 1,2 addition (dependent on stereochemistry) and subsequent cyclisation or Michael cyclisation.



Scheme 23: Mechanism of 2-hexanone (**54**) self-aldol condensation, addition and cyclisation. MgAlO^* hydrotalcite calcined at 200 °C for 2 hours.

2.4 PREPARATION OF COMPOUND **56** AND **56a**

Compounds **56** and **56a** (Scheme 23) were identified in the literature review from the work of Sacia *et al*¹⁷⁰ as a potential synthetic starting point for the preparation of a novel biobased surfactant.

2-Hexanone (**54**), was used by Sacia *et al* as the starting material for self-aldol condensation and cyclisation in the synthesis of compounds **56** and **56a** (Scheme 24). The route from lignocellulosic biomass to 2-hexanone (**54**) was previously explored and established earlier in the chapter.

The work by Sacia *et al* used a small-scale catalytic screening method using 2-hexanone (compound **54**, 2 mmol), toluene (3 mL) and 200 mg catalyst for 3 hours at 150 °C in a Q-tube reactor (Figure 23):

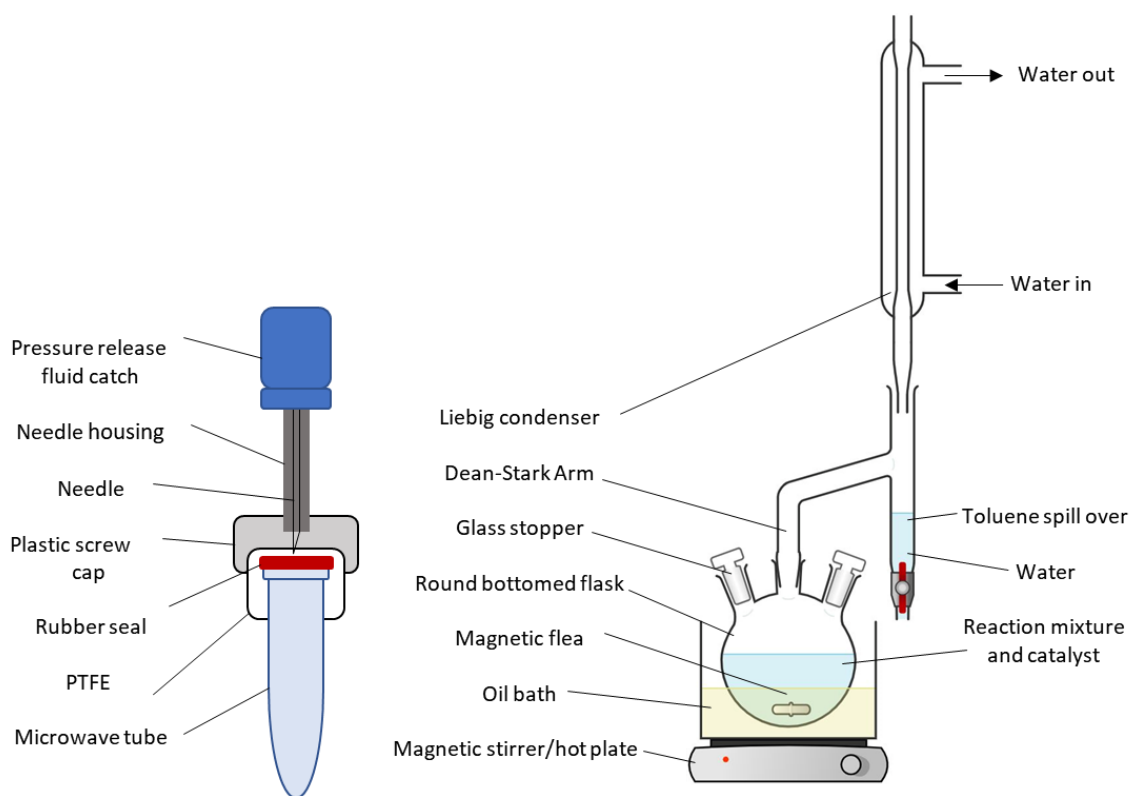


Figure 23: Diagram of Q-tube for small scale reactions (left) and Dean-Stark apparatus set-up for scale-up (right).

A Q-tube is a small capacity (12 mL) toughened glass tube and septa enabling small scale reactions to run under pressure. The pressure is not monitored or adjustable and is produced from the reactants and solvents present at the reaction temperature. In this case the pressure is approximately equal to that produced by 3 mL of toluene at 150 °C. The highest yielding catalyst was also prepared at gram scale by Sacia *et al* in a flask with Dean-Stark apparatus (Figure 23). The conversions of compound **54** reported by Sacia *et al* for the small-scale Q-tube reactions closely matched those reported for the scale up. As the reaction temperature is above the boiling point of toluene and the small-scale reaction is in a sealed environment, there is a pressure difference between the small-scale Q-tube and the larger scale Dean-Stark apparatus. However, no significant change in conversion of **54** was observed when comparing the Q-tube and Dean-Stark methods in their reported work.

The reported conversions of the starting material for the catalytic screening were derived from GC-FID analysis. MgO, TiO₂ and calcined hydrotalcite (Mg-Al-O) produced the highest conversion with respect to the target compounds selected (cyclic trimers, **56**, **56a**) (Table 2):

Table 2: Catalyst screening for the condensation of 2-hexanone (**1**). Reagents and conditions: 2-hexanone (**1**, 2 mmol), toluene (3 mL), 200 mg of catalyst, 150 °C, 3 hours. Work carried out by Sacia et al. * calcined hydrotalcite.

R = (CH₂)₂CH₃ + positional isomers + positional isomers + positional isomers + positional isomers

Entry	Catalyst	Conversion of 54	Dimers (55)	Acyclic trimers (57) And Cyclic (56)	Aromatic trimer (58)
1	MgO	98	3	69	0
2	TiO ₂	99	0	76	16
3	Mg-Al-O*	100	0	93	0

As seen in Table 2, entry 1, MgO enabled a 98% conversion of 2-hexanone (**54**) with 69% selectivity for the cyclic trimer target compounds **56**, 3% of the single aldol condensation products (dimers, **55**) and the remaining 26% to acyclic trimers and higher acyclic/cyclic condensation products. TiO₂ promoted a 99% conversion of 2-hexanone (**54**) with higher selectivity to the target compounds **56** (76%) and 0% conversion to single aldol condensate products. However, it also led to the formation of 16% aromatic products (**58**) which cannot undergo functionalisation to form surfactants due to lack of α,β unsaturated ketones. The calcined hydrotalcite (Mg-Al-O) led to a 100% conversion of 2-hexanone (**54**) with 93% selectivity to the target compounds and 7% to acyclic trimers (**57**) and higher condensation products.

The scale up conditions utilising the Dean-Stark apparatus were replicated using standard lab glassware to avoid incurring unnecessary costs purchasing Q-tube equipment.

The first catalyst investigated was MgO, quoted by Sacia to have a 98% conversion of 2-hexanone (**54**) with cyclic trimers **56** accounting for 69% of the products. MgO was chosen for further studies despite it giving a lower yield of cyclic trimers compared to Mg-Al-O

(MgO, 69%; Mg-Al-O, 93%) as it is a cost effective, non-hazardous catalyst which the research group had previous knowledge of handling. It also did not require pre-treatment in the study by Sacia *et al.*

Using the Dean-Stark set-up **54**, MgO and toluene were charged to the vessel. After 6 hours of vigorous refluxing (entry 1, Table 3) TLC analysis indicated that no products had formed:

Table 3: Reaction conditions for the aldol condensation and cyclisation of 2-hexanone (**54**). Dean-Stark set up. * conversion by mass.

Entry	Catalyst	T / °C	t / h	Conversion of 54
1	MgO, KOH	150	9	0
2	MgO*	150	6	<5

It was hypothesised that the catalyst, which is hygroscopic in nature, may have taken on some water or that a stronger base was needed. To increase basicity, KOH was added, and the reaction heated at reflux for a further 3 hours. No product formation was observed again when analysed by TLC. To work-up the reaction, the reaction mixture was filtered to remove the catalyst and the solvent removed by rotary evaporation. The ¹H NMR spectra of the material recovered identified it as starting material with unidentified minor impurities.

As water is produced during the condensation reaction and the catalyst was in a previously opened bottle, the catalyst, MgO, was calcined for 2 hours at 450 °C prior to the second attempt (entry 2, Table 3) to enhance the surface area and drive off any water present which may have lowered the reaction yield. The reaction was repeated with the calcined MgO (entry 2, Table 3) and after 6 hours reflux a product spot was noted on the TLC. The reaction mixture was worked up however a much smaller than predicted amount of material was recovered. The ¹H NMR of the recovered material however showed starting material with a high level of impurities. As the yield was much lower than expected no further purification was carried out and a different catalyst was selected.

The hydrotalcite derived catalyst (Mg-Al-O) was selected to replace MgO because the catalytic screening by Sacia *et al* reported a 100% conversion of 2-hexanone, 93% selectivity to the target compounds and 7% formation of acyclic trimers which also have the α , β

unsaturated ketone needed for the addition of surfactant head group. Pre-treatment is required to activate at the hydrotalcite which was calcined at 700 °C for 2 h with an oven ramp rate of 2 °C and used within 2 hours of cooling. MgAlO was prepared in this way and used for the aldol condensation of **1** which led to a 57% conversion (entry 1, Table 4) which was lower than expected:

Table 4: Reaction conditions for the condensation of 2-hexanone (**54**). Conversion of **54** determined by GC-FID. MgAlO is hydrotalcite calcined at 700 °C for 2 h with an oven ramp rate of 2 °C prior to use. ** percentage conversion to total products calculated by mass without further analysis after removing remaining **54** through rotary evaporation until no further loss of mass.

Entry	T / °C	t / h	Apparatus description	Conversion of 54 /%
1	111	6	RBF with Dean-Stark arm	57 **
2	165	3	Pressure vessel	31 **
3	160	4	Pressure vessel	63
4	160	4	Pressure vessel	61

As commercial surfactants are commonly compound mixtures the expected level of impurity (7% from acyclic trimers) is acceptable for the end-product however higher purity is beneficial for structure identification and the overall yield is lower than expected.

The reaction set-up was altered for entry 2, Table 4 and a pressure vessel used in place of a Dean-Stark condenser with the aim to closely replicate the work done by Sacia *et al* using a Q-tube. Possible reasoning behind the lower yield may have been the ambient atmosphere and the temperature that can be achieved in a pressure vessel. A new batch of hydrotalcite was calcined to Mg-Al-O as the longevity of the catalyst was unknown and the previous yield was lower than expected. Greater care was taken in the storage of the hydrotalcite once calcined and the sample was stored in a vacuum desiccator and used within 2 hours of cooling. 2-Hexanone (**54**, 2 mmol), Mg-Al-O (200 mg) and toluene (3 mL) were charged into a 15 mL sealed steel pressure vessel and heated to 165 °C for 3 hours. However, the increase in temperature, pressure and handling of the catalyst did not improve the yield to the 100% conversion of 2-hexanone (**54**) and 93% cyclic trimers achieved by Sacia *et al*. The yield of total products (31% by mass) was lower than that achieved at reflux under ambient pressure (57%). The smaller scale of the reaction in the pressure vessel may also have been a factor responsible for a small drop in yield.

For entries 3 and 4 a new batch of hydrotalcite was calcined to Mg-Al-O using the same oven method as that described above however, instead of storing under vacuum the hydrotalcite was stored in the cooled crucible under parafilm and used within 5 hours, in another optimisation attempt. The reaction time was also increased to 4 hours to attempt to increase the yield. The yield for entry 3 (63%) was determined by GC-FID (to avoid any losses during work-up) and are close to entry 1 yield (57%). The discrepancy between these yields may have been due to work-up for entry 1. The reaction was repeated, entry 4, under the same reaction conditions using the same batch of Mg-Al-O and has a comparable yield of 61%.

The GC-FID masses were calculated using dodecane as an internal standard using the calibration curve shown in Figure 24:

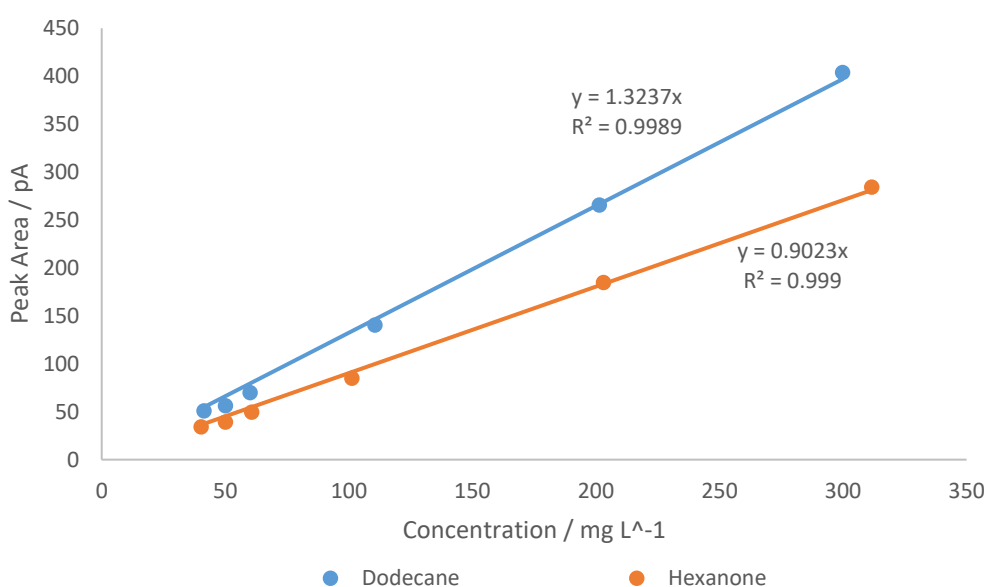


Figure 24: Calibration curve for starting material (hexanone) and internal standard (dodecane).

As the yields quoted by Sacia *et al* remained higher than those accomplished in this project, attention turned to the catalyst and its activation procedure. Hydrotalcite has a brucite-like structure which comprises of sheets of Mg-Al oxides with carbonate and weakly bonded water balancing charges in-between. Upon calcination, the removal of water and carbonate opens pores thereby increasing the surface area and revealing strong (O_2^-) medium (Mg-O) and weak (OH^-) basic sites and mild Lewis acid sites which drastically increases its catalytic

activity.¹⁹³ The mass lost on calcination under an inert N₂ atmosphere was observed by thermogravimetric analysis to be 45%.

The choice of calcination temperatures has previously shown minimal effect on surface area and pore sizes but a significant effect on the basicity. Hydrotalcite derived catalysts have tuneable basicity to an extent *via* the choice of calcination temperatures. It has been found that the basicity correlates with the catalytic activity of Guerbet conversion of ethanol to 1-butanol, aldol condensation of acetaldehyde and heptanal and methanolysis of soybean oil.¹⁹⁴⁻¹⁹⁶

To further understand the effect of handling the catalyst after calcination, the effect of exposure of the catalyst to CO₂ was investigated. The catalyst, Mg-Al-O, is derived from hydrotalcite, Mg₆Al₂(CO₃)(OH)₁₆•4H₂O, thus removal of carbonate is a key part of the catalysts preparation and it follows that reformation of carbonate species would deactivate the catalyst. The calcination of hydrotalcite replicated exactly the method reported in a 2015 paper by Sacia *et al*¹⁷⁰: 700 °C for 2 hours with an oven ramp rate of 2 °C / min (Table 5).

Table 5: Catalyst treatment after calcination at 700 °C for 2 h with an oven ramp rate of 2 °C. Reagents and condition: 2-hexanone (compound **54**, 2 mmol), toluene (3 mL) and 200 mg of catalyst reacted under pressure at 170 °C.

Entry	Catalyst	T / °C	t / h	Apparatus description	Conversion of 54 /%
1	Mg-Al-O _a Used immediately after calcination	170	3	Pressure vessel	63
2	Mg-Al-O _b CO ₂ treated before use	170	3	Pressure vessel	65
3	Mg-Al-O _c stored on the benchtop for 24 h before use	170	3	Pressure vessel	74
4	Mg-Al-O stored on bench for 48 hours	150	3	Q-tube	92

Therefore, it was hypothesised that instead we may have reformed carbonates due to how the catalyst was handled after the initial activation. The MgAlO catalyst used to produce the reaction yields shown in Entry 1 of Table 5 was removed from the oven at 200 °C, quickly weighed and transferred to a flask containing toluene and hexanone and produced a yield of: 63% yield with 33% hexanone remaining. The catalyst used for entries 2 and 3 (Table 5) were removed from the oven at 200 °C and quickly transferred to a sample vial and stored in a vacuum desiccator until cool. Entry 2 catalyst was subsequently treated with CO₂ in an attempt to replicate prolonged exposure to the atmosphere. The catalyst was put into a porous thimble and charged with supercritical CO₂ at 150 bars for 1 hour before use, resulting in a condensation product yield of 65% with 33% hexanone unreacted. The catalyst used for entry 3, once cooled in the vacuum desiccator, was left on the bench outside the vacuum desiccator for 24 h prior to reaction and produced a 74% yield with 23% hexanone unreacted.

The similarity in conversion of 2-hexanone in entries 1 and 2 (Table 5), despite the CO₂ treatment of one of the samples, suggests that the catalytic activity is not linked to carbonate adsorption due to air exposure but may be linked to exposure to moisture during cooling. To expose the catalyst to more moisture, the catalyst sample was left for another 24 hours on the benchtop before use. A similar yield to that reported by *Sacia et al* was achieved suggesting that the moisture rather than exposure to CO₂ played a role in activating the catalyst.

Further investigation into the literature led to a greater understanding in the process of exposing the basic sites on the catalyst needed for the aldol condensation. As mentioned previously the thermal decomposition of double-layered lamellar type structures, such as hydrotalcite, removes water and carbonate counterions leaving a well dispersed mixture of metal oxides. This process changes the crystal structure of the material. If the material is exposed to a carbonate-free water atmosphere, the metal oxides show a memory-like effect in which the lamellar structure is reformed. This leads to meixnerite (magnesium aluminium oxides hydrate) with OH⁻ sites interlaced in the material.¹⁹⁷ The catalytic ability of meixnerite is related to the basicity of the material, which is determined by two key factors: temperature of calcination and method of rehydration. The basicity can be measured by temperature programmed desorption of CO₂ (CO₂-TPD) and is a common method for mixed oxides derived from hydrotalcite.^{193, 194, 198} This method is based on the absorption of different species of CO₂, monodentate, bidentate and bicarbonate ions.

Monodentate and bidentate carbonate formation requires low co-ordinate oxygen anions whereas bicarbonate require surface hydroxy groups.

The difference in calcination temperature causes a significant effect on basicity due to the formation of the lamellar-type structure. At lower temperatures there is an increased likelihood of the formation of a spinel-like phase for example MgAlO_4 , the memory-like reconstruction of the lamellar phase is dependent on the presence of this spinel-like phase. Once the carbonate-free lamellar-type structures have been achieved active OH^- sites can be introduced. The ratio of active to non-active OH^- sites, related strongly to basicity and therefore catalytic activity, is determined by the hydration method. Although the structure-activity relationship of meixnerite is not well understood, an investigation into two rehydration methods was done by Corma *et al*^{199, 200}. The investigation focussed on two methods of rehydration, gas phase and liquid phase. The gas phase introduced water vapour in a carbonate-free environment using nitrogen as a carrier gas. This method relies on the diffusion of water vapour through the material to form OH^- sites. Calcined material rehydrated *via* the gas phase method resulted in a reduction of the porosity of the material compared to the calcined reference material, exhibiting a low BET surface area (from 253 to $57 \text{ m}^2 \text{ g}^{-1}$) and pore volume of ($0.1 \text{ cm}^3 \text{ g}^{-1}$). This has been seen to produce a low number of active OH^- sites and therefore a low activity catalyst. During liquid phase rehydration a mechanical flea is used to mix the solid material with water in a carbonate-free environment. Rehydration *via* liquid phase has been seen to exhibit a remarkable BET surface area of ($270 \text{ m}^2 \text{ g}^{-1}$), a significant increase compared to the calcined reference. This change in the porosity and the BET surface area can be linked to the method of rehydration. The change in the porous characteristics is theorised to be due to the exfoliation of the meixnerite crystals during the stirring of the solution. The stirring of the solution results in a disruption of the crystallinity and therefore an increase in the surface area of the material.

The increase in the surface area in turn increases the proportion of active OH⁻ sites (Figure 25):

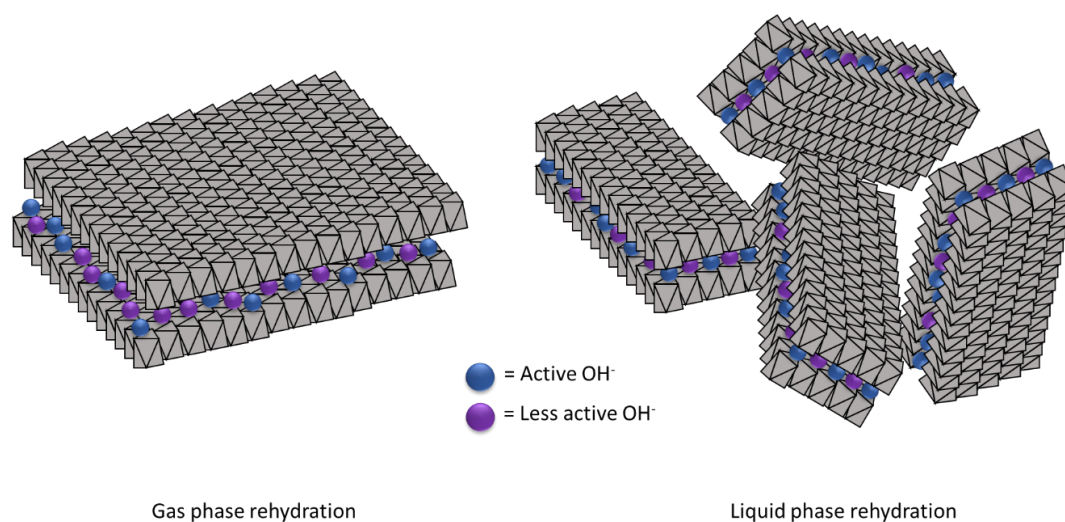


Figure 25: Schematic representation of crystal structure of Mg-Al-O after rehydration *via* liquid phase (top) and gas phase (bottom).¹⁹⁷

De Jong and co-workers²⁰¹ stated that only 5% of the hydroxy ions of the rehydrated samples are active enough to play a role in the reaction. This supports the theory of decreased crystallinity of the material and therefore, an increase in the number of edges of the crystals and sites where active OH⁻ ions are able to play a role in the reaction. The total number of basic sites was found to be higher after rehydration *via* the liquid phase (803.9 mmol g cat⁻¹) than the gas phase (437.7 mmol g cat⁻¹).

Although the temperature of the calcination is a key factor in the overall activity of the catalyst, the rehydration method also has a large impact on the overall activity of the final catalyst and this linked to basicity of the meixnerite. Ablo *et al*¹⁹⁷ determined that there were three main components that have an impact: crystallinity, rehydration and porosity or surface area. The calcination and removal of carbonate gives the metal oxide skeletal structure in which the OH⁻ counterions can be re-introduced into the lamellar phase structure. Using the liquid phase rehydration method to disrupt the crystallinity and reveal a greater surface area with more active OH⁻ sites forms an active catalyst for aldol condensations.

The catalyst treatment described by Sacia *et al*¹⁷⁰ stated that hydrotalcite be calcined under static air at 700 °C for 2 hours with an oven ramp rate of 2 °C. Based on the findings discussed above, using this calcination method fails to re-introduce water to create OH⁻ basic sites and therefore decreases the potential catalytic effect. Allowing rehydration through leaving the catalyst open to the air for 48 hours may explain the differences in yield between this study and theirs.

To study the effect of the liquid rehydration method discussed above 36% water (relative to the hydrotalcite mass) was added to the reaction vessel and another reaction under the same conditions was run without the presence of water. Conversion and the percentage of each product relative to total products is shown in Figure 26:

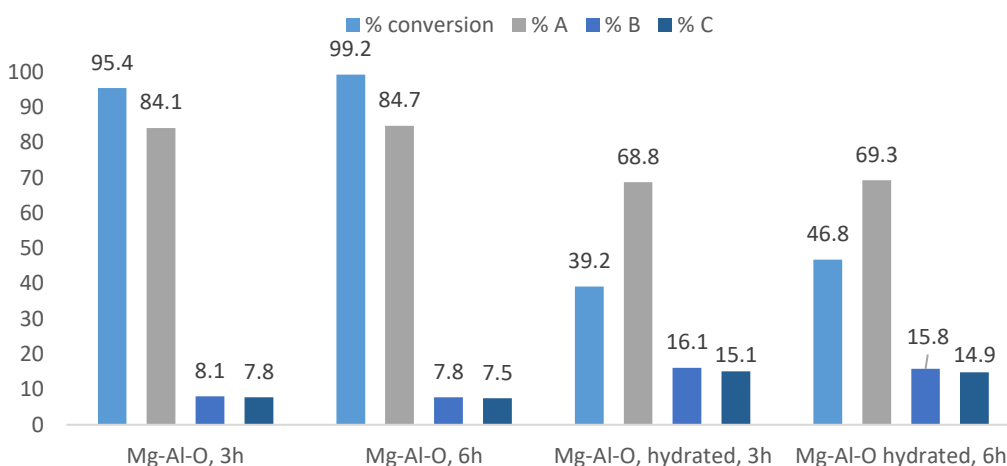


Figure 26: Effect of water addition to catalyst. % conversion = conversion of 2-hexanone. % A = major cyclic isomer. % B minor cyclic isomer, %C minor cyclic isomer.

As seen in Figure 26, the addition of liquid water to the catalyst decreased the conversion of 2-hexanone from 95.4% to 39.2% over 3 hours. Over 6 hours the conversion improved slightly to 46.8%. The addition of water also increased the ratio of trimers produced, doubling the percentage of the two minor isomers, and reducing the percentage of products from the major isomer from 84% to 69%. As aldol condensations produce water and their products are often in equilibrium, it is likely that the reduction in 2-hexanone conversion (54), when additional water is present, is due to the effects of Le Chatelier's principle.

As toluene is a petrochemically based solvent; hence, greener solvents were considered for this reaction. 2,2,5,5-tetramethyloxolane (TMO) is a recently developed solvent designed as a replacement for toluene.²⁰²⁻²⁰⁴ TMO was investigated as a drop-in replacement for toluene. In this case TMO reduced the conversion of 2-hexanone (**54**) after 3 hours by 32.1% and altered the distribution of products (Figure 27):

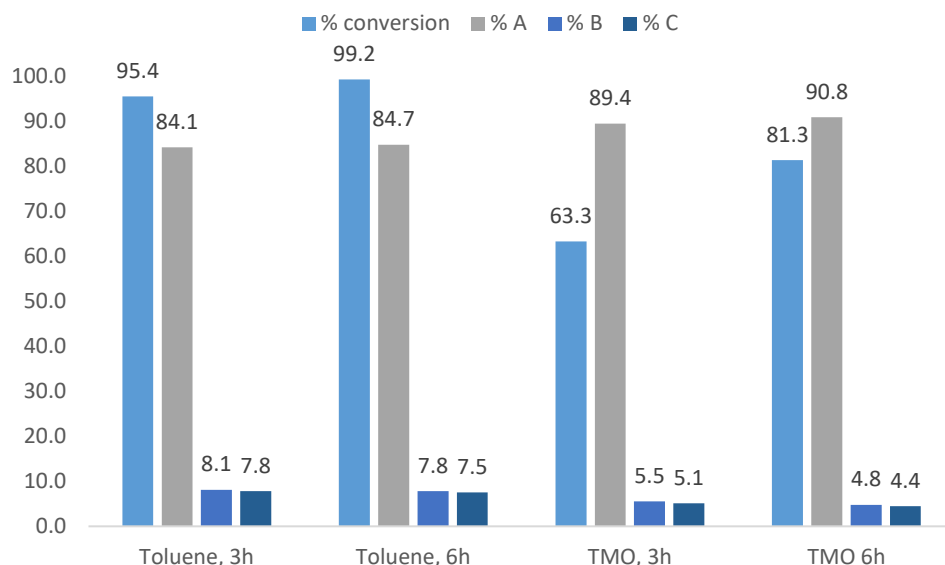


Figure 27: Investigating a greener solvent replacement for toluene. % conversion = conversion of 2-hexanone (**54**). % A = major cyclic isomer. % B minor cyclic isomer, %C minor cyclic isomer.

As seen in Figure 27, the selectivity to the major isomer was increased by 5.3% over 3 hours and 5.9% over 6 hours however the conversion of 2-hexanone (**54**) significantly decreased by 32.1% over 3 hours. The yield can be somewhat recovered by longer reaction times, after 6 hours the conversion of **54** increased to 81.3% using TMO. The reduction in yield and the need for greater energy consumption through heat produced over longer reaction times means TMO is not an ideal drop-in replacement for this reaction (for reaction see Scheme 23 or Table 2).

2.5 STRUCTURAL IDENTIFICATION OF COMPOUND 56

2.5.1 Infrared spectroscopy

A notable difference between the IR spectra of 2-hexanone (**54**) and the crude isolated products of RD130 is the addition of the absorption at 1618 cm^{-1} , which can be assigned to a C=C stretch of an α,β unsaturated ketone (Figures 28 and 29, Table 6) which is characteristically lower in frequency than that expected of non-conjugated alkenes.

This is accompanied by a shift in the frequency of the C=O bond stretch from 1714 cm^{-1} characteristic of a typical aliphatic ketone to 1687 cm^{-1} for the conjugated α,β -unsaturated ketone. There also appears to be a decrease in intensity of the C=O as the ratio of C=O to C-H changes from 1:12 in 2-hexanone (**54**) to 1:32 in compound **56** and **56a**. This indicates the formation of compounds **56** and **56a**.

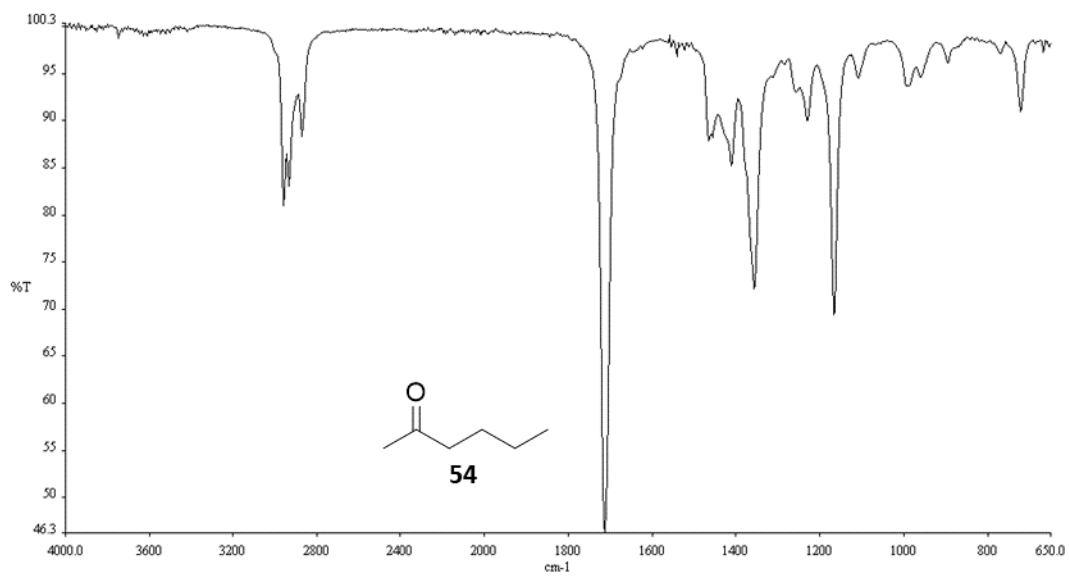


Figure 28: Infrared spectra of 2-hexanone (54).

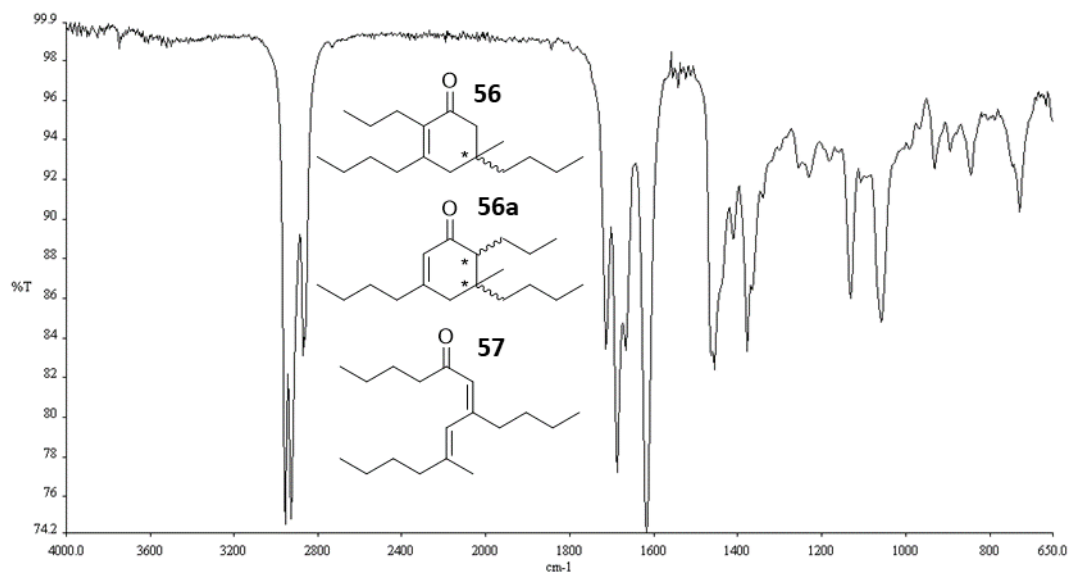
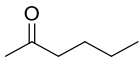
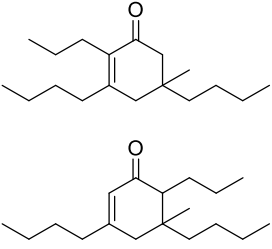


Figure 29: Infrared spectra of a mixture of compounds 56, 56a and 57.

Table 6: Infrared spectral data and assignments for 2-hexanone (**54**) and compound **56/56a**.

Compound	Absorption / cm^{-1}	Transmission / %	Group	Environment
 54	2959	81	C-H	Stretch - alkane
	2934	83	C-H	Alkane
	2874	88	C-H	Alkane
	1714	46	C=O	Aliphatic ketone
	1465	87	C-H	Bending - alkane
 56, 56a	2957	74	C-H	Stretch - alkane
	1714	83	C=O	Aliphatic ketone
	1687	77	C=O	Conjugated ketone
	1618	74	C=C	Stretch - α,β -unsaturated ketone
	1378	83	C-H	Bending - alkane

2.5.2 Gas chromatography and mass spectrometry

The GC-FID spectrum shows 2-hexanone (**54**, boiling point 127 °C) eluting from the column at 2.56 minutes (Figure 30):

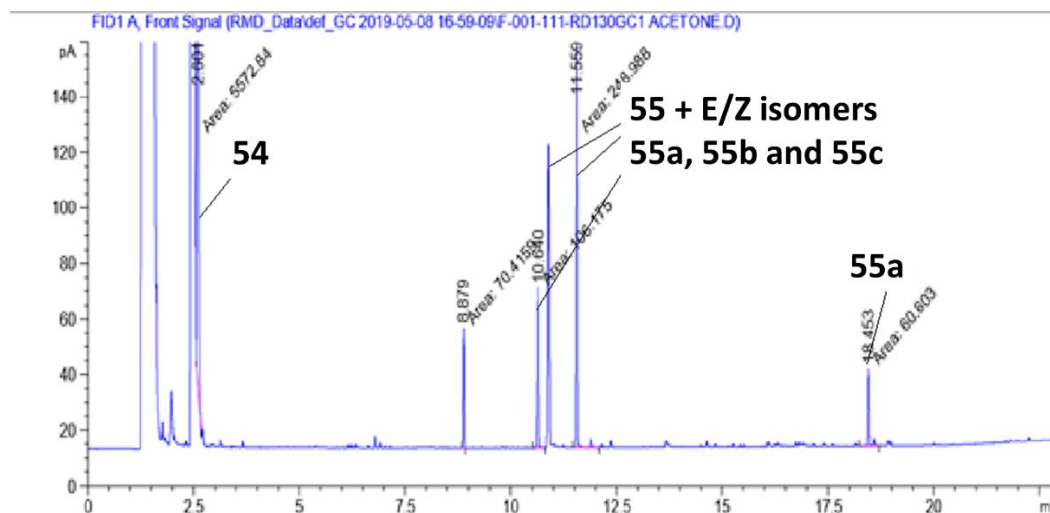


Figure 30: GC-FID chromatogram for reaction mixture, Table 5, Entry 4, in acetone.

As seen in Figure 30, the spectrum also shows 3 peaks eluting between 10.5 minutes and 11.5 minutes, assumed to be dimers of 2-hexanone (**55**). 2-Hexanone (**54**), dimers and trimers (**55**, **56**) were identified by GC-MS and results displayed in Figure 31:

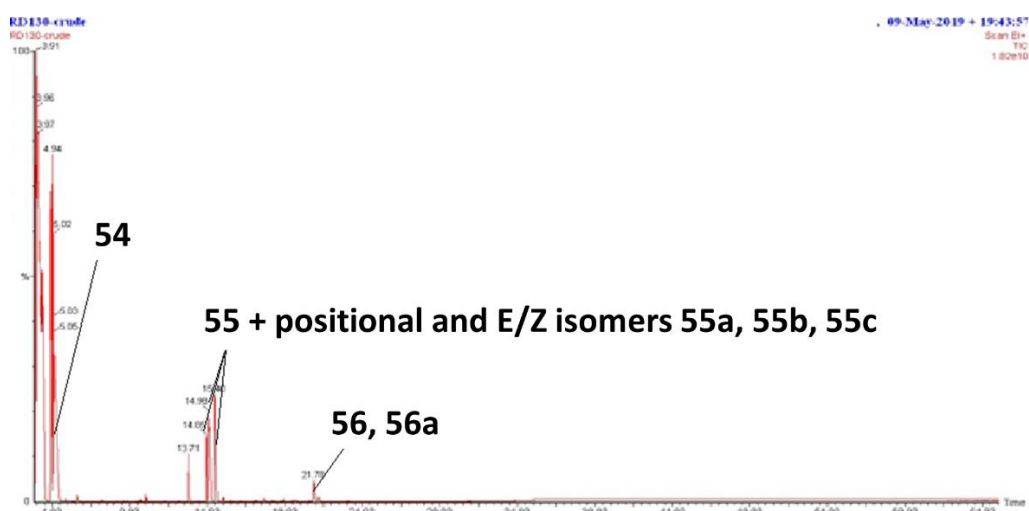


Figure 31: GC-MS Chromatogram for RD130 crude reaction mixture.

The GC-MS indicates the expected mass from the molecular ion peak of the dimer ($C_{12}H_{22}O$) at 182 m/z (Figure 32):

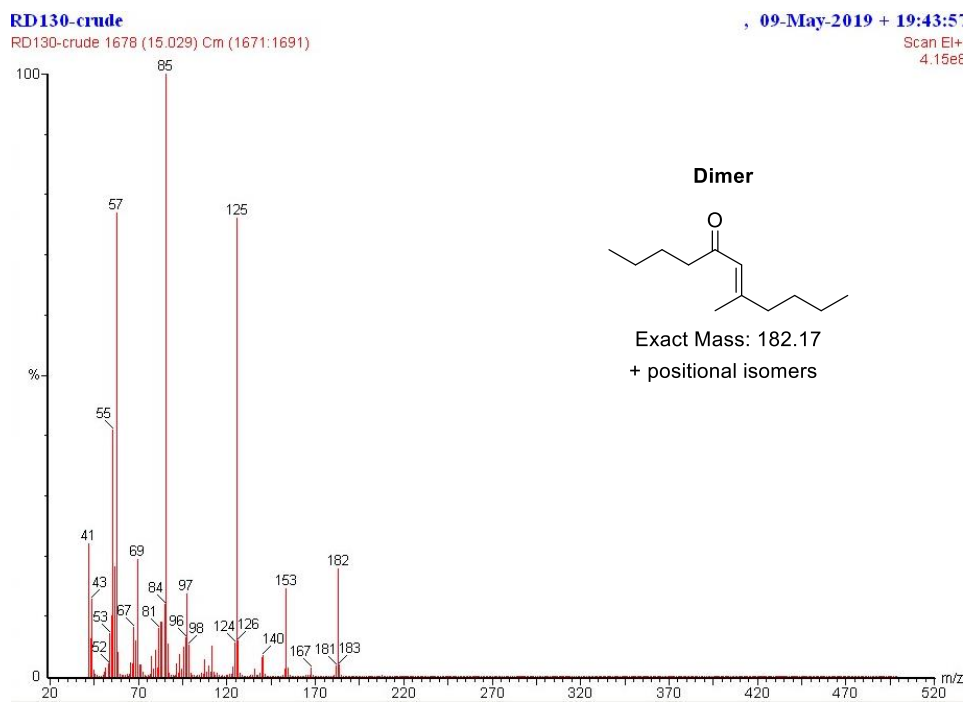


Figure 32: Mass spectra for the peak of dimer from the GC-MS chromatogram.

The elution at 18.45 minutes expected to be trimer ($C_{18}H_{32}O$) has the expected molecular of 264 m/z shown in Figure 33:

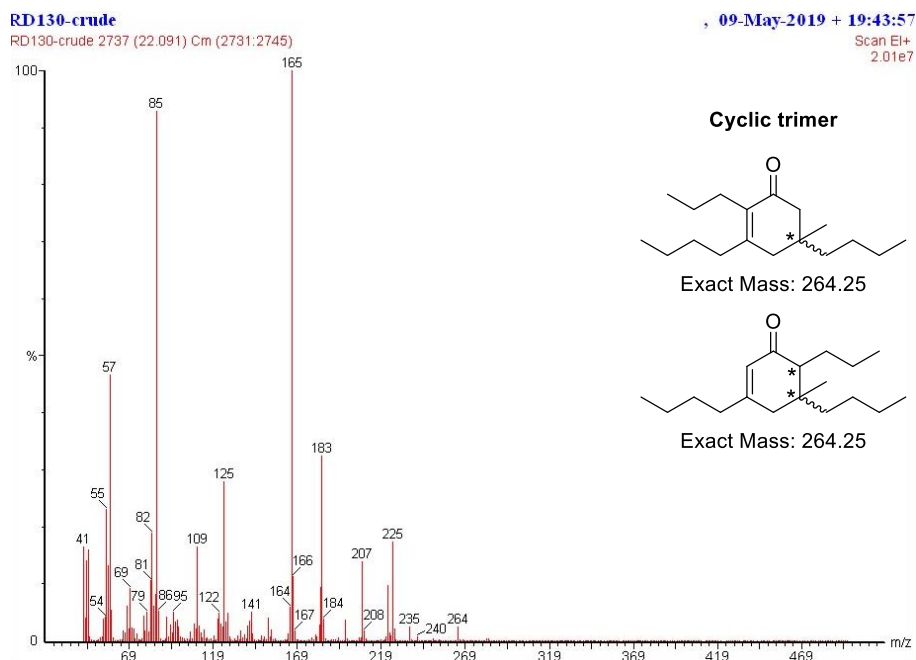


Figure 33: Mass spectra for the peak of trimer from the GCMS chromatogram.

2.5.3 NMR spectroscopy

An NMR spectrum was recorded after Kugelrohr distillation purification of the 2-hexanone (**54**) cyclisation products (Figure 34):

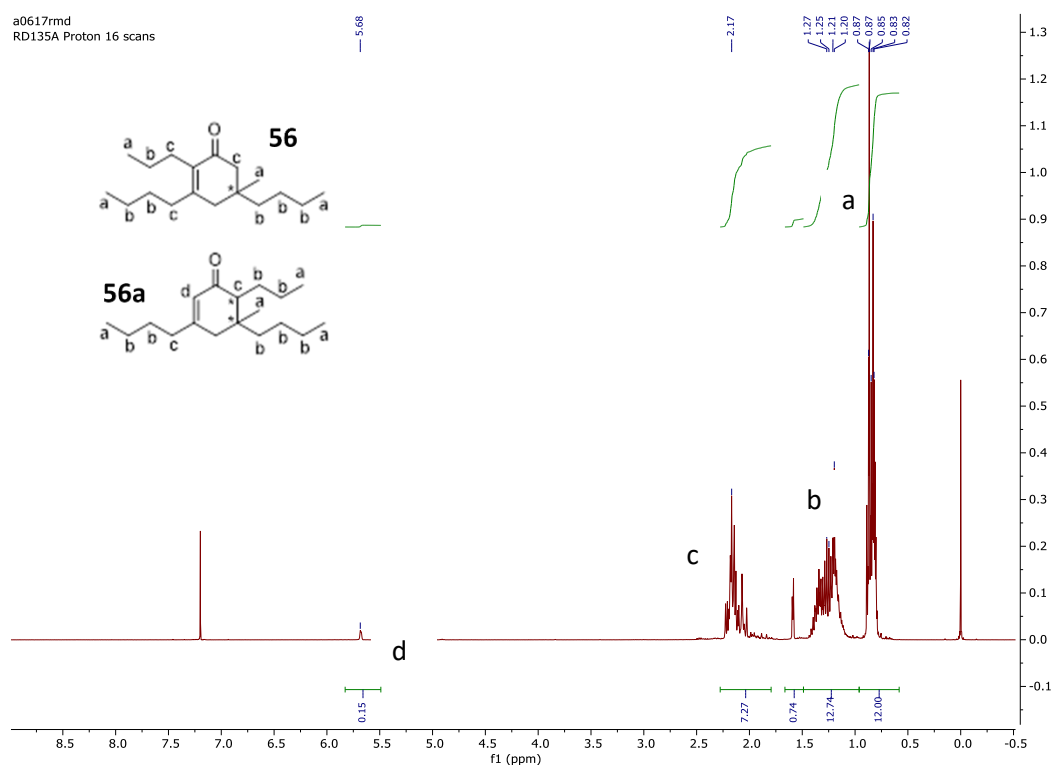


Figure 34: ¹H NMR of product compounds **56**, **56a** (400 MHz, Chloroform-d) δ 5.68 (s, 0.15H), 2.28-1.79 (m, 7H), 1.49-0.96 (m, 13H), 0.96-0.58 (m, 12H).

The NMR spectra shows a mixture of **56** and **56a** and no further separation was attempted. However, the NMR of the pure compounds **56** and **56a** are shown in the supplementary information from the Sacia's paper.¹⁷⁰

The ¹H NMR spectrum assignments can be made based on the level of carbon substitution. Protons on the primary carbons, -CH₃ (a), present in the 0.5-1.0 region. Protons on the secondary carbons, -CH₂- (b), in the 1.0-1.5 region and protons on the tertiary carbons, CH (c), found in the 1.7-2.3 range. Proton d is found only in compound **56a** is easily distinguishable at 5.68 due to the adjacent C=C.

As there are 12 methyl protons at 0.96–0.58 ppm for both compounds, comparison of the integration of proton d shows that compound **56** (no alkene protons) is present at 85% purity with 15% compound **56a** (1 alkene proton) (Figure 35):

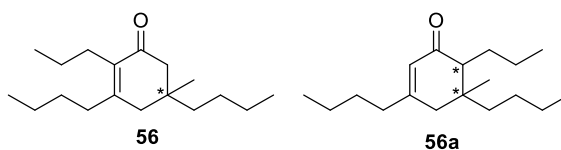
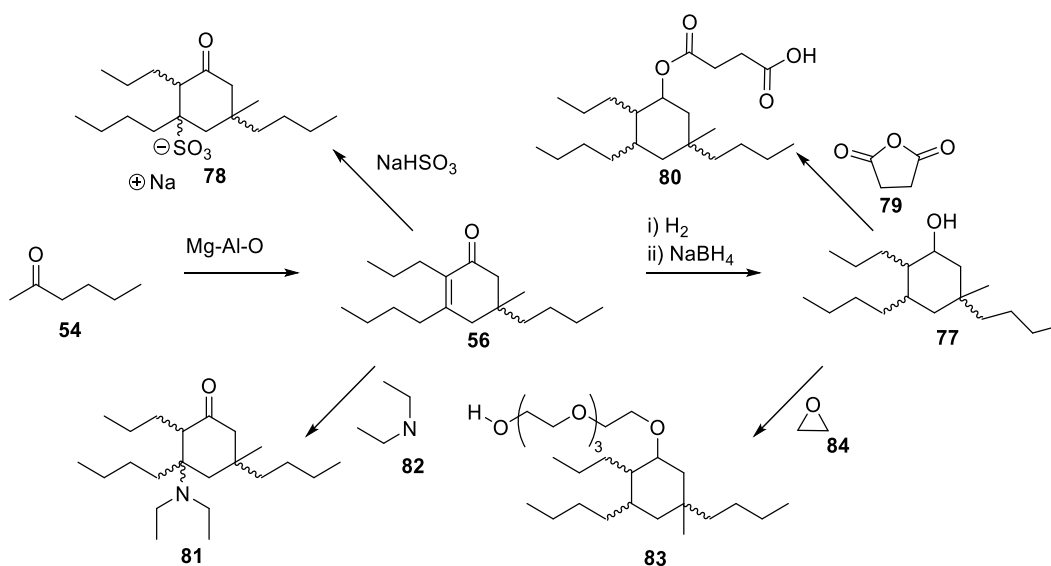


Figure 35: The structure of compound **56** and **56a** with ^1H NMR assignments. * represents the chiral centre.

Further assignment is difficult for compound **56** because it is a mixture of 2 diastereoisomers. It is not surprising that there are significant overlaps in the signals which makes full assignment of the proton NMR difficult.

Following the study on the activation of the catalyst and potential greener solvent replacement compound **56** and its isomers were successfully synthesised at large scale. The next steps involve exploring synthetic routes shown in Scheme 27 to add traditional surfactant head groups. The Michael accepting nature of the α,β -unsaturated ketone (Scheme 27) is expected to enable addition of amines as a precursor to quaternary amines (cationic surfactants) and for addition of bisulfite as a route to sulfonated surfactants (anionic surfactants). A route is also available through the hydrogenation and reduction of the α,β -unsaturated ketone to alcohol and the addition of poly (ethylene glycol) via ester linkage.



Scheme 24: Synthetic routes to surfactants from compound **56**

2.6 CYCLISATION OF 2-NONANONE (**90**) AND 2-DODECANONE (**93**)

Once compound **56** was successfully synthesized experiments began on aldol condensations of longer chain fatty methyl ketones (Figure 36):

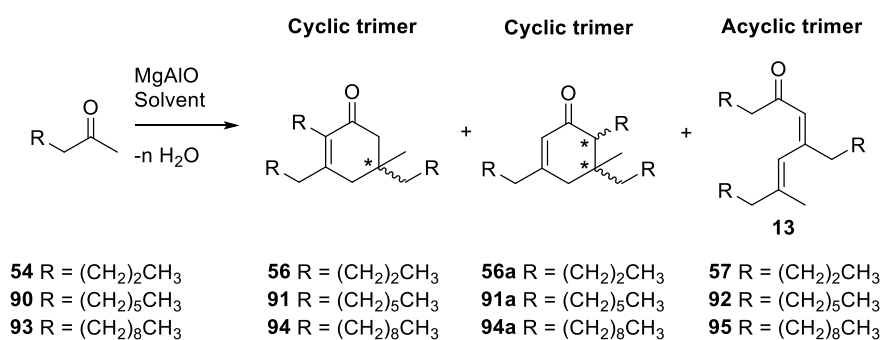


Figure 36: Key reaction products of 2-hexanone (**54**), 2-nonanone (**90**) and 2-dodecanone (**93**).

Nonanone (**90**) was selected as the starting material for the self-aldol condensation because this would extend each of the three branches of the cyclic structure (**56**) by three carbons. Therefore compound **91** would have an additional 9 carbons compared to the double aldol condensate of **54**. This was expected to improve hydrophobicity. Similarly, dodecanone (**93**)

was selected to extend compound **56**'s branches by another 9 carbons, producing compound **94**.

The method from the aldol condensation of 2-hexanone (**54**), was carried over to the attempted aldol condensations of **90** and **93**. The starting material, catalyst and toluene were charged into a round bottomed flask and set to reflux with a condenser and a Dean-Stark arm. The reflux was maintained for the duration of the specified reaction time (see Table 7) and then allowed to cool. Once cool the catalyst was removed by filtration and the solvent removed by rotary evaporation.

The reaction conditions for the initial attempts to synthesise the cyclic aldol condensates (**91**, **94**) of nonanone (**90**) and dodecanone (**93**) are described in Table 7:

Table 7: Reaction details of nonanone (**90**) and dodecanone (**93**) aldol condensations. * Calcined at 450 °C for 2 hours prior to reaction.

Entry	Starting material	Mass of starting material / g	Catalyst	Mass of catalyst / g	Volume of toluene / mL	t / hours	Conversion of starting material / %
1	90	5.60	MgO*	2.30	25	16	<5%
2	93	2.14	MgO*, KOH	2.1, 0.11	15	16	<5%
3	90	5.61	KF/Al ₂ O ₃	3.91	25	6	<5%
4	90	5.82	CaCO ₃	3.83	25	6	<5%
5	90	5.54	MgAlO*	3.81	25	6	<10%
6	90	0.29	MgAlO*	0.25	3	3	<10%

MgO, CaCO₃ and KF/Al₂O₃ were trialled as Lewis bases but produced very poor conversion of the starting material. Less than 5% of the expected mass for each was obtained as crude product with no further purification. Calcined hydrotalcite (MgAlO) was identified by Sacia *et al.* as the catalyst providing the highest conversion and so this was also used (entries 5 and 6, Table 7) which again returned a poor yield of crude product <10% of the expected mass. As toluene is the solvent used by Sacia and co-workers its boiling point of 110 °C is well below the reaction temperature of 160 °C specified it was theorised that pressure may be required for this reaction and so an experiment was conducted under pressure to the

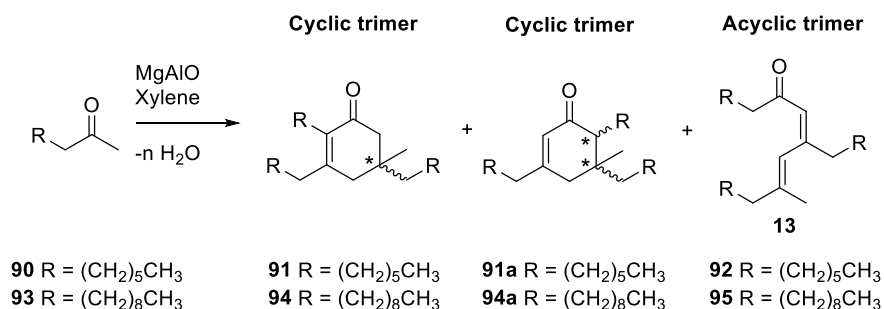
specifications of the small-scale reaction carried out by Sacia.¹⁷⁰ This too however, provided poor yields of crude product.

Additionally, the shape of the resulting surfactant produced from this hydrophobe may be problematic as the tail group size and position of the head group would not be ideal for packing and may encourage reverse micelles.

As described previously compound **56a** and its isomers were successfully synthesised at small scale, however the yields reported in the literature were not achieved and it was speculated that either the specific equipment used by Sacia *et al* (Q-tube) may have been necessary to achieve those yields or a key piece of information had not been disclosed. Since making this conclusion a Q-tube of the same dimensions reported by Sacia *et al* was purchased to examine the effects.

The condensation of 2-nonanone was investigated alongside 2-hexanone because the longer carbon chain length is likely to produce a more hydrophobic cyclic trimer. A number of catalysts were used, and yields were either low or TLC did not confirm products. The catalysts used to carry out the cyclisation were MgO, KF / Al₂O₃, CaCO₃ and Mg-Al-O. None of these catalysts gave a satisfactory yield under the conditions described in Table 7.

The aldol condensation of 2-nonanone and 2-dodecanone (**90**, **93**) were trialled in xylene at reflux to allow a higher reaction temperature.



Scheme 25: Aldol condensation of 2-nonanone and 2-dodecanone (**90**, **93**)

The higher reaction temperature for the aldol condensation of 2-nonanone (**90**) led to a 98% yield. The higher reaction temperature did not have an effect on the reaction of 2-dodecanone (**93**) which was followed by TLC and did not show consumption of **93** or the appearance of products.

2.7 ADDITION OF HEAD GROUPS

2.8 AMINATION

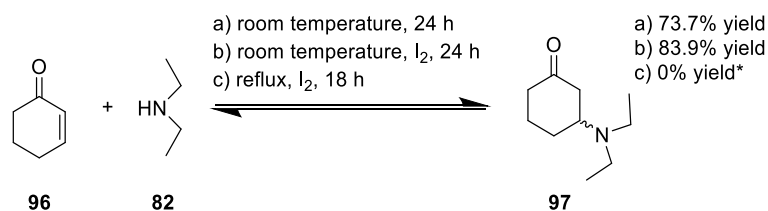
Aza Michael additions are well known C-N bond formation reactions which utilize the electron deficiency at carbon 3 caused by the ketone.²⁰⁵ This creates an electrophilic site on which to add an amine as a precursor to a quaternary ammonium surfactant. The nature of these reactions lend themselves to green chemistry as they are simple addition reactions they benefit from good atom economies and often produce better yields at lower temperatures than at high temperatures.

There are many catalysts in the literature for the aza-Michael addition of amines to α,β -unsaturated carbonyls including molecular iodine, alumina, SnCl₄, AlCl₃, TiCl₄ and combinations of aniline or pyridine with various MOFs, K₂CO₃, KF/Al₂O₃ and DMAP.²⁰⁶⁻²⁰⁸ For this set of reactions molecular iodine was chosen as it is relatively inexpensive and successful use of I₂ has been reported in the literature for 1,4 addition of amines to α,β -unsaturated ketones and esters.^{184, 207, 209, 210} More traditional metal catalysts (SnCl₄, AlCl₃, TiCl₄) can lead to the generation of environmentally damaging waste streams.²⁰⁷

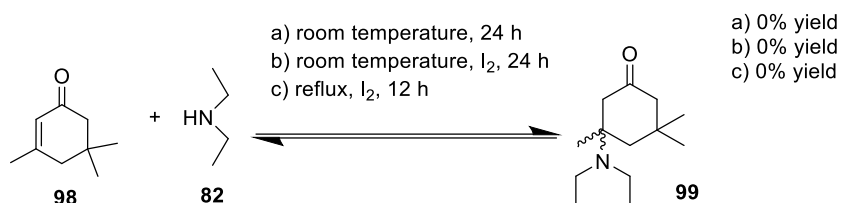
The proposed mechanisms for iodine catalysis are via hidden Bronsted base catalysis, Lewis acid catalysis or catalysis by iodonium.^{211, 212} Molecular iodine can be used to activate α,β -unsaturated carbonyls for nucleophilic attack through Lewis acid catalysis/halogen bond catalysis²¹² and in some cases performs better than traditional Bronsted acids.^{210, 213}

Previous work by Borah *et al* found that aliphatic amines undergo aza-Michael addition onto a range of α,β -unsaturated carbonyl compounds under mild conditions in the presence of iodine however no work was reported on α,β -unsaturated ketones.²⁰⁷

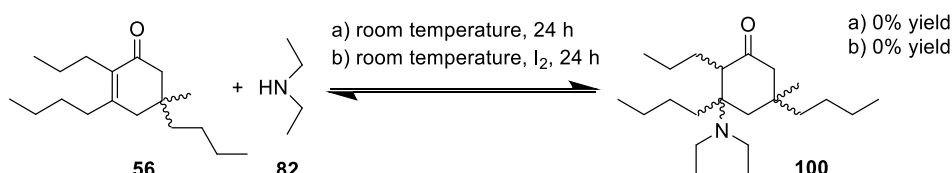
Aminations of cyclohexanone (**96**), isophorone (**98**) and compound **56** with diethyl amine are shown in Schemes 29-31:



Scheme 26: Amination of cyclohexenone (3 mmol) (**96**) with excess diethyl amine (**82**, 24 mmol). Solvent free reaction with stirring. Yields determined by GC-FID analysis of reaction mixtures *100% conversion of cyclohexenone with 0% selectivity to the desired product.



Scheme 27: Amination of isophorone (2.4 mmol) (**98**) with excess diethyl amine (**82**, 19 mmol). Solvent free reaction with stirring. Yields determined by GC-FID analysis of reaction mixtures.



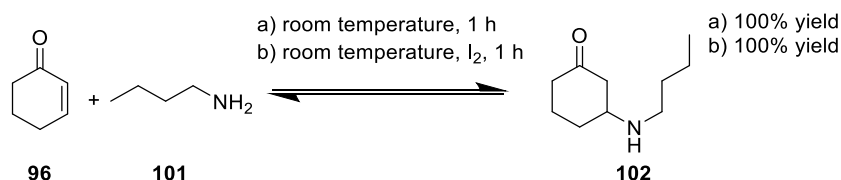
Scheme 28: Amination of compound **56** (1.5 mmol) with excess diethyl amine (**82**, 12 mmol). Solvent free reaction with stirring. Yields determined by GC-FID analysis of reaction mixtures.

Mild conditions for the addition of diethyl amine (DEA, **82**) to compound **56** with iodine as a catalyst did not yield the desired product (compound **100**). As a result of this cyclohexenone (**96**) and isophorone (**98**) aminations were studied, to better understand if the iodine catalyst was active for addition to cyclic α,β -unsaturated ketones and the effect of steric hindrance through use of inexpensive and readily available isophorone.

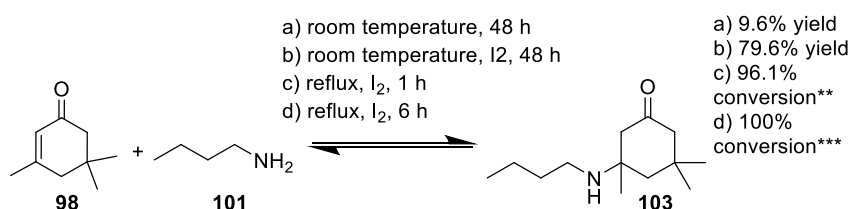
At ambient temperature the 1,4 addition of DEA (**82**) to cyclohexenone (**96**) in the presence of iodine gave a yield of 83.9% (compound **97**). This was a 10% increase compared to the same reaction conditions without a catalyst, an indication that iodine has some effect on

the yield. The reaction was also carried out at reflux. The conversion from starting materials to products with catalyst at reflux was 87.5% however the desired product peak was not present and retention times suggest that further reactions have taken place to heavier compounds with later retention times. This is evidence that the product is not stable at high temperatures.

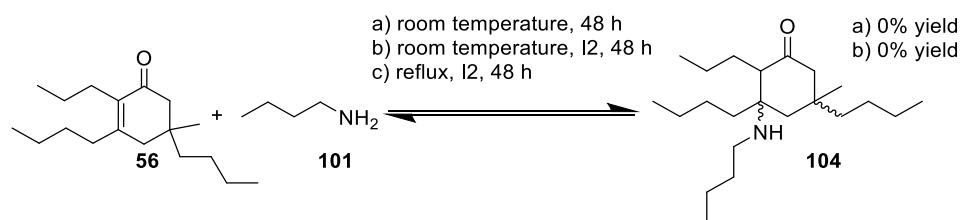
Addition of DEA to isophorone (**98**) and **56** was unsuccessful at room temperature or under reflux in the presence of iodine. It is hypothesised that the products of these reversible reaction were under too much steric hindrance to be favourable. To address this issue a primary amine, butyl amine (BA, **101**) was selected and subjected to the same reaction conditions (Schemes 32-34):



Scheme 29: Amination of cyclohexenone (3 mmol) (**96**) and excess butyl amine (24 mmol)(**101**). Solvent free reaction with stirring. Yields determined by GC-FID analysis of reaction mixtures.



Scheme 30: Amination of isophorone (2.4 mmol) (**98**) and excess butyl amine (19 mmol)(**101**). Solvent free reaction with stirring. Yields determined by GC-FID analysis of reaction mixtures. **96.1% conversion of starting material with 33% selectivity to the desired product **100% conversion of starting material with 31% selectivity to the desired product.



Scheme 31: Amination of **1** (1.5 mmol) (**56**) and excess butyl amine (15 mmol) (**101**). Solvent free reaction with stirring. Yields determined by GC-FID analysis of reaction mixtures.

Without the need of catalyst cyclohexenone (**96**) was fully converted to compound **102** after 1 hour at room temperature. Isophorone required much longer reaction times at ambient temperature producing a low yield of compound **103** after 48 hours. Catalytic iodine (0.2 mol% w.r.t.) much improved the yield at room temperature from 9.6% to 79.6% yield after 48 hours in the presence of iodine. At reflux full conversion of **98** was achieved after 6 hours however at the elevated temperature (78 °C) selectivity to **103** was reduced to 33%. These yields suggest that iodine is acting as a Lewis acid to catalyse the reaction and that the use of a primary amine in place of a secondary much improves the steric hindrance.

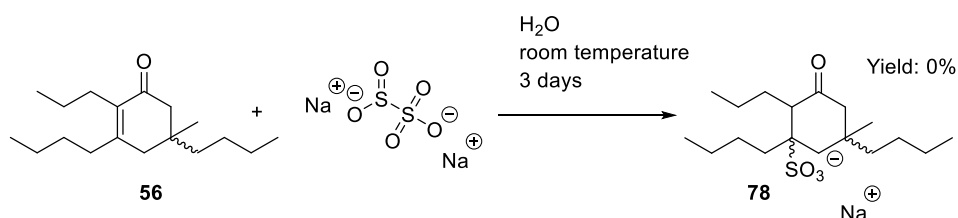
Based on these findings it was expected that compound **56** would require a catalyst and as predicted, compound **104** was not formed at room temperature after 48 hours without one. However, the presence of iodine did not overcome the steric hindrance as seen with isophorone and the addition of butylamine onto **56** did not go at room temperature or at reflux. If steric hindrance is blocking reactivity at carbon 3 of **56** it may be more feasible to attack at carbon 1 or attack with a smaller nucleophile.

The addition of amines to the α , β -unsaturated ketone of compound was unsuccessful. This is possibly due in part to steric hinderance around the alkene bond or deactivation of the site due to the inductive effect pushing electron density towards carbon 3 and therefore decreasing the δ^+ and making this site less accepting of nucleophiles. Addition of amine to the ketone may be possible through reductive amination. The addition of 4-methoxy-aniline to sterically hindered camphor was possible under conditions reported by Podyacheva²²⁴ and the use of Rh/CO as a catalyst. There is the possibility of further work to look at the reductive amination of **56** with the same catalyst and conditions.

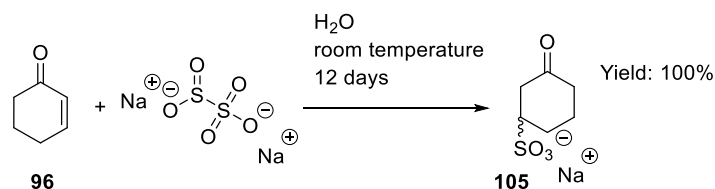
2.9 SULFONATION

Sulfonation through Michael addition of metabisulfite and bisulfite to unsaturated ketones benefits from the same good atom economies and preference for lower temperatures as the aza Michael additions, and are also well established.²¹⁴⁻²¹⁶ However a key difference is that the sulfonation with sodium metabisulfite/bisulfite is the final synthetic step whereas the aza Michael additions require another synthetic step to quaternise.

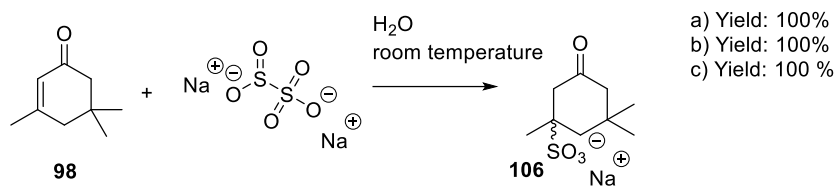
In this study, the sulfonation of compound **56**, cyclohexanone and isophorone are shown in Schemes 35-37:



Scheme 32: Sulfonation of **56** (4 mmol) with sodium metabisulfite (4 mmol) in aqueous solution (10 mL deionised water) with stirring. Solvent removed by rotary evaporation before analysis by FT-IR and ^1H NMR.



Scheme 33: Sulfonation of cyclohexenone (**96**) (3 mmol) with sodium metabisulfite (3 mmol) in aqueous solution (2.5 mL deionised water) with stirring. Solvent removed by rotary evaporation before analysis by FT-IR and ^1H NMR.



Scheme 34: Sulfonation of isophorone (**98**) (2 mmol) with sodium metabisulfite (2 mmol) in aqueous solution (2.5 mL) deionised water with stirring. Solvent removed by rotary

evaporation before analysis by FT-IR and ^1H NMR. Conditions: a) H_2O , room temperature, 30 minutes with ultrasonic probe (RD187-A) b) H_2O , 50 $^\circ\text{C}$, 30 minutes with ultrasonic probe (RD187-B) c) H_2O , room temperature, 12 days (RD190-A)

To attain the target molecule **78** sulfonation was initially tested under the mildest conditions, at room temperature with stirring for 3 days, (Scheme 35) however there was no conversion of compound **56** to compound **78**. Before experimenting with reaction conditions to obtain compound **78**, the same reaction was attempted using readily available cyclohexanone (**96**) and isophorone (**98**) to gain an insight to the reactivity of the molecule.

Cyclohexenone (**96**) was stirred at room temperature for 12 days in an aqueous solution of sodium metabisulfite (Scheme 36). Similar conditions were used by Kerp *et al*, who used sulphurous acid as a SO_3^- source.²¹⁷ The reaction mixture was vigorous stirring to increase the interfacial area between the two phases (cyclohexenone/water) which became miscible as the reaction progressed. The loss of the alkene protons at 5.9 ppm and 6.9 ppm in the ^1H -NMR shown in Figure 37 confirms that the α , β unsaturated ketone was sulfonated with full conversion under these mild conditions.

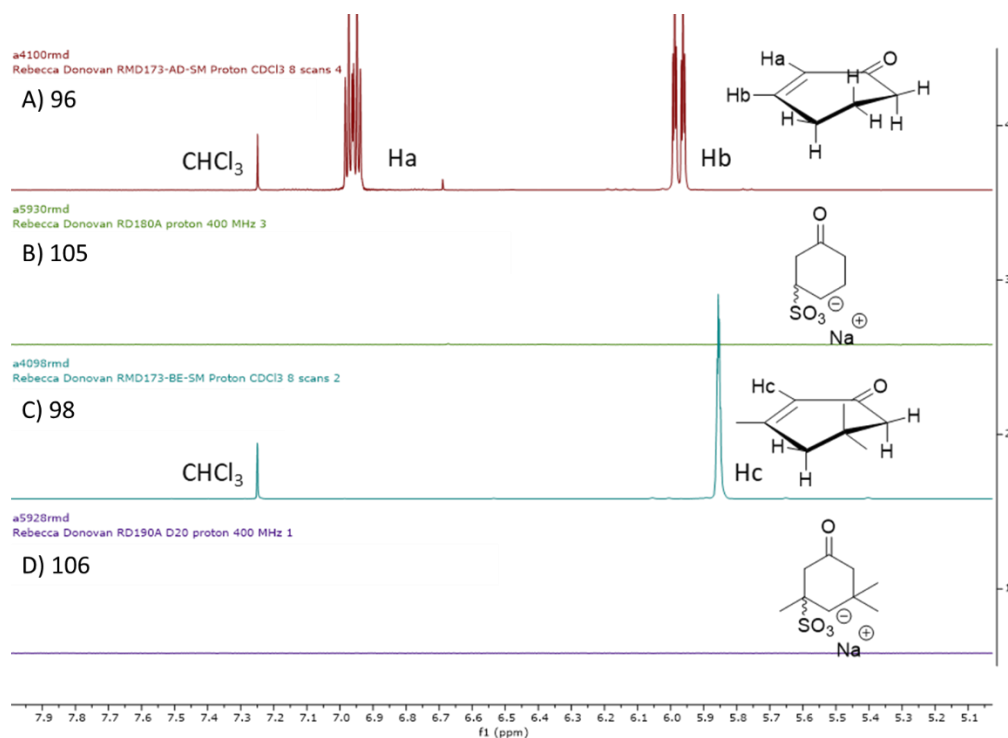
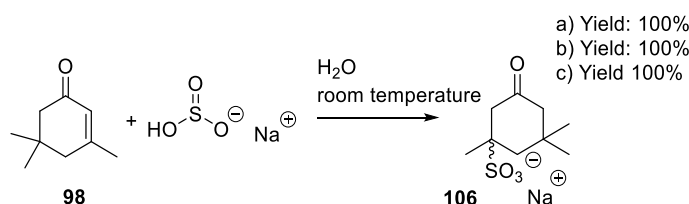


Figure 37: ^1H NMR snapshot comparing the alkene region of cyclohexenone (a), the sulfonation product of cyclohexenone (b), isophorone (c) and isophorone's sulfonation product (c).

Isophorone was subjected to the same mild conditions as shown in Scheme 37. This was done to determine whether the increased steric hindrance caused by the methyl groups in the 3 and 5 positions would affect reaction rate and/or reversibility and therefore the yield. Full conversion is indicated by the loss of alkene protons in Figure 37, spectra d. The isophorone/water phases took several days to combine, despite a high rate if mechanical stirring. This could be due to the poor solubility of the isophorone in the aqueous layer where the reaction takes place. This indicates a slow rate of reaction, though as product forms it may act as a phase transfer catalyst, aiding further reaction. Further work would be required to give an accurate rate.

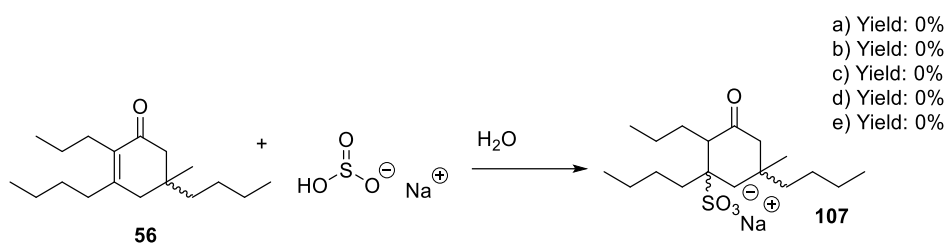
An ultrasonic probe was used to find conditions to increase the reaction rate. The reaction mixture consisted of two phases and therefore the amount of isophorone available to the nucleophile in the aqueous solution was restricted. An ultrasonic probe was used under the hypothesis that the superior mixing would increase the rate of the reaction. Two solutions were trialled: the first without any temperature control, in which the solution reached 60 °C and the second within an ice bath used to dissipate the heat produced by the probe. Full conversion was achieved *via* both methods after 45 minutes.

A second source of SO_3^- , sodium bisulfite, was used for comparison and fully converted isophorone to the sulfonation product (Scheme 20):



Scheme 35: Sulfonation of isophorone (**5**) with sodium bisulfite with stirring. Solvent removed by rotary evaporation before analysis by FT-IR and ^1H NMR. a) **4** (2.8 mmol) and sodium bisulfite (8.5 mmol) in deionised water (20 mL) b) **4** (2.8 mmol), sodium bisulfite (8.5 mmol) and acetic acid (0.5 mL) in deionised water (20 mL) c) isophorone (3 mmol) and sodium bisulfite (6 mmol) in deionised water (10 mL) and isopropanol (10 mL). Conditions: a) H_2O , room temperature, 12 days (RD190-B) b) H_2O , acetic acid, room temperature, 12 days (RD190-C) c) Isopropanol, H_2O , 50 °C, 65 hours (RD192)

Work by Gassama *et al* reported mild conditions for isophorone sulfonations and addressed the two-phase reaction issue by using an isopropanol and water blend and heating to 60 °C.²¹⁸ This work was repeated here and achieved full conversion after 65 hours (Scheme 39):



Scheme 36: Sulfonation of **1** (3.3 mmol) with sodium bisulfite (6.6 mmol) in specified solvents with stirring. Yields determined through ^1H NMR and FT-IR after removal of solvent via rotary evaporation. Conditions: a) H_2O , isopropanol, $50\text{ }^\circ\text{C}$, 24 hours b) H_2O , isopropanol, $65\text{ }^\circ\text{C}$, 3 days c) H_2O , isopropanol, reflux, 24 hours d) H_2O , cyrene, reflux, 4 days e) H_2O , toluene, reflux, 4 days

The isopropanol and water solvent system failed to dissolve both compound **56** and sodium hydrogen sulphite. The solvent system was altered from the previously used 50:50 mixture which was successful for the isophorone sulfonation shown in Scheme 37 to a 60:40 isopropanol water mix. This solvent system appeared to improve the solubility of the reactants, however a hazy solution persisted. After 24 hours at $50\text{ }^\circ\text{C}$, 3 days at $65\text{ }^\circ\text{C}$ and 24 hours at reflux no reaction occurred.

2.9.1 HSPiP's predictive role in alternative solvents for compound **56** dissolution

Alternative solvents and mixtures were compared using Hansen solubility parameters *via* HSPiP predictions. The solvents in the database closest to compound **56** within the Hansen space are most likely to dissolve compound **56**. This includes limonene, cyclopentyl methyl ether, fatty acid methyl esters and toluene amongst others. This can be seen in the graphical representation shown in Figure 38. Of the many solvents identified by HSPiP the only solvent likely to dissolve compound **56**, which is also either able to dissolve salts or is miscible with water to enable the dissolution of the sodium salts is toluene. HSPiP was also used to predict the highest amount of toluene in a toluene and water mixture likely to enable dissolution of compound **56**. This shown by the blue spheres in Figure 38.

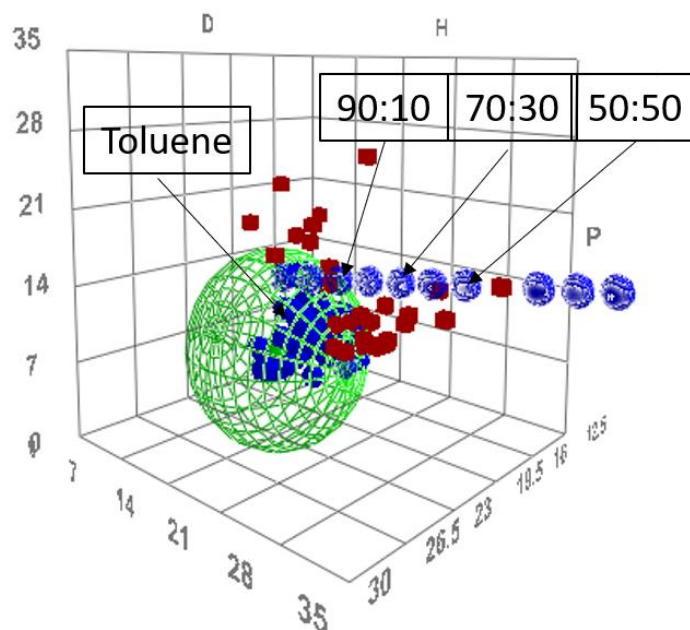
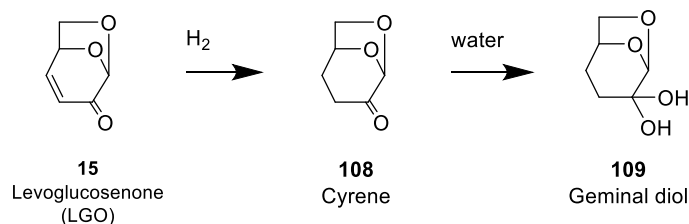


Figure 38: Graphical representation of different solvents in Hansen space. Compound **56** at the centre of the mesh sphere. Solvents within the sphere are most likely to dissolve the target molecule. Toluene and water ratios (90:1, 70:30, 50:50) calculated from predictions.

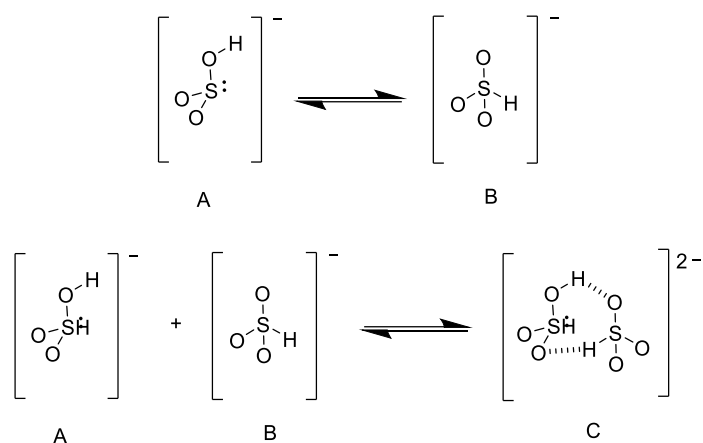
Cyrene[®], a solvent derived from hydrogenation of levoglucosenone, developed as a greener alternative to solvents such as NMP was also used mixed with water.²¹⁹ Although HSPiP predicts that Cyrene is further away than toluene to compound **56** within the Hansen space, a Cyrene and water mixture of 50:50 was used. Cyrene has been shown to form a geminal diol (ketone hydrate) upon interaction with water (Scheme 40) and has been reported exhibiting some surfactant like behaviour which may enhance dissolution.²²⁰



Scheme 37: Showing the hydrogenation of levoglucosenone (LGO) to form Cyrene and hydration of Cyrene to the geminal diol.

Prior to work by Fini and co-workers, the simplest form of addition of bisulfite to form sulfonic acids was discovered over a century ago with some later developments by Kellogg²²¹ and Crowley²²², in which the procedures required large excesses of reagents and

high temperatures. Fini *et al* describe a mild procedure for the sulfonations of several α , β -unsaturated ketones at ambient temperature using triethylamine as a Bronsted base. The effects of sodium hydrogen sulphite concentrations in aqueous solution on the rate of the sulfonations was explored by Fini *et al*²²³ In aqueous media sodium bisulfite exists in two equilibria, shown in Scheme 41:



Scheme 38: Two equilibrium present in bisulfite solution.

At high concentration (5 M) sodium bisulfite exists mostly as the unreactive, non-nucleophilic dimer. At low concentrations however, the reactive species A is maximised. A combination of low concentration bisulfite and the use of triethylamine is believed to push the equilibrium to reactive species A. This allowed for the sulfonation of a wide range of activated ketones under mild conditions. Less activated olefins, some examples of which are shown in Figure 39, under similar conditions required much longer reaction times and resulted poor yields:

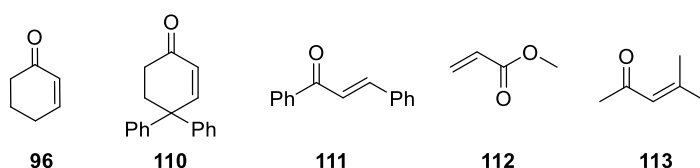


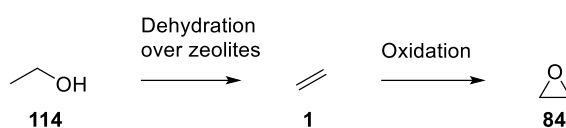
Figure 39: Reagents used by Fini *et al* for sulfonation that produced low yields after 4 days at 22 °C.

The Michael addition of sodium metabisulfite and sodium bisulfite to **56** was unsuccessful, possibly with similar reasoning to the failed amination attempts such as steric hinderance and inductive effects deactivating the reaction site. The addition of triethylamine rather than I_2 may increase reactivity through Bronsted base catalysis rather than promoting the

reaction through halogen bond formation. The addition of bisulfite to the ketone may also be possible as an alternative route.

2.10 ADDITION OF TETRAETHYLENE OXIDE (115)

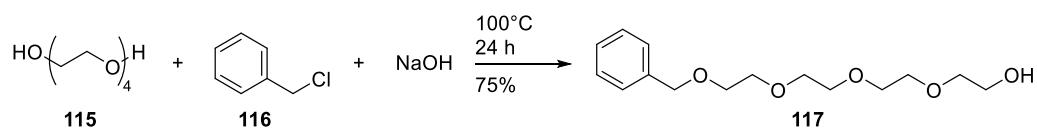
After failed attempts at sulfonation and amination the choice of tail group was reconsidered. Croda have a line of fully bioderived surfactants, the ECO range, which have poly(ethylene oxide) based tail groups sourced from bioethanol.²²⁴ The bioethanol is dehydrated and oxidised to produce ethylene oxide (Scheme 42):^{225, 226}



Scheme 39: Route to bioethylene oxide from bioethanol through ethylene.

An ethoxylated chain was chosen as the head group for the synthetic target molecules because scale up to industry could make use of Croda's established biobased route to ethoxylated surfactants. Tetraethylene oxide was selected over replicating the use of ethylene oxide to produce an ethoxylated head group for two reasons. Firstly, eliminating use of ethylene oxide greatly reduces risk in the lab because ethylene oxide is flammable, toxic and can react explosively. Secondly, tetraethylene oxide can be bought at high purity which makes structural determination of products much simpler. If the structures designed in this study were found to have merit as surfactants then longer ethoxylate chains could be trialled. Any realistic industrial scale up would produce a range of ethoxylate chain lengths.

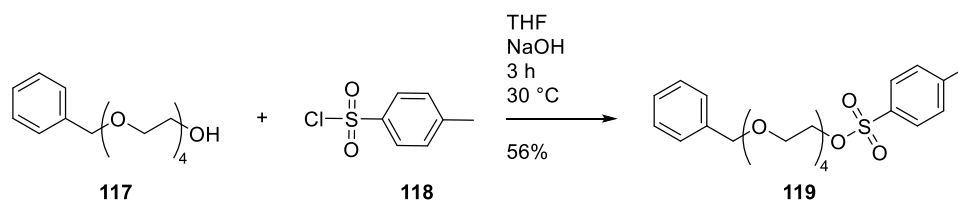
The use of tetraethylene oxide, while simplifying structural analysis and safety procedures does require an additional protection and deprotection step to prevent reaction with the alcohol group on both sides. To protect on one side only a large excess of tetraethylene oxide was used, 10:1, compared to benzyl chloride and sodium hydroxide (Scheme 43):



Scheme 40: Synthetic route to tetraethylene glycol monobenzyl ether (75%) from tetraethylene glycol (1 mol), benzyl chloride (0.1 mol) and sodium hydroxide (0.12 mol) heated to 100 °C for 24 hours

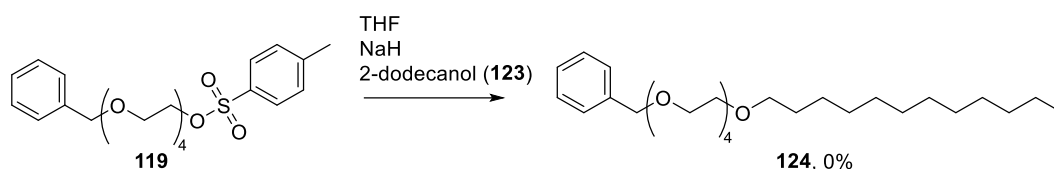
The large excess greatly reduces the probability that the sodium hydroxide will strip the hydrogen from both alcohol groups on one molecule and react with two benzyl chloride molecules. Tetraethylene oxide is water soluble and was easily washed from the final product.

Compound **117** was dissolved in THF and cooled to 0 °C before adding an aqueous solution of sodium hydroxide and stirring for 10 minutes. Toluenesulfonyl chloride in THF was added to the flask and then the reaction mixture was allowed to come to room temperature before heating to 30 °C for 3 hours. The reaction mixture was then acidified to pH 2 and the product extracted with DCM. The product was purified by flash column chromatography and afforded compound **119** (56%).



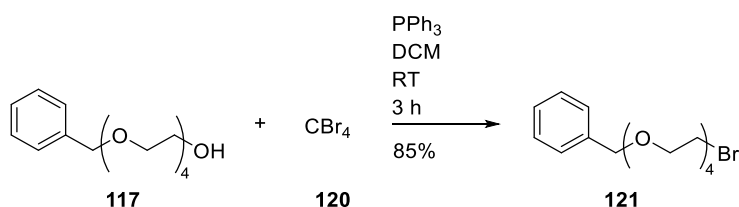
Scheme 41: Synthesis of compound **119**

The synthetic step described by Scheme 44 was designed to add a leaving group onto compound **117** so an ether link can be made between the head group (compound **117**) and fatty alcohol tail groups as proposed in Scheme 45:



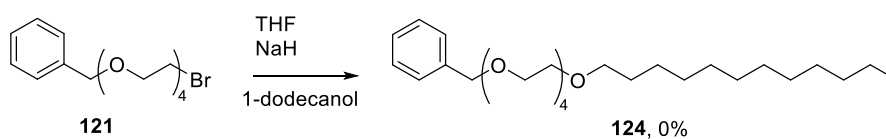
Scheme 42: Unsuccessful etherification of compound **119** and 2-dodecanol

The etherification in Scheme 45 was monitored by TLC and no products were identified. Scheme 46 shows an Appel reaction to form the alkyl bromide **121**, an alternative leaving group to the tosylate group. Compound **117** was dissolved in DCM and cooled in an ice bath before adding carbon tetrabromide and triphenyl phosphine and stirring for 3 hours at room temperature. The reaction was monitored by TLC and upon completion the reaction mixture was pouring into an excess of ethyl acetate, filtered and purified by flask column chromatography. Compound **121** was isolated in an 85% yield.



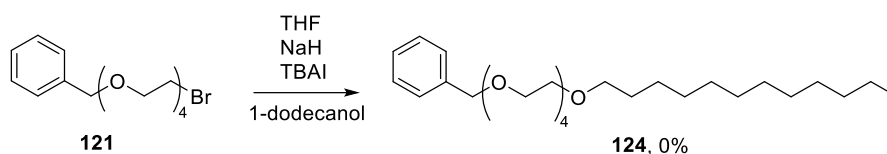
Scheme 43: Appel reaction to produce alkyl bromide from compound **117**

The Williamson ether synthesis in Scheme 47 was attempted using compound **121** and sodium hydride in dry THF. The mixture was monitored by TLC but no products identified.



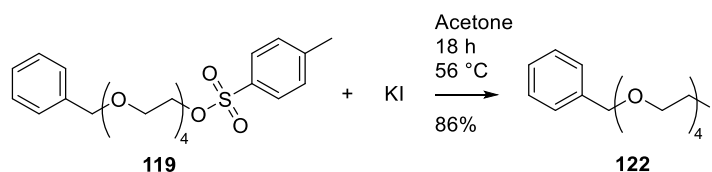
Scheme 44: Unsuccessful etherification of compound **121**

The etherification using the alkyl bromide was attempted again under different conditions, Scheme 48. TBAI was added to the reaction mixture to promote a Finkelstein reaction; however TLC confirmed starting materials remained after stirring at room temperature overnight and heating to 40 °C for 1 hour.



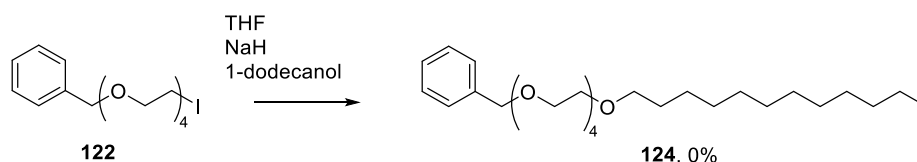
Scheme 45: Finkelstein reaction with TBAI for the etherification of compound **121**

As the tosylate and bromide leaving groups were unsuccessful in the etherification attempts, an iodide leaving group was considered. Compound **119** was dissolved in acetone and potassium iodide added to the solution. The reaction mixture was heated to reflux for 18 hours, cooled, filtered and the salts washed with acetone. The filtrate was concentrated *in vacuo*, diluted with DCM and washed with sodium thiosulfate and brine. The combined organics were dried and concentrated, and the product purified by flash column chromatography, and isolated in 86% yield.



Scheme 46: Synthesis of alkyl iodide **122**

The etherification in Scheme 50 was attempted using compound **122** in dry THF with sodium hydride. The reaction mixture was monitored by TLC, the starting material remained and no additional spots were observed, indicating the desired product was not formed.

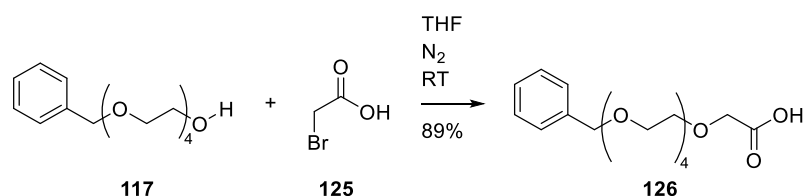


Scheme 47: Proposed etherification of compound **122** and 1-dodecanol (**124**)

No attempts were made using shorter alcohols because the aim of the project at this time was to seek out a singular method of bringing together the head and tail groups and the linear, unhindered dodecanol was of a

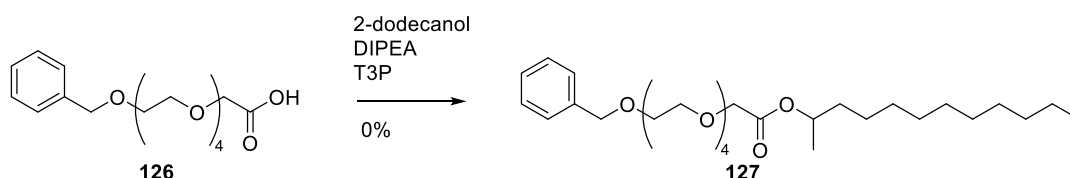
2.11 ESTERIFICATION

After unsuccessful attempts at etherification, an ester link instead of an ether link was considered instead. An additional advantage of switching to an ester link is that it is likely to be much better in terms of biodegradation than the ether link. The fatty groups intended for use as the hydrophobic tail groups of the surfactants are all either ketones or alcohols. Therefore, addition of a carboxylic acid containing fragment to the protected tetra ethylene oxide chain (**117**) was done, by reacting **117** with bromoacetic acid **125** as shown in Scheme 51, affording **126** in high yield.



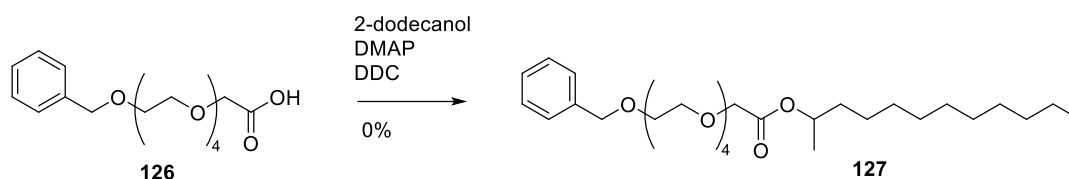
Scheme 48: Addition of carboxylic acid to compound **117** using bromoacetic acid

The first esterification attempt using **126** (Scheme 52) was done with T3P, which was chosen because of recent knowledge within the Unsworth group.²²⁷ Compound **126** was dissolved in dry toluene in a flask under nitrogen containing T3P (1.3 eq) and DIPEA (2.6 eq) and the reaction mixture left overnight at room temperature. The reaction mixture was assessed by TLC which showed starting material remained and no new product spots. The reaction mixture was purified by column chromatography which yielded the starting materials only.



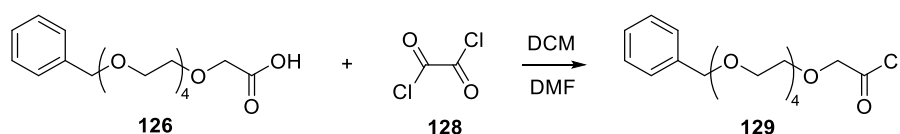
Scheme 49: T3P mediated esterification attempt

Scheme 53 shows another esterification attempt, this time using DMAP and DCC in dry DCM under N₂. The reaction mixture was assessed by TLC which showed starting material remained and no new product spots.

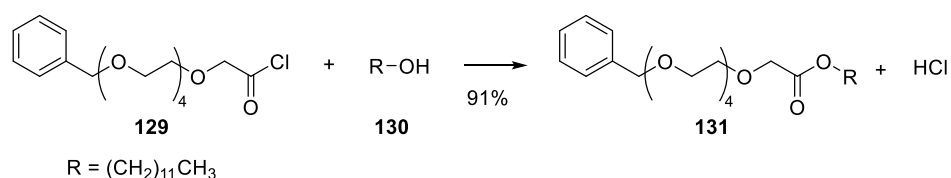


Scheme 50: Steglich esterification attempt using compound **126** and 2-dodecanol

Another route to the ester was therefore attempted, this time using an acyl chloride as an intermediate. To make the acid chloride, acid **126** was dissolved in DCM with oxalyl chloride and DMF (**87**) was used to catalyse the reaction. The resulting product **129** was taken on directly to the esterification without additional purification or characterisation.



Scheme 51: Using oxalyl chloride to produce an acyl chloride for esterification with fatty alcohols

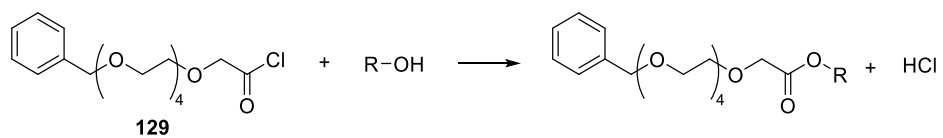


Scheme 52: Esterification with fatty alcohol via acyl chloride formation

With the acid chloride **129** in hand, attention moved onto testing the esterification. Pyridine was used in the acyl chloride reaction with the various alcohols, which acts both a base, and as a nucleophilic catalyst to form an acylpyridium ion which is a better electrophile than RCOCl.

Pleasingly, the esterification via the acyl chloride with dodecanol (Scheme 55) produced a 91% yield. Therefore, the same conditions were used for the esterification of the various fatty alcohols, presented with their yields, in Table 8.

Table 8: Reaction conditions and yields for the reaction between the benzyl protected acyl chloride of poly (ethylene glycol) and fatty alcohols



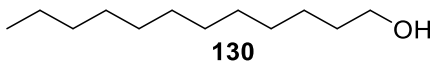
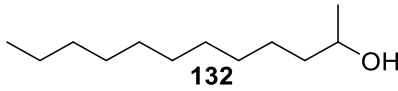
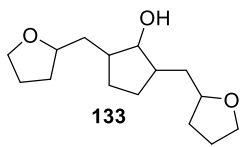
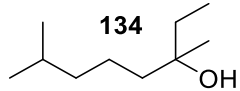
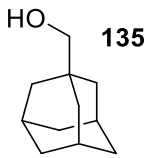
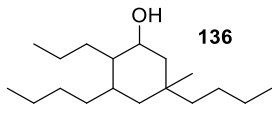
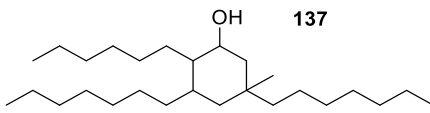
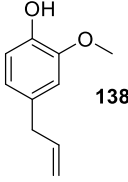
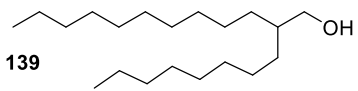
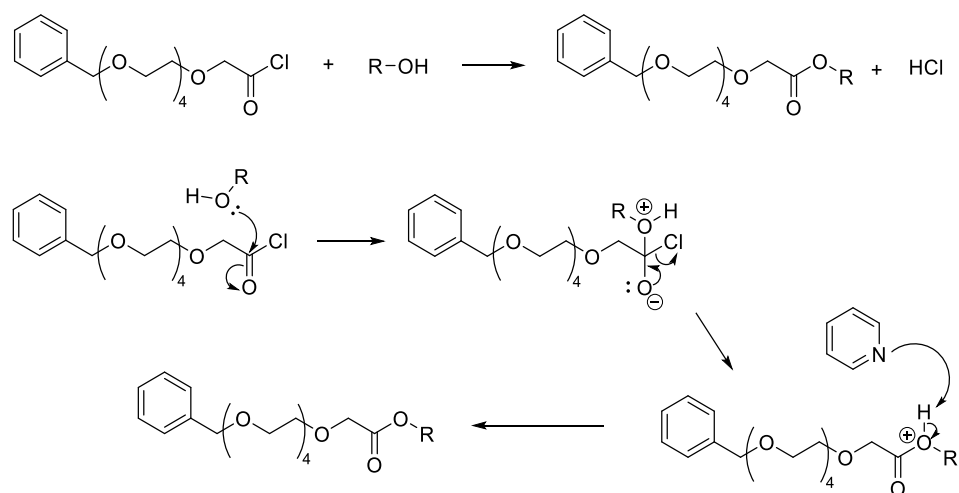
R	Yield / %
 <p>130</p>	91
 <p>132</p>	85
 <p>133</p>	14
 <p>134</p>	20
 <p>135</p>	57
 <p>136</p>	21
 <p>137</p>	29
 <p>138</p>	14
 <p>139</p>	79

Table 8 shows a small decrease in yield between the primary alcohol 1-dodecanol (**131**) from 91% to 85% with the secondary alcohol 2-dodecanol (**132**). This yield is dramatically reduced to 20% with tertiary alcohol **134**. Alcohols **133**, **136** and **137** also had poor yields, 14%, 21% and 29% respectively, despite being secondary alcohols, likely because of the increased steric hindrance. Primary alcohols **135** and **139** had yields of 57% and 79% which are lower than with primary alcohol 1-dodecanol (**131**). A general mechanism for the esterification via the acyl chloride is shown in Scheme 56.



Scheme 53: Esterification mechanism via acyl chloride

2.12 ALDOL CONDENSATIONS AND THE HYDROGENATION AND REDUCTION OF ALDOL CONDENSATES

One of the fatty alcohols used in the esterification reactions above, **133** (Figure 40), had to be synthesised, and importantly, can be derived from biomass. This was done by first starting with the aldol condensation of **36** and **40**, as shown in Scheme 57, using the method described in chapter 1.

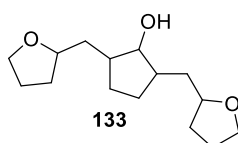
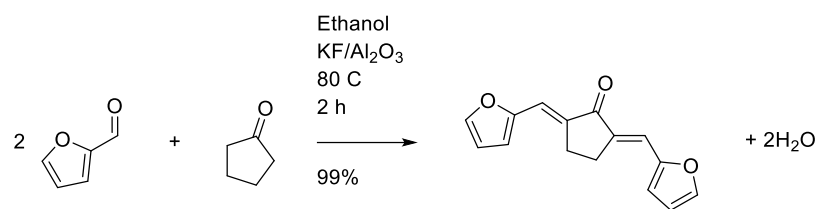
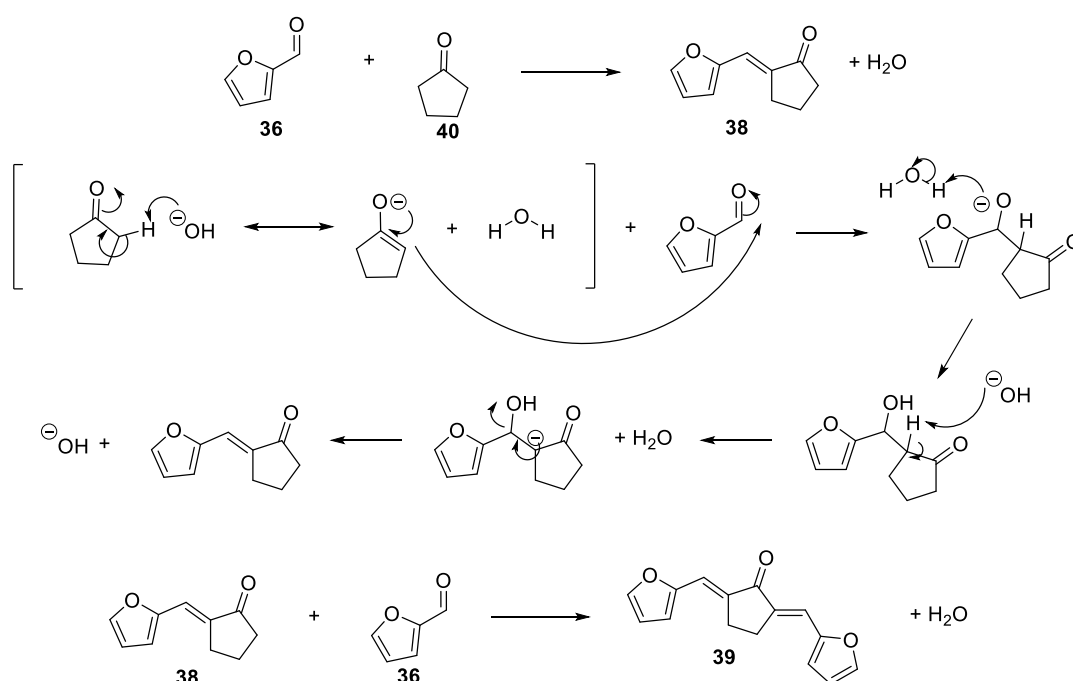


Figure 40: Structure of compound **133**



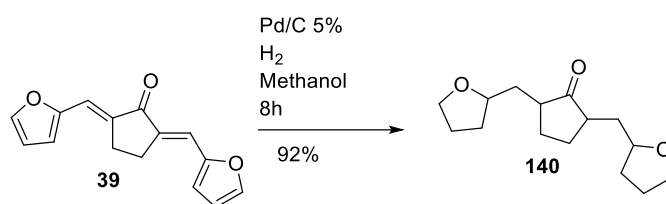
Scheme 54: Aldol condensation of furfural (**36**) and cyclopentanone (**40**)

The proposed mechanism for the aldol condensation of furfural (**36**) and cyclopentanone (**40**) is shown in Scheme 58.



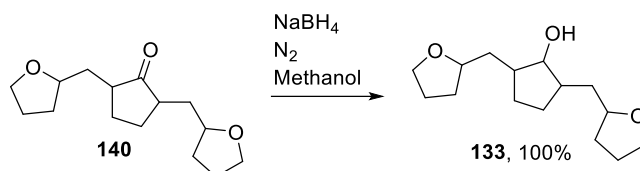
Scheme 55: Cross aldol condensation mechanism of furfural (**36**) and cyclopentanone (**40**)

The double aldol condensate product **39** was then hydrogenated and reduced to produce fatty alcohol **133**. Compound **39** was hydrogenated first, using a standard hydrogenation over Pd/C as shown in Scheme 59. Pd/C was added to a flask which was then purged with N₂. Methanol was added via syringe followed by compound **39** in methanol. The reaction mixture under nitrogen was then purged with H₂ 3 times before leaving stirring vigorously at room temperature for 8 hours. The catalyst was filtered out and the product extracted in ethyl acetate at 92% yield.



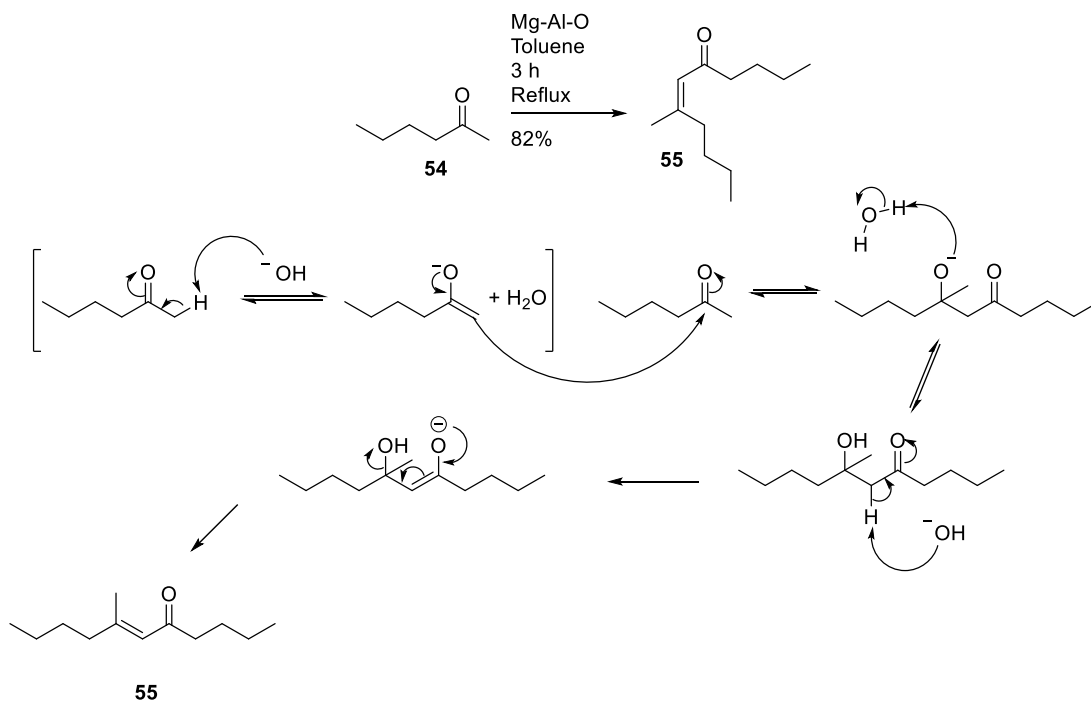
Scheme 56: Hydrogenation of aldol condensate product **39**

The ketone **140** was then reduced with sodium borohydride in methanol under N_2 as shown in Scheme 60. The reaction was followed with TLC until completion before quenching with deionise water dropwise and extraction with ethyl acetate. Once the reduction was complete, compound **133** was used in the esterification described above in Table 8.



Scheme 57: Sodium borohydride reduction of compound **140**

Another fatty alcohol identified from biofuel research derivable from biomass is compound **56**. Scheme 61 shows the aldol condensation mechanism for compound **54**.



Scheme 58: Proposed mechanism for the aldol condensation of compound **54**

The cross-aldol condensation of **54** and **55** produces compound **56** which when hydrogenated and reduced under the same conditions as seen previously, yields compound **136** (Figure 41).

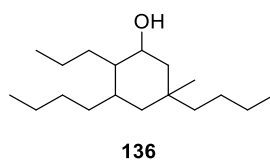
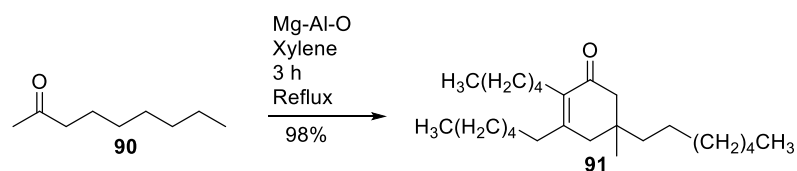
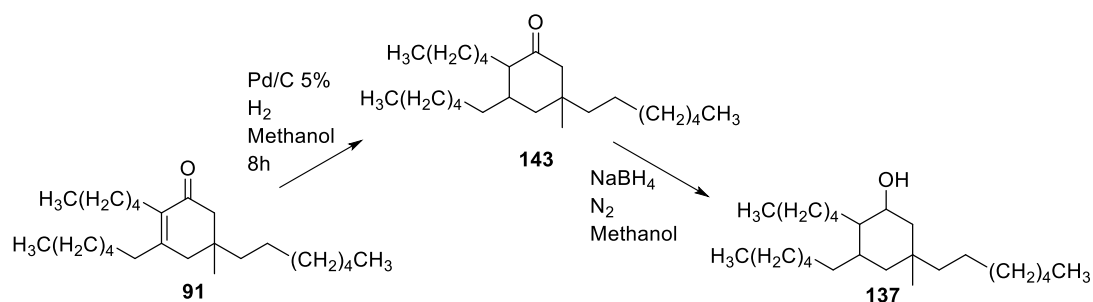


Figure 41: Structure of compound **136**

Compound **137** was produced in a similar manner. The aldol condensate of 2-nonanone (**90**, Scheme 62) is hydrogenated and reduced (Scheme 63) to afford compound **137**, as described in Scheme 63.



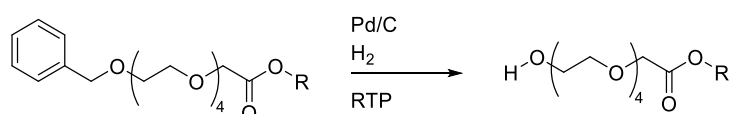
Scheme 59: Aldol condensation of 2-nonanone (**90**)



Scheme 60: Hydrogenation over Pd/C and reduction with sodium borohydride of 2-nonanone double aldol condensate.

2.13 DEPROTECTION

As noted above, the surfactant tail and head groups were joined together through ester synthesis (Scheme 56). Once the tail groups (fatty alcohols, R-OH Scheme 56) were attached to the head group (**129**) the head group needed to be deprotected. This was achieved through hydrogenation to yield the final compounds (Scheme 65). The final compounds are listed in Figure 42.



Scheme 61: Deprotection of head group to yield final compounds with surfactant potential

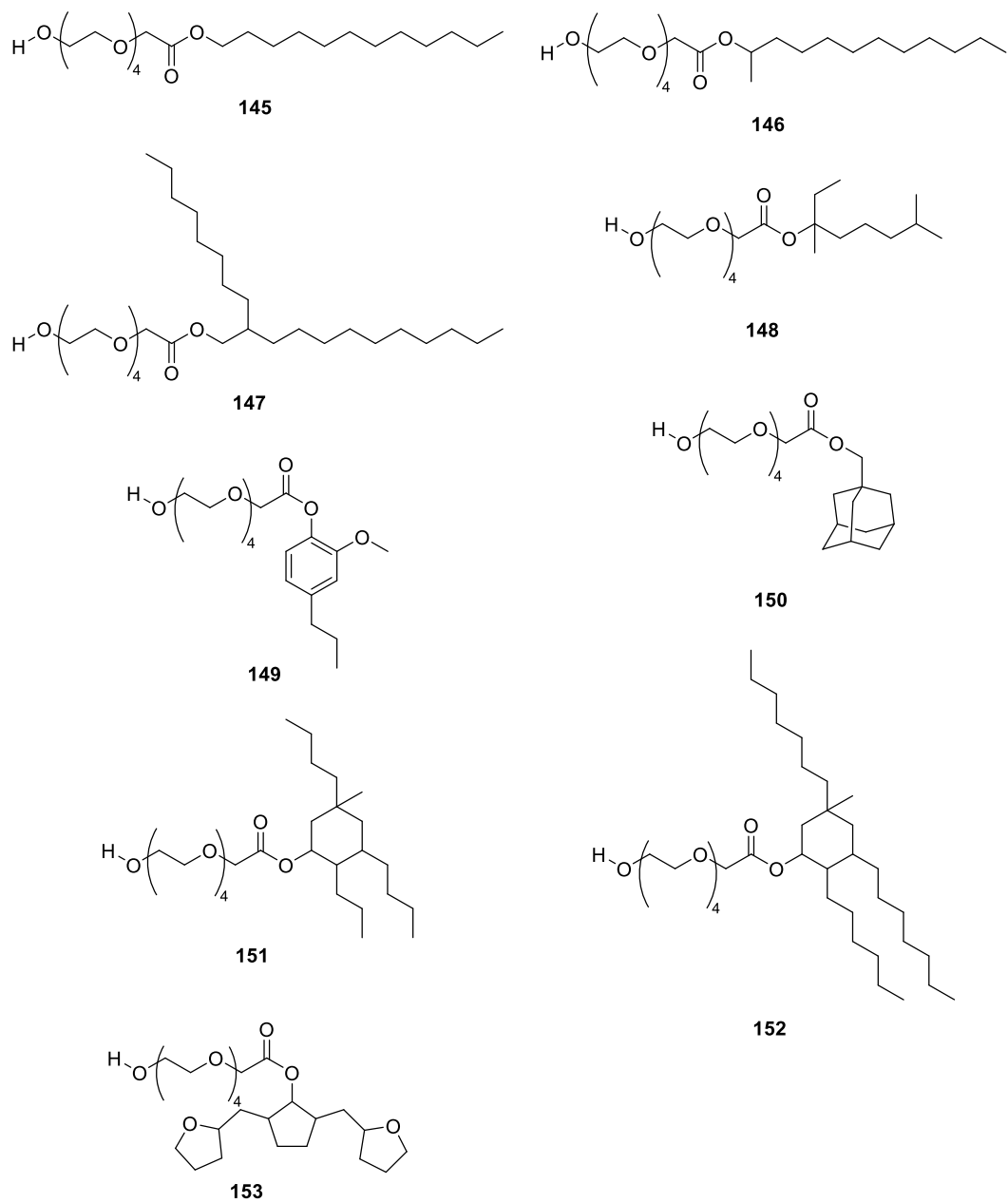


Figure 42: Final synthetic compounds with surfactant potential

2.14 CONCLUSION

Fatty ketones from biomass research were identified and synthesised through aldol condensations. The α,β -unsaturated ketones were then hydrogenated and reduced to produce alcohols for addition of a surfactant head group. Attempts to add anionic (sulfonate) and cationic (quaternary amine) head groups to the hydroxyls failed. Focus moved to the addition of a non-ionic head group, poly (ethylene oxide). To simplify compound identification by NMR in the first instance tetraethyleneoxide was chosen as the synthetic starting point.

One of the two terminal hydroxyls of tetraethylene oxide was protected with a benzyl group to avoid reaction on both ends of the head group. From here Williamson ether synthesis was attempted. Tosylate, iodide and bromide leaving groups were used under different conditions to promote etherification but to no avail.

An ester link rather than an ether link was decided upon and thus a carboxylic acid was added via the terminal hydroxyl on the protected tetraethylene oxide because the selected tail groups all have hydroxyl groups. The carboxylic acid was added via bromoacetic acid.

Attempts at esterification through T3P mediated esterification and Steglich esterification failed. Esterification through acyl chloride was successful and was used to produce 9 novel compounds with potential to exhibit surfactant characteristics after deprotection through hydrogenation to remove the benzyl group. Their properties were explored as described in the following chapter.

2.15 EXPERIMENTAL

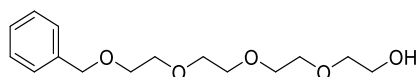
2.15.1 General Experimental

All reagents, except where stated, were purchased from commercial sources and used without further purification. Anhydrous DCM and THF were obtained from an innovative technology Inc. PureSolv[®] solvent purification system. Anhydrous DMF was purchased from Merck. Unless stated otherwise, all ¹H and ¹³C NMR spectra were acquired at 293 K and recorded on a JEOL ECS400A, operating at 400 MHz (100 MHz for ¹³C) or a Bruker AVIII300NB, operating at 300 MHz (75 MHz for ¹³C). Chemical shifts (δ) are quoted in parts per million (ppm) and the residual solvents peak for CDCl₃, δ_{H} 7.26 and δ_{C} 77.0 were used as reference peaks. Coupling constants are denoted as J and reported in Hertz (Hz) to the nearest 0.1 Hz. Abbreviations used to describe multiplicity are: s singlet, d doublet, t triplet, q quartet, dt doublet of triplets, m multiplet. Infrared (IR) spectra were recorded on a Bruker Alpha II platinum ATR. Mass spectra (high-resolution) were obtained by the University of York Mass Spectrometry Service, using Electrospray Ionisation (ESI) on a Bruker Daltonics, Micro-TOF spectrometer. Melting points were determined using Gallenkamp apparatus. Thin layer chromatography was carried out on Merck silica gel 60F₂₅₄ pre-coated aluminium foil sheets and were visualised using UV light (254 nm) and stained with basic aqueous potassium permanganate. Flash column chromatography was carried out using slurry packed Fluka silica gel (SiO₂), 35–70 μm , 60 Å, under a light positive pressure, eluting with the specified solvent system.

2.16 REACTION PROCEDURES AND EXPERIMENTAL

2.16.1 Preparation of ether, carboxylic acid and intermediates

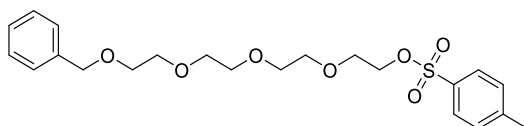
Compound 117: Tetraethylene glycol monobenzyl ether



Tetraethylene glycol (172 mL, 1.00 mol) and a 50% aq. Sodium hydroxide solution (4.75 g in 9.50 mL water, 0.120 mol) was stirred at room temperature for 15 minutes. Benzyl chloride

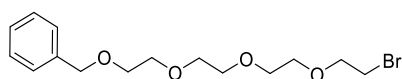
(12.4 mL, 0.100 mol) was added dropwise and the reaction mixture heated to 100 °C for 24 hours. The reaction mixture was allowed to cool to room temperature and quenched with cold water (150 mL). The aqueous phase was washed with hexane (2 x 100 mL) and then extracted with ethyl acetate (6 x 200 mL). The extracted organics were washed with ice-cooled water (2 x 150 mL), dried with magnesium sulphate and concentrated *in vacuo* affording the title compound (22.0 g, 75%) as a light yellow free flowing oil which was used without further purification. R_f : 0.26 (0.5% MeOH in DCM); $\nu_{\max}/\text{cm}^{-1}$ (neat) 3449, 2865, 1102; δ_{H} (300 MHz, Chloroform-*d*) 7.36 – 7.22 (m, 5H, H_{Ar}), 4.54 (s, 2H, PhCH_2), 3.73 – 3.53 (m, 16H, $\text{OCH}_2\text{CH}_2\text{O}$). δ_{C} (75 MHz, Chloroform-*d*) 138.2 (CH_{Ar}), 128.3 (2C, CH_{Ar}), 127.7 (2C, CH_{Ar}), 127.6 (CH_{Ar}), 73.2 (CH_2), 72.6 (CH_2), 70.5 ($\text{CH}_2 \times 4$), 70.2 (CH_2), 69.4 (CH_2), 61.5 (CH_2). These data are in accordance with those found in the literature.²²⁸

Compound 119: 1-Phenyl-2,5,8,11-tetraoxatridecan-13-yl 4-methylbenzenesulfonate



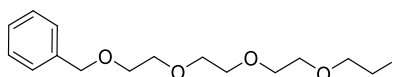
Compound **117** (424 mg, 1.50 mmol) in THF (5 mL) was cooled to 0 °C and combined with sodium hydroxide (237 mg, 5.90 mmol) in deionised water (3.5 mL) and stirred for 10 minutes at 0 °C. Toluenesulfonyl chloride (412 mg, 2.21 mmol) in THF (5 mL) was added to the flask and the reaction mixture was allowed to come to room temperature then heated to 30 °C for 3 hours and subsequently poured into cold deionised water (50 mL) and acidified to pH 2 using 3 M HCl. The product was extracted with DCM (3 x 30 mL), dried over magnesium sulfate and concentrated *in vacuo*. Purification by flash column chromatography (1:1 hexane: ethyl acetate) afforded the title compound (343 mg, 56%) as a light yellow viscous oil; R_f : 0.30 (1:1 hexane : ethyl acetate), δ_{H} (400 MHz, Chloroform-*d*) 7.82 – 7.68 (m, 2H, H_{Ar}), 7.42 – 7.18 (m, 7H, H_{Ar}), 4.52 (s, 2H, PhCH_2), 4.17 – 4.10 (m, 2H, CH_2), 3.73 – 3.46 (m, 16H, $\text{OCH}_2\text{CH}_2\text{O}$), 2.39 (s, 3H, CH_3). These data are in accordance with those found in the literature.^{229,230,231}

Compound 121: 13-Bromo-1-phenyl-2,5,8,11-tetraoxatridecane



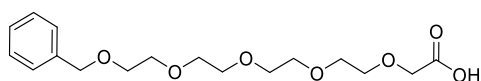
Compound **117** (284 mg, 1.00 mmol) was dissolved in DCM (5 mL) with stirring at 0 °C. Carbon tetrabromide (410 mg, 1.21 mmol) was added to the flask followed by triphenyl phosphine (420 mg, 1.62 mmol) and the reaction mixture was allowed to come to room temperature and stirred for 3 hours. The reaction mixture was concentrated *in vacuo* and poured into ethyl acetate (20 mL). The white precipitate formed was removed via vacuum filtration and the mixture was concentrated *in vacuo*. Purification by flash column chromatography (100% ethyl acetate) afforded the title compound (300 mg, 85%) as a yellow oil; R_f : 0.52 (ethyl acetate); R_f : 0.30 (1:1 ethyl acetate hexane); δ_H (400 MHz, Chloroform-*d*) 7.42 – 7.17 (m, 5H, H_{Ar}), 4.55 (s, 2H, $BzCH_2$), 3.79 (t, $J = 6.3$ Hz, 2H, CH_2), 3.70 – 3.58 (m, 14H, OCH_2CH_2), 3.45 (t, $J = 6.3$ Hz, 2H, CH_2). These data are in accordance with those found in the literature.²³²

Compound 122: 13-Iodo-1-phenyl-2,5,8,11-tetraoxatridecane



Compound **119** (438 mg, 1.00 mmol) was dissolved in acetone (1.7 mL), potassium iodide (498 mg, 2.99 mmol) was added and the reaction mixture heated to reflux for 18 hours. Once cooled the reaction mixture was filtered and the salts washed with acetone (5 x 10 mL). The filtrate was concentrated *in vacuo* and diluted with DCM then washed with saturated sodium thiosulphate (3 x 25 mL) and brine (2 x 25 mL). The organics were dried over magnesium sulphate and concentrated. Purification by flash column chromatography (ethyl acetate: hexane 9:1), afforded the *title compound* as a light yellow oil (334 mg, 86%); R_f : 0.36 (33% ethyl acetate in hexane); δ_H (300 MHz, Chloroform-*d*) 7.42 – 7.21 (m, 5H, H_{Ar}), 4.57 (s, 2H, $PhCH_2$), 3.75 (t, $J = 6.7$ Hz, 2H, CH_2), 3.71 – 3.61 (m, 12H, OCH_2CH_2O), 3.25 (t, $J = 6.7$ Hz, 2H, CH_2). Expected mass of $C_{15}H_{23}IO_4 = 394.06$, mass found $C_{15}H_{23}INaO_4 = 417.0533$, error [mDa] 0.1. These data are in accordance with those found in the literature.²³³

Compound 126: 1-phenyl-2,5,8,11,14-pentaoxahexadecan-16-oic acid

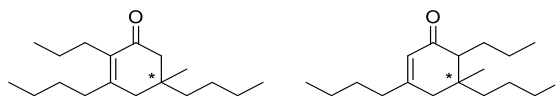


Compound **117** (9.09 g, 32.01 mmol) was dissolved in dry THF (45 mL) with stirring under a nitrogen atmosphere and cooled to 0 °C. NaH (60% in mineral oil, 2.40 g, 60.0 mmol) was

added and stirred under nitrogen for 15 minutes. Bromoacetic acid (4.45 g, 32.03 mmol) was added to a flask containing dry THF (45 mL) and cooled to 0 °C with stirring. The solutions were combined and stirred at room temperature for 24 hours. Deionised water (50 mL) was added to the reaction mixture and acidified to pH 2 with HCl (2 M). The product was extracted with DCM (4 x 50 mL) and the organic layer dried with magnesium sulphate and concentrated *in vacuo*. Purification by flash column chromatography (ethyl acetate: hexane 4:1 → ethyl acetate: methanol 1:1), afforded the *title compound* (9.74 g, 89%) as a light yellow oil; R_f : 0.21 (ethyl acetate: methanol 1:1); $\nu_{\max}/\text{cm}^{-1}$ (neat) 3031, 2867, 1804; δ_{H} (300 MHz, Chloroform-*d*) 7.40 – 7.18 (m, 5H, H_{Ar}), 4.56 (s, 2H, PhCH_2), 4.11 (s, 2H, CH_2COO), 3.78 – 3.53 (m, 16H, $\text{OCH}_2\text{CH}_2\text{O}$). These data are in accordance with those found in the literature.²³⁴

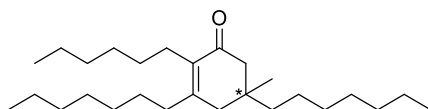
2.16.2 Aldol Condensations

Compound 56 and 56a: 3,5-Dibutyl-5-methyl-2-propylcyclohex-2-en-1-one



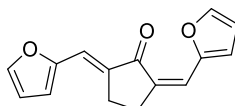
Toluene (160 mL) was added to a flask containing Mg-Al-O* (See 2.11.7 for preparation details, 3.84 g) and fitted with a Dean-Stark arm and condenser. Hexanone (11.45 g, 0.11 mol) was added to the flask at room temperature and the reaction mixture brought to reflux with vigorous stirring for 6 hours. After this time the reaction was allowed to cool and the catalyst was filtered off and washed with toluene (3 x 20 mL) and ethyl acetate (3 x 20 mL). The filtrate and was combined with the washings, dried over magnesium sulphate and concentrated *in vacuo* to afford **56** and **56a** in a roughly 6:1 ratio as a colourless oil (7.90 g, 82%); $\nu_{\max}/\text{cm}^{-1}$ (neat) 2957, 2929, 2870, 1664, 1624; δ_{H} (400 MHz, Chloroform-*d*) δ 5.68 (s, 0.15H, **56a**), 2.28-1.79 (m, 7H), 1.49-0.96 (m, 13H), 0.96-0.58 (m, 12H). These data are in accordance with those found in the literature.¹⁷⁰

Compound 91 and 91a: 3,5-Diheptyl-2-hexyl-5-methylcyclohex-2-en-1-one



Mg-Al-O* (2.69g), nonanone (3.82g, 26.9 mmol) and xylene (80 mL) were added to a flask fitted with a Dean-Stark arm and condenser. The reaction mixture was heated at reflux and stirred for 18 hours. After this time the reaction was allowed to cool and the catalyst was filtered off and washed with xylene (2 x 20 mL). The filtrate and washings were combined and the solvent removed *in vacuo* to afford the *title compound* as a colourless oil (3.42 g, 98%); $\nu_{\max}/\text{cm}^{-1}$ (neat) 3406, 2954, 2924, 2854, 1665, 1625; δ_{H} (300 MHz, Chloroform-*d*) 2.33–1.97 (6H, m, C=CCH₂), 1.48 (2H, s, COCH₂), 1.29–1.10 (28H, m, CH₂), 0.89–0.74 (12H, m, CH₃); expected mass C₂₇H₅₀O: 390.39, mass found C₂₇H₅₀NaO: 413.3760, error[mDa] -1.4.

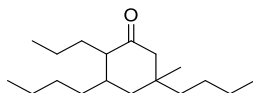
Compound 39: (2Z,5E)-2,5-bis(furan-2-ylmethylene)cyclopentan-1-one



Cyclopentanone (10 mmol, 0.84 g) and furfural (20 mmol, 1.92 g) were added to a flask containing ethanol (40 mL) and potassium fluoride on aluminium oxide (5.5 mmol F⁻g⁻¹, 0.20 mg) fitted with a waterless reflux condenser. The reaction mixture was stirred and heated to 80 °C for 2 hours. After 2 hours the reaction mixture was allowed to cool to room temperature before addition of ice cooled deionised water (50 mL). The resulting orange-brown precipitate was filtered out of solution and washed with cold deionised water. The addition of ice-cold water and subsequent filtration was repeated twice or until no further precipitate was formed. The precipitate was dissolved in sufficient DCM and the solid catalyst filtered from solution and washed with DCM until white. The aqueous solution was extracted with DCM (3 x 40 mL) and the solvent from the combined organics was removed by rotary evaporation to afford the *title compound* which was used without further purification as an orange-brown powder (2.37 g, 99%); δ_{H} (300 MHz, Chloroform-*d*) δ 7.52 (2H, d, J = 1.8 Hz, C=CHO), 7.28 (2H, s, C=CH), 6.63 (2H, d, J = 3.5 Hz, C=CH), 6.47 (2H, dd, J = 3.5, 1.8 Hz, CH=CHO), 3.02 (4H, s, CH₂). Melting point: 164-165; expected mass C₁₅H₁₂O₃ 240.08, mass found C₁₅H₁₂NaO₃: 263.0679 error[mDa] -0.2. These data are in accordance with those found in the literature.¹⁶⁴

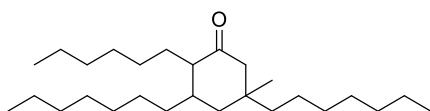
2.16.3 Hydrogenation of aldol condensates

Compound 141: 3,5-dibutyl-5-methyl-2-propylcyclohexan-1-one



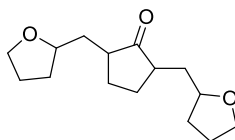
Pd/C (5 % wt/wt loading, 1.13 g) was added to a 2 necked flask fitted with a suba seal and a 3-way gas tap connected to the vacuum line and a balloon. The flask was carefully purged and filled with nitrogen through a balloon which was repeated 3 times. Methanol (50 mL) was added to the flask through a needle and syringe to maintain the nitrogen atmosphere followed by compound the mixture of **56** and **56a** (7.32 g, 27.7 mmol). The balloon was exchanged for a hydrogen balloon and the flask purged and refilled with hydrogen 3 times then left vigorously stirring for 8 hours. After this time the catalyst was removed through Buchner filtration and washed with ethyl acetate (3 x 30 mL). The solvent organics from the washes were combined and solvent removed by rotary evaporation to afford the *title compound* which was not further purified and was a light yellow oil (6.78 g, 92%); $\nu_{\max}/\text{cm}^{-1}$ (neat) 2956, 2927, 2871, 2860, 1708.

Compound 143: 3,5-Diheptyl-2-hexyl-5-methylcyclohexan-1-one



Pd/C (5 % wt/wt loading, 2.2 g) was added to a 2 necked flask fitted with a suba seal and a 3 way gas tap connected to the vacuum line and a balloon. The flask was carefully purged and filled with nitrogen through a balloon which was repeated 3 times. Methanol (50 mL) was added to the flask through a needle and syringe to maintain the nitrogen atmosphere followed by compound **VII** (7.12 g, 18.2 mmol). The balloon was exchanged for a hydrogen balloon and the flask purged and refilled with hydrogen 3 times then left vigorously stirring for 8 hours. After this time the catalyst was removed through Buchner filtration and washed with ethyl acetate (3 x 30 mL). The solvent organics from the washes were combined and solvent removed by rotary evaporation to afford the *title compound* which was not further purified and was a light yellow oil (6.62 g, 93%); $\nu_{\max}/\text{cm}^{-1}$ (neat) 2955, 2925, 2855, 1715.

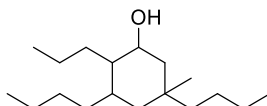
Compound 140: 2,5-bis((tetrahydrofuran-2-yl)methyl)cyclopentan-1-one



Pd/C (5 % wt/wt loading, 200 mg) was added to a 2 necked flask fitted with a suba seal and a 3-way gas tap connected to the vacuum line and a balloon. The flask was carefully purged and filled with nitrogen through a balloon which was repeated 3 times. Ethyl acetate (40 mL) was added to the flask through a needle and syringe to maintain the nitrogen atmosphere followed by compound **39** (241 g, 1.0 mmol). The balloon was exchanged for a hydrogen balloon and the flask purged and refilled with hydrogen 3 times then left vigorously stirring for 8 hours. After this time the catalyst was removed through Buchner filtration and washed with ethyl acetate (3 x 30 mL). The solvent organics from the washes were combined and solvent removed by rotary evaporation to afford the *title compound* which was not further purified and was a light yellow oil (242 mg, 95.6%); R_f : 0.10 (20% ethyl acetate in hexane); $\nu_{\max}/\text{cm}^{-1}$ (neat) 2935, 2864, 1731; δ_{H} (300 MHz, Chloroform-*d*) 3.98–3.69 (4H, m, CH₂OCH), 3.69–3.48 (2H, m, CH₂OCH), 2.29–2.11 (2H, m, CH), 2.11–1.57 (12 H, m, CH₂), 1.57–1.14 (4H, m, CH₂).

2.16.4 Sodium borohydride reduction of ketones

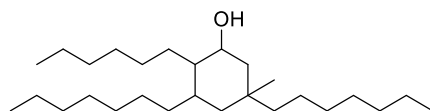
Compound 136: 3,5-dibutyl-5-methyl-2-propylcyclohexan-1-ol



Methanol (30 mL) was added to a 2-neck flask which was purged with N₂ and cooled in an ice bath for 10 minutes before adding sodium borohydride (1.77 g, 46.9 mmol) and purging with nitrogen again. In a separate flask compound **143** (8.31 g, 31.2 mmol) was diluted in methanol (20 mL) and then added via syringe to the first flask. The reaction mixture was allowed to come to room temperature under stirring and the reaction was monitored by TLC until completion. Deionised water was added dropwise to the reaction mixture to quench. Deionised water (20 mL) and HCl (20 mL) were added to the reaction mixture and the products extracted with ethyl acetate (3 x 50 mL). The organics were combined, dried over magnesium sulphate and concentrated *in vacuo* to remove solvent to afford the *title compound* as a colourless oil (8.26 g, 99%); $\nu_{\max}/\text{cm}^{-1}$ (neat) 3461, 2954, 2925, 2871, 2859; δ_{H} (300 MHz, Chloroform-*d*) 3.6 (1H, s, CHOH), 2.29–0.93 (23H, m, CH₂, CH), 0.90–0.68 (12H,

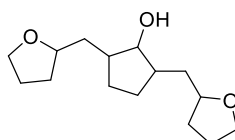
m, CH₃). Expected mass for C₁₈H₃₆O: 268.28, mass found C₁₈H₃₄NaO: 289.2502 error [mDa] -0.7.

Compound 137: 3,5-diheptyl-2-hexyl-5-methylcyclohexan-1-ol



Methanol (30 mL) was added to a 2-neck flask which was purged with N₂ and cooled in an ice bath for 10 minutes before adding sodium borohydride (0.957 g, 25.3 mmol) and purging with nitrogen again. In a separate flask compound **143** (6.62 g, 16.9 mmol) was diluted in methanol (20 mL) and then added via syringe to the first flask. The reaction mixture was allowed to come to room temperature under stirring and the reaction was monitored by TLC until completion. Deionised water was added dropwise to the reaction mixture to quench. Deionised water (20 mL) and HCl (20 mL) were added to the reaction mixture and the products extracted with ethyl acetate (3 x 50 mL). The organics were combined, dried over magnesium sulphate and concentrated *in vacuo* to remove solvent to afford the *title compound* as a colourless oil (6.55 g, 98%); $\nu_{\max}/\text{cm}^{-1}$ (neat) 3541, 2954, 2921, 2853.

Compound 133: 2,5-bis((tetrahydrofuran-2-yl)methyl)cyclopentan-1-ol

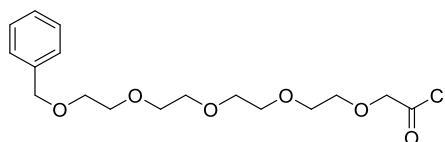


Methanol (5 mL) was added to a 2-neck flask which was purged with N₂ and cooled in an ice bath for 10 minutes before adding sodium borohydride (45.4 mg, 1.2 mmol) and purging with nitrogen again. In a separate flask compound **140** was diluted in methanol (5 mL) and then added via syringe to the first flask. The reaction mixture was allowed to come to room temperature under stirring and the reaction was monitored by TLC until completion. Deionised water was added dropwise to the reaction mixture to quench. Deionised water (5 mL) and HCl (5 mL) were added to the reaction mixture and the products extracted with ethyl acetate (3 x 15 mL). The organics were combined, dried over magnesium sulphate and concentrated *in vacuo* to remove solvent to afford the *title compound* as a colourless oil (218.5 mg, 87%); R_f: 0.02 (20% ethyl acetate in hexane); $\nu_{\max}/\text{cm}^{-1}$ (neat) 3439, 2939, 2863, 2145; δ_{H} (300 MHz, Chloroform-*d*) 3.95–3.72 (4H, m, CH₂OCH), 3.72–3.50 (2H, m, CH₂OCH),

3.24–3.09 (1H, m, CH), 2.99–2.43 (2H, m, CH), 2.10–1.57 (12H, m, CH₂), 1.57–1.17 (4H, m, CH₂).

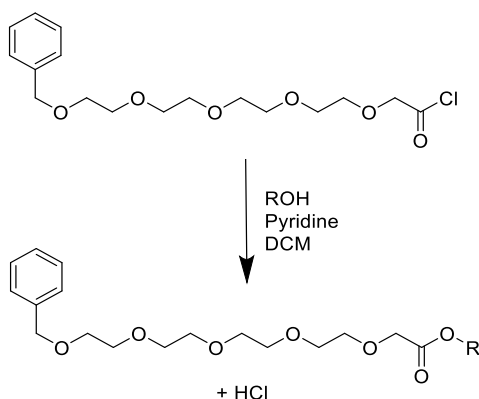
2.16.5 Preparation of esters from acyl chloride

Compound 129: 1-phenyl-2,5,8,11,14-pentaoxahehexadecan-16-oyl chloride



Oxalyl chloride (2 M solution in DCM, 15 mL, 30.0 mmol) was added to a solution of compound **126** (3.43 g, 10.0 mmol) in DCM (50 mL) followed by a catalytic amount of DMF (5 drops) under a nitrogen atmosphere. The resulting solution was stirred at room temperature for 1 hour and concentrated *in vacuo* to remove all the solvent and excess oxalyl chloride and afford the *title compound* as a colourless oil (3.61 g, <99% based on ¹H NMR). δ_{H} (300 MHz, Chloroform-*d*) 7.27 (m, 5H, H_{Ar}), 4.50 (s, 2H, PhCH₂), 4.42 (s, 2H, CH₂COCl), 3.64 – 3.50 (m, 16H, OCH₂CH₂O). Product was predicted to be unstable and was used immediately without further purification or additional characterisation in the following syntheses of esters.

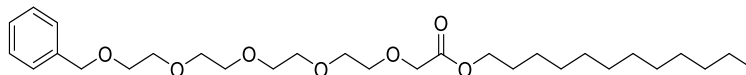
General procedure for the preparation of esters from acyl chloride



The selected alcohol (10.0 mmol) and pyridine (0.8 mL, 10.0 mmol) were added to a solution of compound **129** (3.61 g, 10.0 mmol) in DCM (50 mL) with stirring at room temperature. The reaction was followed by TLC and once complete the resulting organic solution was washed with deionised water (4 x 30 mL) and the aqueous extract washed with DCM (30 mL). The organics were combined and dried over magnesium sulphate and concentrated *in*

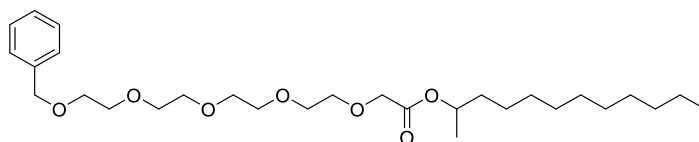
vacuo to remove solvent and purified by flash column chromatography to yield the desired product.

Compound 154: Dodecyl 1-phenyl-2,5,8,11,14-pentaoxahehexadecan-16-oate



1-Dodecanol (1.86 g, 10.0 mmol) and acid chloride **129** (3.61 g, 10.0 mmol) were reacted using the general procedure for the preparation of esters from acyl chloride. Purification by flash column chromatography (40% ethyl acetate in hexane) afforded the *title compound* as a light yellow oil (4.64 g, 91%); R_f : 0.10 (40% ethyl acetate in hexane); $\nu_{\max}/\text{cm}^{-1}$ (neat) 2922, 2854, 1753, 1101; δ_{H} (300 MHz, Chloroform-*d*) 7.41 – 7.22 (m, 5H, H_{Ar}), 4.59 (s, 2H, PhCH_2), 4.14 (t, 2H, COOCH_2), 3.88 – 3.52 (m, 16H, $\text{OCH}_2\text{CH}_2\text{O}$), 1.65 (p, $J = 7.0$ Hz, 2H, $\text{COOCH}_2\text{CH}_2$), 1.43 – 1.18 (m, 18H, $(\text{CH}_2)_9\text{CH}_3$), 0.90 (t, 3H, CH_2CH_3); δ_{C} (75 MHz, Chloroform-*d*) 170.5 (C=O), 138.3 (CH_{Ar}), 137.5 (CH_{Ar}), 128.3 (CH_{Ar}), 128.4 (CH_{Ar}), 127.7 (CH_{Ar}), 127.6 (CH_{Ar}), 74.7 (CH_2), 73.2 (2C, OCH_2), 70.9 (2C, OCH_2), 69.4 (2C, OCH_2), 68.6 (OCH_2), 64.9 (OCH_2), 31.9 (CH_2), 29.6 (2C, CH_2), 29.5 (CH_2), 29.5 (2C, CH_2), 29.3 (CH_2), 29.2 (2C, CH_2), 28.6 (CH_2), 25.8 (CH_2), 22.7 (CH_2CH_3), 14.1 (CH_3).

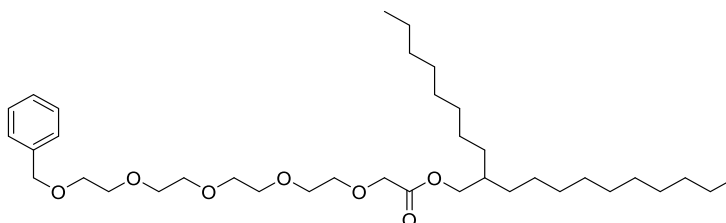
Compound 155: Dodecan-2-yl 1-phenyl-2,5,8,11,14-pentaoxahehexadecan-16-oate



2-Dodecanol (1.86 g, 10.0 mmol) and acid chloride **129** (3.61 g, 10.0 mmol) were reacted using the general procedure for the preparation of esters from acyl chloride. Purification by flash column chromatography (3:2 ethyl acetate: hexane) afforded the *title compound* (4.35 g, 85%) as a light yellow free flowing oil. R_f : 0.16 (3:2 ethyl acetate: hexane); $\nu_{\max}/\text{cm}^{-1}$ (neat) 2923, 2854, 1748; δ_{H} (300 MHz, Chloroform-*d*) 7.34 (5H, m, H_{Ar}), 4.99 (m, 1H, OCH), 4.57 (s, 2H, PhCH_2), 4.11 (s, 1H, CH_2COOCH), 3.79 – 3.53 (m, 16H, OCH_2), 1.67 – 1.16 (m, 22H, $\text{CH}_3\text{CH}(\text{CH}_2)_9$), 0.98 – 0.76 (t, 3H, CH_3). δ_{C} (75 MHz, Chloroform-*d*) 170.0 (COO), 138.3 (CH_{Ar}), 128.3 (2C, CH_{Ar}), 127.6 (2C, CH_{Ar}), 127.5 (CH_{Ar}), 73.1 (OCH_2), 71.6 (OCH_2), 70.8 (OCH_2), 70.6

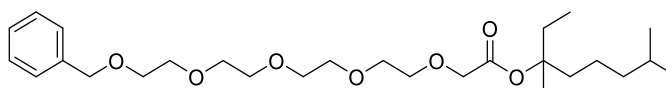
(OCH₂ x 6), 69.4 (OCH₂), 68.7 (OCH₂), 35.8 (CH₂), 31.9 (CH₂), 29.5 (CH₂ x 2), 29.5 (CH₂), 29.4 (CH₂), 29.3 (CH₂), 25.3 (CH₂), 22.6 (CH₂), 19.9 (CH₂), 14.1 (CH₃).

Compound 156: 2-Octyldodecyl 1-phenyl-2,5,8,11,14-pentaoxahexadecan-16-oate



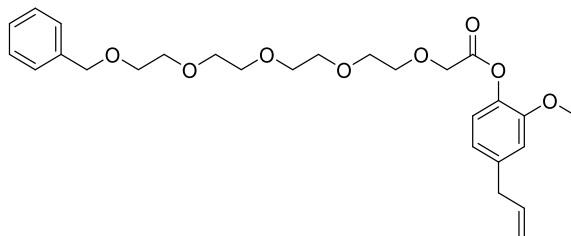
2-Octyl-1-dodecanol (2.98 g, 10.0 mmol) and acid chloride **129** (3.61 g, 10.0 mmol) were reacted using the general procedure for the preparation of esters from acyl chloride. Purification by flash column chromatography (20% ethyl acetate in hexane → 30% ethyl acetate in hexane) afforded the *title compound* as a colourless viscous oil (4.93 g, 79%); R_f: 0.1 (30% ethyl acetate in hexane); $\nu_{\max}/\text{cm}^{-1}$ (neat) 2923, 2855, 1740; δ_{H} (300 MHz, Chloroform-*d*) 7.29 (5H, m, H_{Ar}), 4.56 (2H, s, PhCH₂), 4.13 (3H, s, OCH₂COO), 4.04 (2H, d, *J* = 5.8 Hz, COOCH₂), 3.84 – 3.57 (16H, m, OCH₂CH₂O), 1.44 – 1.16 (32H, m, CH₂), 0.97 – 0.80 (6H, t, CH₂CH₃).

Compound 157: 3,7-dimethyloctan-3-yl 1-phenyl-2,5,8,11,14-pentahexadecan-16-oate



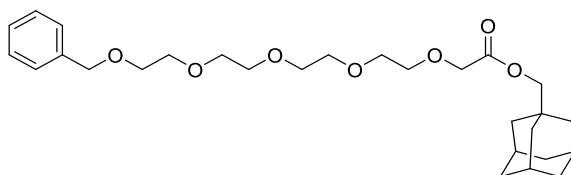
Tetrahydrolinalool (2.27 g, 14 mmol), compound **126** (7.58 g, 22 mmol), pyridine (7.3 mL, 90 mmol) and oxalyl chloride (6.93 mL, 80 mmol) were reacted using the general procedure for the preparation of esters from acyl chloride. Purification by flash column chromatography (50% ethyl acetate in hexane) afforded the *title compound* as a light yellow oil (2.18 g, 20%); R_f: 0.24 (50% ethyl acetate in hexane); $\nu_{\max}/\text{cm}^{-1}$ (neat) 2901, 1744, 1723; δ_{H} (300 MHz, Chloroform-*d*) 7.34 (5H, m, H_{Ar}), 4.57 (s, 2H, PhCH₂), 3.96 (2H, s, ROCH₂COOCR), 3.68 – 3.50 (16H, m, OCH₂CH₂O), 1.91-1.57 (5H, m, CH₂, CH), 1.34 (s, 3H, COOCCH₃), 1.28-0.98 (4H, m, CH₂), 0.89-0.69 (9H, m, CH₃). δ_{C} (75 MHz, Chloroform-*d*) 169.9 (C=O), 86.9 (C=OOC), 72.8 (OCH₂COO), 70-71 (6C, overlapping peaks, OCH₂CH₂O), 69.0 (OCH₂CH₂O), 61.9 (COH), 39.4 (CH), 38.4 (CH₂), 31.2 (CH₂), 28.1 (CH₂), 23.7 (CH₂), 22.8 (2C, CHCH₃CH₃), 8.3 (CH₃).

Compound 157: 4-allyl-2-methoxyphenyl 1-phenyl-2,5,8,11,14-pentaoxahexadecan-16-oate



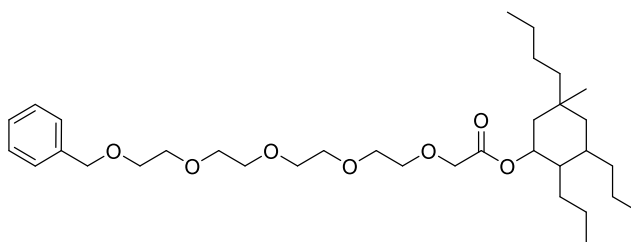
Eugenol (174 mg, 1.06 mmol) and acid chloride **129** (1.5 mL, 17.06 mmol) were reacted using the general procedure for the preparation of esters from acyl chloride. Purification by flash column chromatography (60% ethyl acetate in hexane) afforded the *title compound* as a light yellow oil (141 mg, 28%); R_f : 0.8 (60% ethyl acetate in hexane).

Compound 158: ((3r,5r,7r)-adamantan-1-yl)methyl 1-phenyl-2,5,8,11,14-pentaoxahexadecan-16-oate



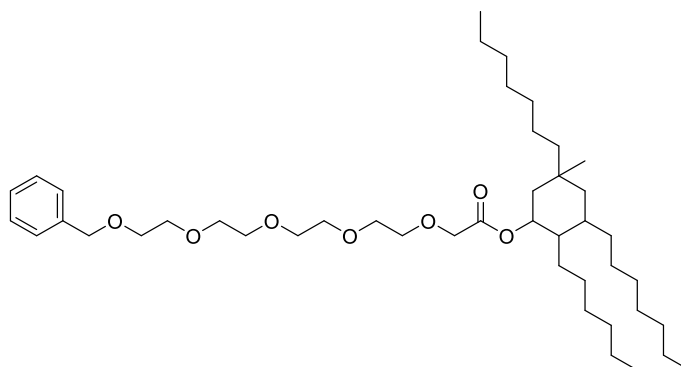
Adamantane methanol (171 mg, 1.0 mmol), compound **126** (353 mg, 1.0 mmol) and oxalyl chloride (1.5 mL, 17 mmol) were reacted using the general procedure for the preparation of esters from acyl chloride. Purification by flash column chromatography (40% ethyl acetate in hexane) afforded the *title compound* as a light yellow oil (288 mg, 57%); R_f : 0.08 (30% ethyl acetate in hexane); δ_H (300 MHz, Chloroform-*d*) 7.33–7.14 (5H, m, H_{Ar}), 4.07 (2H, s, OCH_2COO), 3.67 (2H, s, $COOCH_2$), 1.95–1.83 (3H, m, CH_2), 1.71–1.53 (6H, m, CH_2), 1.49–1.39 (6H, m, CH_2).

Compound 160: 3,5-dibutyl-5-methyl-2-propylcyclohexyl 1-phenyl-2,5,8,11,14-pentaoxahexadecan-16-oate



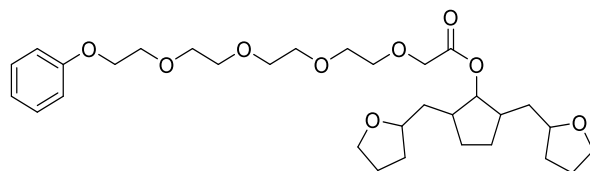
Compound **136** (3.21 g, 11.9 mmol) and acid chloride **129** (3 mL, 35.0 mmol) were reacted using the general procedure for the preparation of esters from acyl chloride. Purification by flash column chromatography (% ethyl acetate in hexane) afforded the *title compound* as a light yellow oil (1.48 g, 21%); R_f : (% ethyl acetate in hexane); $\nu_{\max}/\text{cm}^{-1}$ (neat) 2954, 2927, 2860, 1748; δ_{H} (300 MHz, Chloroform-*d*) 7.41–7.09 (5H, m, H_{Ar}), 4.48 (2H, s, PhCH_2), 4.08–3.98 (2H, m, OCH_2COO), 3.69–3.41 (16H, m, $\text{OCH}_2\text{CH}_2\text{O}$), 2.02–1.87 (2H, m, CH), 1.87–0.93 (20H, m, CH_2), 0.93–0.59 (12H, m, CH_3).

Compound 161: 3,5-Diheptyl-2-hexyl-5-methylcyclohexyl 1-phenyl-2,5,8,11,14-pentaoxahexadecan-16-oate



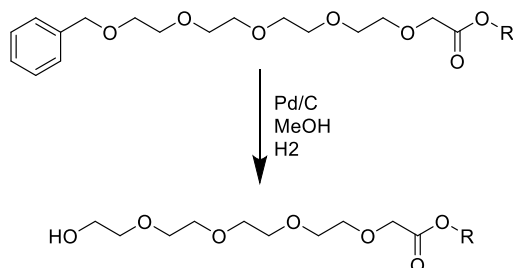
Compound **126** (1.04 g, 2.6 mmol), compound **137** (1.01 g, 2.9 mmol) and oxyalyl chloride (1.5 mL, 17.5 mmol) were reacted using the general procedure for the preparation of esters from acyl chloride. Purification by flash column chromatography (% ethyl acetate in hexane) afforded the *title compound* as a light yellow oil (0.63g, 30%); (% ethyl acetate in hexane); $\nu_{\max}/\text{cm}^{-1}$ (neat) 2923, 2855, 1748.

Compound 162: 13-((2,5-bis(cyclopentylmethyl)cyclopentyl)oxy)-1-phenyl-2,5,8,11-tetraoxatridecane



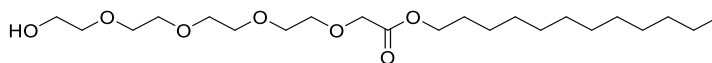
Compound **126** (0.79 g, 3.1 mmol), compound **133** (1.06 g, 3.12 mmol) and oxalyl chloride (1.5 mL, 17.5 mmol) were reacted using the general procedure for the preparation of esters from acyl chloride. Purification by flash column chromatography (% ethyl acetate in hexane) afforded the *title compound* as a light yellow oil (0.25 g, 14 %); R_f : 0.16 (60% ethyl acetate in hexane); $\nu_{\max}/\text{cm}^{-1}$ (neat) 2309, 2869, 1742; δ_{H} (300 MHz, Chloroform-*d*) 7.38-7.12 (5H, m, H_{Ar}), 4.49 (2H, s, $\text{H}_{\text{Ar}}\text{CH}_2$), 4.39–4.25 (1H, m, COOCH), 4.25–4.16 (2H, m, OCH), 4.15–3.97 (2H, m, CH_2), 3.97–3.68 (6H, m, CHOCH_2), 3.68–3.46 (6H, m, $\text{OCH}_2\text{CH}_2\text{O}$), 2.20–0.73 (12H, m, CH_2).

General procedure for the Pd/C hydrogenative deprotection of the benzyl protecting group



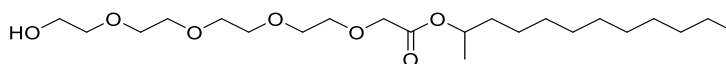
Pd/C (5 % wt/wt loading, 240 mg) was added to a 2 necked flask fitted with a 3 way gas tap and slowly purged with nitrogen. The catalyst was wetted with methanol (6 mL) under nitrogen via septa and syringe and the benzyl protected alcohol (1.00 mmol) was added to the suspension in the same fashion. The nitrogen was purged and replaced with hydrogen at atmospheric pressure and the reaction left at room temperature under vigorous agitation for 16 hours. The reaction was followed by TLC and ^1H NMR and once complete the gas was evacuated from the flask via the vacuum line and was flushed with nitrogen, this process was repeated 3 times. The reaction solution was filtered through a celite pad which was sequentially washed thoroughly with methanol (3 x 10 mL), ethyl acetate (3 x 10 mL) and DCM (3 x 10 mL). The resulting organics were combined and dried over magnesium sulphate and concentrated *in vacuo* and no further purification was required.

Compound 145: dodecyl 14-hydroxy-3,6,9,12-tetraoxatetradecan-16-oate



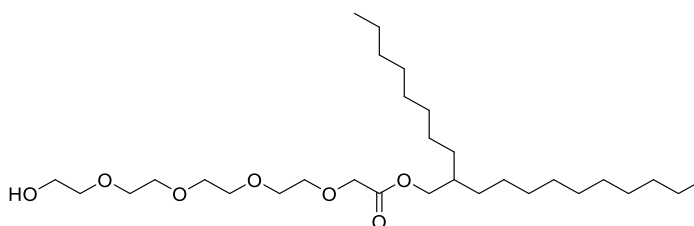
Compound **154** (4.64 g, 9.10 mmol) was hydrogenated via the general procedure for the Pd/C hydrogenative deprotection of the benzyl protecting group to afford the *title compound* as a light yellow oil (3.60 g, 94%); $\nu_{\max}/\text{cm}^{-1}$ (neat) 3420, 2922, 2853, 1754; δ_{H} (300 MHz, Chloroform-*d*) 4.13 (s, 2H, CH_2COO), 3.76 – 3.50 (m, 18H, $\text{OCH}_2\text{CH}_2\text{O}$), 2.61 (s, 1H, OH), 1.51 (t, $J = 7.0$ Hz, 2H, $\text{COOCH}_2\text{CH}_2$), 1.24 (m, H, (CH_2)), 0.90 – 0.74 (m, 3H, CH_3). δ_{C} (75 MHz, Chloroform-*d*) δ 170.8 (C=O), 72.6 (CH_2O), 70.8 (CH_2O), 70.5 (2 x CH_2O), 70.4 (2 x CH_2O), 70.2 (CH_2O), 68.5 (CH_2O), 62.5 (COCH_2COO), 61.5 (COOCH_2), 32.6 (CH_2), 31.8 (CH_2), 29.5 (4 x CH_2), 29.4 (CH_2), 29.2 (CH_2), 25.7 (CH_2), 22.5 (CH_2), 14.0 (CH_3); expected mass $\text{C}_{22}\text{H}_{44}\text{NaO}_7$: 443.2979, mass found $\text{C}_{22}\text{H}_{44}\text{NaO}_7$: 443.2980, error[ppm] -0.1.

Compound 146: dodecan-2-yl 14-hydroxy-3,6,9,12-tetraoxatetradecanoate



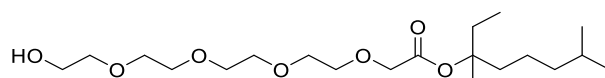
Compound **155** (4.35 g, 8.50 mmol) was hydrogenated using the general procedure for the Pd/C hydrogenative deprotection of the benzyl protecting group to afford the *title compound* as a light yellow oil (3.37 g, 94%); $\nu_{\max}/\text{cm}^{-1}$ (neat) 2923, 2854, 1748, 1105; δ_{H} (300 MHz, Chloroform-*d*) 4.96 (m, 1H, OCH), 4.10 (s, 2H, CH_2COC), 3.66 (m, 16H, $\text{OCH}_2\text{CH}_2\text{O}$), 2.52 (s, 1H, OH), 1.64 – 1.10 (m, 21H, (CH_2)₉ $\text{CH}(\text{O})\text{CH}_3$), 0.93 – 0.77 (4H, t, $J = 6.9$ Hz, CH_2CH_3). δ_{C} (75 MHz, Chloroform-*d*) 169.9 (C=O), 72.4 (CH_2O), 71.5 (CH_2O), 70.6 (CH_2O), 70.4 (CH_2O), 70.3 (CH_2O), 70.3 (CH_2O), 70.3 (CH_2O), 70.1 (CH_2O), 68.5 (CO), 61.2 (CO), 35.7 (CH_2), 31.7 (CH_2), 29.6 – 29.0 (5C, CH_2), 25.1 (CH_2), 22.4 (CH_2), 19.7 (CH_2), 13.9 (CH_2CH_3); expected mass $\text{C}_{22}\text{H}_{44}\text{NaO}_7$: 443.2979, mass found $\text{C}_{22}\text{H}_{44}\text{NaO}_7$: 443.2984, error[ppm] -1.0.

Compound 147: 2-octyldodecyl 12-hydroxy-3,6,9,12-tetradecanoate



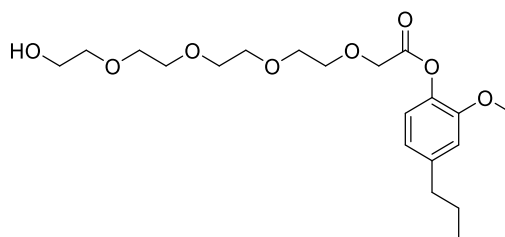
Compound **156** (6.71 g, 10.77 mmol) was hydrogenated via the general procedure for the Pd/C hydrogenative deprotection of the benzyl protecting group to afford the *title compound* as a light yellow oil (5.55 g, 97%); $\nu_{\max}/\text{cm}^{-1}$ (neat) 3450, 2922, 2853, 1748, 1122; δ_{H} (300 MHz, Chloroform-*d*) 4.14 (s, 2H, COCH₂COO), 4.04 (d, J = 5.8 Hz, 2H, COOCH₂), 3.83–3.55 (m, 16H, OCH₂CH₂O), 1.63 (m, 1H, CH(CH₂)₇CH₃(CH₂)₉CH₃), 1.39–1.10 (m, 32H, CH(CH₂)₇CH₃(CH₂)₉CH₃), 0.86 (t, J = 6.5 Hz, 6H, 2 x CH₃). δ_{C} (75 MHz, Chloroform-*d*) 170.8 (C=O), 73.1 (OCH₂COO), 72.7 (C=OOC), 70.9 (OCH₂CH₂O), 70.7 (OCH₂CH₂O), 70.5 (OCH₂CH₂O), 70.4 (OCH₂CH₂O), 70.1 (OCH₂CH₂O), 68.7 (CH), 67.7 (CH₂), 65.8 (CH₂), 40.5 (CH₂), 37.3 (CH₂), 31.9 (CH₂), 31.2 (CH₂), 31.0 (CH₂), 30.1 (CH₂), 30.0 (CH₂), 29.7 (CH₂), 29.6 (CH₂), 29.4 (CH₂), 29.3 (CH₂), 26.9 (CH₂), 26.7 (CH₂), 22.7 (CH₂), 14.2 (CH₃), 14.1 (CH₂); expected mass C₃₀H₆₁O₇: 533.4111, mass found C₃₀H₆₁O₇: 533.4386, error[ppm] -4.7.

Compound 148: 3,7-dimethyloctan-3-yl 14-hydroxy-3,6,9,12-tetraoxatetradecanoate



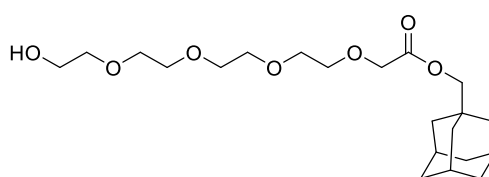
Compound **157** (2.18 g, 4.11 mmol) was hydrogenated via the general procedure for the Pd/C hydrogenative deprotection of the benzyl protecting group to afford the *title compound* as a light yellow oil (1.76 g, 97%); $\nu_{\max}/\text{cm}^{-1}$ (neat) 3465, 2950, 2869, 1743; δ_{H} (300 MHz, Chloroform-*d*) 3.96 (2H, s, CH₂COOCR), 3.68 – 3.50 (16H, m, OCH₂CH₂O), 1.91–1.57 (6H, m, 3 x CH₂), 1.34 (s, 3H, COOCCH₃), 1.28–0.98 (4H, m, 2 x CH₂), 0.89–0.69 (9H, m, CH₃). δ_{C} (75 MHz, Chloroform-*d*) 169.9 (C=O), 86.9 (C=OOC), 72.8 (OCH₂COO), 70–71 (6C, overlapping peaks, OCH₂CH₂O), 69.0 (OCH₂CH₂O), 61.9 (COH), 39.4 (CH), 38.4 (CH₂), 31.2 (CH₂), 28.1 (CH₂), 23.7 (CH₂), 22.8 (2C, CHCH₃CH₃), 8.3 (CH₃); expected mass C₂₀H₄₀NaO₇: 415.2666, mass found C₂₀H₄₀NaO₇: 415.2671, error[ppm] -1.0.

Compound 149: 2-Methoxy-4-propylphenyl 14-hydroxy-3,6,9,12-tetraoxatetradecanoate



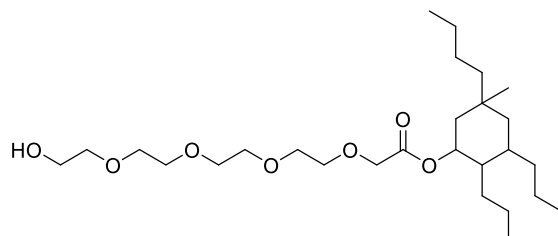
Compound **158** (5.40 g, 10.02 mmol) was hydrogenated via the general procedure for the Pd/C hydrogenative deprotection of the benzyl protecting group to afford the *title compound* as a light yellow oil (4.28 g, 95%); $\nu_{\max}/\text{cm}^{-1}$ (neat) 3435, 2926, 2870, 1754, 1601. δ_{H} (300 MHz, Chloroform-*d*) 6.83–6.63 (3H, m, H_{Ar}), 5.49 (1H, s, OH), 4.15 (2H, s, CH_2COO), 3.86 (3H, s, OCH_3), 3.75–3.57 (16H, m, $\text{OCH}_2\text{CH}_2\text{O}$), 1.66 (2H, t, $\text{CH}_2\text{CH}_2\text{CH}_3$), 1.63 (2H, q, $\text{CH}_2\text{CH}_2\text{CH}_3$), 0.91 (3H, t, $\text{CH}_2\text{CH}_2\text{CH}_3$). δ_{C} (75 MHz, Chloroform-*d*) 171.1 (C=O), 146.3 (C_{Ar}), 143.6 (C_{Ar}), 134.8 (C_{Ar}), 121.0 (CH_{Ar}), 114.1 (CH_{Ar}), 111.1 (CH_{Ar}), 72.6 ($\text{OCH}_2\text{CH}_2\text{O}$), 71.0 ($\text{OCH}_2\text{CH}_2\text{O}$), 70.7 ($\text{OCH}_2\text{CH}_2\text{O}$), 70.63 ($\text{OCH}_2\text{CH}_2\text{O}$), 70.61 ($\text{OCH}_2\text{CH}_2\text{O}$), 70.4 ($\text{OCH}_2\text{CH}_2\text{O}$), 68.7 ($\text{OCH}_2\text{CH}_2\text{O}$), 61.7 ($\text{OCH}_2\text{CH}_2\text{O}$), 55.9 (CH_2COO), 51.9 (OCH_3), 37.8 ($\text{CH}_2\text{CH}_2\text{CH}_3$), 24.9 ($\text{CH}_2\text{CH}_2\text{CH}_3$), 13.8 ($\text{CH}_2\text{CH}_2\text{CH}_3$); expected mass $\text{C}_{20}\text{H}_{32}\text{O}_8$: 401.2097, mass found $\text{C}_{20}\text{H}_{32}\text{O}_8$: 401.2170.

Compound 150: ((3*r*,5*r*,7*r*)-Adamantan-1-yl)methyl 14-hydroxy-3,6,9,12-tetraoxatetradecanoate



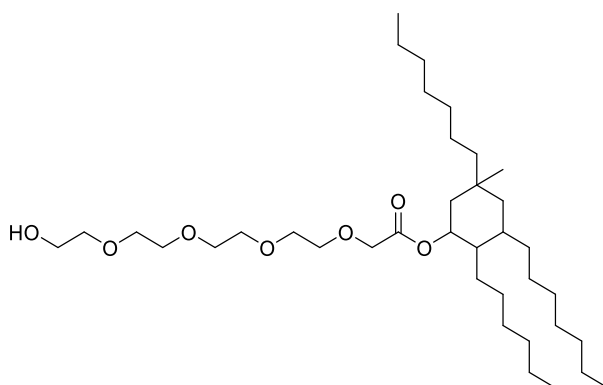
Compound **159** (4.92 g, 9.14 mmol) was hydrogenated via the general procedure for the Pd/C hydrogenative deprotection of the benzyl protecting group to afford the *title compound* as a light yellow oil (4.05 g, 99%); $\nu_{\max}/\text{cm}^{-1}$ (neat) 3463, 2900, 2848, 1750; δ_{H} (300 MHz, Chloroform-*d*) 4.09 (2H, s, OCH_2COO), 3.80–3.84 (2H, m, COOCH_2), 3.70 – 3.55 (16H, m, $\text{OCH}_2\text{CH}_2\text{O}$), 1.94–1.85 (3H, m, CH), 1.71–1.52 (6H, m, CH_2), 1.48–1.41 (6H, m, CCH_2). δ_{C} (75 MHz, Chloroform-*d*) 171.0 (C=O), 74.3 (C=OOC), 73.9 (OCH_2COO), 73.1 (OCH_2), 72.6–70.1 (8C, overlapping peaks, $\text{OCH}_2\text{CH}_2\text{O}$), 68.6 (COH), 39.5–28.1 (CH, CH_2 , 10C, 10 peaks); expected mass $\text{C}_{21}\text{H}_{36}\text{NaO}_7$: 423.2353, mass found $\text{C}_{21}\text{H}_{36}\text{NaO}_7$: 423.2357, error[ppm] -1.0.

Compound 151: 3,5-Dibutyl-5-methyl-2-propylcyclohexyl 14-hydroxy-3,6,9,12-tetraoxatetradecanoate



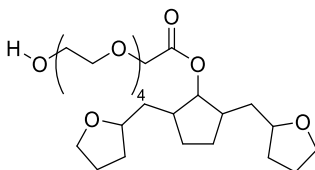
Compound **160** (4.74 g, 8.00 mmol) was hydrogenated via the general procedure for the Pd/C hydrogenative deprotection of the benzyl protecting group to afford the *title compound* as a light yellow oil (3.90 g, 97%); $\nu_{\max}/\text{cm}^{-1}$ (neat) 3480, 2954, 2927, 2871, 1746. δ_{H} (300 MHz, Chloroform-*d*) 4.15-3.93 (3H, m, OCH₂COO, CH), 3.77-3.56 (16H, m, OCH₂CH₂O), 2.08-1.35 (2H, m, CH), 1.35-0.96 (20H, m, CH₂), 0.96-0.71 (12H, m, CH₃). δ_{C} (75 MHz, Chloroform-*d*) 170.2 (C=O), 72.7 (CH₂COO), 72.6 (CH₂COOCH), 70.96 (OCH₂CH₂O), 70.93 (OCH₂CH₂O), 70.68 (OCH₂CH₂O), 70.64 (OCH₂CH₂O), 70.62 (OCH₂CH₂O), 70.60 (OCH₂CH₂O), 70.56 (OCH₂CH₂O), 70.39 (OCH₂CH₂O), 44.3 (CH), 43.8 (CH), 32.8 (CH₂), 32.5 (CH₂), 30.5 (CH₂), 30.17 (CH₂), 26.5 (CH₂), 25.4 (CH₂), 23.9 (CH₂), 23.2 (CH₂), 14.5 (CH₃), 14.4 (CH₃), 14.3 (CH₃), 14.2 (CH₃); expected mass C₂₈H₅₄NaO₇: 525.3762, mass found C₂₈H₅₄NaO₇: 525.3787, error[ppm] -4.8.

Compound 152: 3,5-Diheptyl-2-hexyl-5-methylcyclohexyl 14-hydroxy-3,6,9,12-tetraoxatetradecanoate



Compound **161** (1.40 g, 2.50 mmol) was hydrogenated via the general procedure for the Pd/C hydrogenative deprotection of the benzyl protecting group to afford the *title compound* as a colourless oil (1.15 g, 97%); $\nu_{\max}/\text{cm}^{-1}$ (neat) 3435, 2923, 2855, 1747. δ_{H} (300 MHz, Chloroform-*d*) 5.23-5.02 (1H, m, OCH₂COOCH), 4.18-3.80 (2H, m, OCH₂COOCH), 3.78-3.56 (16H, m, OCH₂CH₂O), 1.72-1.36 (2H, m, CH), 1.36-0.96 (38H, m, CH₂), 0.96-0.73 (12H, m, CH₃). δ_{C} (75 MHz, Chloroform-*d*) 170.2 (C=O), 72.7 (OCH₂COOCH), 72.6 (CH₂COOCH), 70.06 (OCH₂CH₂O), 70.42 (OCH₂CH₂O), 70.61 (OCH₂CH₂O), 70.65 (OCH₂CH₂O), 70.69 (OCH₂CH₂O), 70.93 (OCH₂CH₂O), 33.3 (CH₂), 32.6 (CH₂), 31.9-31.7 (3C, overlapping peaks, CH₂), 30.6 (CH₂), 30.1 (CH₂), 29.2-29.3 (3C, overlapping peaks, CH₂), 29.4 (CH₂), 26.9 (CH₂), 26.02 (CH₂), 24.5 (CH₂), 22.6-22.8 (4C, overlapping peaks), 14.21-14.13 (3C, overlapping peaks, CH₃); expected mass C₃₇H₇₃O₇: 629.5350, mass found C₃₇H₇₃O₇: 629.5333, error[ppm] -2.8.

Compound 153: 2,5-Bis((tetrahydrofuran-2-yl)methyl)cyclopentyl 14-hydroxy-3,6,9,12-tetraoxatetradecanoate



Compound **162** (1.56 g, 2.76 mmol) was hydrogenated via the general procedure for the Pd/C hydrogenative deprotection of the benzyl protecting group to afford the *title compound* as a light yellow oil (1.27 g, 94%); $\nu_{\max}/\text{cm}^{-1}$ (neat) 3437, 2960, 2869, 1742 ; δ_{H} (300 MHz, Chloroform-*d*) 4.31-4.39 (1H, m, COOCH), 4.02-4.11 (2H, m, CH₂COOR), 3.45-3.85 (23H, m, OCH₂CH₂O, CH₂OCH), 1.01-2.21 (18H, m, CH₂CH₂). δ_{C} (75 MHz, Chloroform-*d*) 170.1 (C=O), 72.7 (2C, CH), 72.5 (2C, OCH₂), 70.2-70.4 (7C, OCH₂CH₂O, overlapping peaks), 69.8 (CH₂C=OO), 67.0 (COOCH) 61.3 (COH), 36.0 (CH), 35.7 (CH), 31.7 (2C, CH₂), 31.5 (2C, CH₂), 25.6 (2C, CH₂), 25.5 (2C, CH₂); expected mass C₂₅H₄₄NaO₉: 511.2878, mass found C₂₅H₄₄NaO₉: 511.2871, error[ppm] -1.2.

2.16.6 General procedure for the aldol condensation of 2-hexanone using Q-tube apparatus

2-hexanone (2 mmol), Mg-Al-O (200 mg), dodecane (100 mg, internal GC-FID standard) and toluene (3 mL) are loaded into a Q-tube (12 mL) within a pre-heated aluminium block at 150 °C with vigorous stirring. After 3 hours the reaction mixture is filtered through cotton wool prior to GC-FID analysis.

2.16.7 Preparation of Mg-Al-O

Mg-Al-O was prepared following the literature procedure outlined by Sacia et al¹⁷⁰. Hydrotalcite (magnesium aluminium hydroxycarbonate, $\text{Mg}_6\text{Al}_2(\text{CO}_3)(\text{OH})_{16} \cdot 4\text{H}_2\text{O}$) was calcined (heated to activate the catalyst) at 700 °C for 2 h with an oven ramp rate of 2 °C. Prior to optimisation the catalyst was either stored under vacuum or used within 2 hours of cooling. After optimisation the calcined catalyst was allowed to cool and sit on the benchtop for a minimum of 2 days before use.

Chapter 3

3 INVESTIGATION OF THE PROPERTIES AND FUNCTIONALITY OF NOVEL SURFACTANTS IN COMPARISON WITH INDUSTRIALLY PRODUCED SURFACTANTS IN THE PURSUIT OF SUITABLE APPLICATIONS

3.1 INTRODUCTION AND AIMS

A range of analytical methods were used to determine possible applications and analyse any surfactant properties of the final compounds (Figure 43) produced in this work.

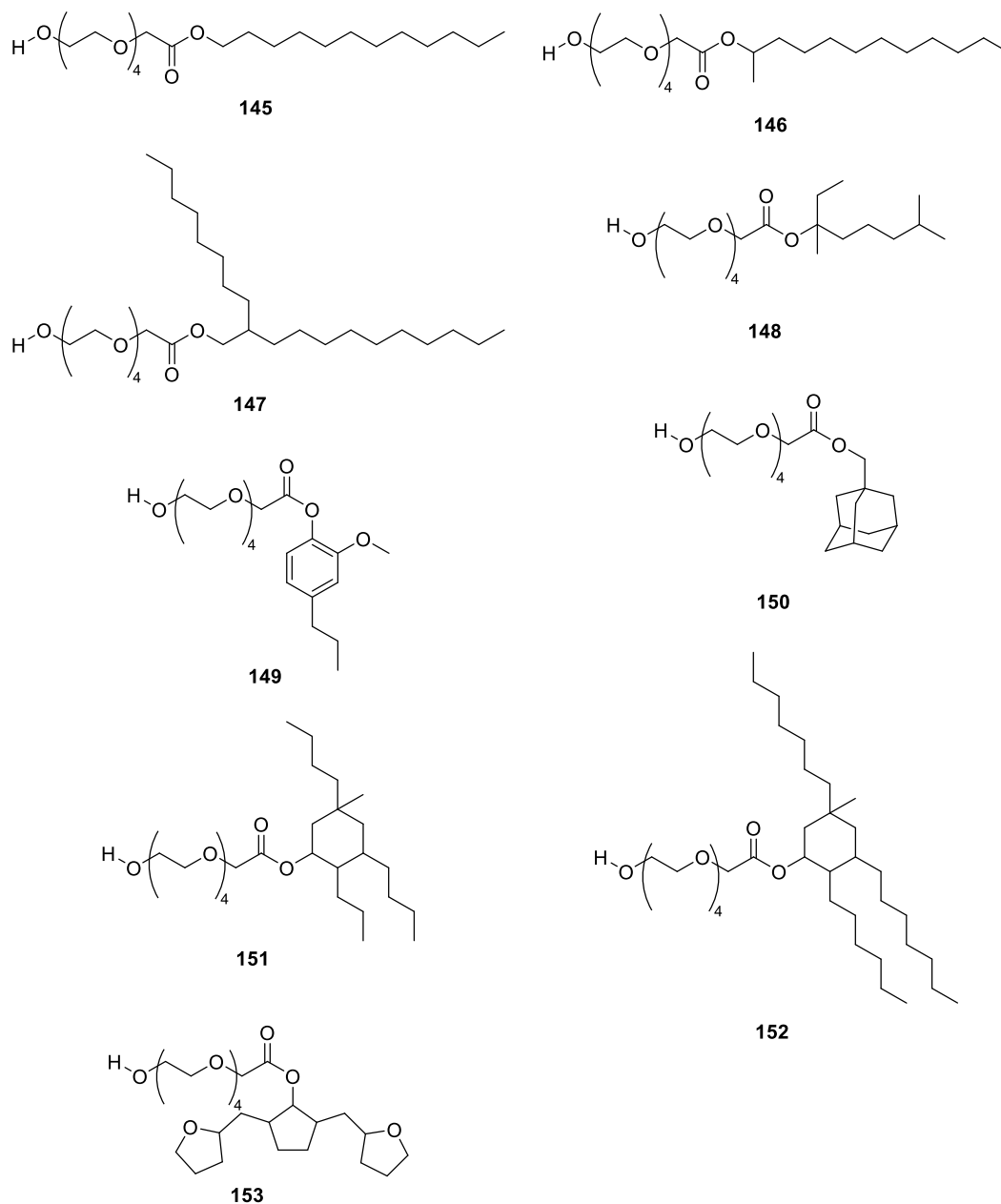


Figure 43: Final compounds **145-153** synthesised in this study and subjected to analysis for identification and comparison of surfactant properties.

Of particular interest was an assessment of whether the range of novel surfactants synthesised during this study (Figure 43) could potentially be used as less harmful,

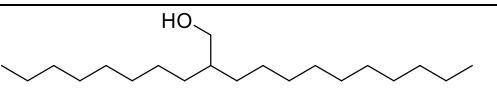
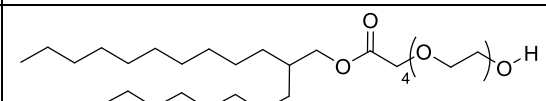
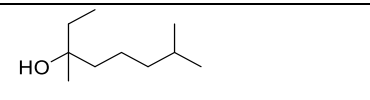
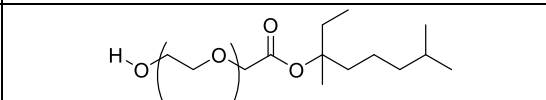
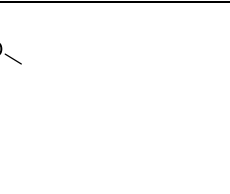
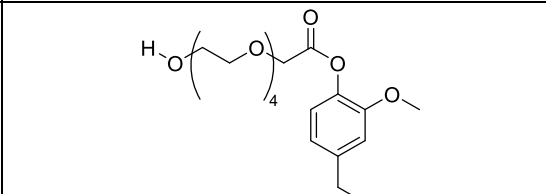

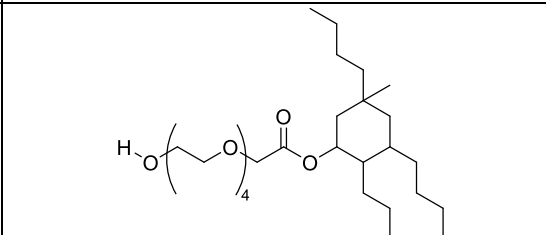
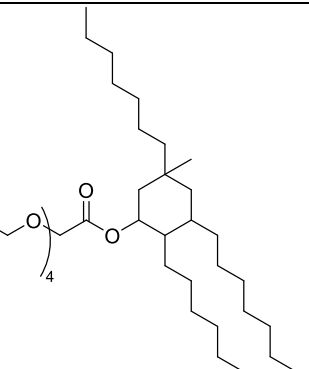
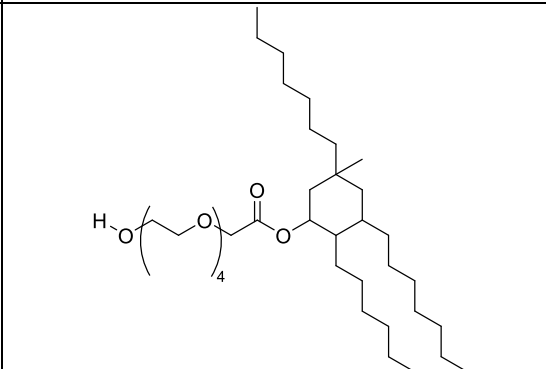

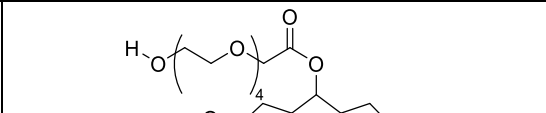
biodegradable replacements for perfluorinated surfactants. Replicating the hydrophobicity of perfluorinated surfactants was chosen as the aim of this study over replicating the resistance to chemical, thermal and biological degradation in order to align with the principles of green chemistry and avoid synthesis of compounds which are persistent in the environment. Hydrophobicity is also a preferable target to oleophobicity as the intention was to use biomass derivable starting materials with which it would be difficult to produce a non-water soluble oleophobic tail group due to the nature of the starting materials.

Several bioderivable alcohols were chosen to use as starting materials for the hydrophobe portion of the surfactant (Table 9). Having a range of bioderivable hydrophobes was a key aspect of this work firstly because waste biomass is a renewable resource and secondly because it increases the likelihood that the final compound will be biodegradable.

Compound **148** is based on linalool, a naturally occurring and extractable terpene found in flowers. Compound **149** is based on eugenol, found in clove oil or derivable from biomass through lignin depolymerisation. The ability to access eugenol from biomass waste as well as extraction from cloves is an advantage because it does not require the sacrifice of food crops for fuel production. Compound **147** is based on a Guerbet alcohol produced by Croda. The Guerbet reaction is utilised by biomass derived fuel researchers as a way to lengthen carbon chains and improve the quality of fuels. Compounds **151** and **152** are based on double self-aldol condensations of methyl ketones derivable from biomass through hydrogenation and hydrolysis of 2,5-DMF (**87**), derived from the platform molecule HMF (**16**) or through Dakin-West reactions. Finally, compound **153** is derived from the alcohol produced by the aldol condensation of cyclopentanone and furfural.

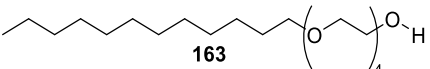
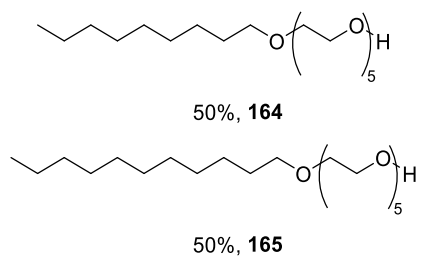
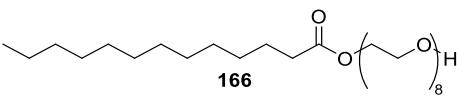
The polyethylene glycol (PEG) hydrophilic head group common to all of the final compounds was chosen because Croda has an existing process which is used for their range of renewable ethoxylated products in their ECO range which are produced through bioethanol. The relatively short PEG chain (4 units) was chosen because a high purity tetraethylene glycol was available commercially which makes structural determination easier during synthesis.

Table 9: Final compounds and the bioderivable alcohols used to produce hydrophobes.

Alcohol	Final compound
	 <p style="text-align: center;">147</p>
	 <p style="text-align: center;">148</p>
	 <p style="text-align: center;">149</p>
	 <p style="text-align: center;">151</p>
	 <p style="text-align: center;">152</p>
	 <p style="text-align: center;">153</p>

Standard industry techniques such as dynamic light scattering and the Wilhelmy plate method were employed to analyse and compare the properties of the surfactants. The laboratories at Croda house the majority of the instruments used in this study to analyse the structure-performance relationship of the surfactants and a comparison of their performance against known industry products (see Table 10) and perfluorooctanoic acid (PFOA).

Table 10: Industrial products and information on manufacture and structure for the industrial produced used for comparison with compounds **145-153**.

Product name	Representative structure	Product information
Brij L4-LQ-(AP)	 <p style="text-align: center;">163</p>	Alpha fatty alcohols (range of chain lengths, predominantly C12:0) with an ethoxylate chain distribution around the nominal figure
Synperonic 91/5-LQ-(RB)	 <p style="text-align: center;">50%, 164</p> <p style="text-align: center;">50%, 165</p>	Alpha fatty alcohols (chain lengths approx. 50% C9:0 and 50% C11:0) with an ethoxylate chain distribution around the nominal figure
Cithrol 4ML-LQ-(RB)	 <p style="text-align: center;">166</p>	Alpha fatty ester (range of chain lengths, predominantly C12:0) with an ethoxylate chain distribution around the nominal figure

Compound **145** (Figure 43) was synthesised in order to establish a route to a fatty chain ethoxylated surfactant that could later be adjusted to add more interesting and novel hydrophobes compared to surfactants produced to industry standards. The industrially produced samples of Brij, Cithrol and Synperonic (Table 44, Figure 44) were chosen for their structural resemblance to compound **145**.

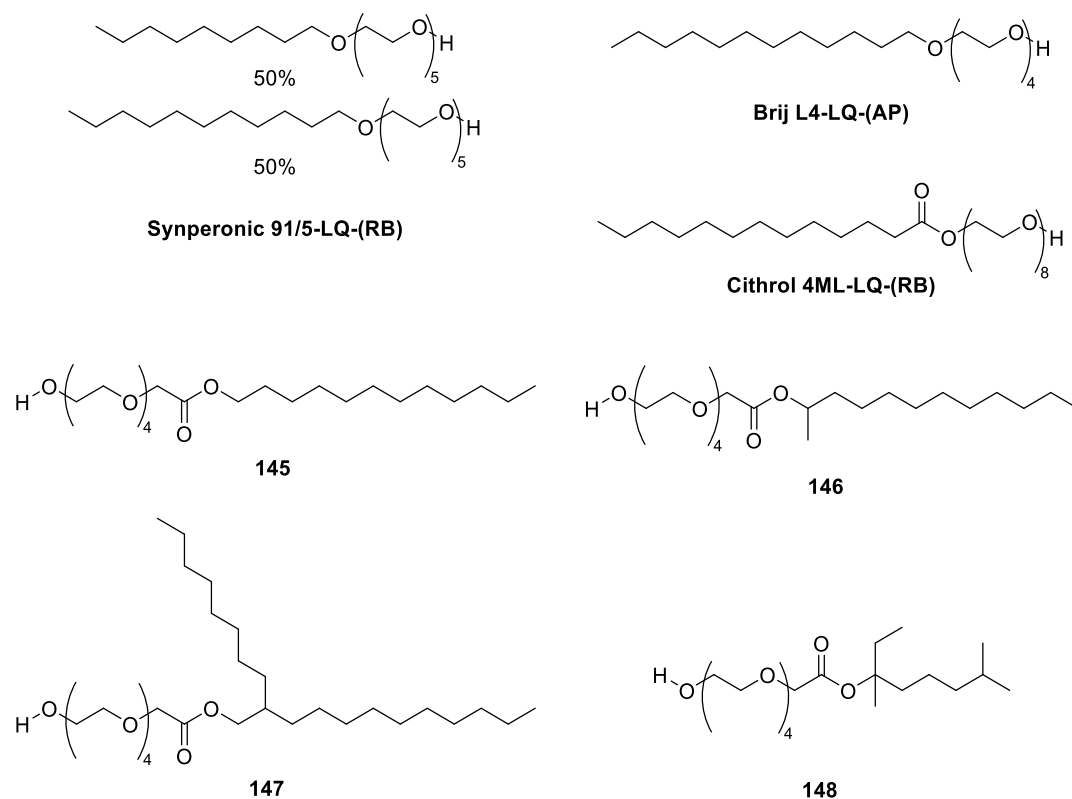


Figure 44: Representative structures for the Industrially produced surfactant samples (purify unknown but likely to be a distribution of fatty chain lengths from natural oils and variation of ethoxylate chain length) alongside the structures of compounds **145-148**.

Brij and Synperonic have predominantly 4 PEG units and a linear alkyl chain however does not have an ester link between the two. Cithrol does have the ester link, however, the orientation of the ester group is reversed, with the hydrophobe portion product coming from a fatty acid then undergoing esterification as opposed to the hydrophobic portion of the final compounds synthesised in this study coming from alcohols before esterification. The comparison between Cithrol, Brij, Synperonic and compound **145** may shed light on the effect the ester linkage has joining the hydrophilic head and hydrophobic tail groups together, compared to direct ethoxylation of the fatty chain.

Cithrol has an average PEG chain length double that of the final compounds produced here. The similar linear alkyl chain lengths of Brij, Synperonic and **145** are useful for observing any difference in solubility and performance doubling the PEG chain length may have when comparing to Cithrol.

Any comparisons between the final compounds and the industrially produced products should be considered with the difference in purity in mind. As is typical with industrially synthesised surfactants, the products are not synthetically pure and are of unspecified purity. Starting materials used for surfactant synthesis are often natural oils such as rapeseed oil and palm oil which contain a distribution of fatty chain lengths (Figure 45):

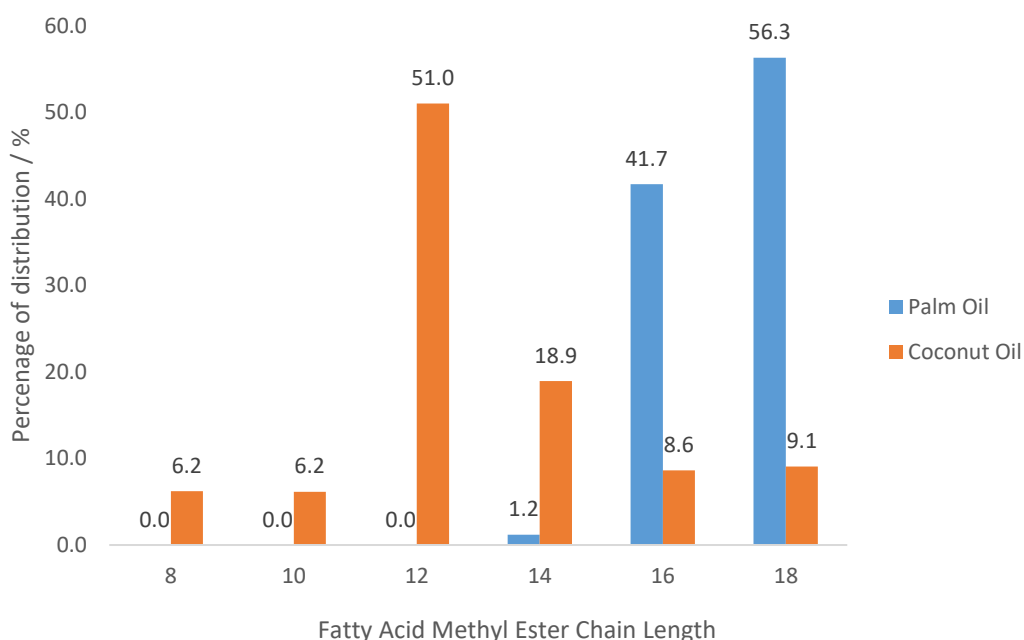
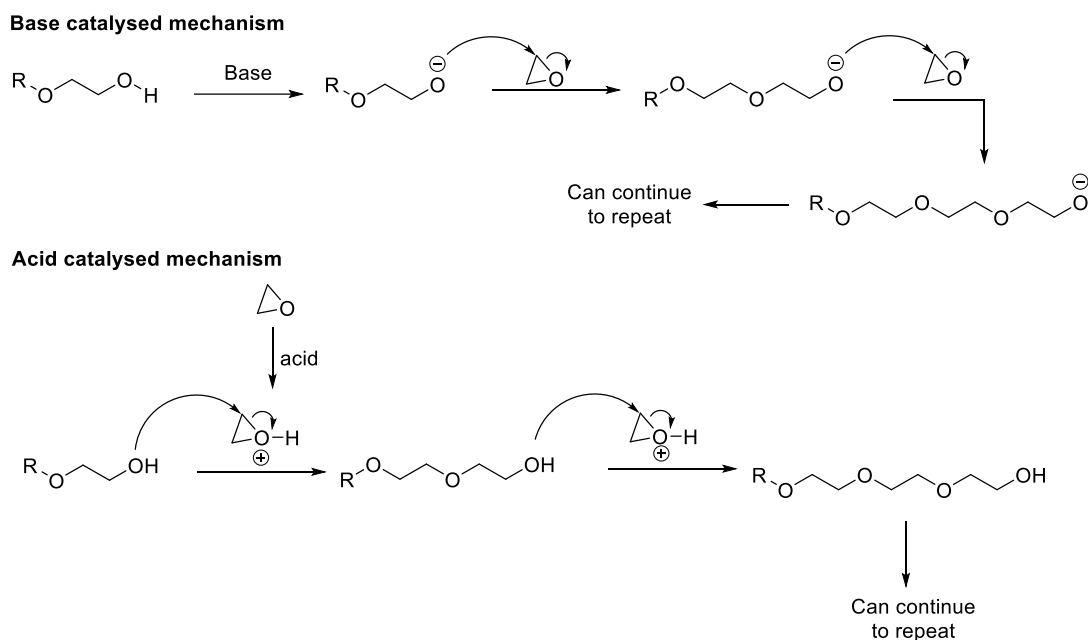


Figure 45: Fatty Acid Methyl Ester Carbon Chain length distribution in Palm Oil and Coconut Oil.

The ethoxylation process, polymerisation through ring opening ethylene oxide, also tends to lead to some variation in ethoxylate chain lengths. This translates to a product with tail groups that have a range of carbon chain lengths and saturation. The products may also have impurities carried through from starting materials or synthetic steps which would not be removed unless the product quality suffered, or the impurity was restricted by law. Caution in interpreting the data produced should therefore be used when comparing the compounds synthesised in this study with those produced industrially.



Scheme 62: Acid and base catalysed mechanisms for the addition of poly(ethylene oxide) head groups.

Typical industrial methods to investigate the properties of surfactants were employed such as critical micelle concentration (CMC) determination through the Wilhelmy plate static surface tension method and dynamic light scattering and dynamic surface tension measurements using the maximum bubble pressure method.

Observing the relationship between the surfactant concentration and surface tension using the Wilhelmy plate static surface tension method gives an insight into the effective concentration of the surfactant through knowledge of the CMC. Dynamic light scattering techniques can also be used to determine CMC and provide information on micelle size. The maximum bubble pressure method can be used to analyse the dynamic surface tension at different concentrations which gives insights into the speed at which the surfactant reaches a newly formed surface and how that can be related to the structure.

Measuring hydrophobicity was initially a major focus of this study because the synthetic aim was to produce surfactants with enhanced hydrophobic tail groups which have the potential to replace perfluorinated surfactants when used for water repellence. Currently hydrophobicity measurements usually apply only to solid surfaces through the contact angle of a droplet of ultra-pure water on a solid surface, as shown in Figure 46:

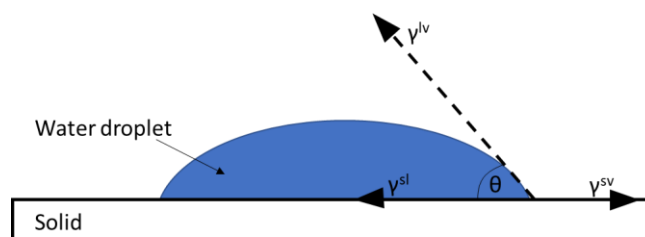


Figure 46: Contact angle of an ultrapure water droplet on a solid surface.

This is known as the sessile drop technique. A quick, simple method of assessing the hydrophobicity of liquid films or adsorbed liquids is not currently known. To produce a solid surface to use for the sessile drop technique the surfactant can be formulated into a plastic sheet by blending the surfactant into the softened plastic during extrusion. The effect the surfactant has on the hydrophobicity of the plastic surface could then be measured through the contact angle between a water droplet and the sheet of plastic. The concentration at which the surfactant is introduced as an additive before extrusion could be varied, starting from an initial concentration between 0-5% wt/wt.

During extrusion the surfactant additive in the plastic is distributed evenly through the plastic. After extrusion and shaping the surfactant typically migrates from the bulk to the surface over a period of time. The contact angle of the surface of the plastic can be measured immediately after shaping and at intervals after this as the surfactant migrates to the surface and affects the surface tension. When no further surfactant reaches the surface, the surface tension measurements would plateau. This technique would give an indication of how quickly the surfactant migrates to the surface and what effect the presence of the surfactant has on the hydrophobicity of the surface. In this manner the optimal surfactant concentration can be determined and a suitable time period for rest after shaping prior to use could be suggested. The structural differences between surfactant compounds could also be studied with respect to the effects on migration time and hydrophobicity of the resulting surface.

Unfortunately, the extruders available for use in York and at Croda require the production of the novel surfactants at a 50-100 g scale, a scale not plausible for some of the target compounds. Initially the aim of this study was to synthesise novel surfactants, analyse them and use the analysis to inform the next round of synthesis. Producing novel surfactants at the scale necessary for extrusion studies would introduce another time pressure and reduce the number of surfactant candidates synthesised. Therefore, the method development was

undertaken by measuring the hydrophobicity of the surfactants without increasing the production scale and using the extruder. This would greatly reduce the time taken to collect data needed to compare the hydrophobicity of perfluorinated surfactants and the synthetic target compounds. The method development centred around techniques to reproducibly adsorb surfactants to a solid substrate. Such a method would mimic the use as a plastic additive whilst making use of a more achievable scale (5 g) of material needed for the range of other analytical techniques at Croda.

3.2 MEASURING HYDROPHOBICITY AND CREATING A SURFACTANT MONOLAYER ON A SOLID SUBSTRATE

This study aims to design and synthesise novel biobased surfactants which can enhance the hydrophobicity of surfaces. In order to assess the effect of the surfactants on the hydrophobicity of the surfaces method development was needed to enable contact angle measurement of a liquid. This would remove the necessity of scale up and allow small amounts of surfactants to be synthesised in the lab and tested more frequently, enabling a more informed design process.

3.2.1 The Sessile drop technique

The hydrophobicity of a solid surface can be quantified using contact angle measurements obtained using the sessile drop technique. The measurement of angle θ created by a droplet of high purity water placed on a smooth surface to provide a direct measurement of hydrophobicity of the solid surface based on Young's Equation as shown in Figure 47:^{235, 236}

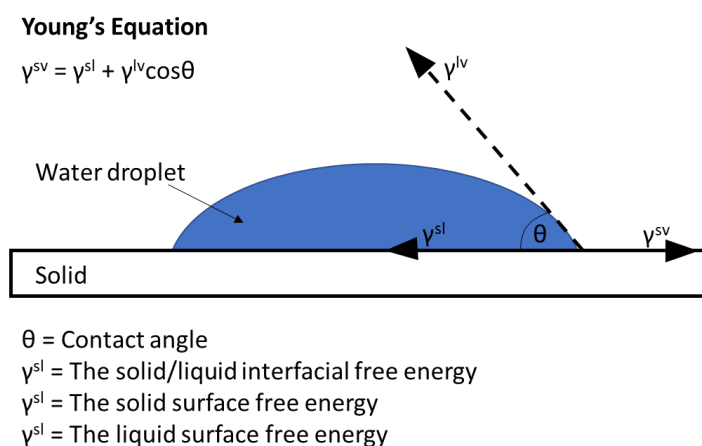


Figure 47: Schematic of the measurement of contact angle of water droplet on solid substrate.

The contact angle θ (Figure 47) measured using the sessile drop technique gives an indication of the wetting properties of that solid. A contact angle of 0° describes the complete wetting of a surface, an acute angle (1° - 90°) is described as a hydrophilic surface.

A hydrophobic surface is defined as a surface with an obtuse contact angle in the 90-150° range when water is the wetting liquid, whilst a surface giving $\theta > 150^\circ$ the surface is considered to be superhydrophobic (Figure 48).

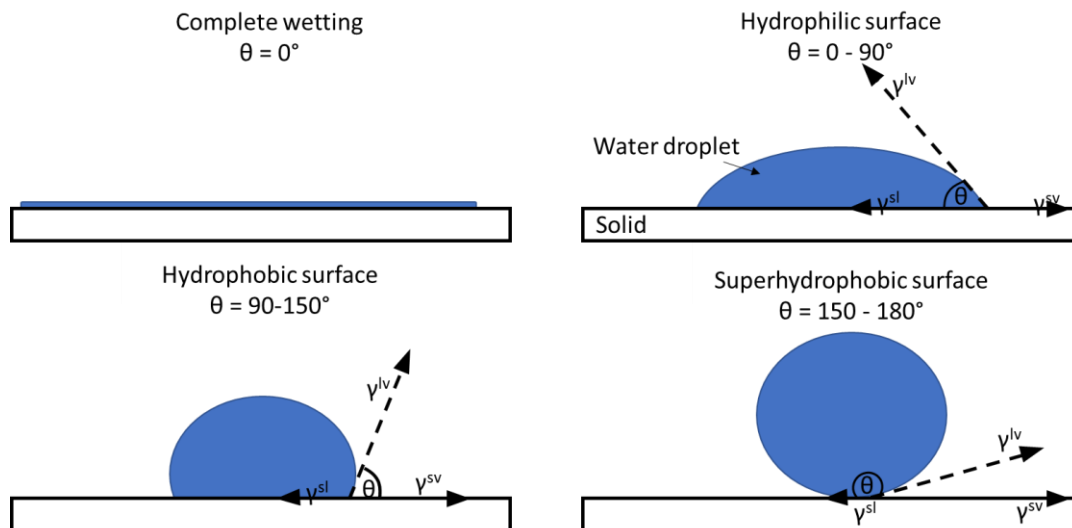


Figure 48: Surface descriptions based on the degree of wetting of that surface with a droplet of water using the sessile drop technique.

A contact angle goniometer uses a high-definition camera to take close-up images of droplets of $<10 \mu\text{L}$, as up to this point the effect of gravity on the droplet is negligible. The software can then automatically assign the contact angle, or it can be determined manually.

Measuring a contact angle is a quick and easy way to assess the hydrophobicity of a solid surface, however reproducibility can be an issue. Measurements are affected greatly by a number of factors: droplet size, time since surface was created, humidity and temperature. As a result, measurements are usually taken as an average of several values preferably in a temperature and humidity-controlled room using an automated liquid dispenser that can deliver the same droplet volume reliably. In this study the measurements were repeated several times on several places along the same solid sample. Despite precautions minor inconsistencies on a surface such as dust or dirt and variation in roughness and uniformity of the surface can have a large impact on the contact angle and therefore contact angle measurements should be repeated frequently and treated with caution.

3.2.2 The Retraction Method

In order to measure the hydrophobicity of liquids using contact angle measurements they must first be loaded onto a solid substrate. The creation of a surfactant monolayer which is loaded onto a clean, 'high energy' smooth solid surface was the work of Zisman *via* the retraction method (Figure 49):²³⁷

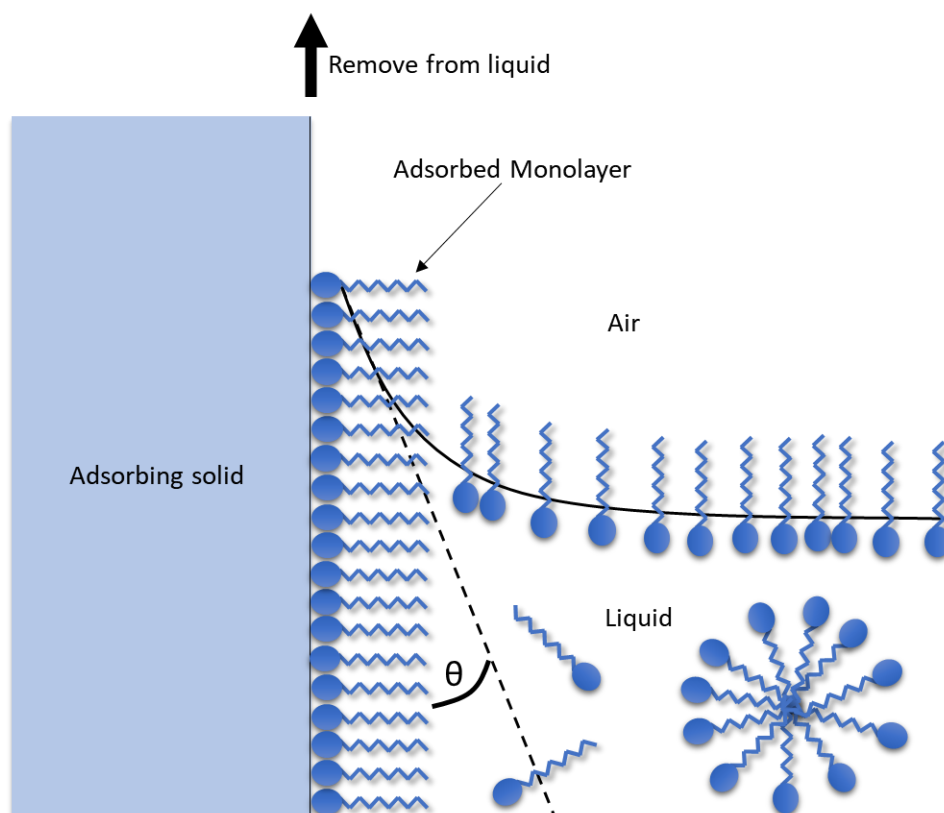


Figure 49: Schematic of the retraction method²³⁷.

This process involves immersing a solid, for example a glass slide or metal plate, into a solution of solvent and the surfactant of interest. The surfactant concentration must be equal to or above the critical micelle concentration (CMC) for absorption of a monolayer. The surfactant molecules adsorb along the surfaces, including that of the glass slide, and the glass slide can be removed vertically leaving a surface coated with a surfactant monolayer, which is of lower energy.

This method is subject to temperature dependence and the solvent used must have a greater surface tension than the critical surface tension of the solid (coated with the monolayer) to achieve a dry monolayer upon removal.

Zisman commented on the possibility of solvent molecules that due to their shape (*i.e.*, octadecylamine used as a retraction solvent for steric acid) could penetrate the monolayer and therefore produce mixed films. It was also established that these mixed films were metastable. Given enough time for the adsorption equilibrium to be established at the surface a true monolayer was produced.²³⁷

Perfluorooctanoic acid (PFOA, **25** in Figure 50) was selected for this experiment as a model compound in our method development because PFOA is a surfactant known to be superhydrophobic, toxic and persistent in the environment, currently under heavy regulation and requiring replacement in many applications. Octanoic acid (**167** in Figure 50) was chosen because it has the same carbon skeleton as PFOA without the perfluorination and has been chosen for this experiment to provide a comparison between the hydrophobicity of perfluorinated surfactants and a more traditional linear surfactant tail groups. Any differences between the two can be attributed to the perfluorination.

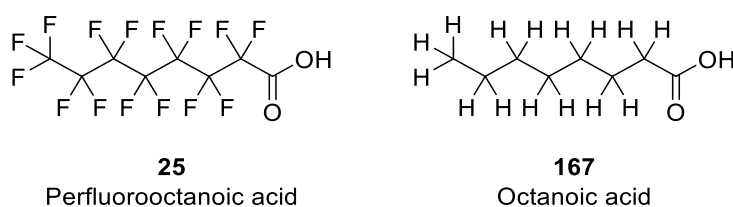


Figure 50: A comparison of perfluorooctanoic acid (**25**, PFOA) and octanoic acid (**160**).

As PFOA is known to produce superhydrophobic anti-stain surfaces, an angle of 150° or above was expected when de-ionised water is applied to glass slides coated with a monolayer of PFOA. Octanoic acid is expected to have a hydrophobic contact angle $\theta = 90-150^\circ$.²³⁸

The glass slides were cleaned in de-ionised water and acetone in the sonic bath and dried with compressed air to keep the surface as clean as possible to promote an even coverage. The cleaned glass slides were then left in their solutions for 48 hours to allow the molecules at the surface to come into equilibrium before removal. In theory, when

equilibrium is reached the surfactant molecules should have produced a monolayer on the surface of the glass. When this slide is removed vertically from the solution the monolayer is extracted intact and the remaining surfactant is left in solution. Figure 51 is a schematic of this theoretical result:

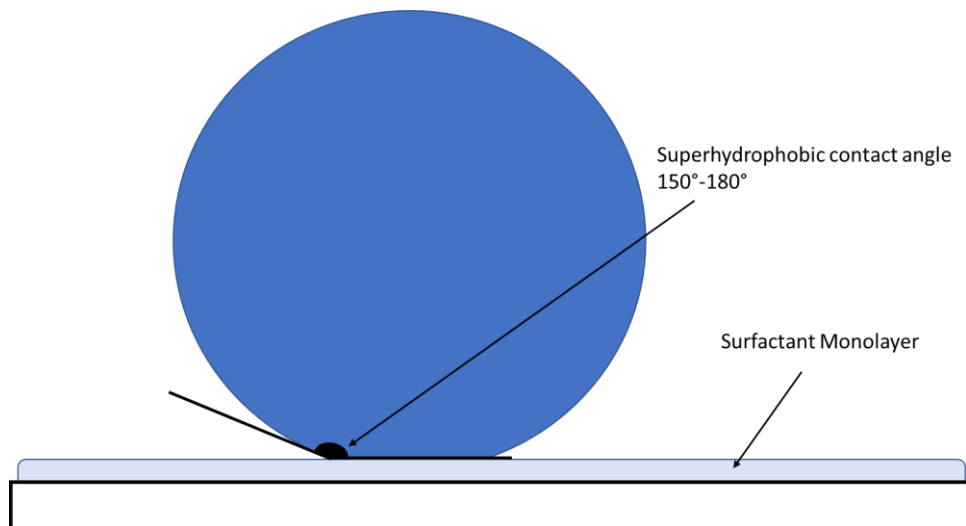


Figure 51: Schematic of water droplet on top of fluorosurfactant monolayer exhibiting superhydrophobic contact angle.

The results detailed in Figure 52 and Table 11 show that eleven glass slides were cleaned and four of the slides had contact angle measurement taken of the surface to see if a reliably clean surface could be produced:

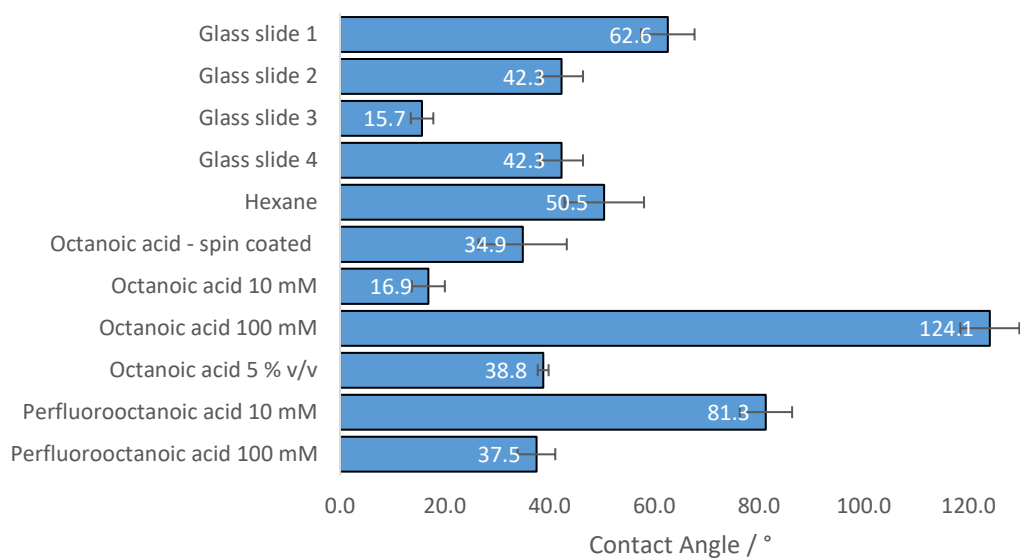


Figure 52: Bar chart for a visual representation of the contact angles described in Table 11. Error bars are based on one standard deviation.

Table 11: Contact angle and water droplet volume results obtained via the retraction method of sample preparation.

Sample Description	Contact angle / °	Contact angle STD/ °	Droplet Volume / μL	Droplet Volume STD / μL
Glass slide 1	62.61	5.10	5.09	1.10
Glass slide 2	42.33	4.08	5.37	4.60
Glass slide 3	15.67	2.15	2.49	0.86
Glass slide 4	42.33	4.08	5.37	4.60
Hexane	50.46	7.59	4.23	3.19
PFOA (10 mM)	81.34	5.01	4.31	1.88
PFOA (100 mM)	37.51	3.60	2.44	0.92
Octanoic acid - spin coated	34.89	8.42	3.79	4.01
Octanoic acid (10 mM)	16.87	3.14	1.78	0.27
Octanoic acid (100 mM)	124.11	5.64	6.43	6.43
Octanoic acid (5% v/v)	38.79	1.04	1.59	0.16

There is a large variation (15.7° to 62.2°) in the data from the four glass slides prepared in the same manner. The slide immersed in hexane had a contact angle of 50.5°, within the range observed for the clean glass slides. The slide immersed in octanoic acid (10 mM) and spin coated with octanoic acid both also produced contact angles within the same range as the clean glass slides. The more concentrated octanoic acid solution (100 mM) significantly increased the contact angle produced to 124.1° ±5.64, to within the expected range for a hydrophobic surface (90-150°).

Assuming a higher concentration may be key to producing the monolayer, a higher concentration solution of octanoic acid was prepared (5% v/v) (Table 3). This theory was confirmed to be incorrect as the higher concentration solution produced a 38.8° contact angle (hydrophilic). Neither of the slides immersed in PFOA had the expected superhydrophobic contact angle (150°-180°) nor did the contact angles reflect the increase in concentration as seen with octanoic acid. The lower concentration solution (10 mM) produced an angle of 81.3° and the higher concentration 100 mM) produced an angle of 37.5°.

The contact angles for the clean glass slides show large disparity between one another, the slides submerged in PFOA produced hydrophilic contact angles instead of the expected superhydrophobic angles and one slide produced from octanoic acid solution (100 mM) had a contact angle within the predicted range. However, there seemed to be no reasonable trend with respect to the concentrations of octanoic acid and there were large standard deviations and very poor reproducibility throughout and therefore the data is deemed unreliable.

Visual inspection of a slide submerged into the 100 mM PFOA showed an uneven coverage. Figure 53 shows a backlit visual inspection of the slide after measurement and what appears to be an uneven deposition of PFOA on the surface of the glass and possible crystallisation in a non-uniform manner.

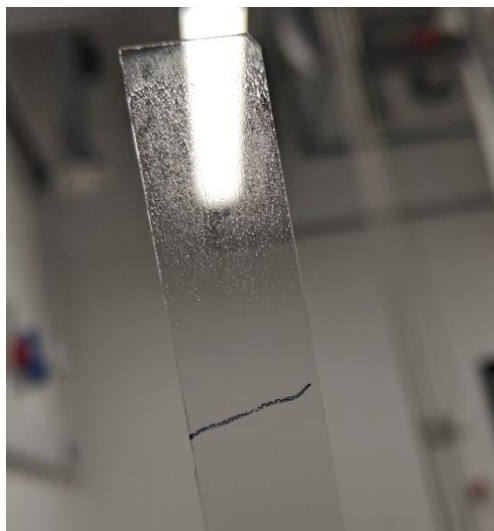


Figure 53: Photograph of back-lit sample slide prepared *via* the retraction method.

Figure 54 is a schematic of a possible mechanism to the uneven deposition seen in Figure 53:

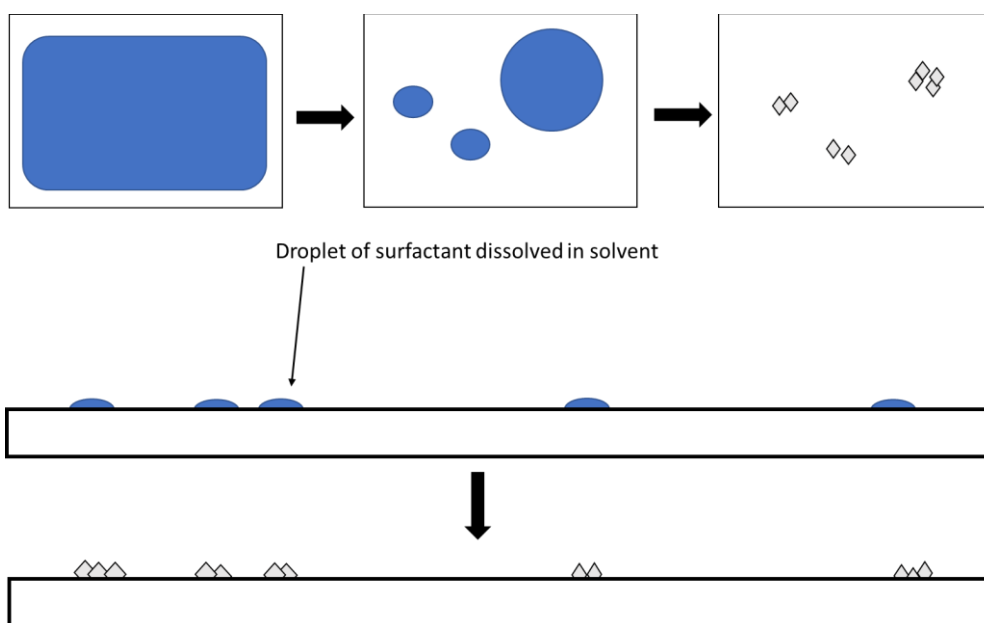


Figure 54: Schematic of drying and crystallisation process during the drying time of the retraction method.

As seen in Figure 54, using PFOA (100 mM) as an example, the slide is removed from the solution and placed on a flat surface with some liquid still visible on the surface. As the

solvent from the PFOA solution begins to evaporate, the larger droplets of solution form smaller droplets, keeping the surfactant in solution until the droplet volume decreases beyond the solubility limit and PFOA is deposited onto the glass in a non-uniform manner. The results do not suggest a monolayer deposition has been achieved. The concentration of surfactant (or compound) of interest, the solvent choice, the choice of a glass surface, the cleanliness of the glass and the drying time are all factors which would influence the success of a monolayer deposition. Furthermore the non-uniform deposit of crystals suggests that the crystal lattice energy could be stronger than the acid-glass interactions and suggest the glass could be of an unsuitable surface energy for a monolayer deposition.

Although it is likely that the non-uniform surface coverage and inconsistent cleaning method is responsible in the majority for the lack of reproducibility, the use of the theta lite contact angle goniometer also introduces error into the experiment as it has manual liquid dispensing. The amount of de-ionised water deposited onto the glass is manually controlled through a screw top syringe and to achieve a consistent volume between 0-10 μL is very difficult in this way. A goniometer with computer-controlled syringe would greatly reduce human error and improve reliability. We therefore concluded this method requires much time-consuming development and a more robust method with better reproducibility is required for reliable data.

3.2.3 Loading hydrophobic liquids onto silica

To improve upon the method attempted above a different solid support was chosen: K60 silica. A solution of the compound/surfactant of interest was added to K60 silica and the solvent removed by rotary evaporation. A more even distribution of product was expected due to the constant rotation of the sample vial and gradual removal of solvent during rotary evaporation. The removal of solvent also removes any issues with mixed films that may have been produced using the retraction method.

Octanoic acid and PFOA were used in this study to enable comparison with the retraction method and octanol samples were also analysed to assess the effect of a change of head group. Octane was also analysed because if a hydrophobic molecule could be successfully analysed then the effects of chain length, unsaturation, branching and ring and cage structures could be assessed without the necessity of sourcing the compound with the specific head group or adding to a synthetic route.

K60 silica was chosen as the solid support as it has a narrow particle size distribution which helps to make the method reproducible and is not costly, an important consideration for a method which may be utilised throughout the project.

It was hypothesised that the silica particles would be evenly coated with the compound of interest as the solvent was removed during rotary evaporation. The hydrophobic silica would then repel a water droplet to different extents, different contact angles, depending on the compound used for coating. Figure 55 is a schematic of the expected result:

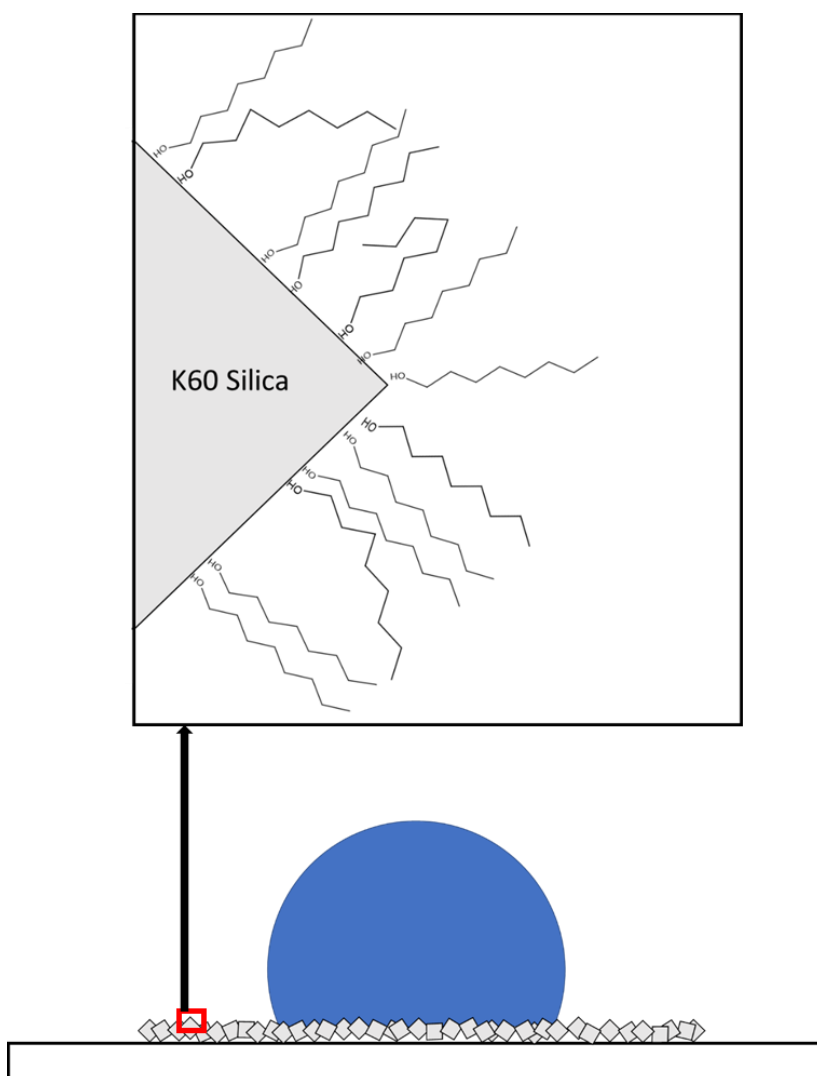


Figure 55: Schematic of the expected effect on contact angle with a de-ionised water droplet of coating silica in octanol.

Figure 56 is an image of the silica samples treated with octane, octanol and octanoic acid:

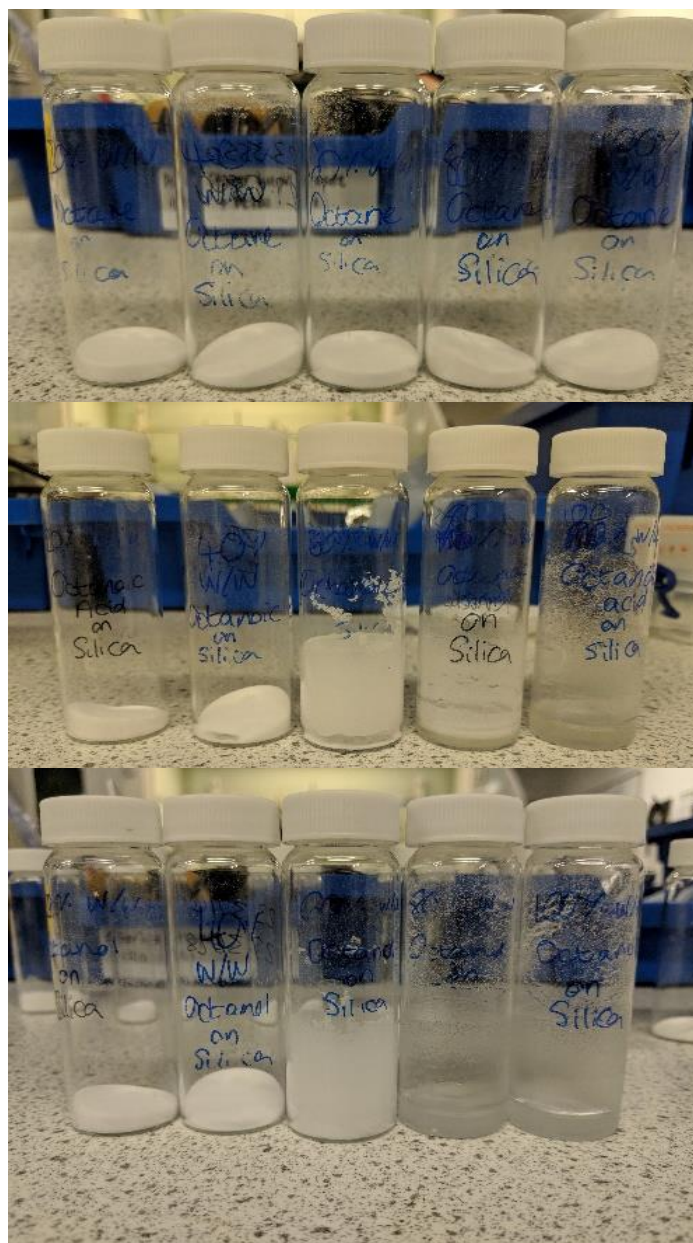


Figure 56: Silica samples treated with octane (top), octanol (middle) and octanoic acid (bottom) at 20%, 40%, 60%, 80% and 100% w/w with respect to silica from left to right.

A visual inspection of the samples showed that for octane all the samples were free flowing powder, whereas for octanol and octanoic acid the samples began to form a gel-like substance at 80% wt/wt. The free-flowing powders for all loadings of octane once solvent was removed suggests that much of the octane may have been removed during rotary evaporation.

All free-flowing powder samples were poured over adhesive tape and pressed to create as flat a surface as possible for contact angle measurement. Those samples which were not

free-flowing were spread onto glass slides and flattened with a spatula. During this process the silica appeared to dry out considerably within 10 seconds.

Figure 57 shows a schematic of the rapid wetting of the slide:

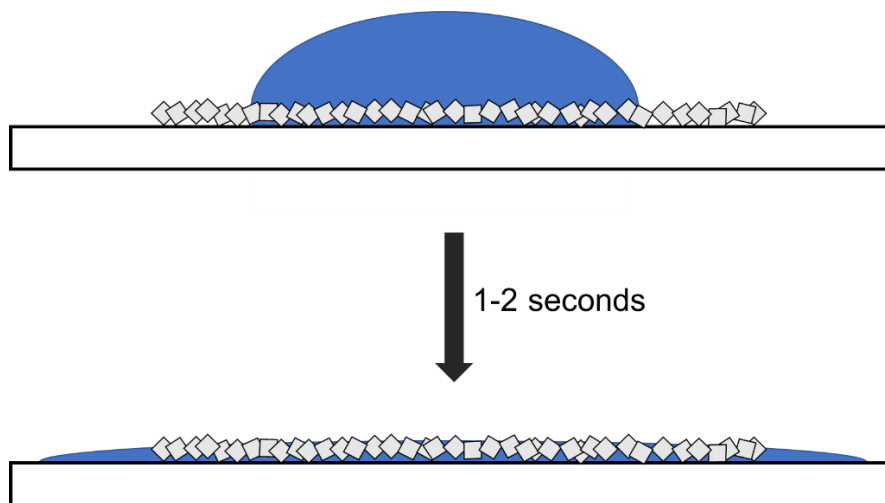


Figure 57: Schematic of the wetting mechanism of coated silica on a glass slide.

The droplet, instead of sitting on top of the treated silica, sank immediately into the spaces between the silica particles. All samples, including those made up to saturation by eye, showed immediate and complete wetting (contact angle $<1^\circ$) on the glass slides.

Figure 58 shows a microscope image of an octanoic acid treated silica sample coated onto adhesive tape on a glass slide:

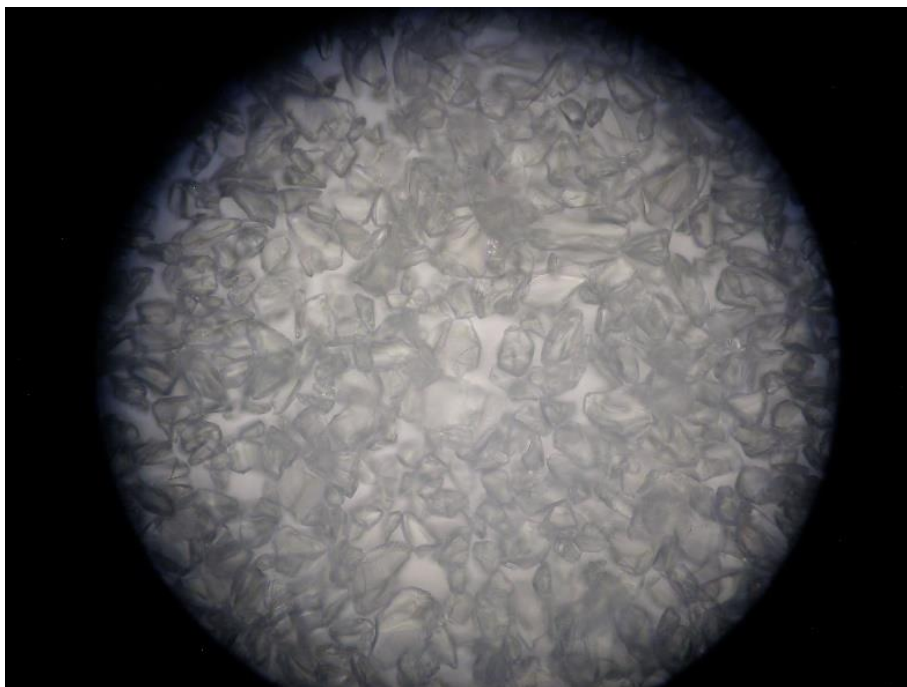


Figure 58: Microscope image of silica treated with octanoic acid spread across adhesive tape.

The roughness and porosity of the silica seen in the microscope image is the likely reason that any hydrophobicity caused by octane, octanol and octanoic acid on the silica is dwarfed and does not provide a measurable effect on contact angle. It is also possible that octane, octanol and octanoic acid do not have enough affinity for K60 silica to coat it. The octanol and octanoic acid may have run off when depositing on the slide, leaving dry silica which would explain the observation of the saturated sample very quickly 'drying out'.

3.2.4 Airbrushing

To improve the uniformity of the surfactant layer and avoid large droplets which leads to non-uniform deposition from solution as described in the retraction method section, an airbrush was used in an attempt to distribute surfactant onto the surface of glass slides and a plastic sheet. The nebulisation at the airbrush head produces a fine mist over the glass slide resulting in rapid solvent evaporation.

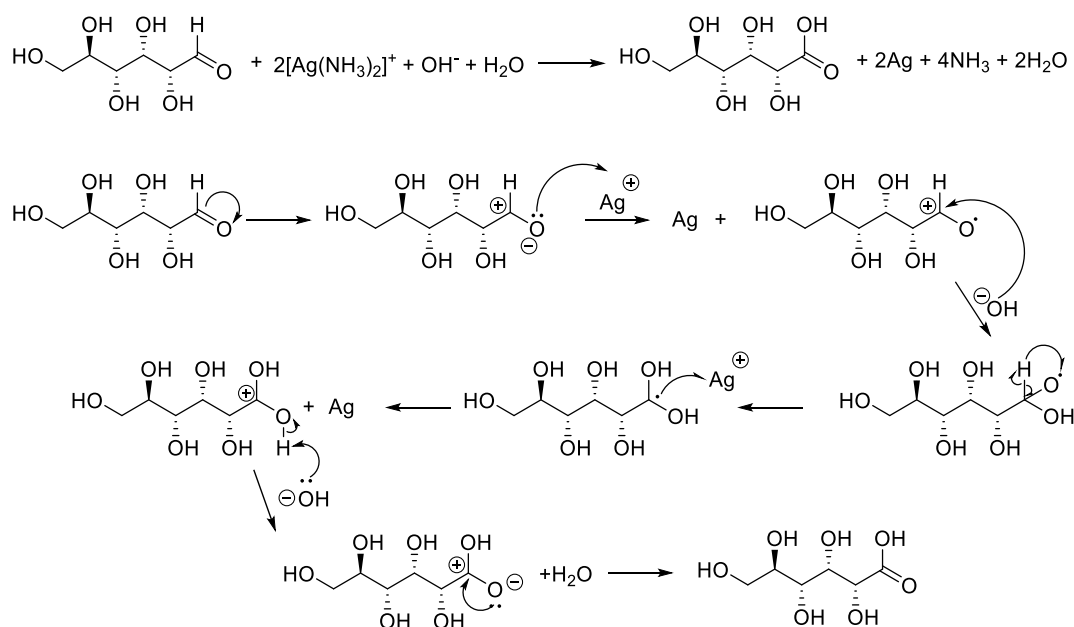
Although solvent evaporation was much faster using the airbrushing method than the retraction method, a fine powder of PFOA could be seen on the glass slide which was denser in some areas and less visible in others. This again led to unreliable and unreproducible

contact angle measurements. Despite spraying a smaller volume of solution over a defined area for a known number of seconds the results acquired were no more consistent and still resulted in depositing a fine powder which is likely evidence that PFOA was in an extreme excess of that required for a monolayer.

3.2.5 Depositing compounds onto silver

One possible cause of the uneven distribution of PFOA on glass slides in the previously described methods is that the glass and silica surfaces were too low in surface energy to cause significant attraction of the polar head group. This was investigated using a higher energy surface, silver.

A silver mirror was precipitated onto clean glass slides using Tollens reagent ($\text{Ag}(\text{NH}_3)_2\text{OH}$) and dextrose solution. In the basic solution the dextrose is enolized to the aldehyde and produced a positive Tollens' test through the precipitation of silver onto the glass slide. The mechanism is shown in Scheme 67:



Scheme 63: Mechanism of the reaction between dextrose and Tollens' reagent.

The silver-plated glass slides were rinsed with de-ionised water and dried with a heat gun. Solutions of varying concentrations of PFOA and octanoic acid were run over the silver plate from pipettes (Figure 59):

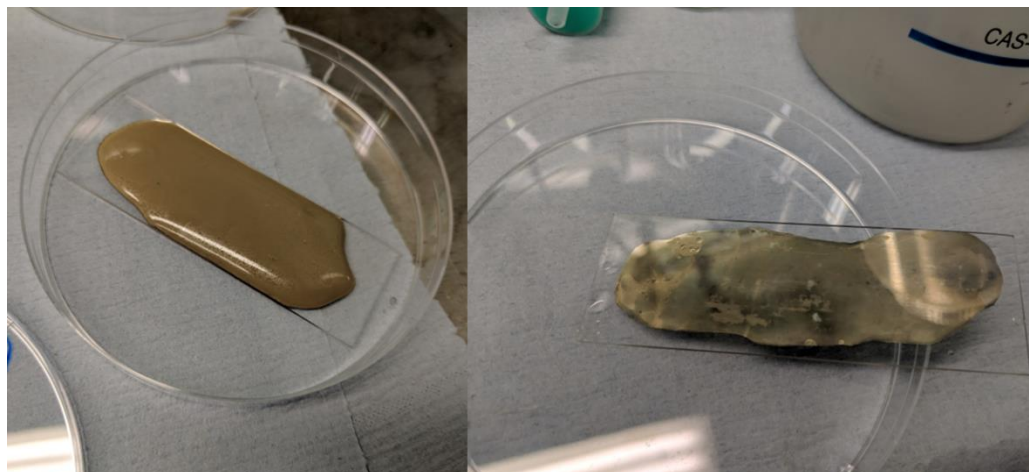


Figure 59: Photographs of the slide preparation process using Tollen's reagent to produce a silver coated slide (left) and the silver coated slide raised up on the side of a petri dish ready for the solution of the component of interest to be pipetted over (right).

The contact angles recorded are presented in Table 12:

Table 12: Contact angle measurements of the silver coated glass slides after treatment with PFOA and octanoic acid solutions of different concentrations.

Sample description	Contact angle / °	Contact angle STD	Volume / μL	Volume STD
Glass slide	49.2	9.3	3.7	1.1
Silver surface blank	19.0	13.8	2.1	2.2
PFOA 10 mM	>150	-	-	-
PFOA 100 mM	<5	-	-	-
PFOA 1 M	<5	-	-	-
Octanoic acid 2 mM	104	26	7.8	1.5
Octanoic acid 4 mM	86	20	5.9	1.7
Octanoic acid 6 mM	138	19	9.5	0.9

Octanoic acid 8 mM	147	18	9.0	2.6
Octanoic acid 10 mM				
-tarnished section	156.7	3.7	11.4	0.7
Octanoic acid 10 mM	103.4	4.4	5.8	1.6
Octanoic acid 20 mM	120	7		
Octanoic acid 100 mM	32.9	12.3	2.9	1.0
Octanoic acid 1 M	43.3	1.0	2.4	0.3

The lowest concentration of PFOA (10 mM) produced a superhydrophobic surface. A measurement of the angle was not possible because the droplets would rapidly run off the horizontal plate. To control the size of the droplet the method used in this study was to expel a small droplet from the syringe and whilst it was still attached to the syringe, carefully raise the sample platform, and touch the droplet to the surface. This created difficulties in dispensing a droplet because the droplet had no affinity to the PFOA coated silver surface and the stage could be raised to press the droplet onto the surface but remain attached to the syringe when the platform was lowered again. To overcome this a larger droplet was dispensed which would fall under its own weight onto the sample.

The higher concentration solutions of PFOA (100 mM, 1 M) were found to enhance the wetting properties of the silver surface to the opposite extreme. Again, contact angles were not recorded as the contact angle was too low, $< 5^\circ$, for the software to identify.

The octanoic acid samples (Table 12) also produced a superhydrophobic surface at 10 mM, however only on a section of silver that appeared tarnished. This section is discoloured possibly because of partial oxidation of the surface which remains unconfirmed as further investigation followed a different direction. The tarnished section produced an average contact angle of 156.7° , whereas the non-tarnished section produced a hydrophobic surface with an average contact angle of 103.4° . The higher concentrations decreased in hydrophobicity as seen with PFOA, with the 100 mM producing an average contact angle of 32.9° and the 1 M solution producing a 43.3° average contact angle. Beyond those comparison a scatter plot (Figure 60) of the contact angle produced against the concentration of octanoic acid shows no identifiable trends.

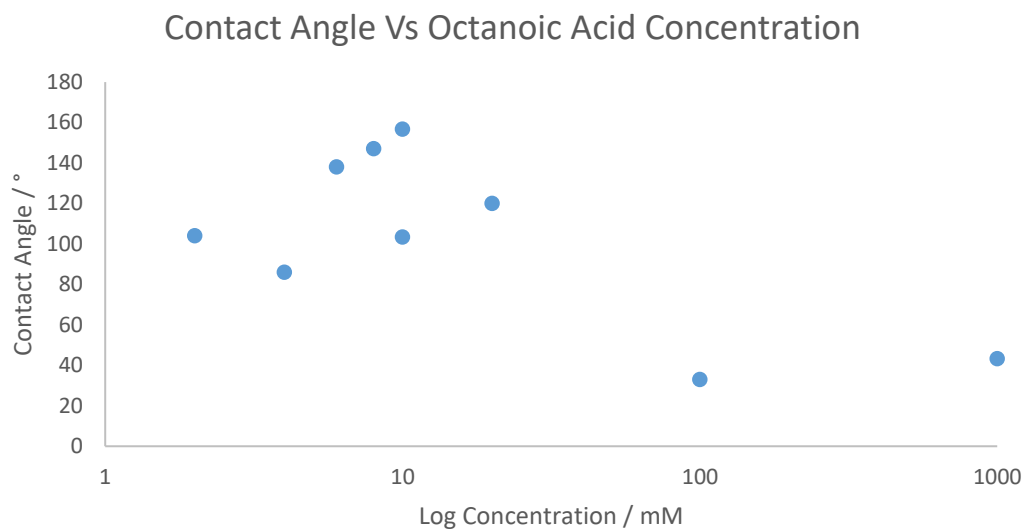


Figure 60: Scatter plot of contact angles produced by octanoic acid on a silver surface described in Table 12.

Upon coating the silver slides with 10 mM of perfluorooctanoic acid and octanoic acid superhydrophobic surfaces were produced. However, due to difficulty achieving a stationary droplet and difficulty with the software's ability to read the angles, no contact angle for the perfluorinated surface were effectively recorded though by eye. The superhydrophobicity was clear for the octanoic acid coated surface (Figure 61), and a contact angle of 155 ° was recorded in Figure 62:

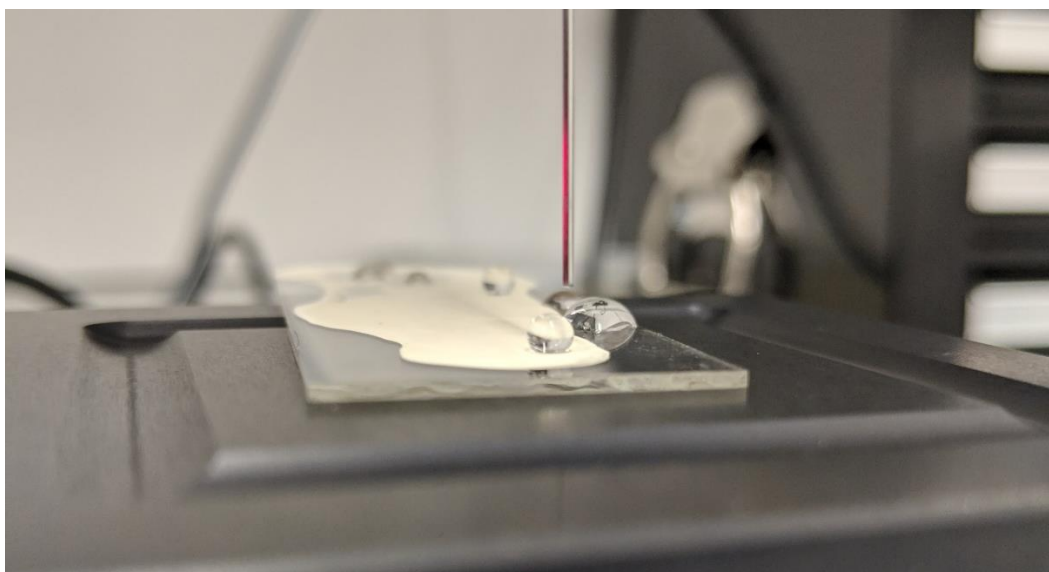


Figure 61: Superhydrophobic surface with droplets of water showing large contact angle.

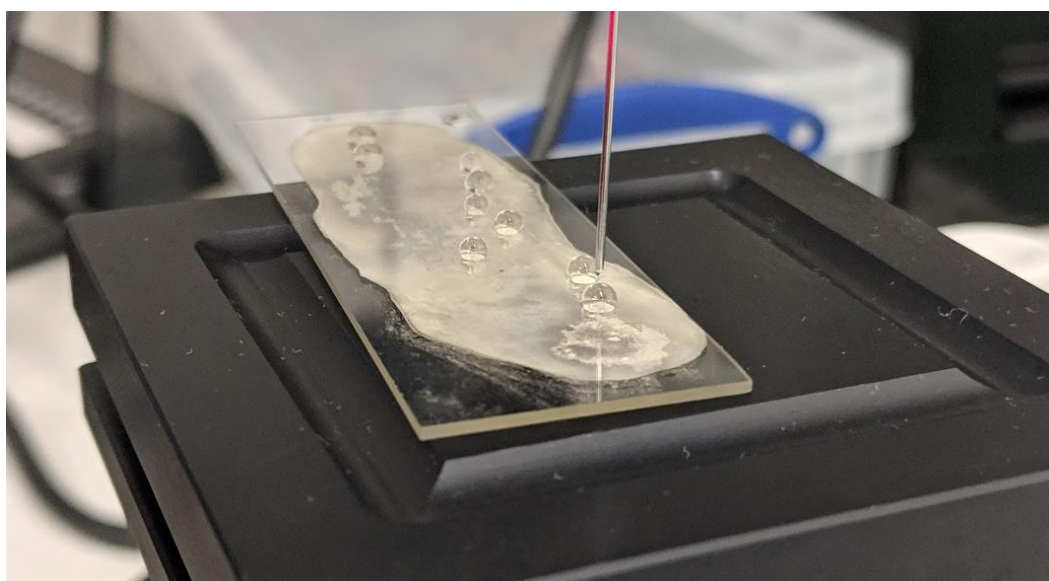


Figure 62: Photograph of the hydrophobic effects of octanoic acid at 10 mM.

The higher concentrations of 0.1 M and 1 M both gave hydrophobic surfaces for octanoic acid and perfluorooctanoic acid however for perfluorooctanoic acid the spreading was close to 0° and too low for the software to measure.

It is possible that the PFOA and the octanoic acid in 10 mM solutions had a strong affinity to the slightly charged, high energy surface of the metal and formed a monolayer which produced excellent repellence. It is feasible that a well aligned monolayer would produce

superhydrophobic surfaces. It is also possible that the more concentrated samples formed other secondary structures, such as micelles or bilayers, on top of the monolayer. As the monolayer would theoretically have hydrophobic chains at the interface with air, the secondary structures would be arranged in reverse micelles or simply with the hydrophilic head groups at the interface with air, making the surface hydrophilic, enhancing wetting.

The contact angles acquired during this work were either unrecordable or had large standard deviations (as large as 26 °) and very poor reproducibility. A more advanced goniometer with an automated droplet dispenser in a temperature and humidity-controlled room may help improve the reproducibility to an acceptable standard. However, if both octanoic acid and perfluorooctanoic acid can produce a superhydrophobic surface then this method could not be used to identify improvements to hydrophobicity through changing surfactant structure.

This method has shown that a superhydrophobic surface can be produced with a hydrocarbon-based surfactant on a high surface energy surface. The contact angle produced by the 10 mM solution of octanoic acid at 103.4 ° (156.7 ° on the tarnished section) raises questions about how distinguishable small changes in structure would be with this method, which would be made less so by the poor precision demonstrated thus far. Difficulty remains in transforming these findings into a robust and practical method.

3.2.5.1 Atmospheric-pressure plasma jet surface modification

Several methods of coating surfactants onto solid substrates such as glass, silica and silver for contact angle analysis have been described earlier in this chapter and have given inconsistent results due to issues such as uneven evaporation, poor attraction to the surface and/or the low surface energy of the glass slide or silica. The most consistent method so far established was the coating of metallic silver with surfactants. The surfactant appeared to be coated evenly across the silver and a superhydrophobic surface produced. At 10 mM octanoic acid and PFOA produced superhydrophobic surfaces and above 10 mM it appeared that the surface was saturated and concentrations above 10 mM increased the wettability of the silver surface possibly due to bi-layers or secondary structures. This confirmed that the higher energy surface worked well to orient the surfactants to produce the desired effect. Visual inspection of the silver surface however showed homogeneous tarnished areas and these coated areas gave better water repellence. Furthermore, all of

the contact angles measured had high standard deviations due to a lack of control over the droplet size and the temperature and humidity of the room. The high standard deviation coupled with the uneven tarnishing resulted in poor reproducibility and it should also be noted that this method generates a lot of waste.

Using a polypropylene sheet would eradicate the need to use an intensive cleaning procedure and would be a closer model to the application as a plastic additive and would be cheaper and produce less waste than coating silver slides. However, it is clear that a high energy surface is needed for good, even distribution of surfactant.

A method used in industry to help with the coating of surfaces is corona treatment. Corona treatment involves bombarding the surface with high energy corona discharge plasma which partially oxidises the surface. Corona treatment equipment is expensive and rarely comes in a size suitable for a laboratory environment. In lieu of this the York Plasma Institute houses an atmospheric pressure helium plasma jet showed in Figure 63:

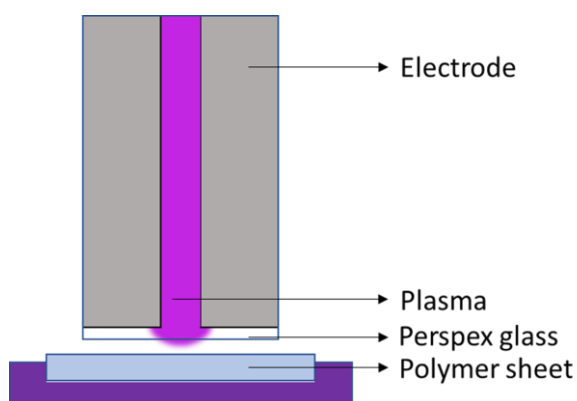


Figure 63: Schematic of plasma jet treatment of a polymer sheet.

The plasma jet was used under ambient conditions to ionise the surface of polypropylene films and the mechanism of surface alteration was investigated.²³⁹ It may be possible to use the plasma jet in much the same way corona treatment is used in industry, to produce a higher energy surface which would be suitably attractive to the hydrophilic, polar head group of a surfactant.

To properly establish this method, the exposure of the polymer surface to the plasma jet would need to be kept consistent. A robotic arm currently moves the jet backwards and forwards at a variable rate. Initial experiments did not see a difference between the blank and the surfactant treated polymer film, however, this may be because the surface was not

exposed for long enough and the desired effect was not realised. Further experiments with longer exposure times (30 minutes per microscope slide) however did not improve the attraction of the surface. This led to the belief that the voltage on the plasma jet was not high enough and therefore the plasma not powerful enough to achieve the desired effect.

Tantec LTD, a company which provides corona treatment equipment for industry, was sought out and agreed to aid in method development. A sample of the sheet plastic was treated using various corona treatment methods in their lab however when surfactant solution was applied immediately afterwards the solution could be seen pooling and balling up in an uneven distribution across the plastic surface.

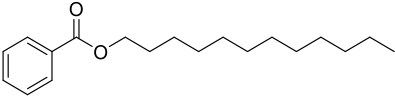
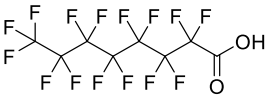
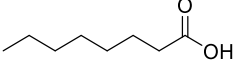
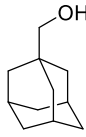
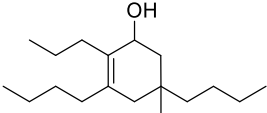
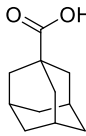
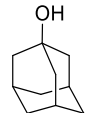
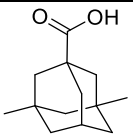
3.2.5.2 Conclusion

After many attempts to create a clean surface which attracts surfactant head groups thereby producing a monolayer of surfactant, the conclusion was drawn that we were unlikely to produce a reliable method in the time remaining. It was hypothesised that access to a clean room and equipment such as a Langmuir-Blodgett trough may have improved results however this route would be too expensive and time consuming to carry out during this study. Such a method would also likely be very time consuming per sample once established which goes against the aims of the method development to find a fast and simple method to determine the hydrophobicity of liquids.

3.2.6 Contact angles of Crodamol AB solutions on glass

A common solvent was identified for the compounds in Table 13 through a simple visual bench solubility test at 0.5% wt/wt. The solvent was an industrially produced alkyl (C12–15) benzoate, Crodamol AB (see Table 13 for the indicative structure).

Table 13: Contact angles of Crodamol AB with 0.5% additives on glass slides.

Additive	Contact angle / °						SD
	1	2	3	4	5	6	
 <p>Crodamol AB (blank - no additive) Representative structure, product contains C1215 alkyl chains</p>	27.0	27.6	27.8	27.4	27.2	27.2	0.3
 <p>1 Perfluorooctanoic acid</p>	78.0	81.4	80.3	78.7	81.5	81.9	1.5
 <p>Octanoic acid</p>	40.5	41.7	41.0	40.7	41.4	40.9	0.4
 <p>Adamantane methanol</p>	31.7	32.7	34.2	33.2	32.9	35.4	1.2
 <p>Compound RD142</p>	27.5	27.7	28.1	29.9	28.3	28.1	0.8
 <p>Adamantane acetic acid</p>	24.7	26.8	24.2	24.2	24.7	26.8	1.1
 <p>Adamantanol</p>	26.5	32.9	27.0	26.0	26.5	26.7	2.4
 <p>Adamantanol</p>	23.8	23.8	24.0	23.4	23.6	23.8	0.2

Once dissolved the effect on the contact angle of the solvent was investigated. It was hypothesised that the more hydrophobic the tail group of the additive was the larger the contact angle would be. If this were true the addition of surfactants which were more hydrophobic than Crodamol AB would produce a Crodamol solution which is more hydrophobic than Crodamol AB and therefore a larger contact angle. This is explained visually in Figure 64:

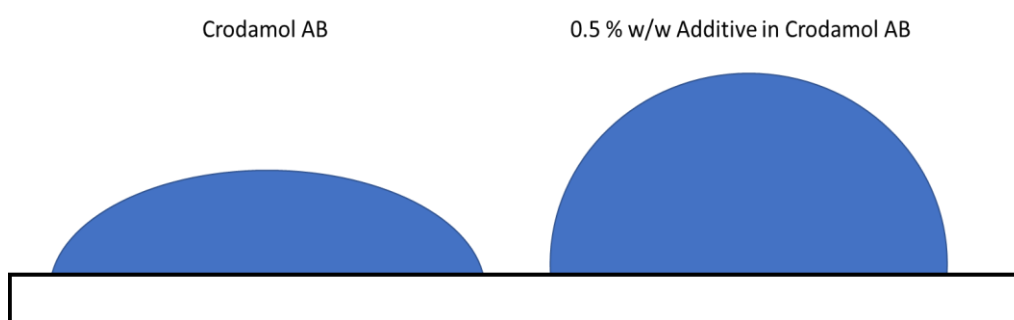


Figure 64: Schematic of the expected effect of adding hydrophobic surfactants to Crodamol AB.

This set of contact angles is expected to have better reproducibility than that previously taken at the University of York because there is much better control over the substrate and test material concentration. The previous methods of coating the surface directly with the the compound under investigation or with a pre-treatment followed by the compound. In these previous attempts the application was inherently more variable both in concentration and homogeneity than the Crodamol AB method. Furthermore, the measurements taken using Crodamol AB were taken in a humidity and temperature controlled room at a laboratory at Croda which has an optical goniometer with automated dispensation (Figure 65):

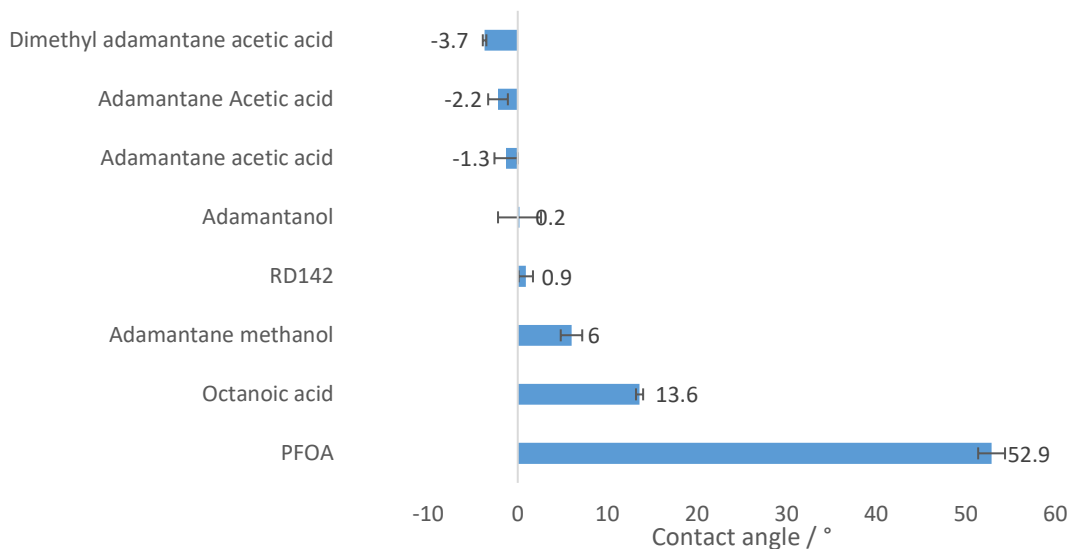


Figure 65: Bar chart showing how the average contact angle of Crodamol AB changed when additives were added at 0.5% wt/wt.

In theory the droplet size should be more consistent than before when done manually and the temperature and humidity variables are somewhat removed. As seen in Figure 65, the standard deviation associated with the measurements decreased dramatically with the use of the automated dispenser and temperature and humidity-controlled room.

The contact angle of Crodamol AB on a glass slide was taken and compared to Crodamol AB with additives from Table 6 at 0.5% wt/wt concentration (Figure 66):

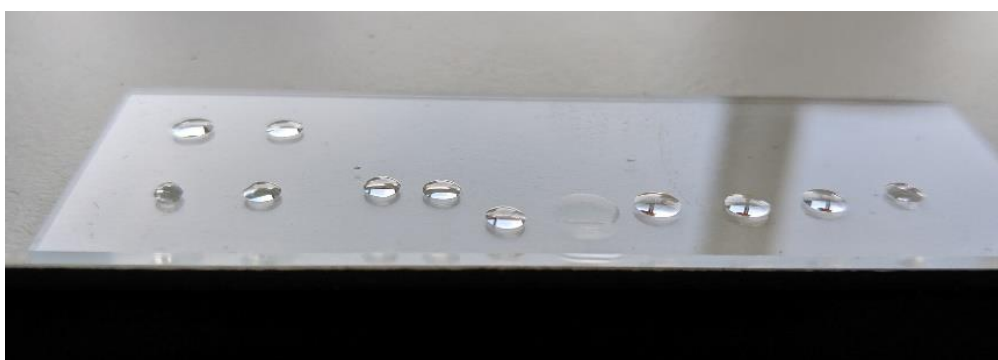


Figure 66: Photograph showing the effect of additives to Crodamol AB on contact angles on a glass surface.

The most extreme was the addition of PFOA which increased the contact angle, and therefore, the hydrophobicity of Crodamol AB. Crodamol AB alone produced a contact angle of 27.4 °, which the addition of PFOA increased to 80.3 °, a notable 55 ° increase.

The adamantane based additives had little effect on the hydrophobicity of Crodamol AB. In the case of dimethyl adamantane acetic acid the hydrophobicity decreased, producing a contact angle of 23.7 °, a reduction of 5 ° from Crodamol alone. The RD142 sample of the cyclised 2-hexanone condensation products had a similarly minor impact.

It is unclear why the adamantane based compounds showed little effect. It could be that the adamantane at the surface had a similar hydrophobicity to Crodamol or that the adamantane based compounds did not come to the surface of the droplet at all.

The orientation of molecules at the surface is unclear, with the exception of PFOA. The strong effect caused by PFOA addition suggests that the perfluorinated tail group was at the surface, which is known to prefer interactions with the air over organic molecules. The other additives, however, may be aligned with tail groups at the surface, which would account for an increase in contact angle, or a true solution may have been formed with a lower polarity which could also have produced such an effect.

Despite reduced variables providing more reliable data, this method proved to be too ambiguous because the orientation and organisation of the surfactants was unclear.

3.2.7 Surface tension

Surface tension is a property derived from the tendency of liquids to form a surface film of the minimum surface area due to the cohesive forces between molecules overpowering the attraction to the air above it where there are much fewer interactions. Molecules in the bulk of the solution are pulled equally in all directions by cohesive forces between molecules. The molecules at the surface experience the cohesive forces as a net force in a downwards direction resulting in a minimised surface area of the surface film, as shown in Figure 67:

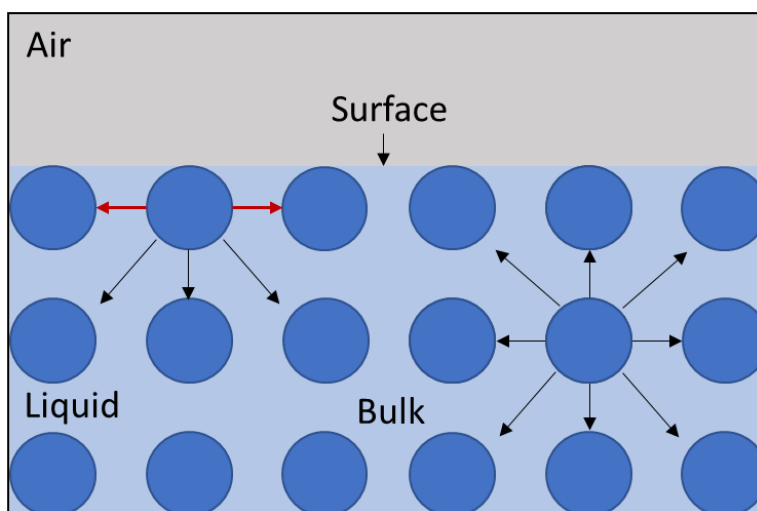


Figure 67: Surface tension diagram.

The definition of a surfactant is a substance that lowers surface tension. Surface tension is a measurement of free energy per unit area and is measured in Dynes per centimeter (dyn/cm) or millinewtons per meter (mN/m) and can be measured using static surface tension methods such as the Wilhelmy plate method, the Du Noüy ring method or the pendant drop method.²⁴⁰⁻²⁴²

3.2.8 CMC definition

Critical Micelle Concentration (CMC) is the minimum concentration at which micelles spontaneously form.²⁴³ At and above the CMC many physical properties of a surfactant solution become distinct, for example surface tension, light scattering and conductance (Figure 68):

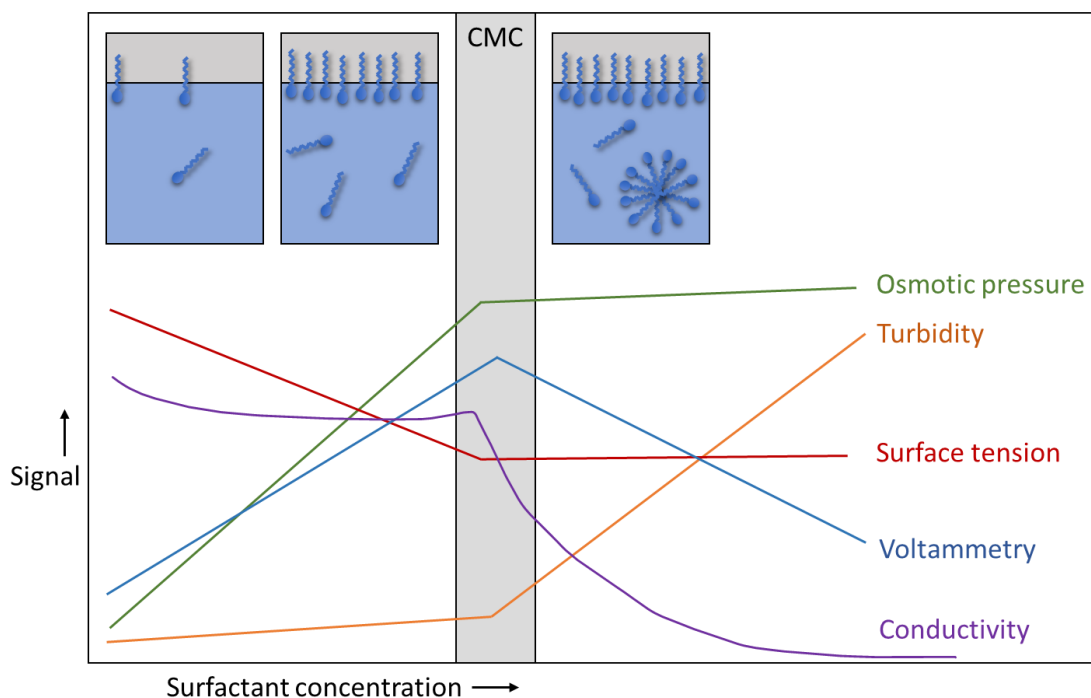


Figure 68: Schematic of the distinct changes in physical properties of a surfactant before and after the critical micelle concentration.

Therefore, CMC determination can be carried out through several methods such as fluorescence, UV-Vis, dynamic light scattering and the Wilhelmy plate static surface tension method. For the purposes of this study CMC measurements were carried out through observation of the surface tension with respect to concentration of surfactant in aqueous solution via the Wilhelmy plate method using a Kruss K100 tensiometer with automated dilution.

3.2.9 Wilhelmy plate static surface tension method

The word surfactant is rooted in the term '*surface active agent*' and the ability to reduce surface tension is a defining characteristic of a surfactant. The relationship between surfactant concentration in deionised water and the surface tension of the resulting solutions can be indicative of the effective concentration of that surfactant. Although this effective concentration or CMC is often far exceeded in formulations, a smaller CMC still indicates that less will be needed in the final formulation compared to a surfactant with a higher CMC. The surface tension reduction can also be useful to compare as a comparison when choosing surfactants as drop-in replacements for others.

The Wilhelmy plate static surface tension method is based on the observations made by Wilhelmy in 1863²⁴⁴ that a thin plate, such as the platinum plates used in modern equipment, will support the weight of a meniscus and that the corresponding weight can be described quite accurately by Equation 1:

$$W_{tot} = W_{plate} + \gamma\rho \quad \text{Eq. 1}$$

W_{tot} = Total weight

ρ = perimeter of the plate

W_{plate} = Weight of the plate

γ = force per unit length (surface tension)

In practice modern equipment consists of a high accuracy balance which weighs the mass of the platinum plate, moves it slowly towards the liquid and measures the difference upon the plate touching the platinum attached to the balance. The surface tension is then calculated *via* Equation 2, with the angle θ assumed 0° when using platinum due to it is very high surface energy:

$$\gamma = \frac{F}{\rho \cos \theta} \quad \text{Eq. 2}$$

F = Force (mN/m)

The instrument used in this study was a Kruss K100 (Figure 69) with automated dispenser allowing measurement of the CMC, which requires measurement across a range of concentrations.

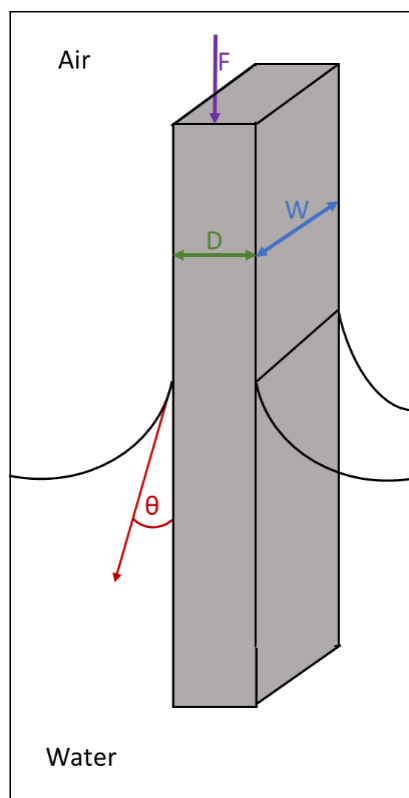


Figure 69: Schematic diagram of Wilhelmy plate static surface tension method.

Prior to carrying out measurements the Wilhelmy plate is held in a flame until it glows red hot. A solution of known surfactant concentration is added to the solution bath beneath the plate. Both are behind a glass windshield and the instrument is on a marble weighing table to reduce weighing errors. The motorised stage raises the bath slowly until the meniscus touches the plate and then takes the weight of the meniscus. When automation is available, tubing pumps deionised water into the solution bath to lower the concentration. In this study the automated dilution function was not available but would have increased the number of data points collected which would have meant that the inflection at the CMC could have been pinpointed more accurately.

Figure 70 shows the photograph of the Kruss K100 with automated dilution used to show the relationship between the concentration of compound **149** and the surface tension of the solution.

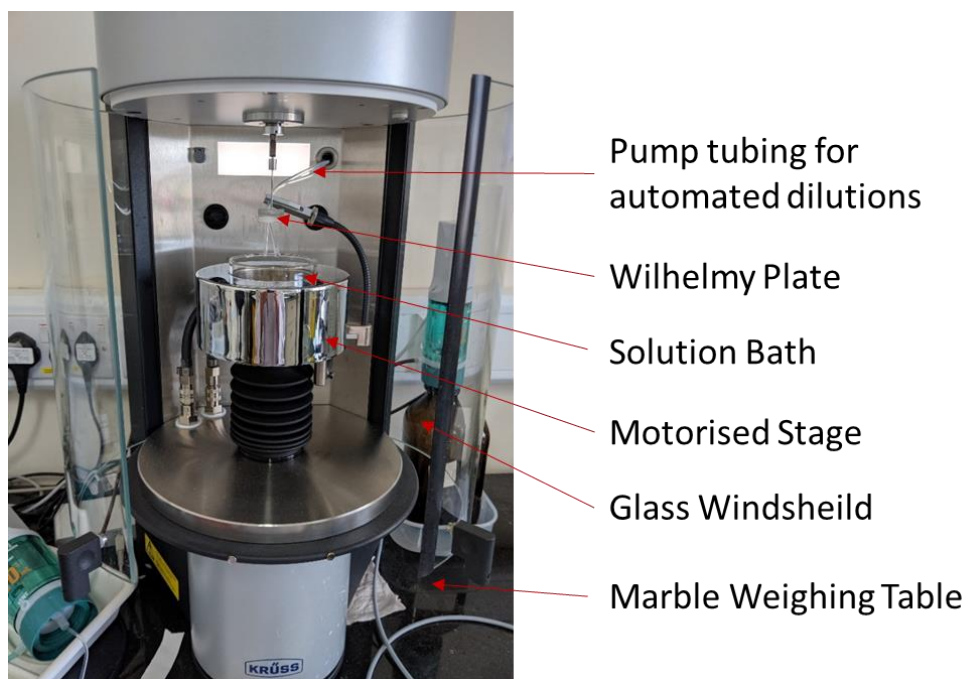


Figure 70: Photograph of the Krüss K100 with automated dilution.

The CMC is found by solving for the coordinates of the intersection between the two lines. This method does not directly measure the presence of micelles but instead assumes that micelles are formed once the surface is 'full' and there is therefore no further surface tension reduction.

The surface tension vs concentration of compound **149** in deionised water are shown in Figure 71 and Table 14:

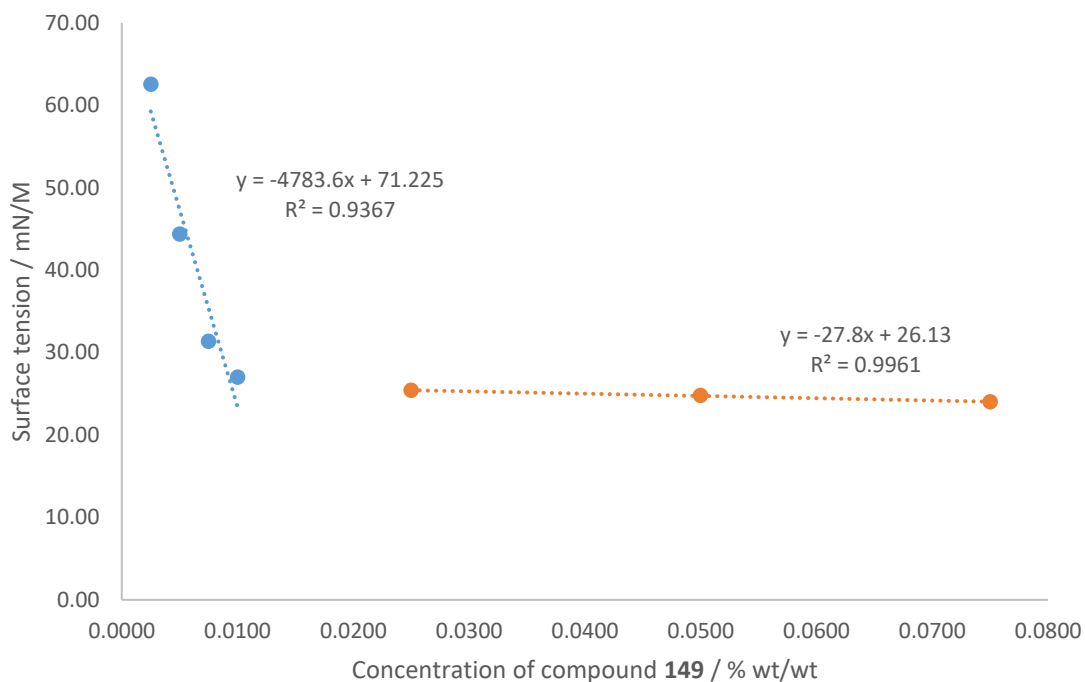


Figure 71: Surface tension vs concentration of compound **149** in deionised water.

Table 14: Results table for the surface tension vs surfactant concentration analysis of compound **149**.

Concentration / % wt/wt	Surface tension / mN/m	SD / mN/m	Temperature / °C
0.0750	24.02	0.006	20.27
0.0500	24.79	0.014	20.19
0.0250	25.41	0.004	20.23
0.0100	27.02	0.006	20.31
0.0075	31.36	0.002	20.28
0.0050	44.39	0.001	20.22
0.0025	62.54	0.041	20.26

At very low concentrations the surface tension approaches that of deionised water (72 mN/m)²⁴⁵ and decreases with the increasing surfactant concentration as more surfactant comes to the surface and has an effect. The surface tension then begins to plateau as the amount of surfactant at the surface hits a maximum. Above this point, the critical micelle

concentration, it is assumed that all additional surfactant molecules are present in micelles. An equilibrium is established between the surfactant at the surface, the surfactant in the bulk of the solution and the surfactant in the micelles.

Two lines of best fit are utilised to pinpoint the CMC. A line of best fit for the data points up to the plateau and a line of best fit for the data points after the plateau. The intersection point between the two lines is (0.009, 25.866). The X coordinate of the intersection gives the CMC for compound **149**, 0.009% wt/wt.

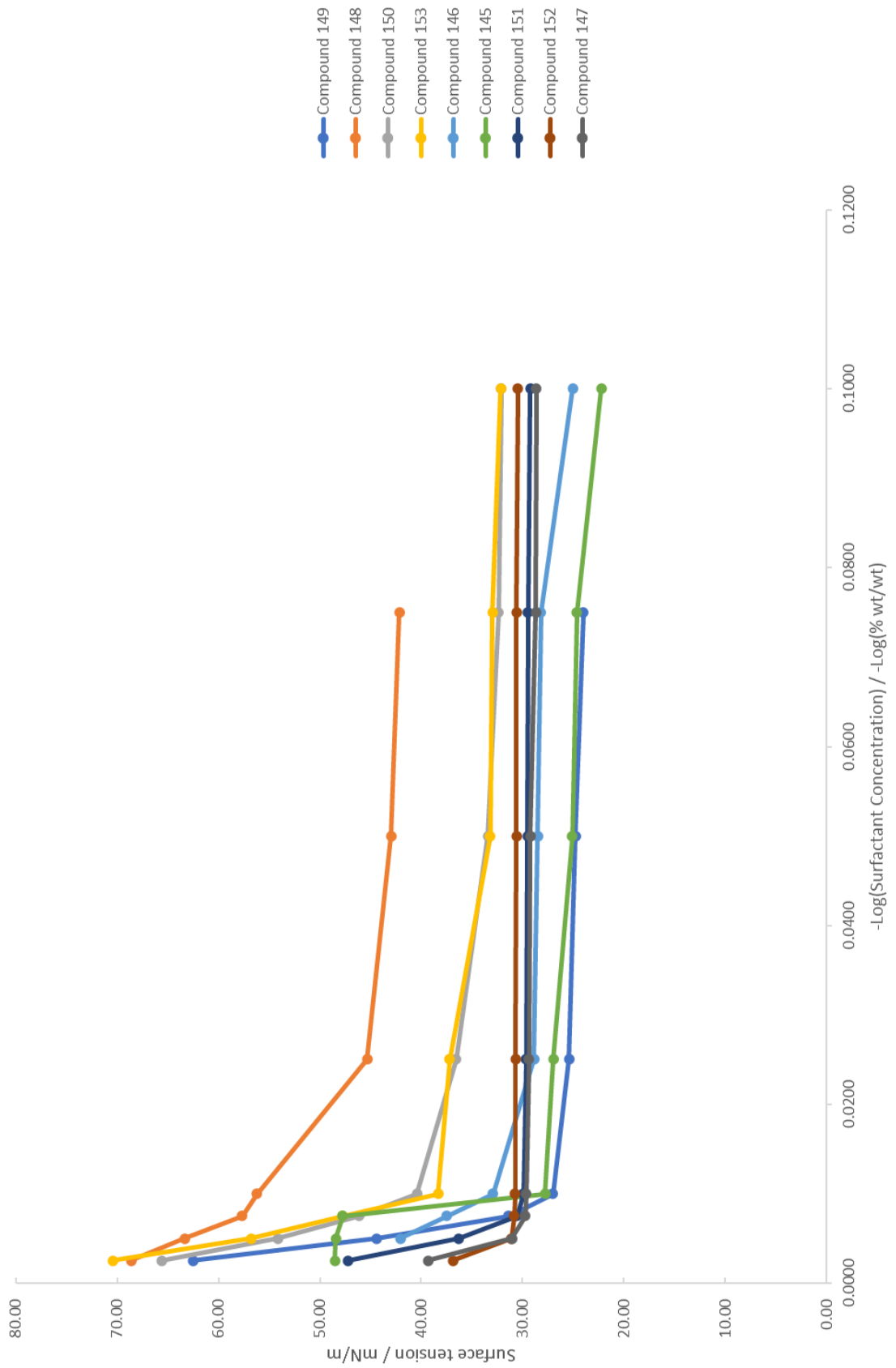


Figure 72: Comparison of surfactant concentration vs surface tension relationships for the final compounds * compound was insoluble in DI water and was dissolved in 5% isopropanol in water.

Figure 72 is a comparison of the surface tension and concentration curves for the compounds listed in the legend. The surface tension reduction curves for compounds **149**, **150** and **153** (with the chemical formulas see in Figure 73) are the steepest. This could be because of the shape of the non-linear cage and ring structures of the tail groups. It is possible that the shape increases the area per surfactant molecule at the surface, decreasing the amount of surfactant molecules that can fit in a monolayer at the surface (a decrease in the surface excess). If fewer molecules were needed to produce a monolayer, the monolayer would therefore be complete at a lower concentration.

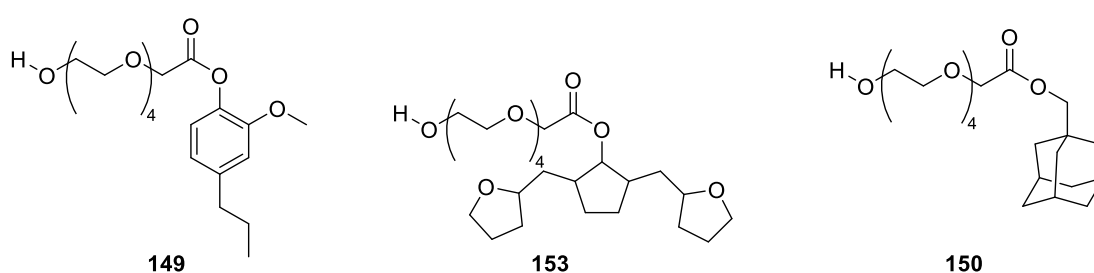


Figure 73: Structures of final compounds **149**, **153** and **150**.

As seen in Figure 72, the greatest surface tension reduction is in compounds **145** and **149**. Compound **149** has the greatest surface tension reduction most likely because it has a relatively short tail in comparison to **145**. There is some polarity in the tail group from the lone pairs on the oxygen of the ether, which could be expected to increase the CMC but this effect is not observed here. When used for detergency shorter chains help lift oils through greater surface tension reduction and longer chains are effective at stabilising emulsified oils because the longer tail groups put a greater distance between the polar water molecules and the oil in the centre of the micelle.

The next shortest chain structure is compound **148** (Figure 74), which has the least reduction in surface tension, as we might expect from the length of the chain compared to a chain of C12 or more.

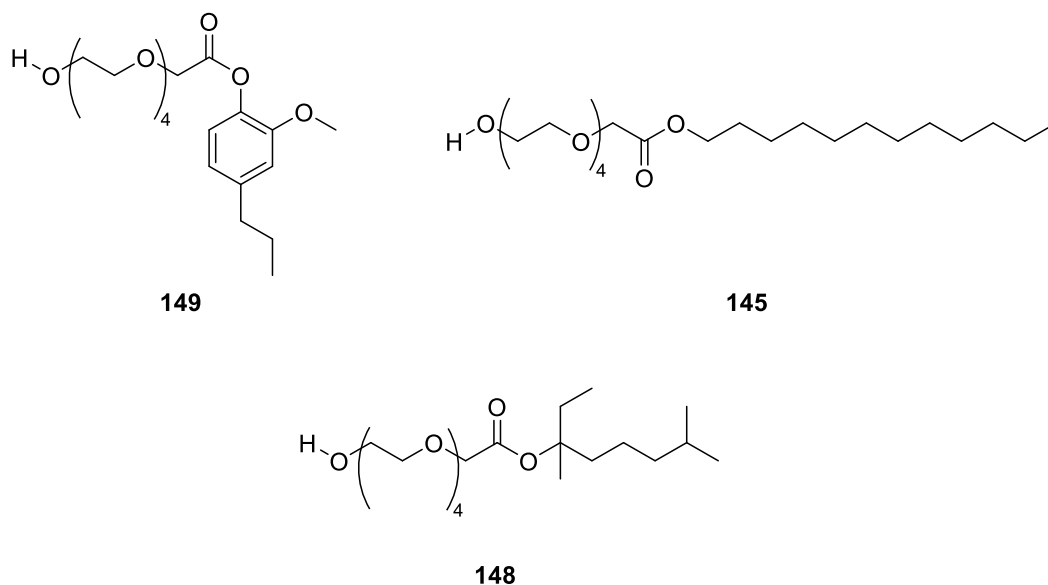


Figure 74: Chemical structures of compounds **149**, **145** and **148**.

This comparison suggests that an additional force may be present such as π - π stacking for compound **149**. This could be influencing how tightly the surfactants are packed at the surface because generally the better the packing the lower the surface tension. If this effect was stronger than the effect of the longer hydrophobic chain length (C12 for compound **145**) this would explain the similar surface tension reductions despite a shorter chain.

Compounds **151** and **152**, which combine some ring/cage character with branching, outperformed the caged and ring structures without branching (compounds **153** and **150** seen in Figure 75).

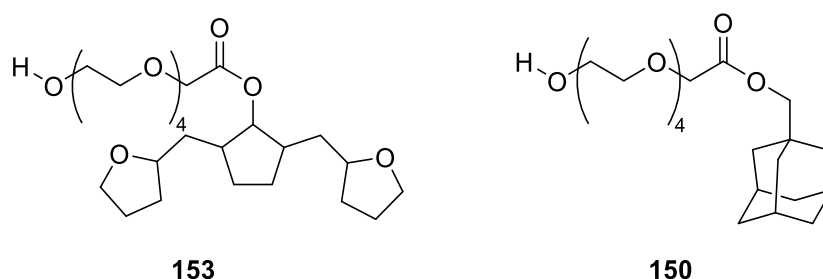


Figure 75: Structures of compounds **153** and **150**.

This could be simply due to the larger hydrophobes for the branched structures or could possibly be due to the branching itself. Future work to investigate this could be to look at

larger cages with no branching and comparing them to smaller cage structures with branching but the same number of carbons as the large, caged structures.

The CMC values calculated from the surface tension vs surfactant concentration curves are presented in Table 15:

Table 15: CMC values for final compounds determined through surface tension measurements using the Kruss K100 vs surfactant concentration. *compound **147** is insoluble in DI water and was dissolved in 5% IPA in DI water prior to CMC analysis.

Compound	CMC / % wt/wt
145	0.2112
148	0.0154
146*	0.0116
150	0.0107
153	0.0101
149	0.0095
151	0.0075
147	0.0054
152	0.0051

The CMC values have been plotted against number of carbons in the tail group (Figure 76). Figure 76 shows weak negative correlation between number of carbons and CMC ($R^2 = 0.6752$). As the head group is the same increasing the number of carbons reduces water solubility and therefore micellization occurs at a lower concentration.

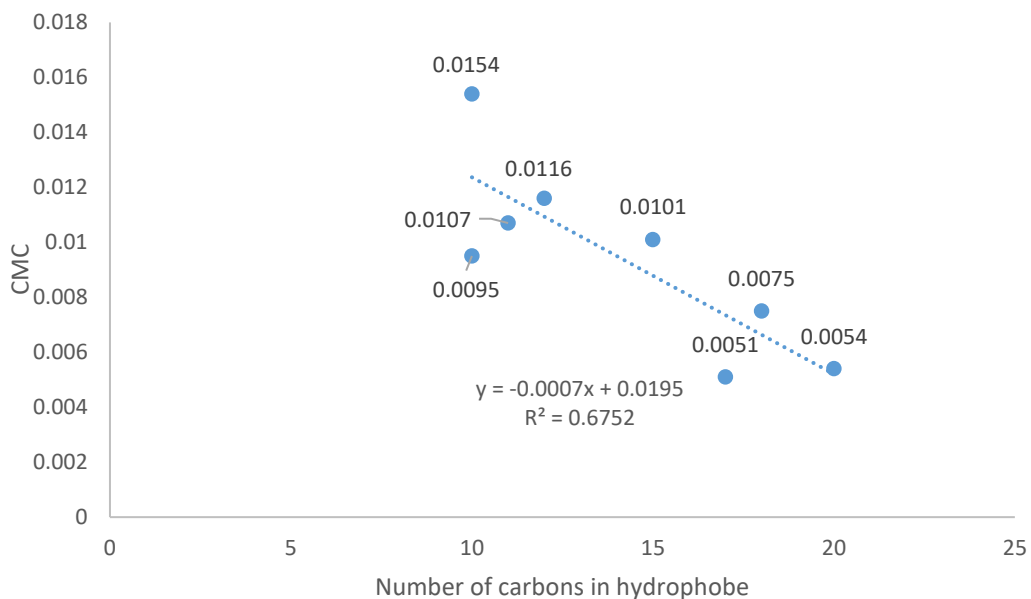


Figure 76: Critical micelle concentration vs number of carbons in the tail group.

Generally, the higher the number of carbons in the hydrophobe the lower the CMC.²⁴⁶ This could simply be because the area per surfactant molecule increases with number of carbons in the tail group; larger tail groups are taking up more space at the interface/surface therefore the concentration needed to 'fill' the surface is lower. There are three potential outliers, compounds **149**, **150** and **153** (see Figure 77 for structures):

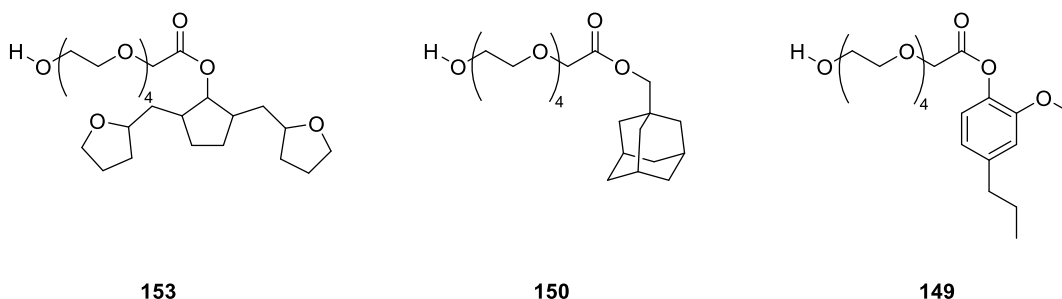


Figure 77: Structures of compounds **153**, **150** and **149**.

If these are removed, there is a significant increase in the negative correlation between the number of carbons in the tail group and the CMC ($R^2 = 0.9651$). All three structures have a ring or cage element. Compound **149** has a lower than expected CMC when considering the number of carbons. This could be because of pi interactions between the rings causing

closer packing at the surface. This could lead to a larger difference between the energy state of the surfactant in the bulk and the energy state of the surfactant in a micelle or at the surface, therefore pushing the equilibrium further towards surfactant at the surface rather than in the bulk.

Neither of the other two structures, compounds **150** and **153**, have linear branching. Compound **150** is a cage structure and compound **153** contains three of 5 membered rings and two oxygens. These two structures therefore have the most drastically different structures to the traditional linear surfactant tail group. Both have lower than expected CMC for the carbon number in the tail group. This suggests that adding ring/cage structures decreases CMC, however as limited samples were synthesised more data would be needed to draw this conclusion.

This is because there is an increase in Van der Waal's forces in longer chains resulting in a lower energy state inside micelles are at the water/air interface. This effect results in lower CMCs for longer hydrophobes.

3.2.10 Dynamic light scattering

The dynamic light scattering (DLS) technique is used to measure the size of micelles.^{247, 248} This method is based on the knowledge that micelles undergo Brownian motion and are large enough to scatter light. A cuvette of sample at the desired concentration, usually in deionised water, is placed in front of a laser within the spectrometer. Bodies large enough to scatter light such as micelles, dust and particulate interfere with the passage of light from the laser to the detector. The frequency of the scattered light is measured, and the particle size determined. The micelle size is determined through its relation to the velocity of the particle, which in turn is related to the frequency shift which occurs when light is scattered by a moving object. This technique is widely used in industry and the literature.²⁴⁹⁻²⁵⁸

The detector collects photons and measures the photon count per second. This is commonly quoted in the more convenient kilo counts per second (kcps). To collect data within the ideal range for the detector an attenuator is used. The attenuator allows only a fraction of the total light present to hit the sensitive detector. The Zetasizer, on which this data was collected, automates this process to achieve an optimal mean count rate for each sample and therefore the attenuation factor for each sample can be different. To enable

comparison between samples the count rate plotted is the derived count rate. The derived count rate is the theoretical count rate that would have been counted if the attenuator had not been used, extrapolated from the mean count rate measured using the attenuator.

The stark difference in size between surfactant molecules in solution below the CMC and the micelles they self-assemble into at concentrations above the CMC produces an obvious change in the intensity of light scattered. As this method can detect the presence and size of micelles it is a more direct measurement than other CMC determination methods for example surface tension measurements. Surface tension methods such as the Wilhelmy plate static surface tension method for CMC determination measure the change in surface tension with relation to concentration.²⁵⁹ The assumption in this method is that the surface tension is at its minimum before formation of micelles. The critical micelle concentration can be determined using the DLS (dynamic light scattering) data.

The Z-average is an estimate of the average particle size based on the integration under the peaks observed. Commonly this is dominated by the two or three main peaks, details of which are in Table 16 for peaks 1 and 2. The chemical structures of the compounds from the Table 16 can be observed in Figure 78:

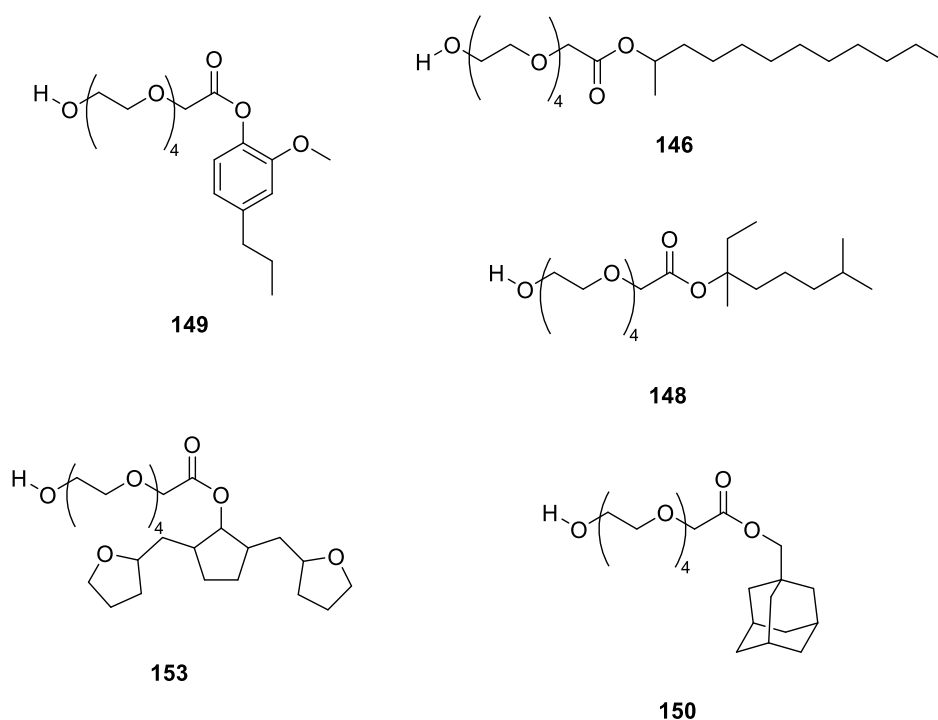


Figure 78: Chemical structures of the compounds from Table 16.

Table 16: Dynamic light scattering data for samples at 0.1% surfactant concentration in ultrapure water measured at 25 °C.

Sample Name	Z-Ave /d.nm	Pdi	Pk 1 Mean Int /d.nm	Pk 2 Mean Int /d.nm	Pk 1 Area Int /%	Pk 2 Area Int /%
Brij	3018	0.5	4659	73.24	90.6	9.4
Synperonic	176.3	0.5	415.7	71.53	82	18
Cithrol	36.42	0.3	53.05	0	100	0
146	562	1	4061	111.8	81.2	18.8
150	491.5	0.4	595.9	165.8	80.7	15.7
152	234.3	0.3	340.4	4571	95.9	4.1
153	176.4	0.2	191.6	5180	97.8	2.2
149	2495	1	183.1	0	100	0

For full raw data including any peak 3 data see appendix. As seen in Table 16, the mean integration for peak 1 and peak 2 is given as well as the peak area integration as a percentage of the signal detected. The polydispersity index (PDI) relates to how broad the particle size distribution. A PDI value approaching 1 is indicative of a very broad curve and therefore a broad distribution of particles/micelles.

The Z-average diameter for **146** is 562 nm however with a PDI of 1, signalling a broad distribution of data, further scrutiny of the data is required. A comparison of peaks 1 and 2 can shed light on PDI and give a better indication of micelle size in some cases. Peaks 1 and 2 fall within the ideal size range selected in the instrument settings and therefore excludes very large particles such as dust or undissolved materials which the PDI and Z-average include. In this case Peak 1 accounts for 81.2% of the scatter and has a mean diameter of 4.061 μm and peak 2, accounting for 18.8% of the scatter, has a mean diameter of 111.8 nm. This indicates that two distinct micelle or particulate sizes are present, which would explain the large PDI. It is possible that peak 1 shows a number of large undissolved droplets of the surfactant of interest and that peak 2 shows the micelle size of that which is dissolved. This is the likely scenario considering the visual inspection of the surfactant solution was hazy. In this case the mean peak intensity of 111.8 nm is a better estimate of the micelle size for **146** than the Z-average of 562 nm.

Compound **150** has a Z-average micelle diameter of 491.5 nm however the peak intensity data suggests two distinct micelle sizes. Peak 1, accounting for 80.7% of the scatter, has an average diameter of 595.9 nm, which would be either a very large micelle or a very small droplet of undissolved material. Peak 2 accounting for 15.7% of the scatter has an average diameter of 165.8 nm. The PDI of 0.4 can be explained by the two distinct particle/micelle sizes. The effective length of the carbon chain of the oleophilic tail group of compound **150** is comparatively short in relation to the tail groups of other synthesised in this study. Therefore it could be expected that compound **150** would produce the smallest micelles however this is not the case. It could be that the cage structure may be interfering with the efficient packing of the micelle and therefore increasing the average diameter. A reasonable prediction would be that compound **146**, with 11 carbons on the backbone and a methyl branch at the intersection of the head and tail group, would produce larger micelles than compound **150**. However, compound **146** appear to have a much smaller micelle size with a micelle diameter of approximately 111 nm compared to compound **150** with an approximate micelle diameter of 165 nm. The free rotation around the C-C bonds in the carbon backbone of **146**'s tail group may have had an effect on micelle size as the chain may have folded back on itself, whereas any rotation on the cage like structure of compounds **150**'s tail group is restricted.

Compound **149** has a Z-average of 2.495 μm and a PDI of 1. Looking deeper into the data for **149** reveals that peak 1 is 100% of the scatter from the ideal size range and has a mean peak diameter of 183.1 nm. This is a strong indication that a large particle such as a dust particle, has crossed the laser and blocked a significant amount of light. As such data would be outside of the ideal range it would not be counted in the peak 1 and 2 integrals but would be included in the PDI and Z-average data, which appears to be skewed as a result.

Compounds **148** and **153** both have a more reasonable PDI of 0.3 and 0.2 respectively. The Z-average for **148** (243.3 nm) is larger than **153** (176.4 nm). This indicates that the micelles are 38% larger due to differences in structure of the tail groups. Compound **148**'s tail group for example has a longer linear carbon chain with methyl and ethyl branching at two carbons in the chain compared to compound **153**, which may explain the larger micelle. However, compound **153** has three ring structures, the central cyclopentanone derived ring with two tetrahydrofuran branches. IT was predicted that this branching would reduce packing efficiency within the micelle however it is possible that some stacking of the ring structures occurred. Similarly compound **149**, containing a benzene ring, has a smaller

micelle size than compound **148**. The benzene ring may have increased packing efficiency here through π - π interaction such as slip stacking.

Many of the samples produced were borderline water insoluble. This was to be expected as the PEG ester head group, chosen to make structural characterisation of the surfactant easier during synthesis, is small compared to PEG and PEG ester surfactants found on the market.

Future work to enable further understanding of how the tail group structure affects micelle packing in water would include synthesizing surfactants with a longer PEG chain, for example an ethoxylate chain of around 20 units (4 units in this study). This would render the surfactants more water soluble and therefore all samples could be analysed in DI water and compared. Higher purity samples would also make findings clearer and more reproducible.

Compounds **145**, **147**, **151** and **153** had poor solubility in DI water. These compounds were dissolved in a 5% solution of isopropanol in DI water for analysis on the Zetasizer. All other compounds were also prepared in the same solvent for comparison.

DLS can also be used to determine CMC. The derived count rate (kcps) vs concentration of compound **149** (Figure 79) is shown in Table 17:

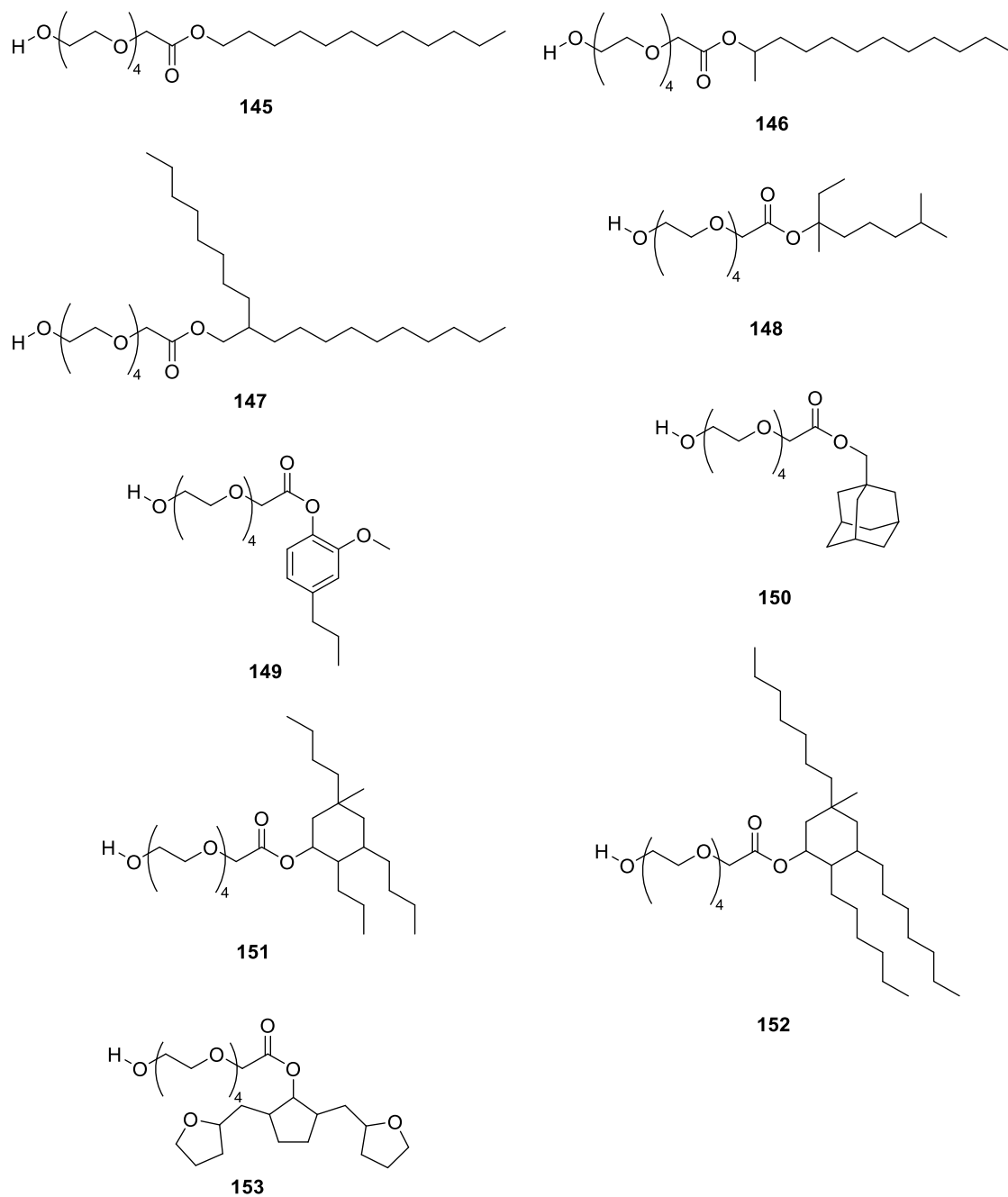


Figure 79: Chemical structures of the compounds **145-153**

Table 17: Dynamic light scattering data for surfactants at 0.1% solution in 5% IPA in DI water at 25 °C. * Blank is 5% IPA in Di water and has a derived count rate of 606 kcps.

Sample Name	Z-Ave /d.nm	Pdl	Pk 1 Mean Int /d.nm	Pk 2 Mean Int /d.nm	Pk 1 Area Int /%	Pk 2 Area Int /%
Blank*	2385	1	304	0	100	0
145	500.4	0.4	483	75.38	93	7
147	219.4	0.2	219.7	0	100	0
151	232.1	0.3	224.5	0	100	0
152	256.4	0.3	269.1	5097	96.6	3.4
149	1791	1	216.1	0	100	0
148	294.5	0.3	435.9	0	100	0
146	227.5	0.5	472	25.12	96	4
153	222.1	0.3	214.9	0	100	0
150	622.7	0.5	372.7	0	100	0
Brij	578.2	1	2556	224.9	73.5	26.5
Cithrol	15.74	0.2	18.8	0	100	0

The CMC is obtained by splitting the data into two series and using the two linear trendlines to find the CMC which is the intercept of the two lines (Figure 80). Compound **149** has a CMC of 0.0268% wt/wt (Table 18).

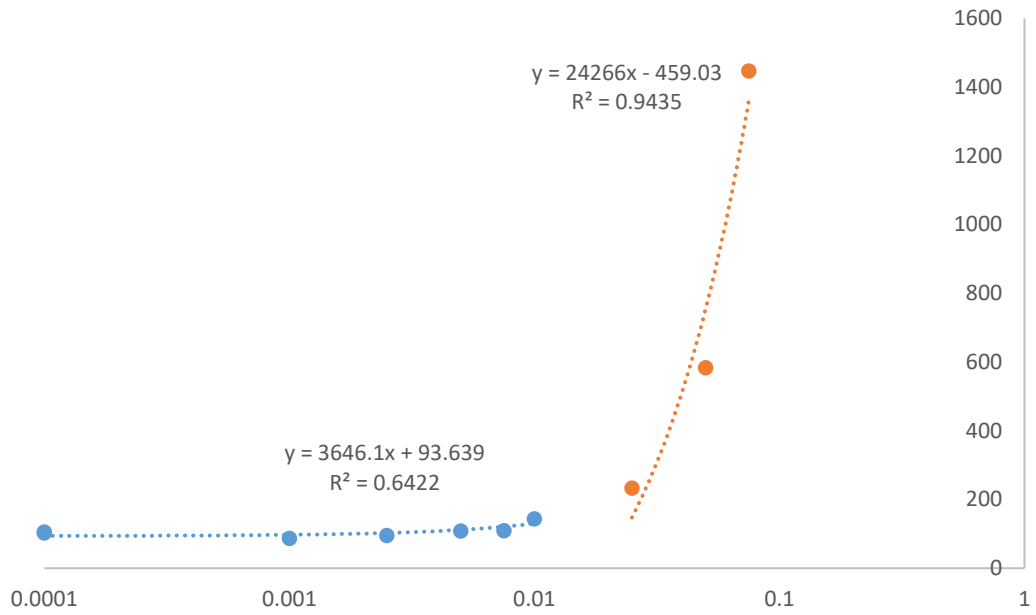


Figure 80: Derived count rate vs concentration of compound **149**.

Table 18: Concentration and derived count rate for CMC determination of compound **149**.

Surfactant concentration / % wt/wt	Derived count rate / kcps
0.075	1446.6
0.05	582.9
0.025	233.3
0.01	143.2
0.0075	109.4
0.0025	95.3
0.001	87.2
0.0001	102.2
0.005	108.4
0.0001	105.3
0.075	1446.6
0.05	582.9
0.025	233.3

Table 19: CMC values determined by DLS (see appendix for data tables, plots, line equations and intercept co-ordinates for each compound).

Compound	CMC (DLS) / % wt/wt
149	0.0268
148	0.0779
150	0.0693
153	0.0749
146	0.0065
151	0.0059
152	0.0546
147	0.0008

3.2.11 Maximum bubble tensiometry

The maximum bubble pressure method is a convenient way of analysing surface tension with respect to time, therefore the dynamic surface tension, of surfactant solutions at different concentrations.²⁶⁰⁻²⁶⁶ Determination of the dynamic surface tension through this method involves a narrow tube submerged into the liquid in question from which an inert gas is blown to produce bubbles which form slowly and break from the neck of the tube. The changes in pressure within the tube are recorded and the surface tension acquired through Equation 3:

$$\Delta P = \frac{2\gamma}{r} \quad \text{Eq. 3}$$

ΔP = the difference in pressure r = radius of the bubble

γ = surface tension

This equation shows that as the size of the bubble decreases the pressure of the gas within increases. The minimum radius of a bubble of gas eluting from a small tube is the radius of the tube, as shown in Figure 81. When the bubble is hemispherical the radius of the tube is equal to the radius of the bubble and therefore the maximum pressure is reached.

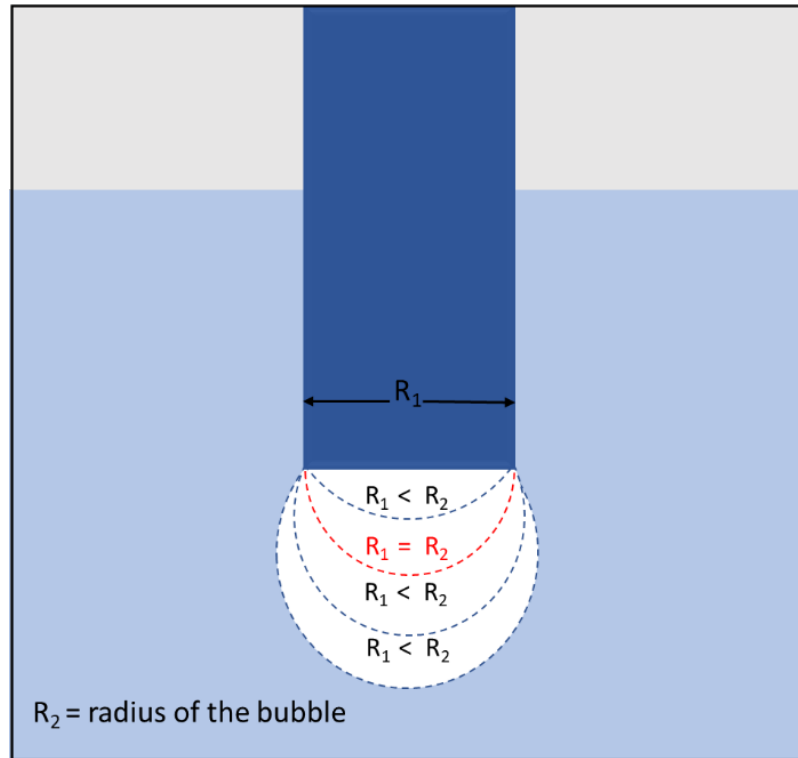


Figure 81: Radius size of gas bubble eluting from a capillary tube.

As a bubble elutes from the tube the radius of curvature of that bubble decreases to a minimum (Figure 82, points A and B), when the bubble is a hemisphere (Figure 82, point B), the maximum pressure is achieved. Following this the radius of curvature increases as the bubble grows (Figure 82, point C) and is detached from the tube (Figure 82, point D). This allows measurement of the surface tension via the relation of pressure to radius and surface tension presented in Equation 3.

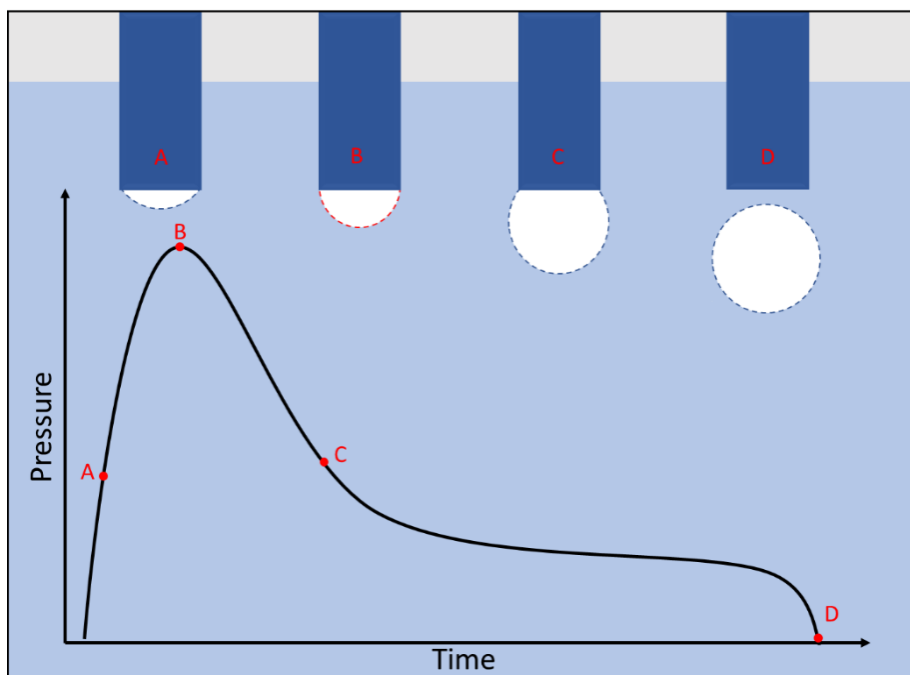


Figure 82: Schematic representing the change of gas pressure over time as a bubble elutes from a capillary tube.

Maximum bubble tensiometry is a useful method to assess how efficiently a surfactant can form an emulsion or lift debris from a surface. A faster dynamic surface tension often greatly reduces the mechanical work required to produce an emulsion.

The presence of surfactant at the liquid/air interface reduces surface tension and therefore also should reduce the pressure required to elute the bubble. Done sufficiently slowly, this method can be used to measure equilibrium surface tension and can also provide information on how quickly the surfactant comes to the surface. The surface tension decreases with the lifetime of the bubble, as with longer lifetimes more surfactant has reached the new liquid/air interface. This method can be useful to assess the dynamic surface tension at different concentrations, to formulate for the most efficiency and to assess the suitability of a surfactant for applications. For example, polymeric surfactants create very stable emulsions once at the surface however move through solutions more slowly than smaller surfactants. Having measured the dynamic surface tension the formulator is now able to put in a surfactant with a better dynamic surface tension which is less stable but reduces the surface tension faster, so less mechanical energy needs to be put in to create the stable emulsion which can then be stabilised by the polymeric surfactant.²⁶⁷

Figures 83 and 84 describe the dynamic surface tension of the final compounds through a plot of surface tension vs surface lifetime for each compound and the industrially produced samples:

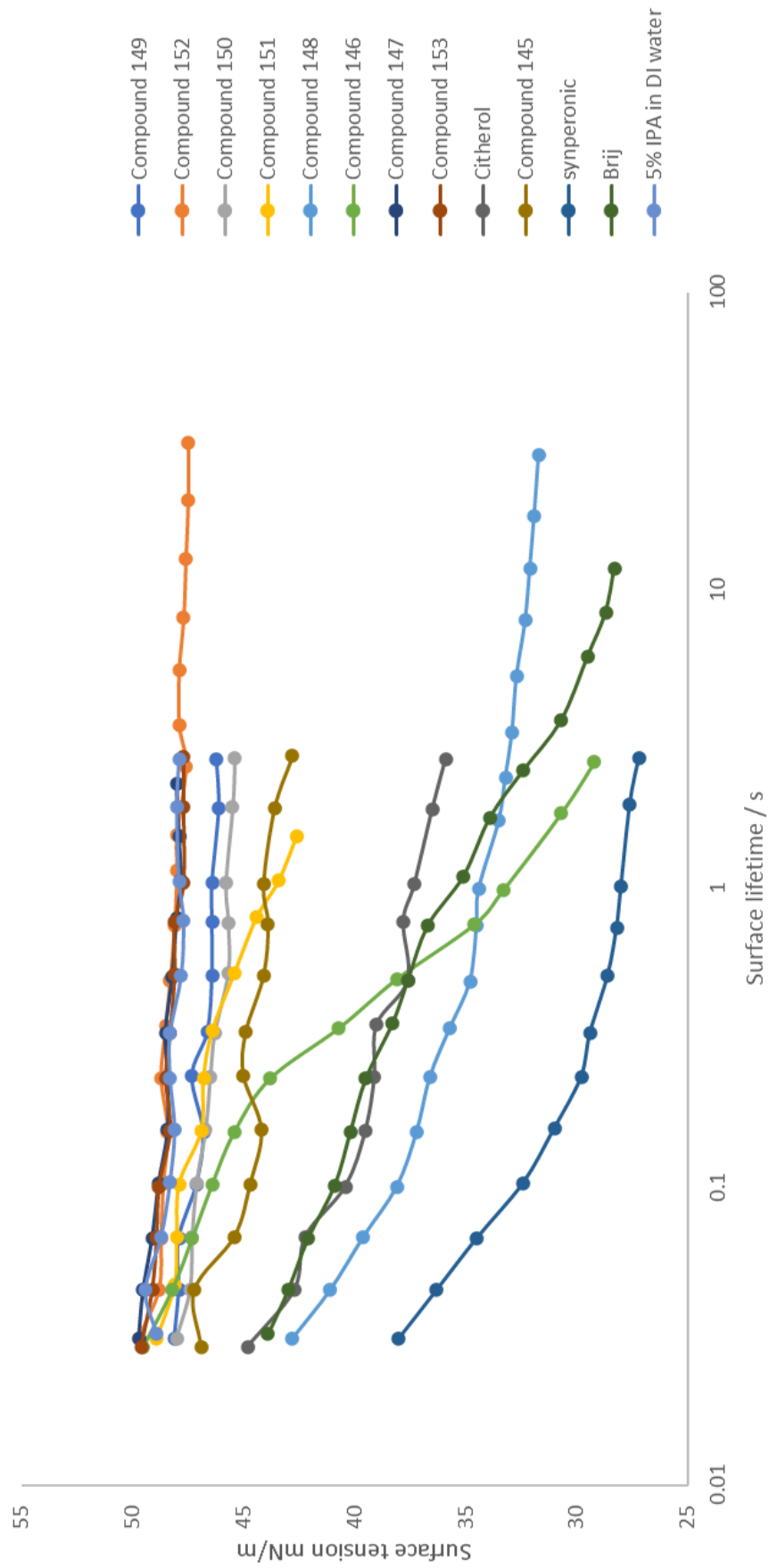


Figure 83: Surface tension vs surface lifetime data collected from the maximum bubble pressure method. Surfactant concentration was 0.1% wt/wt in 5% IPA in deionised water.

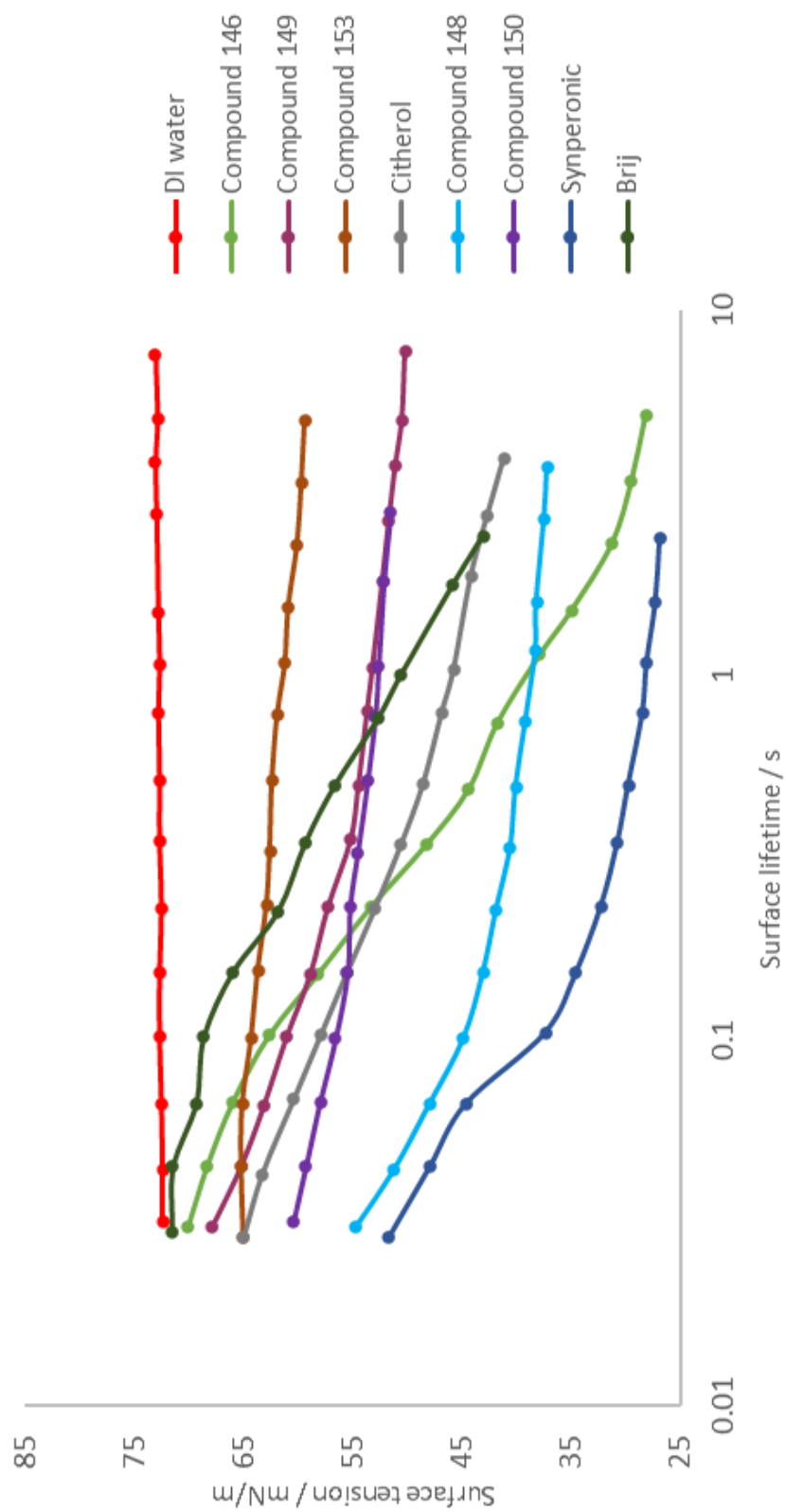


Figure 84: Surface tension vs surface lifetime data collected from the maximum bubble pressure method. Surfactant concentration was 0.1% wt/wt in deionised water.

Not all samples would dissolve in deionised water at 0.1% concentration however all samples would dissolve in deionised water with 5% IPA. Therefore, all samples were dissolved in deionised water with 5% IPA for analysis and compounds which would dissolve fully were also analysed in deionised water only. The effect that the IPA would have was unknown but comparison of Figures 83 and 84 shows that the starting point is a reduced surface tension measurement by 22-25 mN/m. The scale on Figure 84 has been adjusted to better fill the space but clearly shows the blank (5% IPA in deionised water) in red provides a ceiling value to the data, much like deionised water does in Figure 83 as the addition of surfactant can only lower the surface tension from its start point. The slope of the data points tends to be less steep and the surface tension measurements tend to be very close to that seen in DI water only by around 1 second. For example, Synperonic in deionised water with 5% IPA has a surface tension at the shortest surface lifetime of 38 mN/m compared to 51 mN/m in deionised water alone. However, when measured with a surface lifetime of around 1 second both samples have a surface tension around 28 mN/m.

In both Figures 83 and 84 the three industrially produced samples are among the 5 steepest slopes, indicating that they generally reach newly formed surfaces faster than those surfactants synthesised in this study. This could be because the industrially produced samples have an unknown purity and are in fact a mixture of different chain lengths of hydrophobe and hydrophile. This means it is likely that those industrially produced surfactant mixtures will have some shorter chain surfactants within them which can travel to the surface faster as they are less hindered by fewer interactions while moving through solution compared to longer chains.

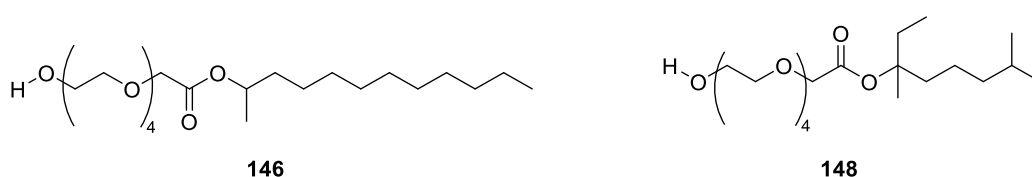


Figure 85: Structures of compounds **146** and **148**.

Compounds **146** and **148** have the steepest slopes of the final compounds synthesised for this study. Therefore, we can surmise that these compounds move through water to newly formed surfaces faster than the other surfactant compounds analysed. This could be because compound **148** has the smallest hydrophobe in terms of carbon number and has no bulky ring or cage structures which may increase the number of interactions when moving through solution. Compound **146** on the other hand has a longer chain, with an 11- carbon chain and a methyl branch but is almost completely linear.

This could suggest that the more bulk in terms of carbon number and presence of rings and cages the slower the surfactant can reach the surface to lower surface tension. This information is useful for the application as a plastic additive as it is likely that if a surfactant takes a long time to reach the surface in a liquid medium it is likely to also take a long time to move to the surface of the plastic, or even prevent it from doing so at all.

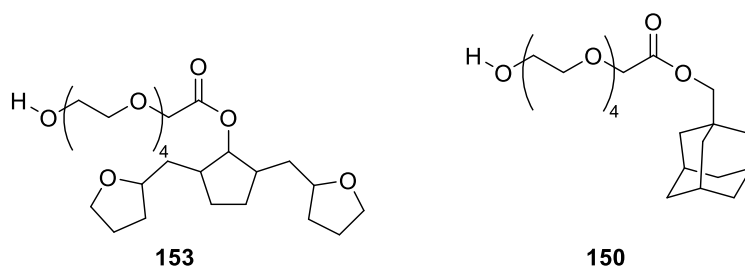


Figure 86: Structures of compounds **153** and **150**.

This theory is further supported by compounds **150** and **153** (Figure 86) whose dynamic surface tension data sets do not have a steep slope, potentially because of the ring/cage structures within.

3.2.12 The Hydrophobic-lipophobic balance (HLB) scale

Hydrophobic-lipophobic balance (HLB) and critical micelle concentration (CMC) have long been quoted by manufacturers of surfactants as standard in the industry to enable formulators to differentiate between surfactants and calculate adjustments to formulate complex surfactant mixtures.

HLB is an empirical scale intended as a measure of preference of surfactants to the water or oil phases. Originally HLB was calculated based on the Griffin equation, given below (Equation 4).

$$HLB = 20 \frac{M_e}{M_m} \quad \text{Eq.4}$$

M_e = Molecular mass of ethoxylate chain M_m = molecular mass

Based on alkyl ethoxylates the equation is a ratio of the number of ethoxy units and the chain length of the alkyl unit. Generally, HLB is useful when formulating with alkyl ethoxylates for example if a surfactant blend is too preferential to the oil phase and needs to incorporate more water a surfactant with a higher HLB can be incorporated and will shift the overall balance and improve the formulation.

HLB can also be used a starting point for formulation as certain ranges of HLB are commonly used for certain applications, for example a detergent would commonly have a much higher HLB than an emulsifier and a wetting or spreading agent would likely have a HLB close to 7. The scale proved to be very useful for categorizing alkyl ethoxylates and was expanded by Davies in 1957 to adjust for the effect of other hydrophobic tail groups (branching, rings, unsaturation) and hydrophilic head groups (ionics, esters etc.).²⁶⁸

3.2.13 The Hydrophobic-lipophobic difference equation

Despite the adjustments to the calculation by Davies, in practice, the further away the surfactant is from a linear alkyl ethoxylate the less useful the HLB becomes as the surfactant does not behave as it's calculated HLB would suggest. This is because the numerical adjustment does not accurately take into account the change in shape of the hydrophobic tail groups and the different area and charges of the hydrophilic head groups. Furthermore, the effect of salinity and temperature (which greatly affect ionics) and a change of oil phase are not taken into consideration. The Griffin and Davies models take into account only the size contribution of the polar and non-polar regions whereas in reality a formulation is a balance between temperature, salinity, oil phase and water and therefore HLB is incapable of providing adequate predictions of surfactant behavior. A more complex model, hydrophobic-lipophobic difference (HLD) (Equation 5), exists to overcome the shortfalls of HLB.

$$HLD = Cc - k \cdot EACN - \alpha \Delta T + f(S) \quad \text{Eq. 5}$$

Cc = Characteristic curvature

α = scaling factor based on the head group temperature effects

T = temperature

k = EACN scaling factor

EACN = effective alkane chain number S = salinity

HLD provides an equation to be manipulated for specific applications in order to balance formulations based on the salinity and temperature of the mixture, and the shape and curvature of the surfactant. An example of its use would be for phase inversion processes. The HLD can be manipulated to near 0 by increasing the temperature of the mixture. At HLD =0 the energy required to produce an emulsion is very low however also not stable. The HLD can also be manipulated to around -1 by decreasing the temperature producing a stable oil in water emulsion. In this way the most efficient emulsion process can be established. Due to the nature of the equation no HLD number can be given to a surfactant

alone, only the system and therefore cannot be quoted here, however k, EACN and Cc may be possible to calculate and included to aid formulation through use of the HLD equation.

3.2.14 Key parameters for surfactant behaviour and performance determined from combinations of analysis

CMC is defined as the concentration above which additional surfactant in aqueous solution forms micelles. However, in formulation the behavior of the surfactant in water at such low concentrations is largely irrelevant as commonly an oil phase is introduced and concentrations several orders of magnitude above the CMC are used to produce the desired effects. The CMC tends to function as the minimum concentration required for effective use of the surfactant rather than an indication of effectiveness.

The surfactant concentration vs surface tension measurements commonly used to calculate the CMC can also be used to calculate other useful factors and will therefore still be quoted for the surfactants produced in this work. The slope of the surfactant concentration vs surface tension, $\frac{d\sigma}{d\ln c}$, can be used to calculate surface excess as described below by Equation 6:

$$\Gamma_m = -\frac{1}{RT} \cdot \frac{d\sigma}{d\ln c} \quad \text{Eq. 6}$$

Γ_m = surface excess R = gas constant σ = surface tension c = concentration

The surface excess, Γ_m , is the saturated concentration of surfactant at the surface and can be used to calculate the area per surfactant molecule (A, Equation 7), an indication of how tightly packed the molecules are at the surface.

$$A = \frac{1}{N_A \cdot \Gamma_m} \quad \text{Eq. 7}$$

A = Head area in angstroms

N_A = Avogadro's number

Once the surface excess is known from the surface tension vs concentration measurements the absorption coefficient can be calculated in combination with dynamic surface tension data from the maximum bubble pressure method through Equation 8:

$$\sigma_t = \sigma_{eq} + \frac{RT\Gamma_m^2}{2c} \left(\frac{Kt}{\pi}\right)^2 \quad \text{Eq. 8}$$

t = surface age

σ_{eq} = surface tension at equilibrium

K = absorption coefficient

σ_t = surface tension at surface age t T = absolute temperature R = gas constant

The absorption coefficient is a measure of the likelihood or preference of the surfactant to be at the surface or within the aqueous phase.

3.2.15 Preliminary bench test for an indication of emulsion type

This rapid qualitative test provides a visual indication of the type of emulsion a surfactant tends to form. To prepare, a sample of surfactant (0.5 g) is added to Arlamol (2 g) and water (8 g) and shaken to form an emulsion. A droplet of the resulting emulsion placed onto a clean glass slide very close to a droplet of water. The glass slide is then carefully tilted to encourage the droplets to touch (Figure 87):

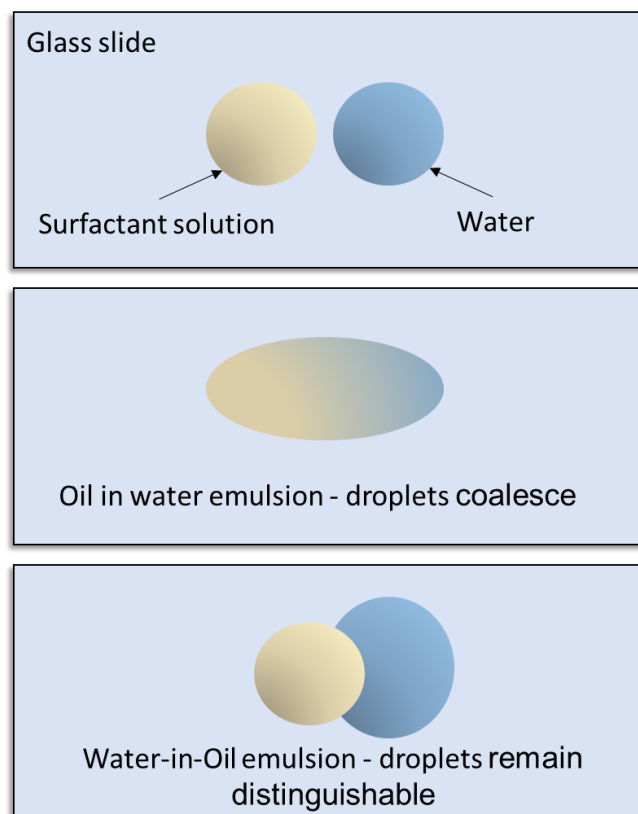


Figure 87: Schematic diagram of the emulsion type bench test.

If the continuous phase of the emulsion is water, as with an oil in water emulsion, the two droplets will coalesce. If the surfactant solution has formed a water in oil emulsion the droplets will retain a clear separation at the shared surface.

Table 20: Masses used and results table for the emulsion type bench test.

Surfactant sample compound name	Surfactant		Oil		Water		Emulsion type (observation)
	Mass (g)	Conc. (%)	Mass (g)	Conc. (%)	Mass (g)	Conc. (%)	
145	0.50	0.048	1.99	0.199	8.01	0.762	Oil in water
146	0.51	0.047	2.00	0.195	8.23	0.767	Oil in water
147	0.50	0.047	1.99	0.198	8.02	0.763	Water in oil
151	0.51	0.048	2.00	0.199	8.00	0.761	Oil in water
148	0.50	0.048	1.99	0.199	8.00	0.762	Oil in water
150	0.50	0.043	2.01	0.177	9.31	0.787	Oil in water
149	0.51	0.048	2.00	0.199	8.01	0.762	Not an emulsifier

As seen in Table 20, the observations from this quick bench test suggested that the 2-octyl dodecyl sample may be more suited to a water-in-oil emulsion formulation. The length of the tail group (the longest chain by 8 carbons) and the free rotation around the C-C backbone means that the tail groups are less likely to pack closely in a typical micelle. Furthermore, the branch on the carbon backbone further increases the likelihood of reverse micelle formation, producing a water-in -oil emulsion. The eugenol-based surfactant formed an unstable Windsor 1 solution which quickly separated.

3.3 CONCLUSION

In chapter 2, the synthesis of 9 novel surfactants was described. Several methods which attempted to measure the relative hydrophobicity of the hydrophobic tail groups compared to one another and to industrially synthesised blends with similar general structures were trialled. Each had their own shortcomings and after much consideration, method development was dropped due to both time pressures and a realisation that a method for comparing hydrophobicity of tail groups was not likely to give representative results as the surfactant should be considered as a whole.

The surfactant properties of each of the 9 novel surfactants were explored and compared to industrially synthesised blends with similar general structures in chapter 3 using standard industry techniques. This included use of the Wilhelmy plate static surface tension method which proved each of the 9 novel compounds did exhibit surfactant properties by reducing the surface tension of water. The static surface tension was also used to produce critical micelle concentrations (CMC) for each surfactant.

The dynamic surface tension of each compound was also explored, describing how quickly each compound migrates to a newly formed surface. Dynamic light scattering was used to assess the size of micelles, shedding light on packing proficiency and also used to produce CMC values for each compound. The combined data suggested that ring and cage structures present in some of the compounds effected packing efficiency negatively. Increasing the number of carbons in the hydrophobic tail group reduced solubility in water and lead to a tendency to form reverse micelles in one case.

Further work to define the surface excess and area per surfactant molecule from the data given would provide further insights to the properties of these surfactants and enable the use of the HLD equation for predicting the behaviour of each compound in a specific solution, were both phases, temperature and salinity are known. Increasing the number of data points collected would have enabled a comparison of the CMCs collected via two different methods however due to time pressures and equipment malfunctions this was not possible. All novel compounds exhibited surfactant properties which were compared to one another through several different analysis methods.

3.4 OVERALL CONCLUSION

Chapter 1 provided a summary of the literature exploring the need to produce replacements for perfluorinated surfactants which are being phased out of production globally due to their toxicity, persistence in the environment and lack of biodegradability. The surge in biofuel research following environment policies in Europe and the U.S. provided several bioderived highly hydrophobic structures which have the potential to be used as a hydrophobic tail groups for biomass derived surfactants. To produce long chain dense alkanes suitable for use as biofuel and jet fuel it was found in the literature that in general to produce fuels platform molecules undergo C-C coupling reactions such as aldol condensations and Diels-Alder condensations to lengthen the carbon chain before hydrodeoxygenation to form alkanes. These high-density alkanes often included branching, ring structures and cage structures which it was hypothesised may help with hydrophobicity when used as a surfactant tail group.

Several of these structures were selected as a synthetic starting point and synthesised through aldol condensation as described in Chapter 3. We chose not to follow the aldol condensations with a hydrodeoxygenation step to preserve the remaining functionality, an α,β -unsaturated ketone. Instead, the α,β -unsaturated ketones were hydrogenated and reduced to form fatty alcohols for the addition of a head group.

Several choices of head groups were attempted including anionic, through sulfonation of the α,β -unsaturated ketones, cationic through amination of the α,β -unsaturated ketones and non-ionic where an ether link was attempted to attach a poly (ethylene glycol) tail group. All attempts were unsuccessful which lead to the use of an ester link between the head and tail group which also promotes degradability. One terminal hydroxyl of tetraethylene oxide was protected and via the other hydroxyl a carboxylic acid was added using bromoacetic acid. Several attempts at the esterification of the carboxylic acid and fatty alcohols were unsuccessful for example Steglich esterification and use of T3P mediated esterification. Eventually esterification was successful using an acyl chloride as an intermediate. After esterification using the 9 selected fatty alcohols the compounds were deprotected through hydrogenation producing 9 novel compounds with potential to behave as surfactants.

Chapter 3 explored method development attempts which aimed to measure and compare the hydrophobicity of surfactant tail groups without extrusion into plastic first. Several methods were trialled however overall it was concluded that a quick comparison of tail groups was difficult because creating a monolayer required specialist equipment and surface effects such as packing efficiency had a large impact could not be ignored.

Standard industry techniques confirmed that all 9 compounds exhibited surfactant properties which were compared to one another and to industrially produced surfactant blends through several different analysis methods. The analysis methods included Wilhelmy plate static surface tension method, dynamic surface tension measurements and dynamic light scattering measurements. From these analysis techniques the size of the micelles formed was discussed, as well as the speeds at which each surfactant migrated to a newly formed surface and the CMCs of each compound were determined.

4 REFERENCES

1. P. T. Anastas and J. C. Warner, *Green chemistry: Theory and practice*, 1998, **29**.
2. P. T. Anastas, *Handbook of green chemistry*, Wiley-VCH, 2013.
3. P. T. Anastas and M. M. Kirchhoff, *Accounts of chemical research*, 2002, **35**, 686-694.
4. P. Anastas and N. Eghbali, *Chemical Society Reviews*, 2010, **39**, 301-312.
5. R. A. Sheldon, *Philosophical Transactions of the Royal Society A*, 2020, **378**, 20190274.
6. P. T. Anastas, M. M. Kirchhoff and T. C. Williamson, *Applied Catalysis A: General*, 2001, **221**, 3-13.
7. J. Wilkinson, P. S. Hooda, J. Barker, S. Barton and J. Swinden, *Environ Pollut*, 2017, **231**, 954-970.
8. W. McDonough and M. Braungart, *The International handbook on environmental technology management*, **33**.
9. F. Bonviu, *Romanian J. Eur. Aff.*, 2014, **14**, 78.
10. O. E. Ogunmakinde, W. Sher and T. Egbelakin, *Clean Technologies and Environmental Policy*, 2021, **23**, 899-914.
11. C. J. Whalen and K. A. Whalen, *Journal of Economic Issues*, 2020, **54**, 628-643.
12. T. J. Farmer and M. Mascal, *Introduction to chemicals from biomass*, 2015, 89-155.
13. M. J. Rosen and J. T. Kunjappu, *Surfactants and interfacial phenomena*, John Wiley & Sons, 2012.
14. T. F. Tadros, *An introduction to Surfactants*, 2014.
15. A. W. Adamson, Gast, Alice P., *Physical Chemistry of surfaces*, John Wiley & Sons, 1997.
16. N. Dave and T. Joshi, *Int. J. Appl. Chem*, 2017, **13**, 663-672.
17. S. Tiwari, *International Journal of Engineering Research and Application*, 2018, **8**, 61-66.
18. T. M. Schmitt, *Analysis of Surfactants*, CRC Press, 2001.
19. C. A. Sperati, Dordrecht, 1986.
20. R. C. Buck, J. Franklin, U. Berger, J. M. Conder, I. T. Cousins, P. de Voogt, A. A. Jensen, K. Kannan, S. A. Mabury and S. P. van Leeuwen, *Integrated Environmental Assessment and Management*, 2011, **7**, 513-541.
21. E. Kissa, *Fluorinated surfactants and repellents*, CRC Press, New York, 2nd edn., 2001.
22. S. Posner, in *Polyfluorinated Chemicals and Transformation Products*, eds. T. P. Knepper and F. T. Lange, Springer Berlin Heidelberg, Berlin, Heidelberg, 2012, DOI: 10.1007/978-3-642-21872-9_2, pp. 25-39.
23. M. P. Krafft, *J Polym Sci Pol Chem*, 2006, **44**, 4251-4258.
24. L. Pauling, *J Am Chem Soc*, 1947, **69**, 542-553.
25. L. Pauling, *J Am Chem Soc*, 1932, **54**, 3570-3582.
26. D. Barriet and T. R. Lee, *Curr Opin Colloid In*, 2003, **8**, 236-242.
27. K. U. Goss and G. Bronner, *J Phys Chem A*, 2006, **110**, 9518-9522.
28. M. Pabon and J. M. Corpart, *Journal of Fluorine Chemistry*, 2002, **114**, 149-156.
29. M. P. Krafft, *Advanced Drug Delivery Reviews*, 2001, **47**, 209-228.
30. E. Dhanumalayan and G. M. Joshi, *Advanced Composites and Hybrid Materials*, 2018, **1**, 247-268.
31. M. P. Krafft and J. G. Riess, *Chemical reviews*, 2009, **109**, 1714-1792.
32. N. Kovalchuk, A. Trybala, V. Starov, O. Matar and N. Ivanova, *Advances in colloid and interface science*, 2014, **210**, 65-71.
33. A. Stefanek, K. Łęczycka-Wilk, S. Czarnocka-Śniadała, W. Frąckowiak, J. Graffstein, A. Ryzko, A. Nowak and T. Ciach, *Colloids and Surfaces B: Biointerfaces*, 2021, **200**, 111603.

34. J. Glüge, M. Scheringer, I. T. Cousins, J. C. DeWitt, G. Goldenman, D. Herzke, R. Lohmann, C. A. Ng, X. Trier and Z. Wang, *Environmental Science: Processes & Impacts*, 2020, **22**, 2345-2373.
35. R. C. Buck, Murphy, Peter M., Pabon, Martial, *Polyfluorinated chemicals and transformation products*, 2012.
36. P. B. a. G. Larsen, Estelle, *Journal*, 2015, 7-83.
37. M. J. Lopez-Espinosa, D. Mondal, B. Armstrong, M. S. Bloom and T. Fletcher, *Environ Health Perspect*, 2012, **120**, 1036-1041.
38. K. Steenland, L. Zhao, A. Winquist and C. Parks, *Environ Health Perspect*, 2013, **121**, 900-905.
39. V. Barry, A. Winquist and K. Steenland, *Environ Health Perspect*, 2013, **121**, 1313-1318.
40. S. M. Bartell and V. M. Vieira, *Journal of the Air & Waste Management Association*, 2021, **71**, 663-679.
41. F. Coperchini, L. Croce, G. Ricci, F. Magri, M. Rotondi, M. Imbriani and L. Chiovato, *Frontiers in Endocrinology*, 2021, **11**.
42. A. M. Calafat, L. Y. Wong, Z. Kuklennyik, J. A. Reidy and L. L. Needham, *Environ Health Perspect*, 2007, **115**, 1596-1602.
43. K. Kato, L. Y. Wong, L. T. Jia, Z. Kuklennyik and A. M. Calafat, *Environ Sci Technol*, 2011, **45**, 8037-8045.
44. Y. Liu, A. Li, Q. An, K. Liu, P. Zheng, S. Yin and W. Liu, *Critical Reviews in Environmental Science and Technology*, 2021, DOI: 10.1080/10643389.2021.1886556, 1-28.
45. T. Cao, A. Qu, Z. Li, W. Wang, R. Liu, X. Wang, Y. Nie, S. Sun, X. Zhang and X. Liu, *Environmental Science and Pollution Research*, 2021, **28**, 67053-67065.
46. C. R. Stein, D. A. Savitz, B. Elston, P. G. Thorpe and S. M. Gilboa, *Reproductive Toxicology*, 2014, **47**, 15-20.
47. Forever chemicals: the hidden threat from the PFAS toxins on your shelf, <https://www.theguardian.com/environment/2021/sep/14/forever-chemicals-the-hidden-threat-from-the-pfas-toxins-on-your-shelf>, (accessed Januray 2022).
48. Storyville: Poisoning America: The Devil we know, <https://www.bbc.co.uk/programmes/b0bs68rr>, (accessed 05/01/2022).
49. L. A. Caldwell and F. Thorp V, *Journal*, 2021.
50. S. Gibbens, *Journal*, 2020.
51. A. M. Phillips, *Journal*, 2019.
52. D. S. Cloud, A. M. Phillips and T. Barboza, *Journal*, 2019.
53. S. Gibbons, Toxic 'forever chemicals' more common in tap water than thought, report says, <https://www.nationalgeographic.com/science/2020/01/pfas-contamination-safe-drinking-water-study/#:~:text=Some%20of%20the%20most%20commonly,safe%20by%20their%20own%20standards.>, (accessed 04/06/2020, 2020).
54. T. Perkins, The forever chemicals fueling a public health crisis in drinking water, The Guardian, <https://www.theguardian.com/society/2020/feb/03/pfas-forever-chemicals-what-are-they>, (accessed July 2023).
55. Dark Waters, *Focus Features*, T. Haynes, M. Ruffalo, C. Vachon, P. Koffler, 2020, 126 minutes.
56. The Today Show, 2020.
57. J. M. Conder, R. A. Hoke, W. De Wolf, M. H. Russell and R. C. Buck, *Environ Sci Technol*, 2008, **42**, 995-1003.
58. J. S. C. Liou, B. Szostek, C. M. DeRito and E. L. Madsen, *Chemosphere*, 2010, **80**, 176-183.
59. M. Houde, J. W. Martin, R. J. Letcher, K. R. Solomon and D. C. G. Muir, *Environ Sci Technol*, 2006, **40**, 3463-3473.
60. M. Houde, A. O. De Silva, D. C. G. Muir and R. J. Letcher, *Environ Sci Technol*, 2011, **45**, 7962-7973.

61. W. J. Zhong, L. Y. Zhang, Y. N. Cui, M. Chen and L. Y. Zhu, *Sci Total Environ*, 2019, **647**, 992-999.
62. S. K. Kim and K. Kannan, *Environ Sci Technol*, 2007, **41**, 8328-8334.
63. D. B. Chan and E. S. K. Chian, *Environmental Progress*, 1986, **5**, 104-109.
64. A. Fath, F. Sacher and J. E. McCaskie, *Water Science and Technology*, 2016, **73**, 1659-1666.
65. K. E. Carter and J. Farrell, *Separation Science and Technology*, 2010, **45**, 762-767.
66. A. Lelek and C. Köhler, *Regulated Rivers: Research & Management*, 1990, **5**, 57-66.
67. J.-C. Le Coze and S. Lim, 2004.
68. M. H. Russell, W. R. Berti, B. Szostek and R. C. Buck, *Environ Sci Technol*, 2008, **42**, 800-807.
69. J. W. Washington, J. J. Ellington, T. M. Jenkins, J. J. Evans, H. Yoo and S. C. Hafner, *Environ Sci Technol*, 2009, **43**, 6617-6623.
70. M. G. Evich, M. J. Davis, J. P. McCord, B. Acrey, J. A. Awkerman, D. R. Knappe, A. B. Lindstrom, T. F. Speth, C. Tebes-Stevens and M. J. Strynar, *Science*, 2022, **375**, eabg9065.
71. L. P. Wackett, *Microbial Biotechnology*, 2022, **15**, 773-792.
72. S. Huang and P. R. Jaffé, *Environ Sci Technol*, 2019, **53**, 11410-11419.
73. Y. Yu, K. Zhang, Z. Li, C. Ren, J. Chen, Y.-H. Lin, J. Liu and Y. Men, *Environ Sci Technol*, 2020, **54**, 14393-14402.
74. V. S. Bondar, M. G. Boersma, E. L. Golovlev, J. Vervoort, W. J. Van Berkel, Z. I. Finkelstein, I. P. Solyanikova, L. A. Golovleva and I. M. Rietjens, *Biodegradation*, 1998, **9**, 475-486.
75. S. A. Hasan, M. I. M. Ferreira, M. J. Koetsier, M. I. Arif and D. B. Janssen, *Applied and environmental microbiology*, 2011, **77**, 572-579.
76. D. P. Dixon, D. J. Cole and R. Edwards, *Archives of biochemistry and biophysics*, 2000, **384**, 407-412.
77. X. Jiao, Q. Shi and J. Gan, *Critical reviews in environmental science and technology*, 2021, **51**, 2745-2776.
78. K. J. Hansen, H. Johnson, J. Eldridge, J. Butenhoff and L. Dick, *Environ Sci Technol*, 2002, **36**, 1681-1685.
79. A. M. Becker, S. Gerstmann and H. Frank, *Chemosphere*, 2008, **72**, 115-121.
80. C. A. Moody, J. W. Martin, W. C. Kwan, D. C. Muir and S. A. Mabury, *Environ Sci Technol*, 2002, **36**, 545-551.
81. J. L. Barber, U. Berger, C. Chaemfa, S. Huber, A. Jahnke, C. Temme and K. C. Jones, *Journal of environmental monitoring*, 2007, **9**, 530-541.
82. L. Ahrens and M. Bundschuh, *Environ Toxicol Chem*, 2014, **33**, 1921-1929.
83. L. Ahrens, W. Gerwinski, N. Theobald and R. Ebinghaus, *Marine Pollution Bulletin*, 2010, **60**, 255-260.
84. L. Gobelius, J. Hedlund, W. Durig, R. Troger, K. Lilja, K. Wiberg and L. Ahrens, *Environ Sci Technol*, 2018, **52**, 4340-4349.
85. M. M. Schultz, D. F. Barofsky and J. A. Field, *Environ Sci Technol*, 2004, **38**, 1828-1835.
86. I. Ericson, J. L. Domingo, M. Nadal, E. Bigas, X. Llebaria, B. Van Bavel and G. Lindström, *Archives of environmental contamination and toxicology*, 2009, **57**, 631-638.
87. M. S. McLachlan, K. E. Holmström, M. Reth and U. Berger, *Environ Sci Technol*, 2007, **41**, 7260-7265.
88. A. Möller, L. Ahrens, R. Surm, J. Westerveld, F. van der Wielen, R. Ebinghaus and P. de Voogt, *Environ Pollut*, 2010, **158**, 3243-3250.
89. N. Yamashita, K. Kannan, S. Taniyasu, Y. Horii, G. Petrick and T. Gamo, *Marine pollution bulletin*, 2005, **51**, 658-668.
90. N. Yamashita, K. Kannan, S. Taniyasu, Y. Horii, T. Okazawa, G. Petrick and T. Gamo, *Environ Sci Technol*, 2004, **38**, 5522-5528.
91. R. Ghisi, T. Vamerali and S. Manzetti, *Environmental research*, 2019, **169**, 326-341.
92. M. F. Rahman, S. Peldszus and W. B. Anderson, *Water research*, 2014, **50**, 318-340.
93. G. B. Post, P. D. Cohn and K. R. Cooper, *Environmental research*, 2012, **116**, 93-117.

94. P. A. Fair, B. Wolf, N. D. White, S. A. Arnott, K. Kannan, R. Karthikraj and J. E. Vena, *Environmental research*, 2019, **171**, 266-277.
95. J. L. Domingo and M. Nadal, *Journal of Agricultural and Food Chemistry*, 2017, **65**, 533-543.
96. H. A. Kabore, S. V. Duy, G. Munoz, L. Meite, M. Desrosiers, J. X. Liu, T. K. Sory and S. Sauve, *Sci Total Environ*, 2018, **616**, 1089-1100.
97. S. Saikat, I. Kreis, B. Davies, S. Bridgman and R. Kamanyire, *Environmental Science: Processes & Impacts*, 2013, **15**, 329-335.
98. C. Fei, J. K. McLaughlin, R. E. Tarone and J. Olsen, *Environ Health Persp*, 2007, **115**, 1677-1682.
99. D. Melzer, N. Rice, M. H. Depledge, W. E. Henley and T. S. Galloway, *Environ Health Persp*, 2010, **118**, 686-692.
100. E. P. o. C. i. t. F. Chain, D. Schrenk, M. Bignami, L. Bodin, J. K. Chipman, J. del Mazo, B. Grasl-Kraupp, C. Hogstrand, L. Hoogenboom and J. C. Leblanc, *EFSA Journal*, 2020, **18**, e06223.
101. N. M. Brennan, A. T. Evans, M. K. Fritz, S. A. Peak and H. E. von Holst, *Int. J. Environ. Res. Public Health*, 2021, **18**, 28.
102. Stockholm convention, <http://www.pops.int/>, (accessed 26/01/2022).
103. S. Brendel, E. Fetter, C. Staude, L. Vierke and A. Biegel-Engler, *Environ Sci Eur*, 2018, **30**.
104. Summary of the Toxic Substances Control Act, <https://www.epa.gov/laws-regulations/summary-toxic-substances-control-act#:~:text=The%20Toxic%20Substances%20Control%20Act%20of%201976%20provides%20EPA%20with,%2C%20drugs%2C%20cosmetics%20and%20pesticides.>, (accessed 15/12/2022, 2022).
105. .
106. X. LIM, Maine's ban on 'forever chemicals' marks a big win for some scientists, <https://www.science.org/content/article/maine-s-ban-forever-chemicals-marks-big-win-some-scientists>, DOI: 10.1126/science.abm1382).
107. A. Blum, S. A. Balan, M. Scheringer, X. Trier, G. Goldenman, I. T. Cousins, M. Diamond, T. Fletcher, C. Higgins, A. E. Lindeman, G. Peaslee, P. de Voogt, Z. Y. Wang and R. Weber, *Environ Health Persp*, 2015, **123**, A107-A111.
108. M. Ateia, A. Maroli, N. Tharayil and T. Karanfil, *Chemosphere*, 2019, **220**, 866-882.
109. J. L. Wilkinson, P. S. Hooda, J. Swinden, J. Barker and S. Barton, *Sci Total Environ*, 2017, **593**, 487-497.
110. Z. Y. Wang, I. T. Cousins, M. Scheringer and K. Hungerbuhler, *Environ Int*, 2013, **60**, 242-248.
111. Z. Y. Wang, J. C. DeWitt, C. P. Higgins and I. T. Cousins, *Environ Sci Technol*, 2017, **51**, 2508-2518.
112. Z. Y. Wang, I. T. Cousins, M. Scheringer and K. Hungerbuehler, *Environ Int*, 2015, **75**, 172-179.
113. Announcement of Final Regulatory Determinations for Contaminants on the Fourth Drinking Water Contaminant Candidate List, <https://www.federalregister.gov/documents/2021/03/03/2021-04184/announcement-of-final-regulatory-determinations-for-contaminants-on-the-fourth-drinking-water>, (accessed 27/01/2022).
114. Fifth Unregulated Contaminant Monitoring Rule, <https://www.epa.gov/dwucmr/fifth-unregulated-contaminant-monitoring-rule>).
115. Clean Water Act Effluent Limitations Guidelines and Standards for the Organic Chemicals, Plastics and Synthetic Fibers Point Source Category, <https://www.federalregister.gov/documents/2021/03/17/2021-05402/clean-water-act-effluent-limitations-guidelines-and-standards-for-the-organic-chemicals-plastics-and>, (accessed 27/01/2022).
116. PFAS Strategic Roadmap: EPA's Commitments to Action 2021-2024, <https://www.epa.gov/pfas/pfas-strategic-roadmap-epas-commitments-action-2021-2024>, (accessed 27/01/2022).

117. Action on 'GenX': Another 'forever chemical' added to the EU list of substances of very high concern, <https://chemtrust.org/genx/>).
118. O. Zenasni, M. D. Marquez, A. C. Jamison, H. J. Lee, A. Czader and T. R. Lee, *Chem Mater*, 2015, **27**, 7433-7446.
119. V. Dichiarante, M. I. M. Espinoza, L. Gazzera, M. Vuckovac, M. Latikka, G. Cavallo, G. Raffaini, R. Oropesa-Nunez, C. Canale, S. Dante, S. Marras, R. Carzino, M. Prato, R. H. A. Ras and P. Metrangolo, *Acs Sustain Chem Eng*, 2018, **6**, 9734-9743.
120. P. Verdia, H. Q. N. Gunaratne, T. Y. Goh, J. Jacquemin and M. Blesic, *Green Chem*, 2016, **18**, 1234-1239.
121. M. P. Krafft and J. G. Riess, *Chemosphere*, 2015, **129**, 4-19.
122. H. Lei, M. N. Xiong, J. Xiao, L. P. Zheng, Y. R. Zhu, X. X. Li, Q. X. Zhuang and Z. W. Han, *Prog Org Coat*, 2017, **103**, 182-192.
123. C. A. Moody and J. A. Field, *Environ Sci Technol*, 2000, **34**, 3864-3870.
124. R. E. Thames, *Journal*, 1999.
125. P. Wang, *Fire Technology*, 2015, **51**, 503-511.
126. F. Dubocq, T. Wang, L. W. Y. Yeung, V. Sjöberg and A. Kärman, *Environ Sci Technol*, 2020, **54**, 245-254.
127. X. Yu, N. Jiang, X. Miao, F. Li, J. Wang, R. Zong and S. Lu, *Process Safety and Environmental Protection*, 2020, **133**, 201-215.
128. V. Dichiarante, R. Milani and P. Metrangolo, *Green Chem*, 2018, **20**, 13-27.
129. S. De, S. Malik, A. Ghosh, R. Saha and B. Saha, *Rsc Adv*, 2015, **5**, 65757-65767.
130. D. J. McClements and C. E. Gumus, *Advances in Colloid and interface Science*, 2016, **234**, 3-26.
131. S. Sirsi and M. Borden, *Bubble Science, Engineering & Technology*, 2009, **1**, 3-17.
132. C. M. Hansen, *Danish Technical: Copenhagen*, 1967, **14**.
133. R. A. Milescu, C. R. McElroy, T. J. Farmer, P. M. Williams, M. J. Walters and J. H. Clark, *Advances in Polymer Technology*, 2019, **2019**.
134. A. Jarray, V. Gerbaud and M. Hemati, *Prog Org Coat*, 2016, **101**, 195-206.
135. K. Adamska, A. Voelkel and M. Sandomierski, *Journal of Chromatography A*, 2020, **1610**, 460544.
136. Y. Kato, T. Osawa, M. Yoshihara, H. Fujii, S. Tsutsumi and H. Yamamoto, *ACS omega*, 2020, **5**, 5684-5690.
137. D. P. Faasen, A. Jarray, H. J. Zandvliet, E. S. Kooij and W. Kwiecinski, *J Colloid Interf Sci*, 2020, **575**, 326-336.
138. M. P. Krafft and J. G. Riess, *Curr Opin Colloid In*, 2015, **20**, 192-212.
139. L. T. Mika, E. Cséfalvay and Á. Németh, *Chemical Reviews*, 2018, **118**, 505-613.
140. Z. Zhang, J. Song and B. Han, *Chemical Reviews*, 2017, **117**, 6834-6880.
141. B. M. Upton and A. M. Kasko, *Chemical Reviews*, 2016, **116**, 2275-2306.
142. M. Besson, P. Gallezot and C. Pinel, *Chemical Reviews*, 2014, **114**, 1827-1870.
143. R. J. Van Putten, J. C. Van Der Waal, E. De Jong, C. B. Rasrendra, H. J. Heeres and J. G. De Vries, *Chemical Reviews*, 2013, **113**, 1499-1597.
144. P. Gallezot, *Chemical Society Reviews*, 2012, **41**, 1538-1558.
145. M. Mascal and S. Dutta, *Fuel Processing Technology*, 2020, **197**.
146. R. C. Neves, B. C. Klein, R. J. da Silva, M. C. A. F. Rezende, A. Funke, E. Olivarez-Gómez, A. Bonomi and R. Maciel-Filho, *Renewable and Sustainable Energy Reviews*, 2020, **119**.
147. H. Wang, B. Yang, Q. Zhang and W. Zhu, *Renewable and Sustainable Energy Reviews*, 2020, **120**, 109612.
148. Y. Nakagawa, M. Tamura and K. Tomishige, *Fuel Processing Technology*, 2019, **193**, 404-422.
149. N. Goyal and F. Jerold, *Environmental Science and Pollution Research*, 2021, 1-22.
150. J. B. Sluiter, R. O. Ruiz, C. J. Scarlata, A. D. Sluiter and D. W. Templeton, *Journal of agricultural and food chemistry*, 2010, **58**, 9043-9053.

151. W.-C. Wang and L. Tao, *Renewable and Sustainable Energy Reviews*, 2016, **53**, 801-822.
152. Y. Lie, P. Ortiz, R. Vendamme, K. Vanbroekhoven and T. J. Farmer, *Industrial & Engineering Chemistry Research*, 2019, **58**, 15945-15957.
153. J. Xu, N. Li, G. Li, F. Han, A. Wang, Y. Cong, X. Wang and T. Zhang, *Green Chem*, 2018, **20**, 3753-3760.
154. F. Chen, N. Li, S. Li, G. Li, A. Wang, Y. Cong, X. Wang and T. Zhang, *Green Chem*, 2016, **18**, 5751-5755.
155. X. Sheng, N. Li, G. Li, W. Wang, J. Yang, Y. Cong, A. Wang, X. Wang and T. Zhang, *Scientific Reports*, 2015, **5**, 9565.
156. Y. Jing, Q. Xia, J. Xie, X. Liu, Y. Guo, J.-j. Zou and Y. Wang, *ACS Catalysis*, 2018, **8**, 3280-3285.
157. F. Chen, N. Li, X. Yang, L. Li, G. Li, S. Li, W. Wang, Y. Hu, A. Wang, Y. Cong, X. Wang and T. Zhang, *Acs Sustain Chem Eng*, 2016, **4**, 6160-6166.
158. G. W. Huber, S. Iborra and A. Corma, *Chemical Reviews*, 2006, **106**, 4044-4098.
159. J. N. Chheda, G. W. Huber and J. A. Dumesic, *Angewandte Chemie - International Edition*, 2007, **46**, 7164-7183.
160. A. Corma Canos, S. Iborra and A. Velty, *Chemical Reviews*, 2007, **107**, 2411-2502.
161. V. W. Faria, G. C. Almeida and C. J. A. Mota, *Química Nova*, 2018, **41**, 601-606.
162. V. W. Faria, G. C. Almeida and C. J. A. Mota, *Química Nova*, 2018, **41**, 601-606.
163. M. Gu, Q. Xia, X. Liu, Y. Guo and Y. Wang, *Chemsuschem*, 2017, **10**, 4102-4108.
164. L. Ao, W. Zhao, Y.-s. Guan, D.-k. Wang, K.-s. Liu, T.-t. Guo, X. Fan and X.-y. Wei, *Rsc Adv*, 2019, **9**, 3661-3668.
165. Y. Liu, Y. Wang, Y. Cao, X. Chen, Q. Yu, Z. Wang and Z. Yuan, *Acs Sustain Chem Eng*, 2020, DOI: 10.1021/acssuschemeng.9b07300.
166. W. Wang, X. Ji, H. Ge, Z. Li, G. Tian, X. Shao and Q. Zhang, *Rsc Adv*, 2017, **7**, 16901-16907.
167. W. Wang, S. Sun, F. Han, G. Li, X. Shao and N. Li, *Catalysts*, 2019, **9**.
168. R. Wang, G. Li, H. Tang, A. Wang, G. Xu, Y. Cong, X. Wang, T. Zhang and N. Li, *Acs Sustain Chem Eng*, 2019, **7**, 17354-17361.
169. Y. Liu, G. Li, Y. Hu, A. Wang, F. Lu, J. J. Zou, Y. Cong, N. Li and T. Zhang, *Joule*, 2019, **3**, 1028-1036.
170. E. R. Sacia, M. Balakrishnan, M. H. Deaner, K. A. Goulas, F. D. Toste and A. T. Bell, *Chemsuschem*, 2015, **8**, 1726-1736.
171. J. Xie, X. Zhang, Y. Liu, Z. Li, X.-t.-f. E, J. Xie, Y.-C. Zhang, L. Pan and J.-J. Zou, *Catal Today*, 2019, **319**, 139-144.
172. G. Li, B. Hou, A. Wang, X. Xin, Y. Cong, X. Wang, N. Li and T. Zhang, *Angewandte Chemie International Edition*, 2019, **58**, 12154-12158.
173. L. Pan, J. Xie, G. Nie, Z. Li, X. Zhang and J.-J. Zou, *AIChE Journal*, 2020, **66**, e16789.
174. S. Li, L. Yan, Q. Liu, J. Liu, Q. Liu, W. Fan, X. Zhao, X. Zhang, C. Wang, L. Ma and Q. Zhang, *Green Chem*, 2020, DOI: 10.1039/D0GC00428F.
175. A. Garcia-Ortiz, K. S. Arias, M. J. Climent, A. Corma and S. Iborra, *Chemsuschem*, 2018, **11**, 2870-2880.
176. S. S. Adkins, X. Chen, Q. P. Nguyen, A. W. Sanders and K. P. Johnston, *J Colloid Interface Sci*, 2010, **346**, 455-463.
177. L. Dalla Vecchia, R. O. M. A. de Souza and L. S. de Mariz e Miranda, *Tetrahedron*, 2018, **74**, 4359-4371.
178. S. M. S. Hussain, A. A. Adewunmi, A. Mahboob, M. Murtaza, X. Zhou and M. S. Kamal, *Advances in Colloid and Interface Science*, 2022, 102634.
179. V. Ashokkumar, R. Venkatkarthick, S. Jayashree, S. Chuetor, S. Dharmaraj, G. Kumar, W.-H. Chen and C. Ngamcharussrivichai, *Bioresource Technology*, 2022, **344**, 126195.
180. S. K. Bhatia, S. S. Jagtap, A. A. Bedekar, R. K. Bhatia, A. K. Patel, D. Pant, J. Rajesh Banu, C. V. Rao, Y.-G. Kim and Y.-H. Yang, *Bioresource Technology*, 2020, **300**, 122724.

181. T. J. Farmer, J. W. Comerford, A. Pellis and T. Robert, *Polymer International*, 2018, **67**, 775-789.
182. T. J. Farmer, D. J. Macquarrie, J. W. Comerford, A. Pellis and J. H. Clark, *Journal of Polymer Science Part A: Polymer Chemistry*, 2018, **56**, 1935-1945.
183. A. Pellis, P. A. Hanson, J. W. Comerford, J. H. Clark and T. J. Farmer, *Polymer Chemistry*, 2019, **10**, 843-851.
184. O. B. Moore, P.-A. Hanson, J. W. Comerford, A. Pellis and T. J. Farmer, *Frontiers in Chemistry*, 2019, **7**.
185. R. Manurung, M. Taufik and H. Inarto, *IOP Conference Series: Materials Science and Engineering*, 2021, **1122**, 012071.
186. E. L. Smith, A. P. Abbott and K. S. Ryder, *Chemical reviews*, 2014, **114**, 11060-11082.
187. L. Chen, Y. Xiong, H. Qin and Z. Qi, *Chemsuschem*, 2022, **n/a**, e202102635.
188. B. Chen, Z. Peng, C. Li, Y. Feng, Y. Sun, X. Tang, X. Zeng and L. Lin, *Chemsuschem*, 2021, **14**, 1496-1506.
189. A. T. Hoang, S. Nižetić and A. I. Ölçer, *Fuel*, 2021, **285**, 119140.
190. Y. Román-Leshkov, C. J. Barrett, Z. Y. Liu and J. A. Dumesic, *Nature*, 2007, **447**, 982-985.
191. S. Zhang, Y. Liu, S. Yang and H. Li, *Energy Technology*, 2021, **9**, 2100653.
192. Y. L. Louie, J. Tang, A. M. L. Hell and A. T. Bell, 2017, **202**.
193. J. I. Di Cosimo, V. K. Diez, M. Xu, E. Iglesia and C. R. Apesteguia, *J Catal*, 1998, **178**, 499-510.
194. D. Tichit, D. Lutic, B. Coq, R. Durand and W. Teissier, *J Catal*, 2003, **219**, 167-175.
195. W. P. Xie, H. Chen, L., 2006.
196. K. K. Ramasamy, M. Gray, H. Job, D. Santosa, X. S. Li, A. Devaraj, A. Karkamkar and Y. Wang, *Top Catal*, 2016, **59**, 46-54.
197. S. Abello, F. Medina, D. Tichit, J. Perez-Ramirez, J. C. Groen, J. E. Sueiras, P. Salagre and Y. Cesteros, *Chem-Eur J*, 2005, **11**, 728-739.
198. J. Y. Shen, M. Tu and C. Hu, *J Solid State Chem*, 1998, **137**, 295-301.
199. M. J. Climent, A. Corma, S. Iborra and A. Velty, *Catal Lett*, 2002, **79**, 157-163.
200. M. J. Climent, A. Corma, S. Iborra and A. Velty, *Green Chem*, 2002, **4**, 474-480.
201. J. C. A. A. Roelofs, D. J. Lensveld, A. J. van Dillen and K. P. de Jong, *J Catal*, 2001, **203**, 184-191.
202. F. Byrne, B. Forier, G. Bossaert, C. Hoebbers, T. J. Farmer, J. H. Clark and A. J. Hunt, *Green Chem*, 2017, **19**, 3671-3678.
203. F. P. Byrne, W. M. Hodds, S. Shimizu, T. J. Farmer and A. J. Hunt, *J Clean Prod*, 2019, **240**, 118175.
204. A. Pellis, F. P. Byrne, J. Sherwood, M. Vastano, J. W. Comerford and T. J. Farmer, *Green Chem*, 2019, **21**, 1686-1694.
205. M. M. Heravi and P. Hajiabbasi, *Molecular Diversity*, 2014, **18**, 411-439.
206. L. Yang, L.-W. Xu, W. Zhou, L. Li and C.-G. Xia, *Tetrahedron Letters*, 2006, **47**, 7723-7726.
207. K. J. Borah, M. Phukan and R. Borah, *Synthetic Communications*, 2010, **40**, 2830-2836.
208. S. W. Pelletier, A. P. Venkov, J. Finer-Moore and N. V. Mody, *Tetrahedron Letters*, 1980, **21**, 809-812.
209. M. S. Yusubov and V. V. Zhdankin, *Resource-Efficient Technologies*, 2015, **1**, 49-67.
210. S. Y. Wang, S. J. Ji and T. P. Loh, *Synlett*, 2003, 2377-2379.
211. D. von der Heiden, S. Bozkus, M. Klusmann and M. Breugst, *The Journal of Organic Chemistry*, 2017, **82**, 4037-4043.
212. M. Breugst and D. von der Heiden, *Chem-Eur J*, 2018, **24**, 9187-9199.
213. B. K. Banik, M. Fernandez and C. Alvarez, *Tetrahedron Letters*, 2005, **46**, 2479-2482.
214. M. L. Crawley, E. McLaughlin, W. Zhu and A. P. Combs, *Organic Letters*, 2005, **7**, 5067-5069.
215. N. Duhamel, F. Piano, S. J. Davidson, R. Larcher, B. Fedrizzi and D. Barker, *Tetrahedron Letters*, 2015, **56**, 1728-1731.

216. M. Moccia, F. Fini, M. Scagnetti and M. F. A. Adamo, *Angew Chem Int Edit*, 2011, **50**, 6893-6895.
217. W. M. Kerp, F, *European Journal of Organic Chemistry*, 1897, 193-235.
218. A. Gassama, C. Ernenwein, A. Youssef, M. Agach, E. Riguet, S. Marinkovic, B. Estrine and N. Hoffmann, *Green Chem*, 2013, **15**, 1558-1566.
219. J. E. Camp, *Chemsuschem*, 2018, **11**, 3048-3055.
220. M. De Bruyn, V. L. Budarin, A. Misefari, S. Shimizu, H. Fish, M. Cockett, A. J. Hunt, H. Hofstetter, B. M. Weckhuysen, J. H. Clark and D. J. Macquarrie, *Acs Sustain Chem Eng*, 2019, **7**, 7878-7883.
221. R. M. Kellogg, J. W. Nieuwenhuijzen, K. Pouwer, T. R. Vries, Q. B. Broxterman, R. F. P. Grimbergen, B. Kaptein, R. M. La Crois, E. de Wever, K. Zwaagstra and A. C. van der Laan, *Synthesis-Stuttgart*, 2003, 1626-1638.
222. M. L. Crawley, E. McLaughlin, W. Y. Zhu and A. P. Combs, *Organic Letters*, 2005, **7**, 5067-5069.
223. F. Fini, M. Nagabelli and M. F. A. Adamo, *Adv Synth Catal*, 2010, **352**, 3163-3168.
224. First Major Milestone in Renewable Manufacturing, <https://www.croda.com/en-gb/news/first-major-milestone-in-renewable-manufacturing>, (accessed 17/12/2022, 2022).
225. M. McCoy, Croda To Produce Bio-Ethylene Oxide, <https://cen.acs.org/articles/93/i18/Croda-Produce-Bio-Ethylene-Oxide.html>, (accessed 17/12/2022, 2022).
226. Croda's renewable ethoxylates add another string to ethanol's bow, <https://www.nnfcc.co.uk/news-croda-ethanol>, (accessed 17/12/2022, 2022).
227. G. Coulthard, W. P. Unsworth and R. J. Taylor, *Tetrahedron Letters*, 2015, **56**, 3113-3116.
228. A. C. French, A. L. Thompson and B. G. Davis, *Angewandte Chemie International Edition*, 2009, **48**, 1248-1252.
229. P. Polavarapu and M. P. Krafft, *Journal of Fluorine Chemistry*, 2015, **171**, 12-17.
230. J.-B. Béquignat, N. Ty, A. Rondon, L. Taiariol, F. Degoul, D. Canitrot, M. Quintana, I. Navarro-Teulon, E. Miot-Noirault, C. Boucheix, J.-M. Chezal and E. Moreau, *European Journal of Medicinal Chemistry*, 2020, **203**, 112574.
231. A. Khanal and S. Fang, *Chemistry – A European Journal*, 2017, **23**, 15133-15142.
232. M. Felber, M. Bauwens, J. M. Mateos, S. Imstepf, F. M. Mottaghy and R. Alberto, *Chemistry – A European Journal*, 2015, **21**, 6090-6099.
233. H. Xu, H. Sabit, G. L. Amidon and H. D. H. Showalter, *Beilstein Journal of Organic Chemistry*, 2013, **9**, 89-96.
234. J. F. W. Keana, J. Cuomo, L. Lex and S. E. Seyedrezai, *The Journal of Organic Chemistry*, 1983, **48**, 2647-2654.
235. T. Huhtamaki, X. L. Tian, J. T. Korhonen and R. H. A. Ras, *Nat Protoc*, 2018, **13**, 1521-1538.
236. K. Seo, M. Kim, J. K. Ahn and D. H. Kim, *Korean J Chem Eng*, 2015, **32**, 2394-2399.
237. W. A. Zisman, *American Chemical Society*, 1964, 1-51.
238. F. L. Heale, K. Page, J. S. Wixey, P. Taylor, I. P. Parkin and C. J. Carmalt, *Rsc Adv*, 2018, **8**, 27064-27072.
239. D. Shaw, A. West, J. Bredin and E. Wagenaars, *Plasma Sources Science and Technology*, 2016, **25**, 065018.
240. C. D. Volpe and S. Siboni, *Surface Innovations*, 2018, **6**, 120-132.
241. R. Macy, *Journal of Chemical Education*, 1935, **12**, 573.
242. J. D. Berry, M. J. Neeson, R. R. Dagastine, D. Y. Chan and R. F. Tabor, *J Colloid Interf Sci*, 2015, **454**, 226-237.
243. M. Nic, L. Hovorka, J. Jirat, B. Kosata and J. Znamenacek, *International Union of Pure and Applied Chemistry, v. Version*, 2005, **2**, 1281-1282.
244. L. Wilhelmy, *Annals of Physics*, 1863, **195**, 177-217.
245. J. Kalova and R. Mareš, *International Journal of Thermophysics*, 2015, **36**.

246. B. E. Brycki, I. H. Kowalczyk, A. Szulc, O. Kaczerewska and M. Pakiet, *Application and Characterization of Surfactants*, 2017, 97-155.
247. C. Beliciu and C. Moraru, *Journal of dairy science*, 2009, **92**, 1829-1839.
248. E. S. Basheva, P. A. Kralchevsky, K. D. Danov, K. P. Ananthapadmanabhan and A. Lips, *Phys Chem Chem Phys*, 2007, **9**, 5183-5198.
249. E. W. Anacker and R. D. Geer, *J Colloid Interf Sci*, 1971, **35**, 441-&.
250. B. J. P. Berne, R, *Dynamic Light Scattering*, Dover Publications inc., New York, 1976.
251. R. D. Falcone, N. M. Correa and J. J. Silber, *Langmuir*, 2009, **25**, 10426-10429.
252. P. Guering, P. G. Nilsson and B. Lindman, *J Colloid Interf Sci*, 1985, **105**, 41-44.
253. T. Inoue, *J Colloid Interf Sci*, 2009, **337**, 240-246.
254. T. Kato, S. Anzai and T. Seimiya, *J Phys Chem-Us*, 1987, **91**, 4655-4657.
255. L. J. Magid, K. Daus and P. Butler, *Abstr Pap Am Chem S*, 1983, **185**, 94-Coll.
256. N. Nishikido, M. Shinozaki, G. Sugihara and M. Tanaka, *J Colloid Interf Sci*, 1981, **82**, 352-361.
257. M. Okawauchi, M. Shinozaki, Y. Ikawa and M. Tanaka, *J Phys Chem-Us*, 1987, **91**, 109-112.
258. F. Tokiwa and K. Aigami, *Kolloid Z Z Polym*, 1970, **239**, 687-&.
259. R. Esteves, B. Dikici Ph D, M. Lehman, Q. Mazumder and N. Onukwuba, *Beyond: Undergraduate Research Journal*, 2016, **1**, 4.
260. F. E. Benedetto, H. Zolotucho and M. O. Prado, *Mater Res-Ibero-Am J*, 2015, **18**, 9-14.
261. N. C. Christov, K. D. Danov, P. A. Kralchevsky, K. P. Ananthapadmanabhan and A. Lips, *Langmuir*, 2006, **22**, 7528-7542.
262. V. B. Fainerman, V. N. Kazakov, S. Lylyk, A. V. Makievski and R. Miller, *Colloid Surface A*, 2004, **250**, 97-102.
263. V. B. Fainerman, V. D. Mys, A. V. Makievski and R. Miller, *J Colloid Interf Sci*, 2006, **304**, 222-225.
264. D. E. Hirt, R. K. Prudhomme, B. Miller and L. Rebenfeld, *Colloid Surface*, 1990, **44**, 101-117.
265. P. Joos and E. Rillaerts, *J Colloid Interf Sci*, 1981, **79**, 96-100.
266. N. A. Mishchuk, V. B. Fainerman, V. I. Kovalchuk, R. Miller and S. S. Duhkin, *Colloid Surface A*, 2000, **175**, 207-216.
267. A. W. Adamson, Gast, Alice P., in *Physical Chemistry of Surfaces*, John Wiley and Sons Inc. , 6 edn., 1997, ch. 2.
268. J. Davies, 1957.

4.1 APPENDIX

4.1.1.1 Compound 149

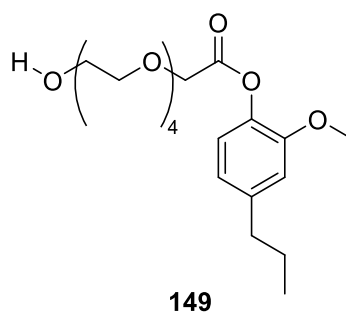


Figure 88: The structure of compound **149**

Table 21: Concentration and derived count rate for CMC determination of compound **149**

Surfactant concentration / % wt/wt	Derived count rate / kcps
0.075	1446.6
0.05	582.9
0.025	233.3
0.01	143.2
0.0075	109.4
0.0025	95.3
0.001	87.2
0.0001	102.2
0.005	108.4
0.0001	105.3
0.075	1446.6
0.05	582.9
0.025	233.3

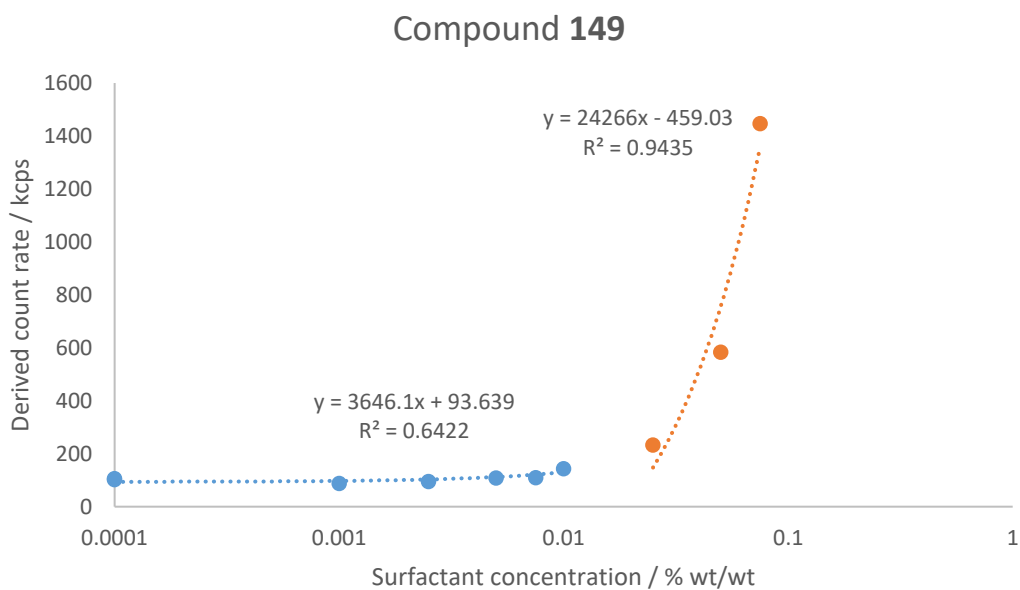


Figure 89: Derived count rate (kcps) vs Surfactant concentration (% wt/wt) for compound **149**

Interception point (0.0268,191.36)

Compound **149** CMC= 0.0268% wt/wt

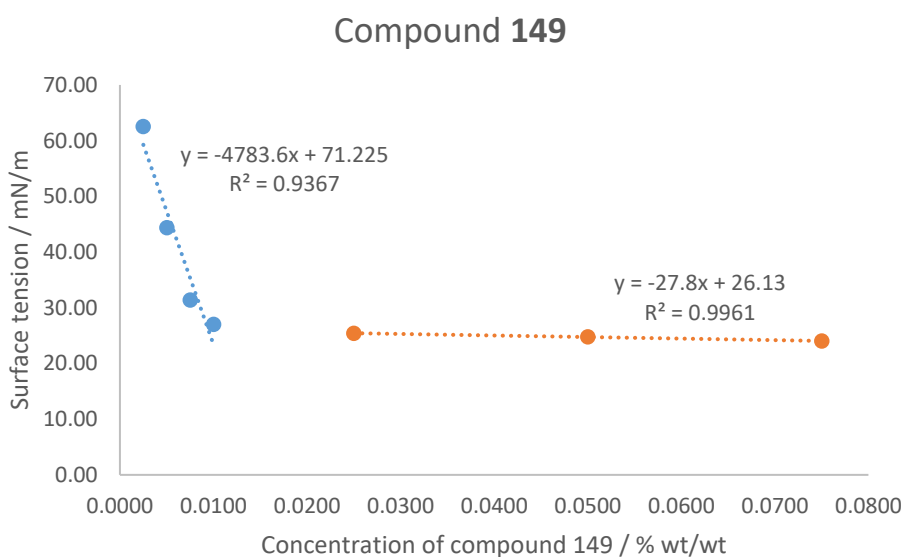


Figure 90: Surface tension vs Concentration of compound **149** in deionised water

Interception point (0.0095, 25.8660)

Compound **149** CMC = 0.0095% wt/wt

Table 22: Results table for the surface tension vs surfactant concentration analysis of compound **149**

Concentration	Surface tension mN/m	SD	Temperature / °
0.0750	24.02	0.006	20.27
0.0500	24.79	0.014	20.19
0.0250	25.41	0.004	20.23
0.0100	27.02	0.006	20.31
0.0075	31.36	0.002	20.28
0.0050	44.39	0.001	20.22
0.0025	62.54	0.041	20.26

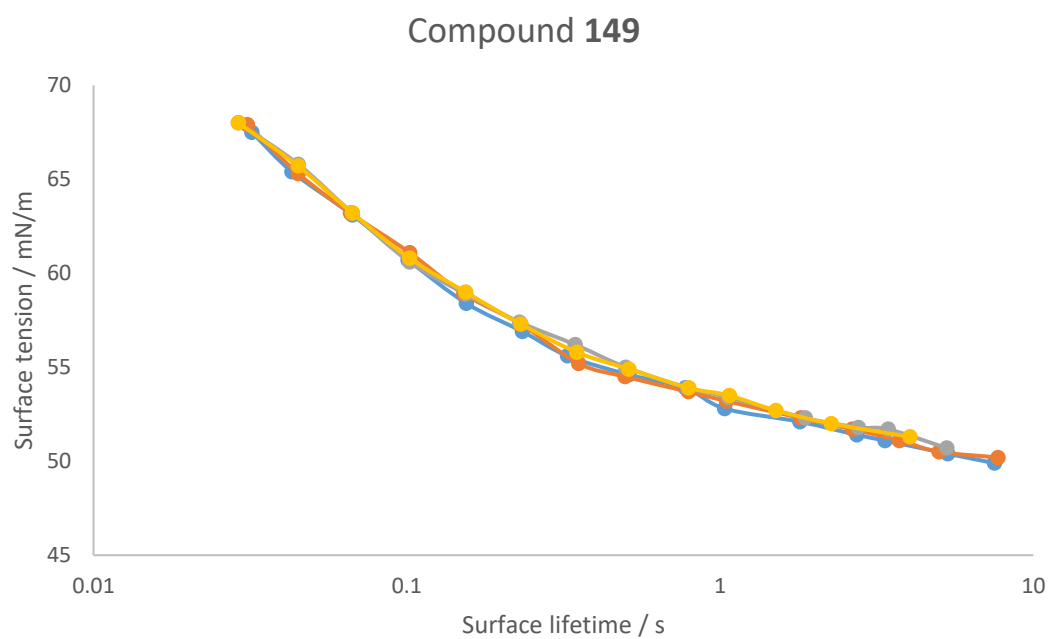
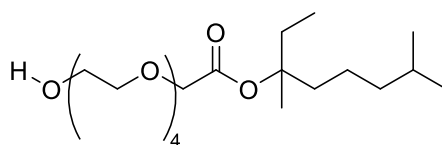


Figure 91: Surface tension vs surface lifetime for compound **149**

Table 23: Surface lifetime (SL) / s and surface tension (ST) / mN/m for compound **149**

Run 1		Run 2		Run 3		Run 4	
SL / s	ST / mN/m	SL / s	ST / mN/m	SL / s	ST / mN/m	SL / s	ST / mN/m
0.032	67.5	0.031	67.9	0.029	68.0	0.029	68.0
0.043	65.4	0.045	65.3	0.045	65.8	0.045	65.7
0.067	63.1	0.066	63.2	0.067	63.2	0.067	63.2
0.101	60.7	0.102	61.1	0.102	60.6	0.102	60.8
0.155	58.4	0.152	58.9	0.154	58.9	0.154	59.0
0.234	56.9	0.231	57.3	0.229	57.4	0.231	57.3
0.326	55.6	0.354	55.2	0.345	56.2	0.349	55.8
0.512	54.6	0.497	54.5	0.5	55.0	0.512	54.9
0.774	53.9	0.793	53.7	0.788	53.9	0.794	53.9
1.035	52.8	1.048	53.2	1.064	53.4	1.07	53.5
1.799	52.1	1.809	52.3	1.87	52.3	1.505	52.7
2.734	51.4	2.644	51.7	2.763	51.8	2.263	52.0
3.365	51.1	3.737	51.1	3.444	51.7	4.041	51.3
5.327	50.4	5.002	50.5	5.298	50.7		
7.512	49.9	7.718	50.2				

4.1.1.2 Compound 148



148

Figure 92: The structure of compound **148**

Table 24: Concentration and derived count rate for CMC determination of compound **148**

Surfactant concentration / % wt/wt	Derived count rate / kcps
0.1	70681.1
0.075	3006.5
0.05	2015.2
0.025	164
0.0075	276.6
0.005	194.3
0.0025	142.4

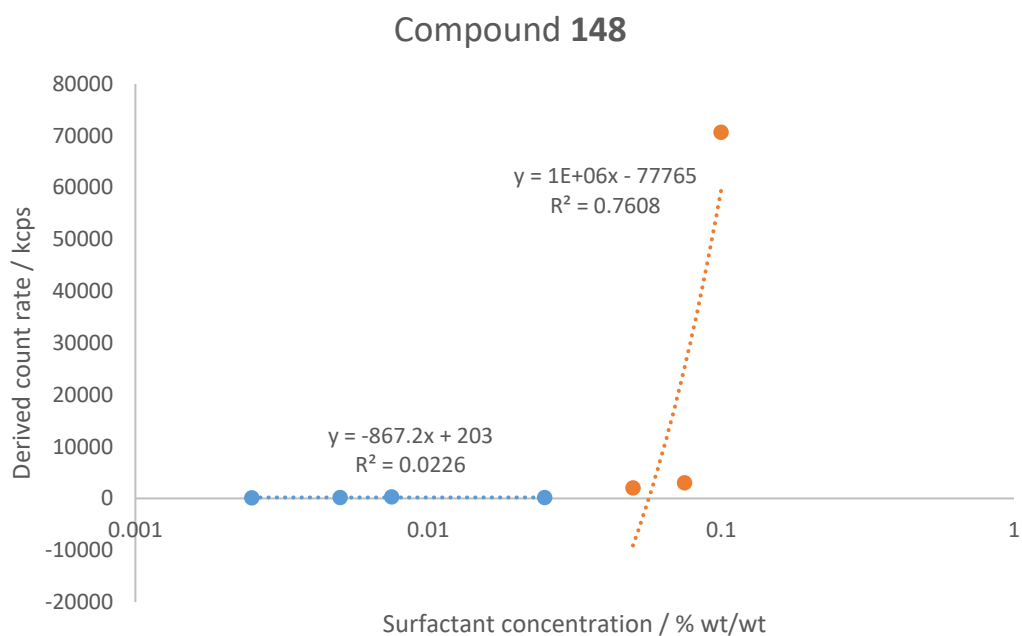


Figure 93: Derived count rate (kcps) vs Surfactant concentration (% wt/wt) for compound **148**

Interception point (0.077900,135.44)

Compound **148** CMC= 0.0779% wt/wt

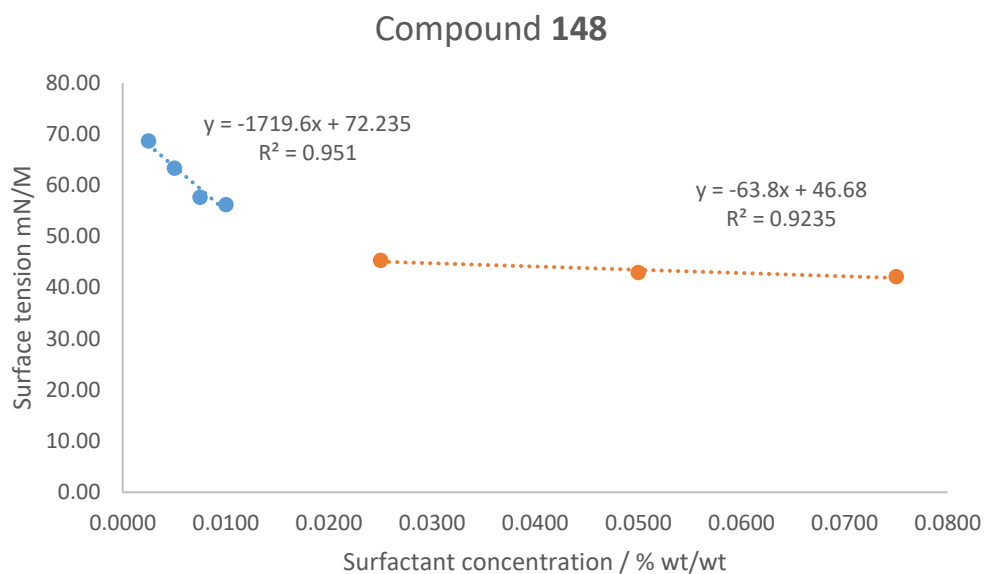


Figure 94: Surface tension vs concentration of compound **148** in deionised water

Interception point (0.0154, 45.695)

Compound **148** CMC= 0.0154% wt/wt

Table 25: Results table for the surface tension vs surfactant concentration analysis of compound **148**

Concentration	Surface tension mN/m	SD	Temperature / °
0.0025	68.66	0.058	19.70
0.0050	63.38	0.011	19.80
0.0075	57.68	0.013	19.77
0.0100	56.23	0.006	19.81
0.0250	45.35	0.083	19.76
0.0500	42.96	0.083	19.73
0.0750	42.16	0.008	19.83

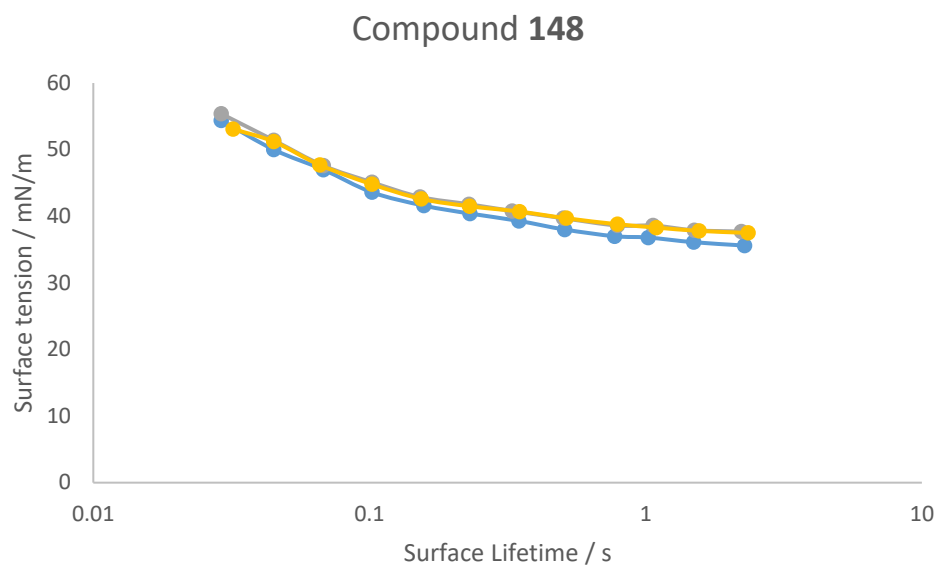
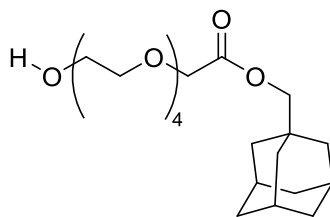


Figure 95: Surface tension vs surface lifetime for compound **148**

Table 26: Surface lifetime (SL) / s and surface tension (ST) / mN/m for compound **148**

Run 1		Run 2		Run 3		Run 4	
SL / s	ST / mN/m	SL / s	ST / mN/m	SL / s	ST / mN/m	SL / s	ST / mN/m
0.029	54.4	0.031	54.7	0.029	55.4	0.032	53.1
0.045	50.0	0.044	51.3	0.045	51.4	0.045	51.2
0.068	47.0	0.067	48.0	0.068	47.6	0.066	47.7
0.102	43.6	0.101	44.9	0.102	45.1	0.102	44.8
0.157	41.6	0.153	43.1	0.152	42.9	0.154	42.6
0.231	40.4	0.228	41.9	0.229	41.8	0.230	41.5
0.347	39.3	0.336	40.6	0.328	40.8	0.349	40.7
0.509	38.0	0.495	40.1	0.503	39.7	0.515	39.7
0.771	37.0	0.746	39.2	0.789	38.6	0.789	38.8
1.020	36.8	1.165	38.3	1.061	38.6	1.091	38.3
1.490	36.1	1.58	38.2	1.498	37.9	1.559	37.8
2.277	35.6	2.677	37.5	2.219	37.7	2.344	37.5
		3.718	37.2				
		5.455	37.0				
		7.822	36.7				
		11.882	36.1				
		22.569	35.8				
		29.863	35.3				

4.1.1.3 Compound 150



150

Figure 96: The structure of compound 150

Table 27: Concentration and derived count rate for CMC determination of compound 150

Surfactant concentration / % wt/wt	Derived count rate / kcps
0.0025	107.4
0.005	113.2
0.0075	143.4
0.025	130.7
0.05	1284.7
0.075	1970.4
0.1	61808

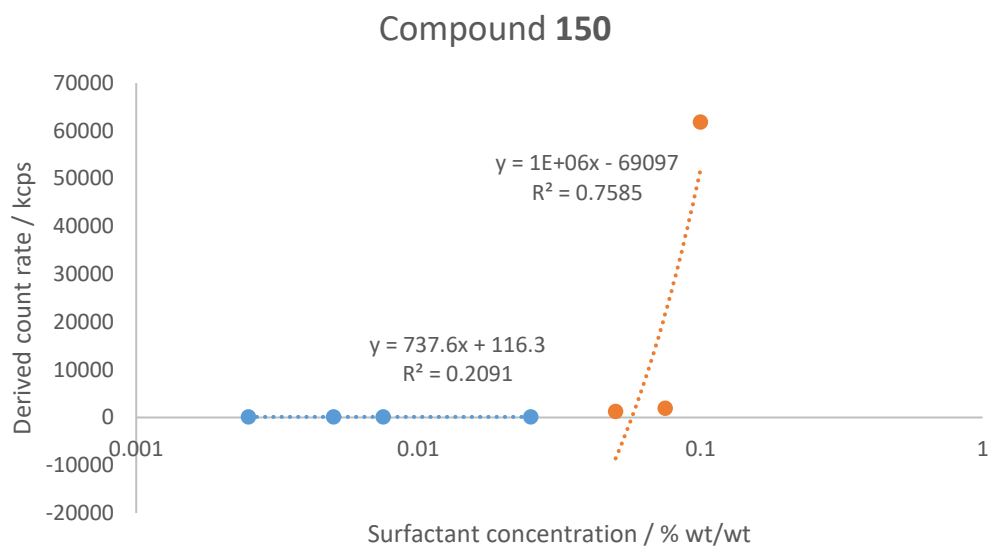


Figure 97: Derived count rate (kcps) vs Surfactant concentration (% wt/wt) for compound **150**

Interception point (0.069264, 167.39)

Compound **150** CMC= 0.0693% wt/wt

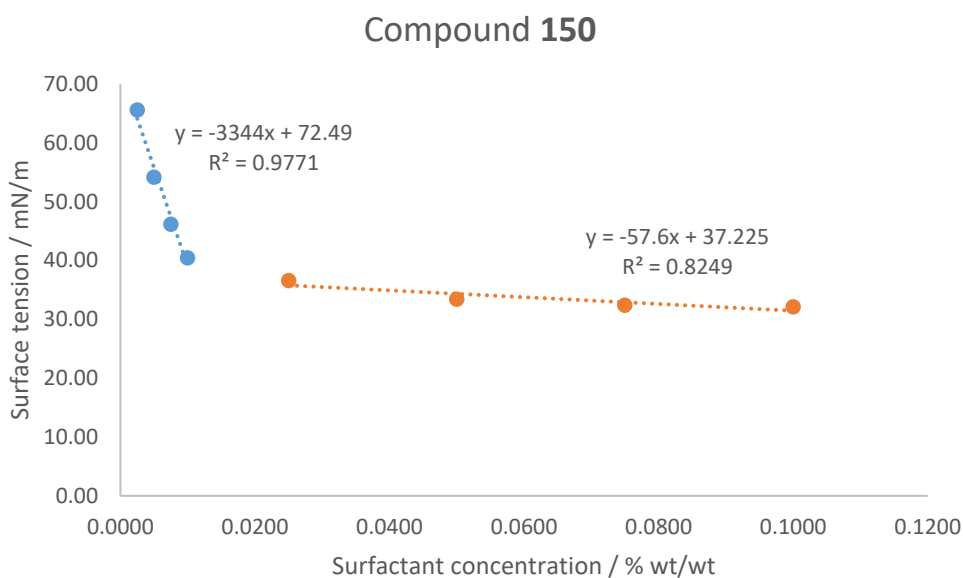


Figure 98: Surface tension vs Concentration of compound **150** in deionised water

Interception point (0.0107, 36.607)

Compound **150** CMC= 0.0107% wt/wt

Table 28: Results table for the surface tension vs surfactant concentration analysis of compound **150**

Concentration	Surface tension mN/m	SD	Temperature / °
0.0025	65.61	0.012	19.54
0.0050	54.18	0.023	19.53
0.0075	46.15	0.018	19.53
0.0100	40.42	0.001	19.66
0.0250	36.58	0.029	19.61
0.0500	33.41	0.013	19.71
0.0750	32.39	0.006	19.64
0.1000	32.12	0.084	19.78

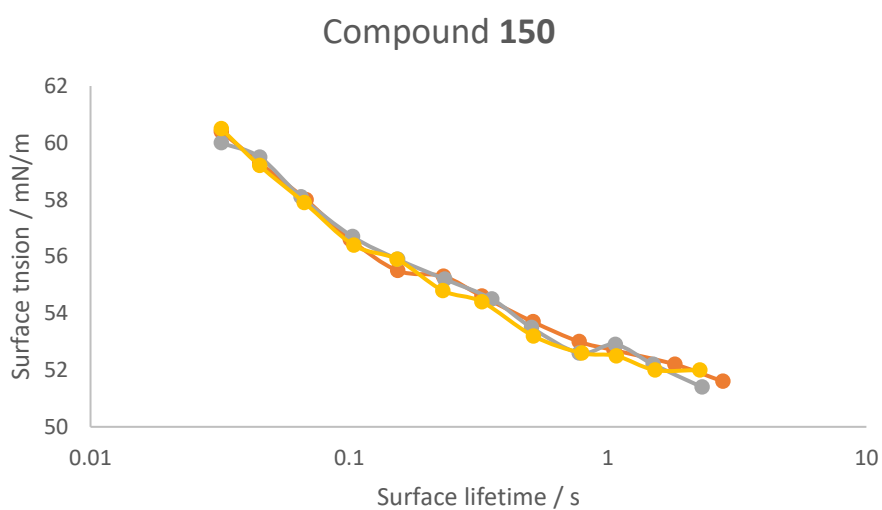


Figure 99: Surface tension vs surface lifetime for compound **150**

Table 29: Surface lifetime (SL) / s and surface tension (ST) / mN/m for compound **150**

Run 1		Run 2		Run 3	
SL / s	ST / mN/m	SL / s	ST / mN/m	SL / s	ST / mN/m
0.032	60.4	0.032	60.0	0.032	60.5
0.045	59.3	0.045	59.5	0.045	59.2
0.068	58.0	0.065	58.1	0.067	57.9
0.101	56.6	0.103	56.7	0.104	56.4
0.154	55.5	0.154	55.9	0.153	55.9
0.231	55.3	0.234	55.2	0.230	54.8
0.326	54.6	0.356	54.5	0.326	54.4
0.513	53.7	0.506	53.5	0.515	53.2
0.774	53.0	0.775	52.6	0.791	52.6
1.057	52.7	1.067	52.9	1.077	52.5
1.815	52.2	1.496	52.2	1.522	52.0
2.783	51.6	2.315	51.4	2.266	52.0

4.1.1.4 Compound 153

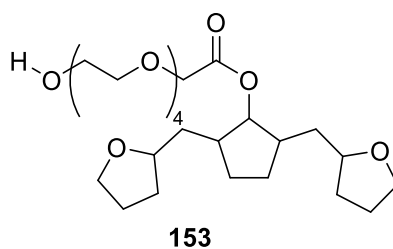


Figure 100: The structure of compound **153**

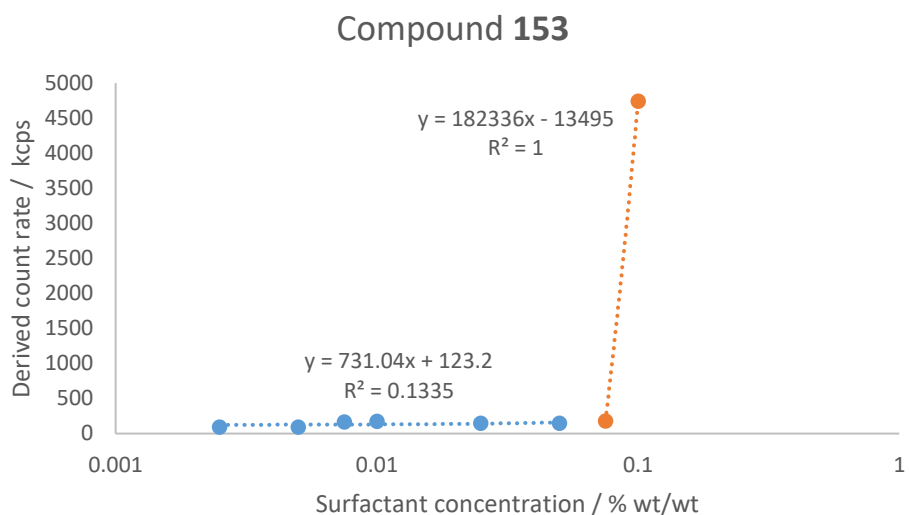


Figure 101: Derived count rate (kcps) vs Surfactant concentration (% wt/wt) for compound **153**

Table 30: Concentration and derived count rate for CMC determination of compound **153**

Surfactant concentration / % wt/wt	Derived count rate / kcps
0.0025	90.3
0.005	90.1
0.0075	163.5
0.01	172.9
0.025	146.6
0.05	148.9
0.075	180.4
0.1	4738.8

Interception point (0.074988, 178.02)

Compound **153** CMC= 0.0749% wt/wt

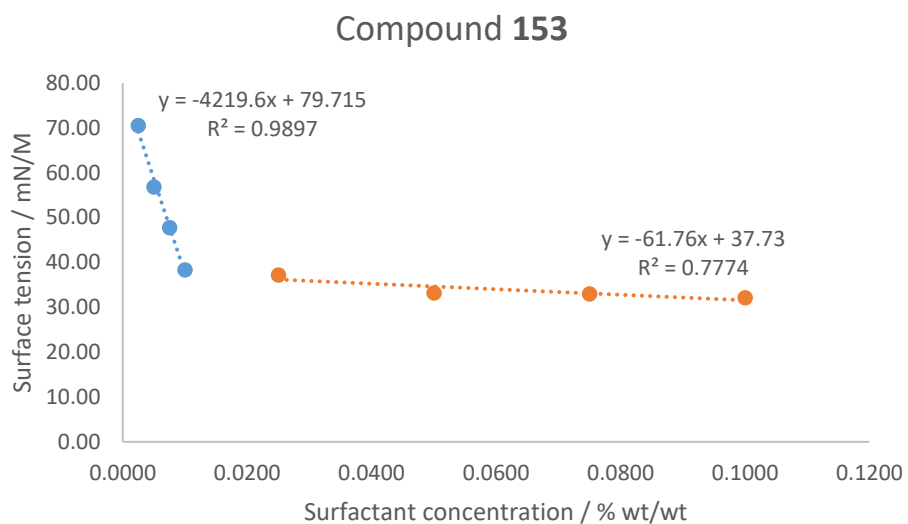


Figure 102: Surface tension vs Concentration of compound **153** in deionised water

Interception point (0.0101,)

Compound **153** CMC= 0.0101% wt/wt

Table 31: Results table for the surface tension vs surfactant concentration analysis of compound **153**

Concentration / % wt/wt	Surface tension / mN/m	SD / mN/m	Temperature / °C
0.0025	70.48	0.025	19.88
0.0050	56.80	0.012	19.60
0.0075	47.76	0.018	20.13
0.0100	38.33	0.011	20.42
0.0250	37.19	0.004	19.55
0.0500	33.21	0.008	19.47
0.0750	32.95	0.008	19.63
0.1000	32.13	0.060	19.36

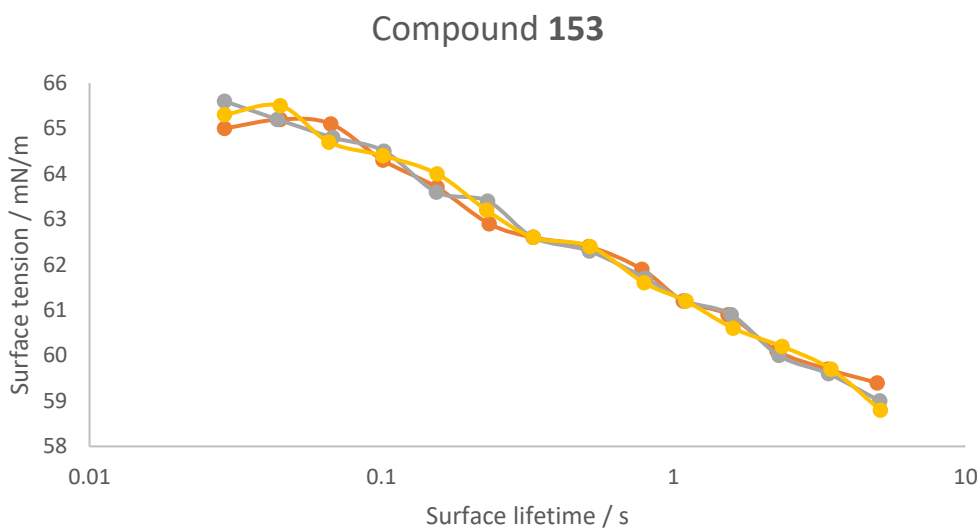


Figure 103: Surface tension vs surface lifetime for compound **153**

Table 32: Surface lifetime (SL) / s and surface tension (ST) / mN/m for compound **153**

Run 1		Run 2		Run 3	
SL / s	ST / mN/m	SL / s	ST / mN/m	SL / s	ST / mN/m
0.029	65.0	0.029	65.6	0.029	65.3
0.045	65.2	0.044	65.2	0.045	65.5
0.067	65.1	0.068	64.8	0.066	64.7
0.101	64.3	0.102	64.5	0.101	64.4
0.155	63.7	0.154	63.6	0.155	64.0
0.234	62.9	0.231	63.4	0.229	63.2
0.330	62.6	0.331	62.6	0.331	62.6
0.513	62.4	0.515	62.3	0.518	62.4
0.780	61.9	0.801	61.7	0.793	61.6
1.079	61.2	1.097	61.2	1.104	61.2
1.536	60.9	1.577	60.9	1.600	60.6
2.264	60.1	2.296	60.0	2.355	60.2
3.369	59.7	3.392	59.6	3.467	59.7
4.986	59.4	5.080	59.0	5.107	58.8

4.1.1.5 Compound 146

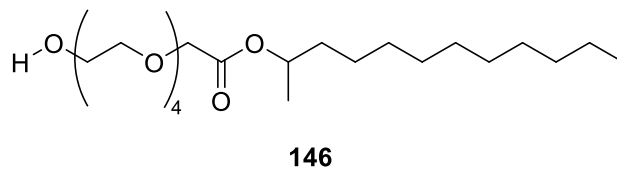


Figure 104: The structure of compound **146**

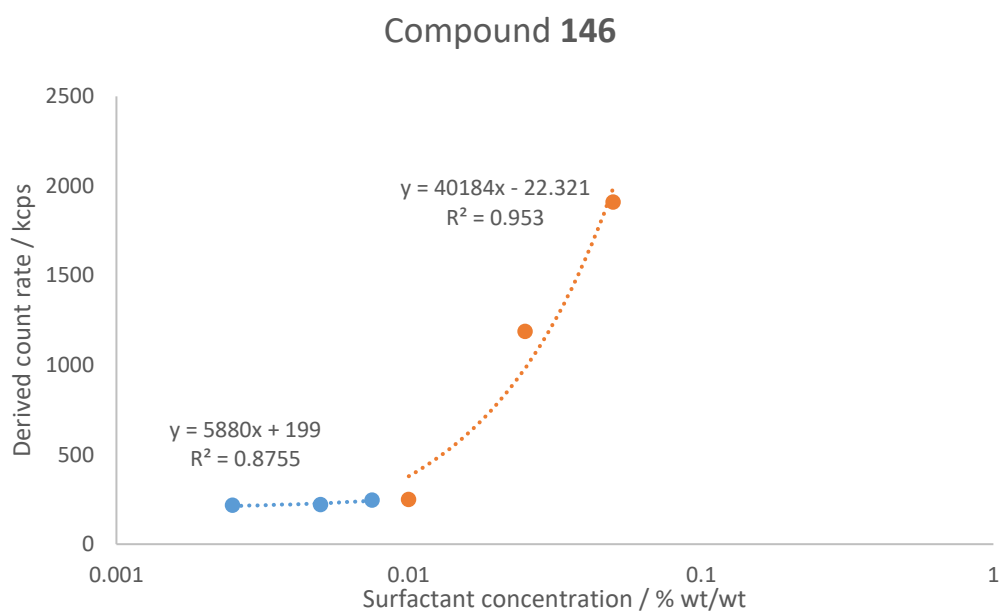


Figure 105: Derived count rate (kcps) vs Surfactant concentration (% wt/wt) for compound **146**

Table 33: Concentration and derived count rate for CMC determination of compound **146**

Surfactant concentration / % wt/wt	Derived count rate / kcps
0.0025	216.9
0.005	222
0.0075	246.3
0.01	250.7
0.025	1188.4
0.05	1909.6

Interception point (0.0064518, 236.94)

Compound **146** CMC= 0.0065% wt/wt

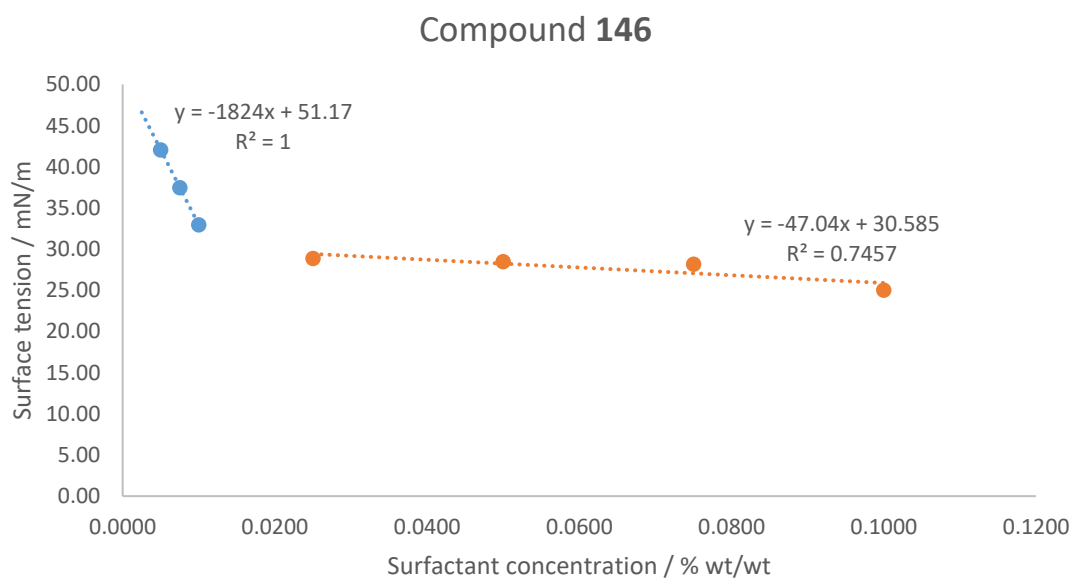


Figure 106: Surface tension vs Concentration of compound **146** in deionised water

Interception point (0.0116,30.400)

Compound **146** CMC= 0.0116% wt/wt

Table 34: Results table for the surface tension vs surfactant concentration analysis of compound **146**

Concentration	Surface tension mN/m	SD	Temperature / °
0.0050	42.06	0.016	20.50
0.0075	37.47	0.017	20.39
0.0100	32.94	0.025	20.44
0.0250	28.86	0.021	20.51
0.0500	28.49	0.076	20.58
0.0750	28.19	0.077	20.51
0.1000	25.04	0.046	20.71

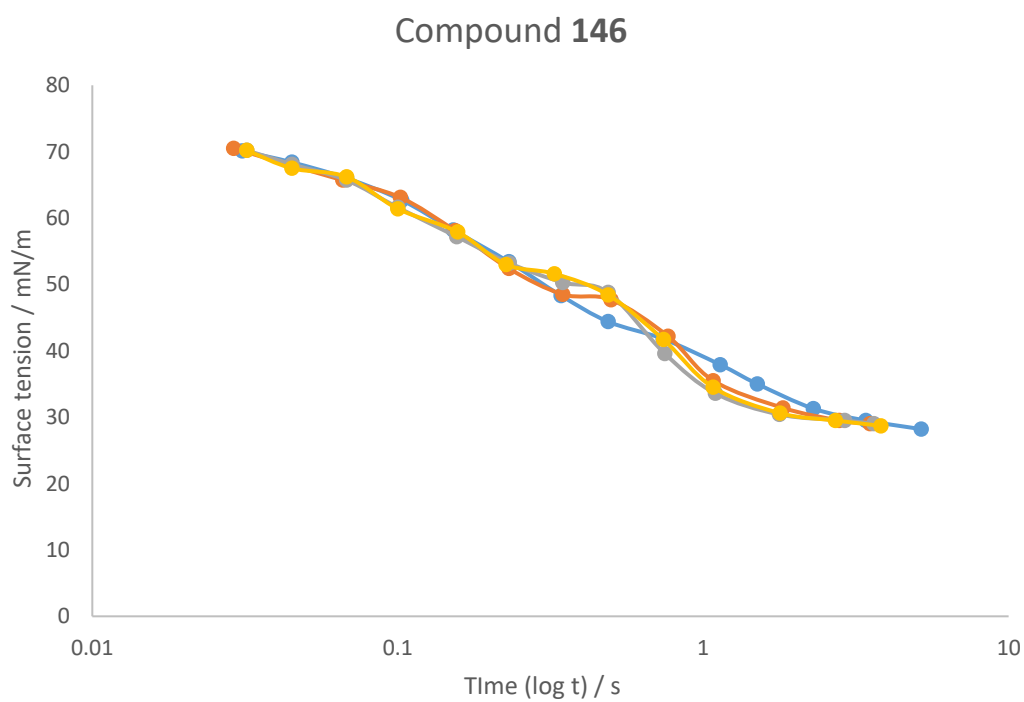


Figure 107: Surface tension vs surface age for compound **146** at 0.1% wt/wt concentration

Table 35: Surface lifetime (SL) / s and surface tension (ST) / mN/m for compound **146**

Run 1		Run 2		Run 3	
SL / s	ST / mN/m	SL / s	ST / mN/m	SL / s	ST / mN/m
0.031	70.1	0.029	70.5	0.032	70.2
0.045	68.4	0.045	67.9	0.045	68.1
0.068	66	0.066	65.7	0.068	65.7
0.103	62.7	0.102	63.1	0.100	61.6
0.152	58.2	0.154	58.1	0.156	57.2
0.231	53.4	0.231	52.4	0.232	53.2
0.343	48.3	0.347	48.5	0.347	50.3
0.488	44.4	0.499	47.7	0.488	48.8
0.739	41.8	0.767	42.2	0.748	39.6
1.138	37.9	1.079	35.5	1.095	33.6
1.505	35	1.825	31.4	1.778	30.4
2.292	31.3	2.792	29.5	2.905	29.5
3.405	29.5	3.516	29	3.622	29.0
5.171	28.2	0.029	70.5		

4.1.1.6 Compound 145

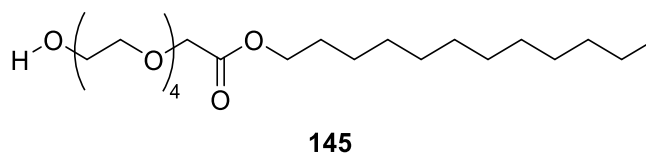


Figure 108: The structure of compound **145**

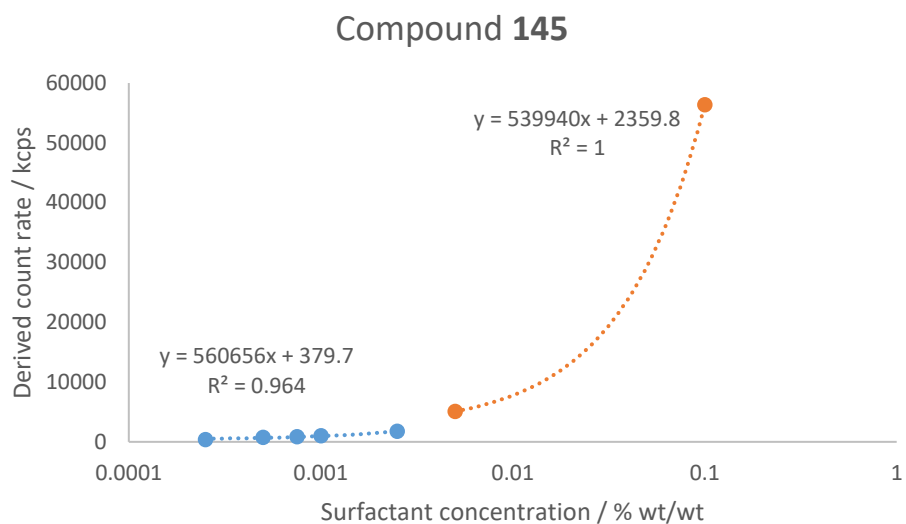


Figure 109: Derived count rate (kcps) vs Surfactant concentration (% wt/wt) for compound 145

Table 36: Concentration and derived count rate for CMC determination of compound 145

Surfactant concentration / % wt/wt	Derived count rate / kcps
0.0025	372.5
0.005	757.0
0.0075	828.5
0.01	999.1
0.025	1744.7
0.05	5059.5
0.1	56353.8

Interception point (0.049386, 3148.4)

Compound 145 CMC= 0.0494% wt/wt

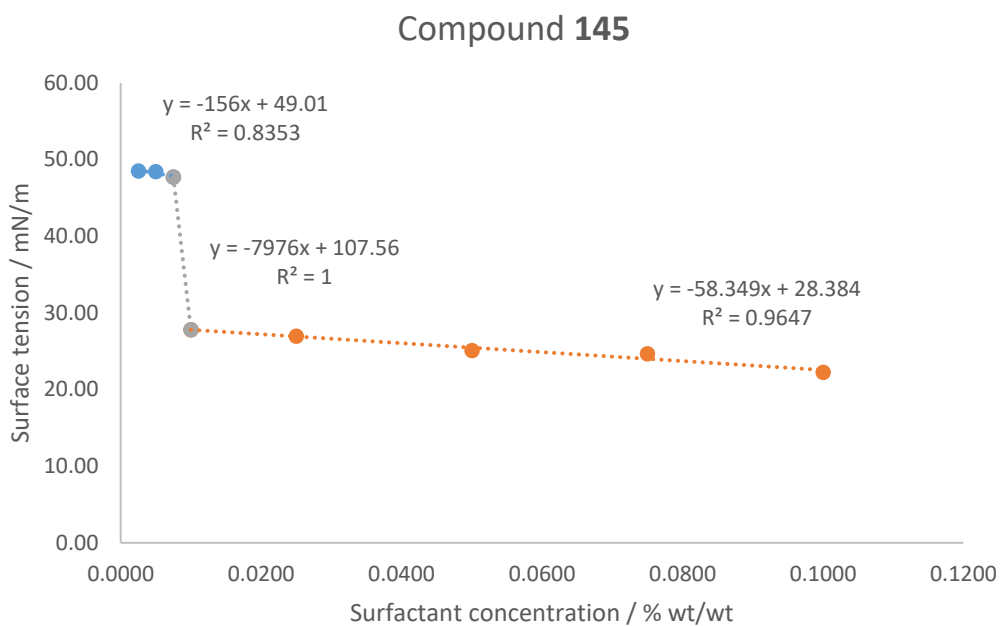


Figure 110: Surface tension vs Concentration of compound **145** in deionised water

Interception point (0.2112, 16.0590)

Compound **145** CMC= 0.2112% wt/wt

Table 37: Results table for the surface tension vs surfactant concentration analysis of compound **145**

Concentration	Surface tension mN/m	SD	Temperature / °
0.0025	48.52	0.071	19.93
0.0050	48.43	0.090	20.04
0.0075	47.74	0.092	19.94
0.0100	27.80	0.330	19.93
0.0250	26.96	0.050	20.08
0.0500	25.09	0.082	20.04
0.0750	24.66	0.021	20.00
0.1000	22.24	0.050	20.05

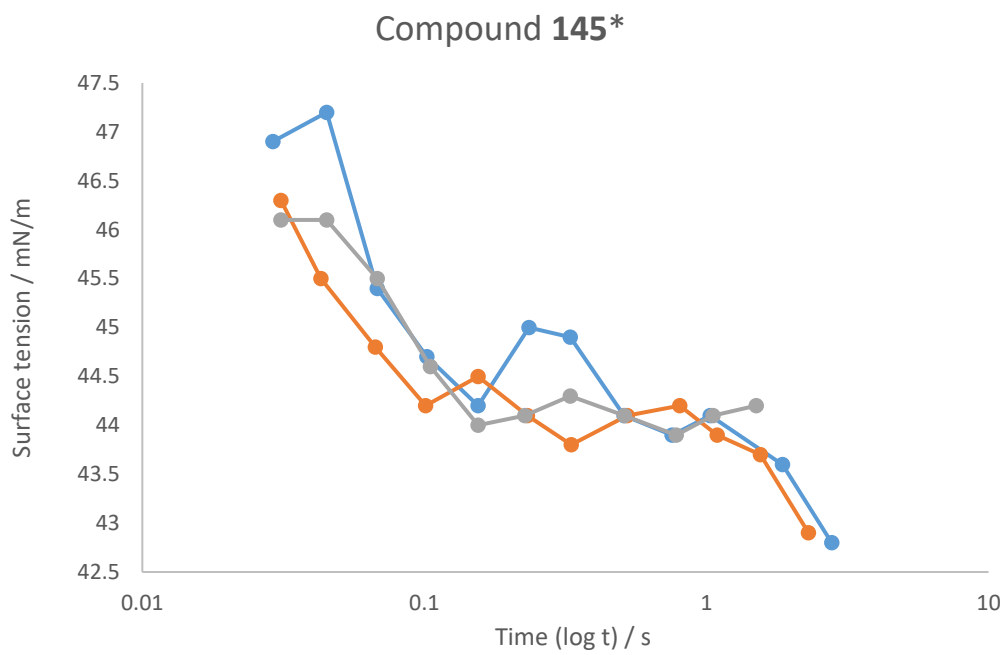


Figure 111: Surface tension vs surface age for compound **145** at 0.1% concentration in deionised water with 5% IPA

Table 38: Surface lifetime (SL) / s and surface tension (ST) / mN/m for compound **145** in deionised water with 5% IPA

Run 1		Run 2		Run 3	
SL / s	ST / mN/m	SL / s	ST / mN/m	SL / s	ST / mN/m
0.029	46.9	0.031	46.3	0.031	46.1
0.045	47.2	0.043	45.5	0.045	46.1
0.068	45.4	0.067	44.8	0.068	45.5
0.102	44.7	0.101	44.2	0.105	44.6
0.155	44.2	0.155	44.5	0.155	44
0.235	45	0.232	44.1	0.227	44.1
0.329	44.9	0.332	43.8	0.329	44.3
0.51	44.1	0.524	44.1	0.512	44.1
0.756	43.9	0.803	44.2	0.781	43.9
1.031	44.1	1.092	43.9	1.054	44.1
1.862	43.6	1.553	43.7	1.5	44.2
2.779	42.8	2.301	42.9		

4.1.1.7 Compound 151

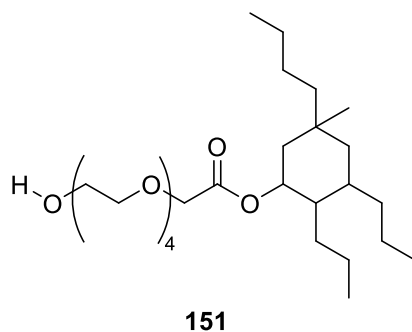


Figure 112: The structure of compound **151**

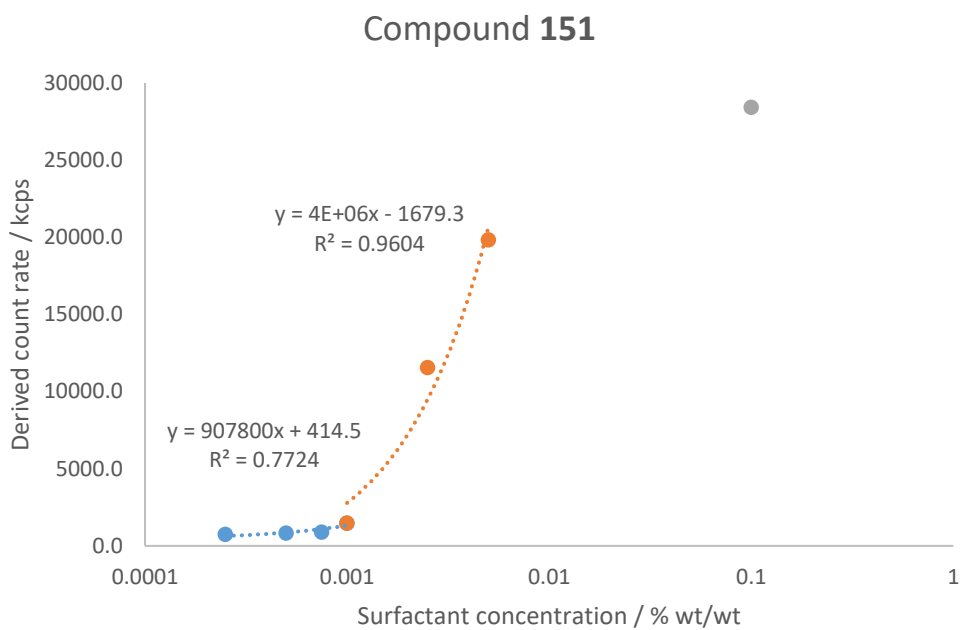


Figure 113: Derived count rate (kcps) vs Surfactant concentration (% wt/wt) for compound **151**

Table 39: Concentration and derived count rate for CMC determination of compound **151**

Surfactant concentration / % wt/wt	Derived count rate / kcps
0.0025	736.5
0.005	829.0
0.0075	889.0
0.01	1473.0
0.025	11564.4
0.05	19837.5
0.1	28424.3

Interception point (0.0058938, 949.54)

Compound **151** CMC= 0.0059% wt/wt

Compound 151

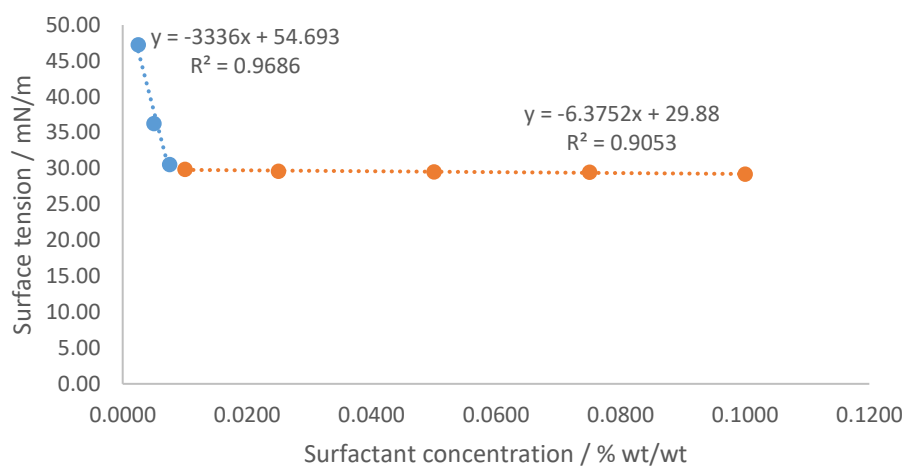


Figure 114: Surface tension vs Concentration of compound **151** in deionised water

Interception point (0.0075, 29.8320)

Compound **151** CMC= 0.0075% wt/wt

Table 40: Results table for the surface tension vs surfactant concentration analysis of compound **151**

Concentration / % wt/wt	Surface tension / mN/m	SD / mN/m	Temperature / °C
0.0025	47.22	0.026	20.03
0.0050	36.28	0.056	20.11
0.0075	30.54	0.043	20.06
0.0100	29.90	0.065	20.07
0.0250	29.63	0.090	20.10
0.0500	29.51	0.160	20.11
0.0750	29.47	0.051	20.07
0.1000	29.23	0.055	20.03

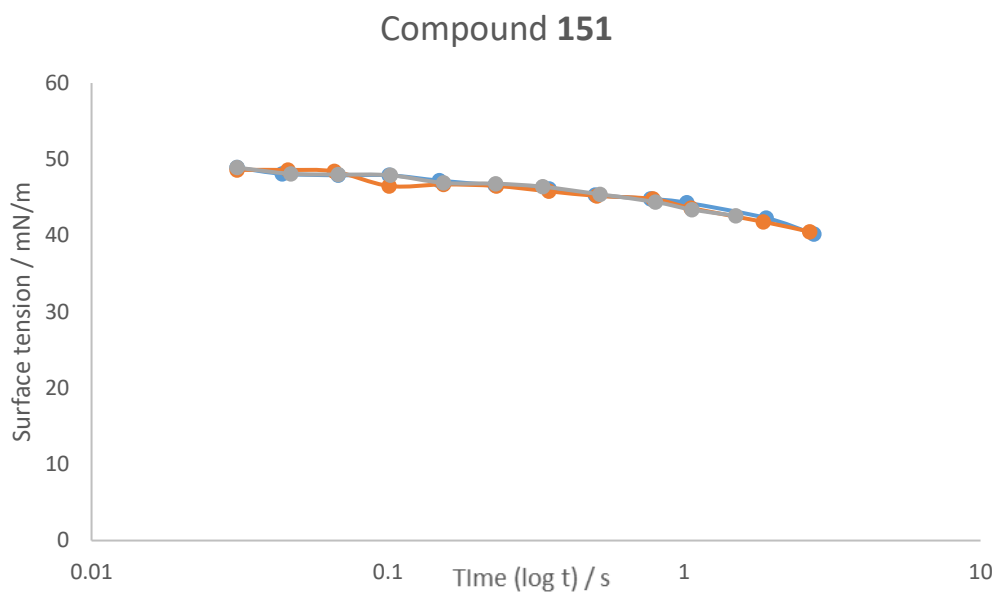


Figure 115: Surface tension vs surface age for compound **151** at 0.1% concentration in deionised water with 5% IPA

Table 41: Surface lifetime (SL) / s and surface tension (ST) / mN/m for compound **151**

Run 1		Run 2		Run 3	
SL / s	ST / mN/m	SL / s	ST / mN/m	SL / s	ST / mN/m
0.031	48.9	0.031	48.6	0.031	48.9
0.044	48.1	0.046	48.6	0.047	48.1
0.068	47.9	0.066	48.4	0.068	48
0.101	47.9	0.101	46.5	0.102	47.9
0.149	47.2	0.154	46.7	0.154	46.9
0.23	46.6	0.232	46.5	0.231	46.8
0.35	46.1	0.349	45.8	0.333	46.4
0.501	45.3	0.507	45.2	0.52	45.4
0.771	44.8	0.784	44.8	0.799	44.4
1.02	44.3	1.053	43.6	1.061	43.4
1.89	42.3	1.849	41.8	1.491	42.6
2.736	40.2	2.652	40.5		

4.1.1.8 Compound 152

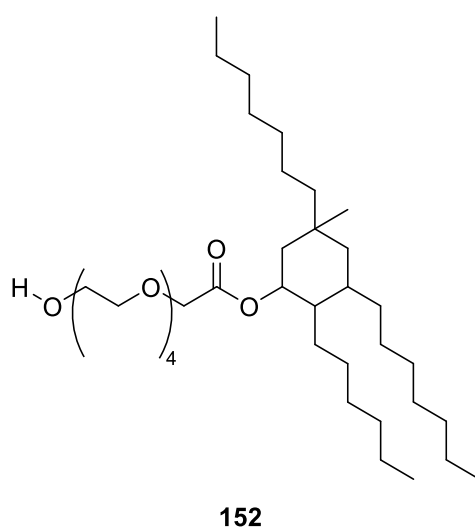


Figure 116: The structure of compound **152**

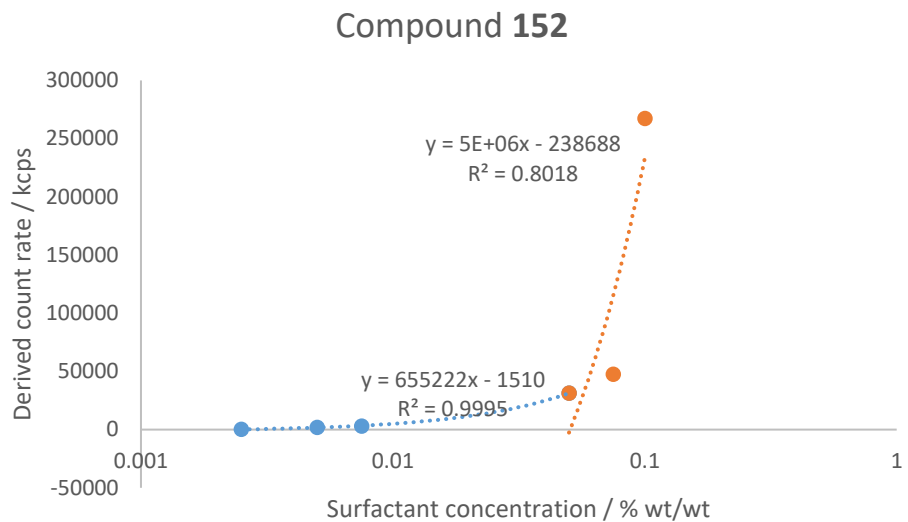


Figure 117: Derived count rate (kcps) vs Surfactant concentration (% wt/wt) for compound **152**

Table 42: Concentration and derived count rate for CMC determination of compound **152**

Surfactant concentration / % wt/wt	Derived count rate / kcps
0.0025	308.5
0.005	2037.2
0.0075	2915.5
0.05	31288.3
0.075	47689.5
0.1	267382.9

Interception point (0.054589, 34258)

Compound **152** CMC= 0.0546% wt/wt

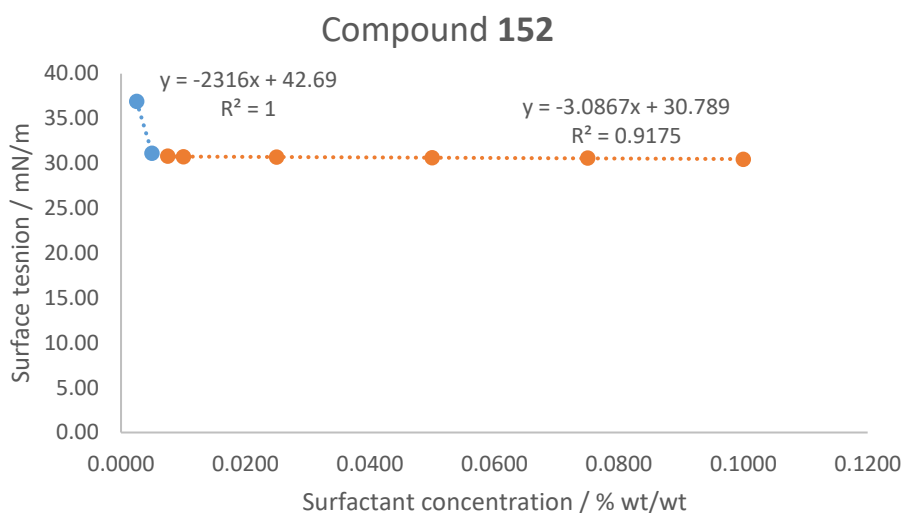


Figure 118: Surface tension vs Concentration of compound **152** in deionised water

Interception point (0.0051,30.7730)

Compound **152** CMC= 0.0051% wt/wt

Table 43: Results table for the surface tension vs surfactant concentration analysis of compound **152**

Concentration / % wt/wt	Surface tension / mN/m	SD / mN/m	Temperature / °C
0.0025	36.90	0.067	19.04
0.0050	31.11	0.097	18.86
0.0075	30.81	0.094	18.97
0.0100	30.72	0.038	18.91
0.0250	30.70	0.083	18.82
0.0500	30.62	0.062	18.79
0.0750	30.60	0.043	18.74
0.1000	30.46	0.098	18.73

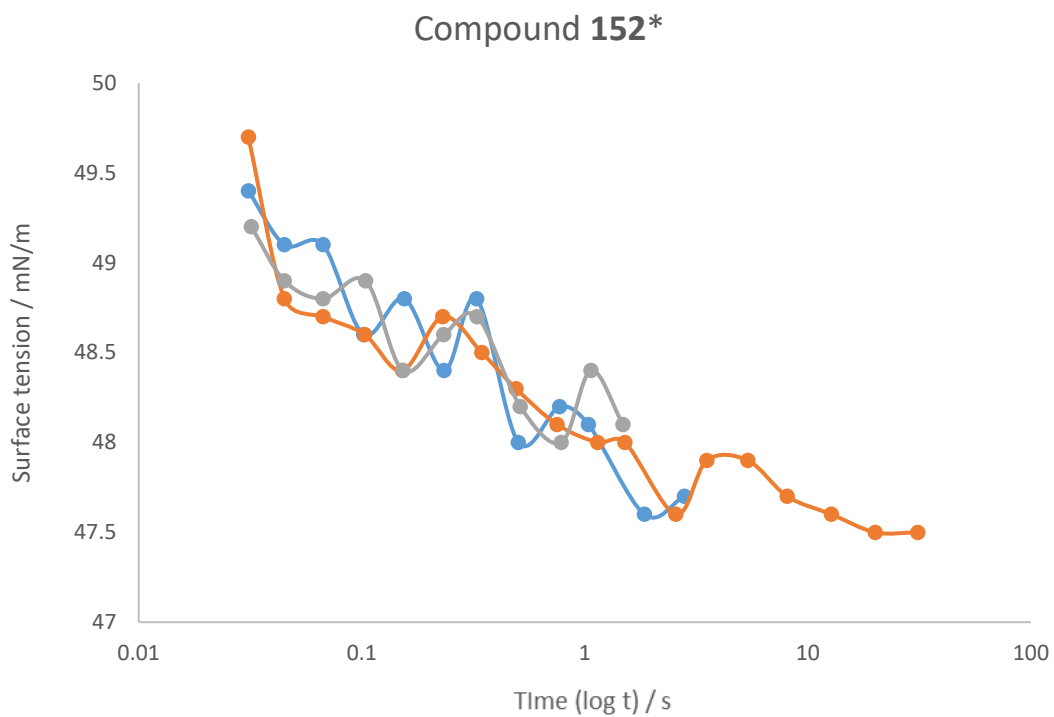


Figure 119: Surface tension vs surface age for compound **152** at 0.1% concentration in deionised water with 5% IPA

Table 44: Surface lifetime (SL) / s and surface tension (ST) / mN/m for compound **152** in deionised water with 5% IPA

Run 1		Run 2		Run 3	
SL / s	ST / mN/m	SL / s	ST / mN/m	SL / s	ST / mN/m
0.031	49.4	0.031	49.7	0.032	49.2
0.045	49.1	0.045	48.8	0.045	48.9
0.067	49.1	0.067	48.7	0.067	48.8
0.102	48.6	0.103	48.6	0.104	48.9
0.155	48.8	0.152	48.4	0.153	48.4
0.234	48.4	0.231	48.7	0.233	48.6
0.327	48.8	0.345	48.5	0.329	48.7
0.504	48	0.491	48.3	0.514	48.2
0.772	48.2	0.752	48.1	0.785	48
1.039	48.1	1.143	48	1.066	48.4
1.852	47.6	1.515	48	1.485	48.1
2.799	47.7	2.563	47.6		
		3.53	47.9		
		5.379	47.9		
		8.092	47.7		
		12.769	47.6		
		20.078	47.5		
		31.129	47.5		

4.1.1.9 Compound 147

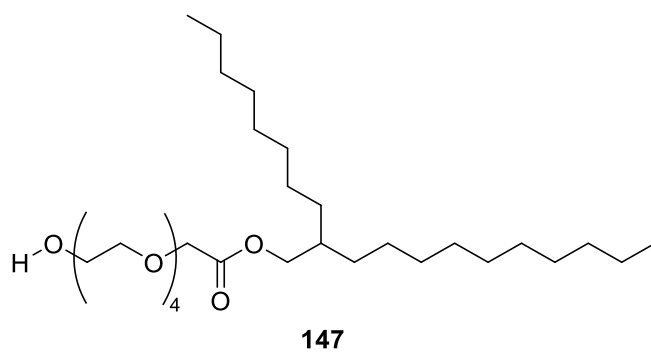


Figure 120: The structure of compound **147**

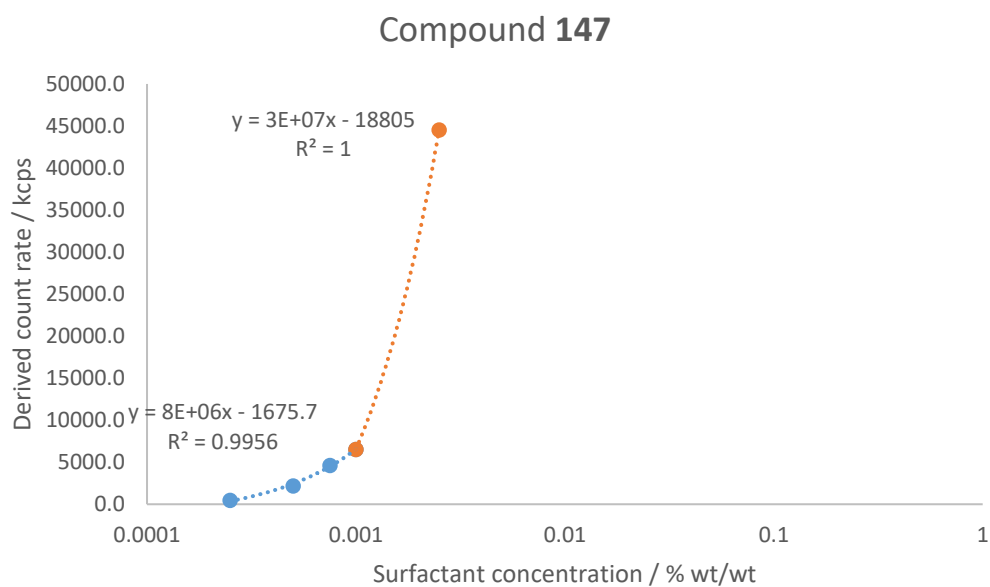


Figure 121: Derived count rate (kcps) vs Surfactant concentration (% wt/wt) for compound **147**

Table 45: Concentration and derived count rate for CMC determination of compound **147**

Surfactant concentration / % wt/wt	Derived count rate / kcps
---------------------------------------	---------------------------

0.00025	496.0
0.0005	2191.2
0.00075	4629.1
0.001	6534.6
0.0025	44544.0

Interception point (0.00077860, 4553.1)

Compound **147** CMC= 0.0008% wt/wt

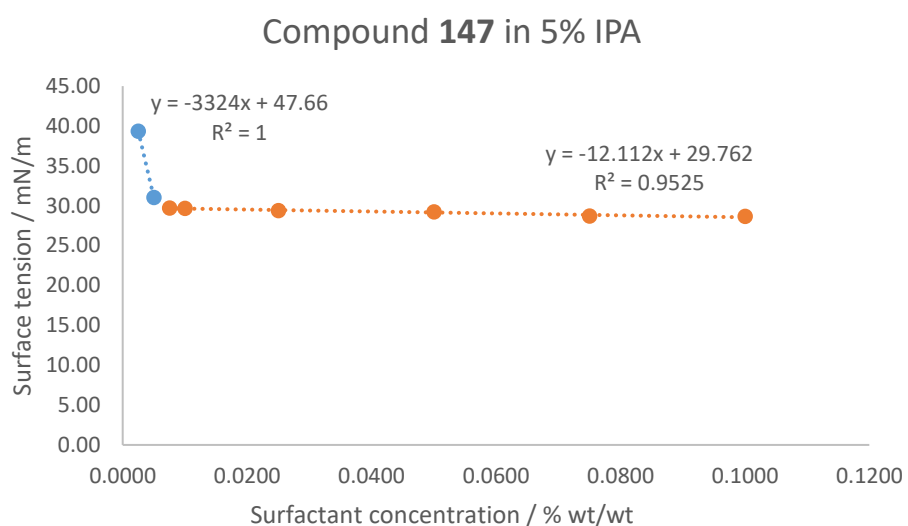


Figure 122: Surface tension vs Concentration of compound **147** in deionised water

Interception point (0.0054,29.6970)

Compound **147** CMC= 0.0054% wt/wt

Table 46: Results table for the surface tension vs surfactant concentration analysis of compound **147**

Concentration / % wt/wt	Surface tension / mN/m	SD / mN/m	Temperature / °C
----------------------------	---------------------------	--------------	---------------------

0.0025	39.35	0.064	18.72
0.0050	31.04	0.043	18.72
0.0075	29.72	0.035	18.74
0.0100	29.66	0.053	18.72
0.0250	29.38	0.021	18.60
0.0500	29.23	0.028	18.63
0.0750	28.69	0.087	18.58
0.1000	28.65	0.073	18.58

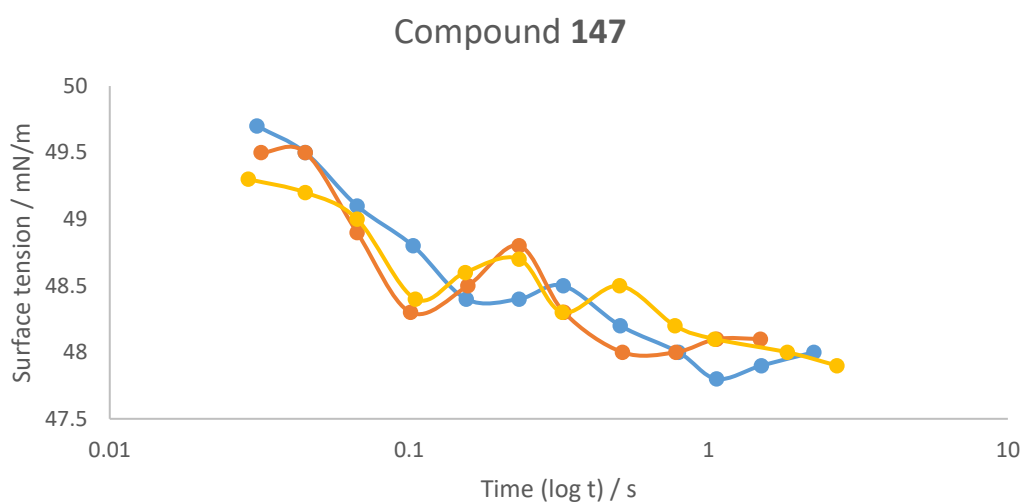


Figure 123: Surface tension vs surface age for compound **147** at 0.1% concentration in deionised water with 5% IPA

Table 47: Surface lifetime (SL) / s and surface tension (ST) / mN/m for compound **147** in deionised water with 5% IPA

Run 1		Run 2		Run 3	
SL / s	ST / mN/m	SL / s	ST / mN/m	SL / s	ST / mN/m
0.031	49.7	0.032	49.2	0.029	49.3

0.045	49.5	0.045	48.7	0.045	49.2
0.067	49.1	0.067	48.1	0.067	49
0.103	48.8	0.105	49.6	0.105	48.4
0.155	48.4	0.15	47.2	0.154	48.6
0.233	48.4	0.22	47.3	0.233	48.7
0.327	48.5	0.345	48.6	0.325	48.3
0.507	48.2	0.492	48.9	0.504	48.5
0.794	48	0.738	48.9	0.772	48.2
1.063	47.8	1.108	47.8	1.047	48.1
1.502	47.9	1.48	48.7	1.831	48
2.25	48	2.537	48.2	2.687	47.9
		3.445	48.2		
		6.191	47.7		
		9.003	48.1		
		13.494	47.6		
		20.292	47.8		
		31.92	47.7		